Large Strain and Fracture of Multiple Network Elastomers

Pierre Michel Millereau

THESE DE DOCTORAT DE
L'UNIVERSITE PIERRE ET MARIE CURIE

Spécialité
Chimie et Physico-Chimie des Polymères
(ED 397, Physique et Chimie des Matériaux)

Présentée par
Pierre MILLEREAU

Pour obtenir le grade de
DOCTEUR de l'UNIVERSITÉ PIERRE ET MARIE CURIE

Sujet de la thèse :

Large Strain and Fracture of Multiple Network Elastomers

Soutenue le 22 Mai 2017 devant le jury composé de :

Mme Anke LINDNER	Examinateur
M. Chung-Yuen HUI	Examinateur
Mme Meredith WISEMAN	Examinateur
M. Costantino CRETON	Directeur de thèse
Mme. Evelyne VAN RUYMBEKE	Rapporteur
M. Christian LIGOURE	Rapporteur

List of abbreviations

ATP	Acetophenone
BA	Butyl Acrylate
BDA	1,4- Butandiol diacrylate
DIC	Digital Image Correlation
DMSO	Dimethylsulfoxyde
DN	Double Network
DSC	Differential Scanning Calorimetry
EA	Ethyl Acrylate
EMCCD	Electron Multiplying Charge Coupled Device
HA	Hexyl Acrylate
HMA	Hexyl Methacrylate
HMP	2-Hydroxyethyl-2-methylpriopiophenone
IPN	Interpenetrated Polymer network
MA	Methyl Acrylate
MDP	1-methyl-2-pyrrolidone
NMR	Nuclear Magnetic Resonance
PAAm	Poly(acrylamide)
PAMPS	Poly(2-acrylamido-2-methylpropanesulfonic acid)
PEG	Poly(ethylene glycol)
QN	Quadruple Network
ROI	Region of Interest
SN	Simple Network
TN	Triple Network
UV	Ultra Violet
ZOI	Zone of Interest

List of symbols

C_∞	Characteristic ratio for an infinite number of monomers
C_N	Characteristic ratio for N monomers
J_1	First invariant
M_x	Average molecular weight between crosslinks
N_A	Avogadro's number
k_B	Boltzmann constant
E_e	Contribution of the entanglements to the Young's modulus
E_x	Contribution of the crosslinks to the Young's modulus
G_c	Fracture toughness
J_m	First invariant for the finite extensibility of the chain
M_e	Average molecular weight between entanglements
M_0	Molecular weight of a monomer
R_{max}	Maximum length of a polymer chain
U_{C-C}	Energy of a carbon bond
Γ	Fracture energy
$\dot{\lambda}$	Strain rate

λ_{cor}	Corrected elongation
λ_h	Hardening elongation
λ_0	Prestretching of the first network
σ_{Mooney}	Mooney Stress
σ_N	Nominal Stress
σ_T	True Stress
χ_{12}	mixing parameter
ϕ_{SN} **or** φ	Fraction of first network in multiple network elastomers
E	Elastic modulus
G'	Storage modulus
G''	Loss modulus
R	Gas constant
T_g	Temperature glass transition
λ_h	Finite extensibility of the chain
ν	Number of elastic polymer chains per unit volume
λ	Stretch
ρ	Polymer network density

Table of Content:

Chapter 3: Mechanical behaviour in Uniaxial Tension of the Reference Sample Family EAe(1.45)

Chapter 5: Fracture properties of multiple network elastomers and visualisation of the crack tip deformation

Chapter 6: Open general discussions

General introduction

Materials made of polymers are continually spreading in different industries and in broad fields. Polymers in general are appreciated for their large spectra of mechanical properties leading to an always larger range of applications. Among polymers, the elastomers are constituting a class of materials that are presenting special properties of elasticity. This property of deforming reversibly even up to high deformation makes them remarkable and stems from their low T_g added to the fact that they are made of long crosslinked and entangled flexible polymer chains. Those chains are constituting a polymer network that gives the deformability of the material. However, all elastomers do not present reversible elasticity to equally large strains. Indeed, soft polymer networks face a trade-off between toughness and stiffness. A highly-crosslinked network has a high modulus but a small reversible domain. On the other hand, a loosely crosslinked network can be highly stretched without damage but has a small Young's modulus.

In order to improve both properties at the same time, research has led to the use of fillers in elastomeric materials. The rubber industry is commonly using hard fillers such as carbon black or silica. As a first result to the use of fillers, the overall Young's modulus is increased. Second and more interestingly, the use of fillers introduces new dissipative mechanisms that favours higher deformations without fracture. Those mechanisms involve higher molecular friction, cavitation or local loss of adhesion at the interface of the fillers. From a mechanical point of view, the addition of fillers displays only advantages, however it changes other properties of the polymer matrix: the transparency of the polymer is removed by the addition of fillers, the viscosity and the density are changed leading to difficulties during the process to obtain thin films. Also, other materials cannot be used with fillers for bio application or specific temperature or U.V. exposure. Therefore, other reinforcement strategy are highly welcome in order to use the interesting mechanical properties of polymer materials in those specific conditions.

Many studies have tried to reach the objective of reinforcing polymer materials by using exclusively polymer networks. Some different techniques have been tried such as mixing short chains and long chains to obtain a synergy but it did not lead to much success at least in the open literature. The use of interpenetrated networks was also tried without much improvement of general properties in terms of fracture toughness or modulus.

Finally, a solution was found for hydrogels: the idea was based on the previously used principle of interpenetrated networks. Hydrogels are very soft polymer networks swollen in water that usually have a very low fracture toughness. Slightly more than a decade ago, a group in Japan led by Gong [1], managed to improve sharply the mechanical properties of their hydrogels. To do that they created interpenetrated polymer networks made of two networks that were presenting separately a stiff but brittle behaviour and a soft and extensible one. The reinforcement idea comes from the asymmetry between the two networks, one has to be very stiff (through prestretching of the chains), highly crosslinked and in minority whereas the other is loosely crosslinked and in majority. The resulting material has a fracture toughness hundred times better than either network on its own.

Six years ago, inspired by the work of Gong's group on hydrogels, the PhD of Etienne Ducrot [2] was started in our group. The objective was to transpose the principle of double networks developed by Gong for hydrogels to the field of elastomers. One of the issue to overcome, in order to make multiple network elastomers, was to sufficiently prestretch the first network to obtain the stiffening and toughening effect. To do so, the highly crosslinked first network was not only swollen with monomer and polymerized once but twice. This created double or triple interpenetrated networks. This strategy was pursued on weak elastomers of methyl or ethyl acrylate and the reinforcement of the mechanical properties was successful. The fracture energy was increased by a factor of 40 and the stress and elongation at break by at least 10 times. The PhD of Etienne Ducrot was a success in transferring the principle of double networks hydrogels towards the field of elastomers. However, some open questions remained:

- Why are double and triple networks so different?
- What is controlling crack propagation and more generally the reinforcement mechanism?
- Is the network architecture strategy working for other monomers?
- How does the failure of the first network occur inside the material?

In order to answer some of those questions and to perform more systematic experiments, another PhD was started on the subject, this is the topic of this manuscript. The present work is divided into 6 chapters.

The first chapter presents some necessary theoretical background regarding the physics and chemistry of polymer networks along with an overview of previous work done on the topic. This bibliographic section describes the work done by Gong *et al.* and by the groups inspired by them.

The second chapter presents the different experiments that have been pursued during this work. The mechanical part is presented along the synthesis path followed to obtain and characterize the multiple network elastomers.

Chapter 3 and 4 describe the mechanical behaviour of different types of multiple networks in uniaxial tension experiments. In those chapters, the mechanical behaviour of the materials is investigated at high strength and different models are used in order to understand and predict the mechanical properties.

Then, in chapter 5, the resistance to crack propagation is studied in a first part. The characterization is done for multiple materials in term of fracture resistance. Then the second section concerns the visualisation of the strain around the crack tip with different techniques: the Digital Image Correlation and the mechanoluminescence.

Finally, in chapter 6, some questions raised by the results are discussed in more detail.

This work will be concluded by a section summarizing the main results of this work and the outlooks and perspectives that could be studied in future work.

References

1. Gong, J.P., et al., *Double-network hydrogels with extremely high mechanical strength.* Advanced Materials, 2003. **15**(14): p. 1155-1158.
2. Ducrot, E., *Double Network Elastomers*. 2013, Université Pierre et Marie Curie: Paris.

Chapter 1: Physical-Chemistry of Polymer Networks and Introduction to Multiple Networks.

Chapter 1: Physical-Chemistry of Polymer Networks and Introduction to Multiple Networks

Introduction

The first chapter of this thesis starts with some theoretical background on polymer networks. We will present the different models and theories that will be used throughout this work in the different chapters. This chapter then presents the state of the art relevant for multiple networks elastomers. This subject was inspired by the pioneering work on double network hydrogels. The notion of double networks appeared in 2003 with the work of Gong *et al.* [1]. Since then, a lot of interest has been shown towards this material design by the scientific community. The aim of this part is to describe the literature that can be found on the topic, starting with the presentation of the notion of double networks as created by Gong. Then, some work done by different groups stemming from this initial discovery will be presented. In a second stage, studies done on the reinforcement of elastomers by using bimodal networks or interpenetrated elastomer networks will be discussed. Finally, we will present the state of the art regarding multiple network elastomers and the previous work done on this project by the former PhD student of our group Etienne Ducrot.

I) Theoretical background

1) Polymer ideal chain model

The model of the ideal polymer chain was developed by Flory [2] and later by Doi and Edwards [3]. It is used to simply describe polymer chains, and is a foundation for the development of many related polymer models. This model is also described in Rubinstein and Colby's book [4]. In this section, we recall its main features.

An ideal polymer chain can be modelled as a succession of $N+1$ atoms defining N segments with length a. Each segment is oriented completely randomly and can be described by a vector $\vec{r_i}$. Using those segments, the end-to-end vector is defined as the sum of the different $\vec{r_i}$ as shown in Eq. (1). As a consequence of the random direction taken by the segments vector, the mean value of the end-to-end vector is zero as shown in Eq. (2). However, the mean square end-to-end distance can be described by Eq. (3) leading to the end-to-end distance expression for an ideal chain in Eq. (4). It can be seen that this distance evolves with the root square of the number of segments which is much smaller than the extended chain length Na. The chain is curled in a random coil.

$$\overrightarrow{\boldsymbol{R_N}} = \sum_{\boldsymbol{i=1}}^{\boldsymbol{N}} \overrightarrow{\boldsymbol{r_i}} \qquad \textbf{Eq. (1)}$$

$$\langle \overrightarrow{\boldsymbol{R_N}} \rangle = \boldsymbol{0} \qquad \textbf{Eq. (2)}$$

$$\langle \boldsymbol{R_N^2} \rangle = \boldsymbol{Na^2} \qquad \textbf{Eq. (3)}$$

$$\langle \boldsymbol{R_N^2} \rangle^{\boldsymbol{1/2}} = \boldsymbol{N^{1/2}a} \qquad \textbf{Eq. (4)}$$

In real chains, the segments are not randomly oriented between each other, but are subject to correlations. Eq. (3) is corrected to account for these correlations in Eq. (5) by the characteristic ratio that is noted C_N. For an infinite number of monomers, as shown in Eq. (6), the characteristic ratio is noted C_∞. This ratio depends on the details of the monomer used, and represents the rigidity or the flexibility of the polymer bonds between each other.

$$\langle \boldsymbol{R_N^2} \rangle = \boldsymbol{C_N Na^2} \qquad \textbf{Eq. (5)}$$

$$\langle \boldsymbol{R_0^2} \rangle = \boldsymbol{C_\infty Na^2} \qquad \textbf{Eq. (6)}$$

The maximum elongation of the chain can also be estimated as shown in Eq. (7) for a chain that presents a rigid angle θ (around 68° for a C-C bond when a is the length of a C-C bond around 0.154 nm) between chain bonds as shown in Figure 1. This maximum elongation can then be used to estimate a parameter that will be used in this work: λ_{limit}. λ_{limit} is the ratio between the length of the fully stretched chain and the end to end mean distance of the chain in its ideal conformation (Eq. (6)) as shown in Eq. (8).

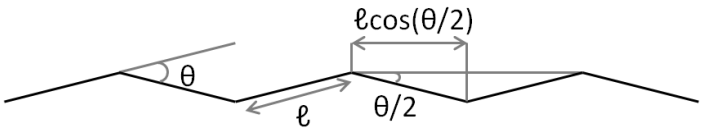

Figure 1: Scheme of a chain in all-trans conformation with a rigid angle θ between following bonds.

$$\boldsymbol{R_{max} = N\, a\, cos\,(\frac{\theta}{2})} \qquad \textbf{Eq. (7)}$$

$$\boldsymbol{\lambda_{limit} = \frac{R_{max}}{\sqrt{\langle {R_0}^2 \rangle}} = cos\,(\frac{\theta}{2})\,\sqrt{\frac{N}{C_\infty}}} \qquad \textbf{Eq. (8)}$$

Entropy and free energy of an ideal chain

The entropy depends on the number of conformations Ω of a freely jointed chain with N monomers and an end-to-end vector $\vec{R}$. Eq. (9) describes the expression of the entropy as a function of N and $\vec{R}$. k_B is the Boltzmann constant.

$$\boldsymbol{S(N,\vec{R}) = k_B\, ln(\Omega(N,\vec{R}))} \qquad \textbf{Eq. (9)}$$

The number of conformations Ω can be deduced from the Gaussian distribution of end-to-end distances around the average value given by Eq. (4). The probability of obtaining a chain with an end-to-end distance between R and $R+dR$ is given by Eq. (10).

$$\boldsymbol{P(N,R)dR = \left\{\left(\frac{3}{2\pi N b a^2}\right)^{3/2} e^{-\frac{3R^2}{2Na^2}}\right\} 4\pi R^2 dR} \qquad \textbf{Eq. (10)}$$

From Eq. (10), the entropy expression can be deduced as shown in Eq. (11). In eq. (11) $S(N,0)$ is a term depending only on N.

$$\boldsymbol{S(N,\vec{R}) = -\frac{3}{2} k_B \frac{R^2}{N.a^2} + S(N,0)} \qquad \textbf{Eq. (11)}$$

Using this result (Eq. (11)), the free energy F can be calculated starting from Eq. (12).

$$\boldsymbol{F = U - T\,S} \qquad \textbf{Eq. (12)}$$

The monomers have no interactions between each other for an ideal chain, so the internal energy U is independent of the end-to-end vector. Then using Eq. (11) and Eq. (12), the free energy can be obtained as shown in Eq. (13).

$$\boldsymbol{F(N,\vec{R}) = \frac{3}{2} k_B T \frac{\vec{R}}{N.a^2} + F(N,0)} \qquad \textbf{Eq. (13)}$$

Polymer network

This section describes ideal chains, but in our system, the chains are connected creating a polymer network. We consider a polymer network made of ideal polymer chains randomly connected to each other. Under load, the first law of thermodynamics can be applied resulting

in the fact that the change in the internal energy is the sum of all energy changes. Those energies are the work due to the network deformation, the heat transmitted to the system and the work due to the change in volume as shown in Eq. (14).

$$\boldsymbol{dF = -S\,dT - p\,dV + f\,dL} \qquad \textbf{Eq. (14)}$$

At constant *T* and *V*, the applied force f to deform the polymer network consists of two contributions:

$$\boldsymbol{f = \left(\frac{\partial F}{\partial L}\right)_{T,V} = \left(\frac{\partial (U - TS)}{\partial L}\right)_{T,V} = \left(\frac{\partial U}{\partial L}\right)_{T,V} - T\left(\frac{\partial S}{\partial L}\right)_{T,V} = f_E + f_S} \qquad \textbf{Eq. (15)}$$

In Eq. (15), f_E is the internal energy term and f_S the entropic one.

In rubbers, it has been shown that the entropic contribution to the force is much more important. For an ideal network f_E ~ 0, and in the rest of this work this contribution is neglected.

2) The affine network model

After describing the model of the ideal chain describing polymer chains, another model needs to be used to understand the behaviour of polymer networks. Its description will be the subject of this section.

We consider a polymer network only composed of crosslinked ideal polymer chains (n polymer chains composed of N monomers between crosslink points) with an average molecular weight between crosslinks M_x smaller than the average molecular weight between entanglements M_e. This means that there are no entanglements present in the system.

The high deformability of such a network arises from the entropic elasticity of the polymer chains that make up the network. The simplest model that captures this idea of rubber elasticity is the affine network model proposed by Kuhn [5-7] almost a century ago. The main assumption of the affine deformation model is that the average deformation of the elastic strands is identical to the macroscopic applied deformation.

A single elastic chain has an initial end-to-end vector $\overrightarrow{R_0}$, its projection in the three different directions of the plane are R_{x0}, R_{y0}, R_{z0}. After deformation, those projections are changed into:

$$\boldsymbol{R_x = \lambda_x R_{x0} \quad R_y = \lambda_y R_{y0} \quad R_z = \lambda_z R_{z0}} \qquad \textbf{Eq. (16)}$$

If there are no interactions between chains, the variation of entropy can be calculated for n crosslinked ideal chains as shown in Eq. (17) so is the free energy shown in Eq. (18).

$$\boldsymbol{\Delta S_{network} = -\frac{nk_B}{2}(\lambda_x^2 + \lambda_y^2 + \lambda_z^2 - 3)} \qquad \textbf{Eq. (17)}$$

$$\boldsymbol{\Delta F_{network} = -T\Delta S_{network} = \frac{nk_BT}{2}(\lambda_x^2 + \lambda_y^2 + \lambda_z^2 - 3)} \qquad \textbf{Eq. (18)}$$

If we now consider a sample of initial dimensions L_{x0}, L_{y0}, L_{z0}, and if the sample is deformed in the three directions by the factors λ_x, λ_y and λ_z, then the dimensions of the deformed sample is given by Eq. (19).

$$\boldsymbol{L_x = \lambda_x L_{x0} \quad L_y = \lambda_y L_{y0} \quad L_z = \lambda_z L_{z0}} \qquad \textbf{Eq. (19)}$$

An assumption that will be made throughout this work is that our materials are incompressible and do not damage by cavitation in uniaxial extension, leading to the hypothesis that the deformation always occurs at a constant volume. This assumption results in Eq. (20).

$$\boldsymbol{\lambda_x * \lambda_y * \lambda_z = 1} \qquad \textbf{Eq. (20)}$$

Case of the uniaxial tension

The uniaxial tension is imposed along the x direction. In accordance with the volume conservation hypothesis, the deformation in every direction can be deduced from the measured stretch λ applied along the x axis as shown in Eq. (21) and Eq. (22). In Eq. (21), ε is the deformation in the x direction starting at 0.

$$\boldsymbol{\lambda_x = \lambda = 1 + \varepsilon} \qquad \textbf{Eq. (21)}$$

$$\boldsymbol{\lambda_y = \lambda_z = \frac{1}{\sqrt{\lambda}}} \qquad \textbf{Eq. (22)}$$

Therefore, the free energy of the system can be calculated using Eq. (20), (21) and (22) as shown in Eq. (23), and the force required to deform the network in the x direction is described by Eq. (24).

$$\boldsymbol{\Delta F_{network} = \frac{n k_B T}{2}(\lambda^2 + \frac{2}{\lambda} - 3)} \qquad \textbf{Eq. (23)}$$

$$\boldsymbol{f_x = \frac{\partial \Delta F_{network}}{\partial L_x} = \frac{1}{L_{x0}} \frac{\partial \Delta F_{network}}{\partial \lambda} = \frac{n k_B T}{L_{x0}}(\lambda - \frac{1}{\lambda^2})} \qquad \textbf{Eq. (24)}$$

The true stress is defined as the ratio between the force f_x and the perpendicular deformed section which is $L_y L_z = \frac{L_{y0} L_{z0}}{\lambda}$. The expression of the true stress is calculated and displayed in Eq. (25). The nominal stress is the ratio of the force in the x direction over the initial cross section, its expression is shown in Eq. (26)

$$\boldsymbol{\sigma_T = \frac{f_x}{L_y L_z} = \frac{n k_B T}{L_{x0} L_{y0} L_{z0}} \lambda \left(\lambda - \frac{1}{\lambda^2}\right) = \frac{n k_B T}{V}(\lambda^2 - \frac{1}{\lambda})} \qquad \textbf{Eq. (25)}$$

$$\boldsymbol{\sigma_N = \frac{f_x}{L_{y0} L_{z0}} = \frac{\sigma_T}{\lambda}} \qquad \textbf{Eq. (26)}$$

The proportionality coefficient observed in Eq. (25) can be linked with the Young's modulus as shown in Eq. (27).

$$\boldsymbol{E = \frac{3 n k_B T}{V} = 3 v k_B T = \frac{3 \rho R T}{M_x}} \qquad \textbf{Eq. (27)}$$

In Eq. (27), $\nu = n/V$ (the number of elastic polymer chains per unit volume), ρ is the network density, R the gas constant and M_x the average molecular weight between crosslinks (in the case of the absence of entanglements).

Using Eq. (27), the affine model gives a prediction for the true stress and the nominal stress as shown in Eq. (28) and (29).

$$\boldsymbol{\sigma_T = \frac{E}{3}\left(\lambda^2 - \frac{1}{\lambda}\right)} \qquad \textbf{Eq. (28)}$$

$$\boldsymbol{\sigma_N = \frac{E}{3}\left(\lambda - \frac{1}{\lambda^2}\right)} \qquad \textbf{Eq. (29)}$$

Provided that the network does not contain entanglements, this model is in good agreement with experiment at small and intermediate strains. Materials following this relationship are called neo-Hookean. Indeed, and at small deformation ($\lambda \approx 1$), Hooke's law is found. At higher strain when the hypothesis of no interactions between chains fails, other models are needed.

3) Contribution of entanglements and crosslinks

In polymer networks, if the crosslinker concentration is low, entanglements can occur. In the presence of entanglements, E is the addition of two components, one coming from the crosslinks E_x and the other from the entanglements E_e as shown in Eq. (30). The assumption that the two components can be added is due to the fact that at small strain the entanglement points behave as temporary crosslink points.

$$\boldsymbol{E = E_x + E_e = \frac{3\,\rho\,R\,T}{M_x} + \frac{3\,\rho\,R\,T}{M_e}} \qquad \textbf{Eq. (30)}$$

To evaluate the respective contributions of the entanglements and crosslinks, the Mooney Rivlin representation can be used [8, 9]. In this approach, Mooney and Rivlin proposed a general expression for the free energy leading to a relation between the Mooney stress (defined in Eq. (31)) and lambda as shown in Eq. (32).

$$\boldsymbol{\sigma_{Mooney} = \frac{\sigma_N}{\lambda - \frac{1}{\lambda^2}}} \qquad \textbf{Eq. (31)}$$

$$\boldsymbol{\sigma_{Mooney} = 2\,C_1 + \frac{2\,C_2}{\lambda}} \qquad \textbf{Eq. (32)}$$

Although this is a fully empirical model, a more molecular qualitative interpretation of the Mooney stress can be given. If there are no entanglements, C_2=0 and the Mooney stress is a constant. This then corresponds to the classical neo-Hookean model. If softening occurs in uniaxial tension then $C_2 > 0$ and, in a simple unfilled rubber network, this is indicative of the presence of entanglements. If hardening appears then C_2 is less than 0, which is attributed to the presence of prestretched chains.

To explore in more detail the different contributions to the modulus, the molecular model proposed by Rubinstein and Panyukov [10, 11] is better suited. The objective of this model is to complete Edwards model and to develop it so it can be used at high deformation. Rubinstein and Panyukov have proposed a non-affine tube model in which the randomness of the crosslinking process is taken into account as well as the deformation of the tube when the sample is stretched. This approach leads to a relation between the Mooney stress and the modulus from entanglements and crosslinks, E_e and E_x respectively as shown in Eq. (33).

$$\sigma_{Mooney} = \frac{\sigma_N}{\lambda - \frac{1}{\lambda^2}} = \frac{1}{3}\left(E_x + \frac{E_e}{\lambda + \lambda^{-0.5} - 1}\right) \qquad \textbf{Eq. (33)}$$

The solution shown in Eq. (33) is in good agreement with uniaxial tension data. On the other hand, to obtain better prediction on the stress in uniaxial compression, Rubinstein and Panyukov have taken into account the fact that chains along the deformation are elongated and compressed on others. Stored length from the compressed directions of the tube can redistribute itself into the stretched directions, balancing the tension in all directions and lowering the free energy and the stress in the network. The resulting dependence of stress on the deformation in the non-affine slip-tube model does not have a simple analytical form. However, the model has been solved numerically and its solution in the experimentally relevant range of $0.1 < \lambda < 10$ can be approximated in a form similar to Eq. (33), as shown in Eq. (34).

$$\sigma_{Mooney} = \frac{\sigma_N}{\lambda - \frac{1}{\lambda^2}} = \frac{1}{3}\left(E_x + \frac{E_e}{0.74\lambda + 0.61\lambda^{-0.5} - 1}\right) \qquad \textbf{Eq. (34)}$$

In Eq. (33), when the deformation tends to 1, Eq. (30) can be recovered.

This equation will be used in this work to fit uniaxial tensile data and to estimation the respective contributions from entanglements and crosslinks to the small strain modulus.

4) Model for large strain deformation: Gent's model

At large strain when the chains are approaching their finite extensibility, a hardening phenomenon occurs. It is observed on stress-strain curves by a sharp increase of the slope between the stress and the strain as shown in Figure 2. It can be seen that starting approximately at an elongation of 2, the slope increases sharply. This phenomenon is called strain hardening by analogy with metallurgy but should really be called strain stiffening since it is not due to plastic deformation events but to non-linear elasticity. For the sake of simplicity, we will refer to it as strain hardening in the rests of the manuscript.

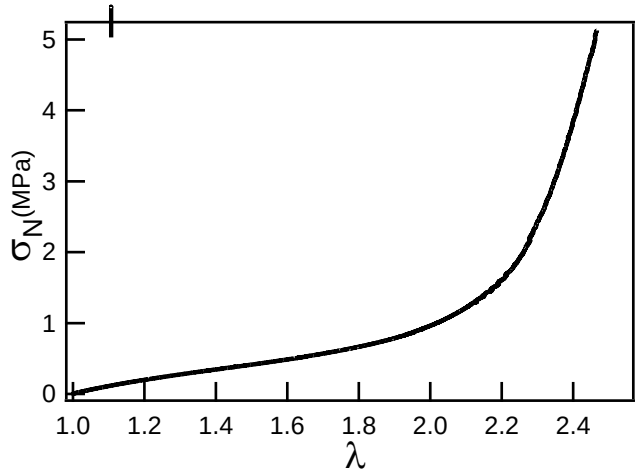

Figure 2: Stress-strain curve of an elastomer showing a hardening phenomenon.

This phenomenon is not described by the previous models presented in this section. To do so, a strain hardening model is needed such as the one developed by Gent [12]. Gent's model introduces the finite extensibility of the polymer chains, and his theory is that the hardening corresponds to the deformation reaching the maximum extensibility of the chains λ_h. This parameter controls mainly the stress and the strain at high deformation as shown in Eq. (35). In this equation, J_1 is the first invariant of the right Cauchy-Green tensor defined in Eq. (36) for uniaxial extension and J_m is the value of this invariant for the finite extensibility of the chain λ_h as shown in Eq. (37).

$$\boldsymbol{\sigma_N = \frac{E\,(\lambda^2 - \frac{1}{\lambda})}{3\,(1 - \frac{J_1}{J_m})}} \qquad \textbf{Eq. (35)}$$

$$\boldsymbol{J_1 = \lambda^2 + \frac{2}{\lambda} - 3} \qquad \textbf{Eq. (36)}$$

$$\boldsymbol{J_m = {\lambda_h}^2 + \frac{2}{\lambda_h} - 3} \qquad \textbf{Eq. (37)}$$

This model will be used to fit experimental curves during this work and gives good results as long as the effect of entanglements is not dominant, i.e. the material is sufficiently crosslinked.

5) Swelling of polymer networks

Upon the swelling of a polymer network, two contrary effects are involved in the mechanism. On one hand, the change of free energy of mixing Δg_{mel} is favourable to the swelling as long as the solvent is a good solvent, while the change of elastic energy Δg_{el} limits the swelling. The change of density of free energy Δg is the sum of those two contributions as shown in Eq. (38).

$$\boldsymbol{\Delta g = \Delta g_{mel} + \Delta g_{el}} \qquad \textbf{Eq. (38)}$$

Using Flory-Rehner theory [13], with the assumption of an isotropic swelling of the network, an expression of Δg_{mel} can be given (Eq. (39)). In Eq. (39), V_1 is the molar volume of the solvent, ϕ_1 and ϕ_2 the respective volume fractions of the solvent and the polymer (with ϕ_1 + ϕ_2 = 1) and χ_{12} is the Flory interaction parameter for the polymer/solvent system.

$$\boldsymbol{\Delta g_{mel} = \frac{R\,T}{V_1}\,(\phi_1\,ln(\phi_1) + \chi_{12}\,\phi_1\,\phi_2)} \qquad \textbf{Eq. (39)}$$

From the model of James and Guth [14], the change of density of free elastic energy can be expressed as shown in Eq. (40).

$$\boldsymbol{\Delta g_{el} = \left(1 - \frac{2}{f}\right)\frac{3RT\nu}{2}\left(\left(\frac{\phi_0}{\phi_2}\right)^{2/3} - 1\right)} \qquad \textbf{Eq. (40)}$$

In Eq. (40), $f$is the functionality of the crosslinker (4 in our system), ν the molar concentration of elastically active chains and ϕ_0 the concentration in polymer at the preparation state.

For an ideal polymer network ν can be estimated as shown in Eq. (41), with Nbeing the mean number of segments between crosslinks.

$$\boldsymbol{\nu = \frac{\phi_2}{NV_1}} \qquad \textbf{Eq. (41)}$$

At the swelling equilibrium, the osmotic pressure (responsible for the swelling) is equivalent inside the network and outside the network. Therefore, using Eq. (39) and Eq. (40), Eq. (42) and then Eq. (43) can be obtained.

$$\boldsymbol{\Pi_{gel} = \Pi_{ext} = 0 = \Pi_{mel} + \Pi_{el} = {\phi_2}^2\frac{\partial}{\partial\phi_2}\left(\frac{\Delta g_{mel} + \Delta g_{el}}{\phi_2}\right)} \qquad \textbf{Eq. (42)}$$

$$\boldsymbol{0 = -\frac{R\,T}{V_1}\left(ln(1-\phi_2) + \phi_2 + \chi_{12}{\phi_2}^2 + (1 - \frac{2}{f})\frac{{\phi_0}^{2/3}{\phi_2}^{1/3}}{N}\right)} \qquad \textbf{Eq. (43)}$$

Using Eq. (43), the swelling ratio at the equilibrium $Q_{eq} = \frac{1}{\phi_2}$ can be predicted. It depends on the quality of the solvent influencing χ_{12}, on the conditions of synthesis through ϕ_0 but it also depends on the number of segments in the chain and therefore on the amount of crosslinker during the synthesis.

The evolution of the Young's modulus as a function of swelling ratio has been theoretically investigated mainly by Panyukov. The Panyukov form of the free elastic energy can be used for swollen or deformed networks as shown in Eq. (44).

$$\boldsymbol{F_{el} = kT\,\frac{(\lambda R_0)^2}{{R_{ref}}^2}} \qquad \textbf{Eq. (44)}$$

In Eq. (44), R_0 was previously described in Eq. (6), λ is the deformation ratio assuming an affine deformation on the length scales of a network strand with $R^2 = (\lambda R_0)^2$ and ${R_{ref}}^2$ is the mean square end-to-end fluctuation of the end-to-end distance of the network strand [4].

The Young's modulus of the swollen gel is proportional to the chain number density (Eq. (41)) multiplied by the elastic free energy per chain giving Eq. (45).

$$E(\phi_2) = \nu kT \frac{(\lambda R_0)^2}{{R_{ref}}^2} = kT \frac{\phi_2}{NV_1} \frac{(\lambda R_0)^2}{{R_{ref}}^2} \qquad \textbf{Eq. (45)}$$

6) Fracture of polymer networks: Lake and Thomas theory [15]

The goal of this theory is to estimate the energy dissipated by the breakage of a single polymer chain. As shown in Figure 3, a polymer chain containing N monomers between crosslinks is considered. This chain is located across the plane of fracture propagation.

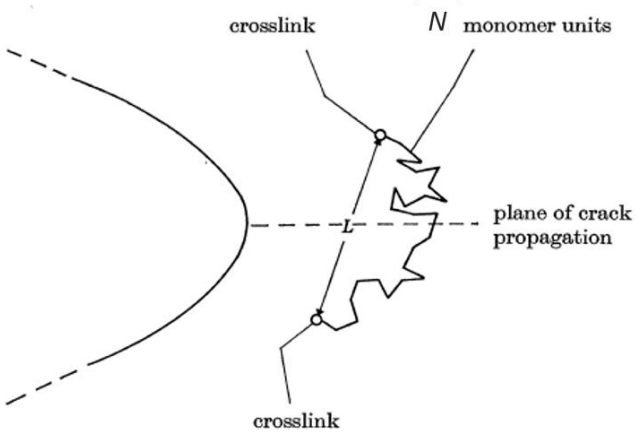

Figure 3: Schematic view of a polymer chain (n monomers unity between crosslink) across the plane of crack propagation[15]

In Figure 3, when the crack propagates, the chain is more and more stretched until it reaches the final force before breakage of f_{max} given by the relationship shown in Eq. (46), where $U_{C\text{-}C}$ is the energy of a carbon-carbon bond (≈ 2 eV) and a is the length of this bond (≈ 1.5 Å). At the same time, when the chain is stretched, it loses some available configuration resulting in the storage of an elastic entropic energy U_{ent}. The general expression of this energy is given by Eq. (47). where k_B is the Boltzmann constant, T is the temperature and $\vec{R}$ the end to end vector of the polymer chain. When the polymer chain is fully stretched to the length $N * a$, this gives a new estimate of the entropic energy of the fully stretched chain in Eq. (48). At the breakage point, the force applied to every monomer reaches f_{max} and when the chains finally breaks, the energy released can be estimated. This released energy $U_{tot\ chain}$ is the addition of the energy released by every monomer according to the Lake and Thomas theory (N times $U_{C\text{-}C}$) and of the entropic energy as described in Eq. (48) resulting in Eq. (49) (the factor 2 comes from the fact that in the studied case, each monomer presents two carbon-carbon bonds in the polymer chain). At ambient temperature, the product k_BT is of the order of 10^{-2} eV while $U_{C\text{-}C}$ has a value of 2 eV. This allows us to make the approximation $NU_{C-C} \gg k_BTN$ resulting in an estimate of the energy dissipated by a broken chain (Eq. (50)).

$$f_{max} = \frac{U_{C-C}}{a} \approx 4\,nN \quad \text{Eq. (46)}$$

$$U_{ent} \approx \frac{3}{2} k_B\,T \frac{\vec{R}^2}{N\,a^2} \quad \text{Eq. (47)}$$

$$U_{ent} \approx \frac{3}{2} k_B\,T \frac{(Na)^2}{Na^2} \approx \frac{3}{2}\,k_B\,T\,N \quad \text{Eq. (48)}$$

$$U_{tot\,chain} \approx 2 * N\,U_{C-C} + U_{ent} \approx 2 * NU_{C-C} + \frac{3}{2}\,k_BTN \quad \text{Eq. (49)}$$

$$U_{tot\,chain} \approx 2 * N\,U_{C-C} \quad \text{Eq. (50)}$$

The result presented in Eq. (50) stands only for one chain but it can be applied to the entire network system. When a network is considered, the crack has to propagate by breaking at least every chain on the fracture plane. This leads to an estimate of a minimal energy Γ_0 needed to propagate a crack with the Lake and Thomas model as described in Eq. (51), where $\Sigma$is the areal density of chains crossing the plane of the fracture. This density can be calculated as shown in Eq. (52) with M_0 being the molar mass of the monomer and N_A the Avogadro's number. This leads to an estimate of Γ_0 with the Lake and Thomas model (Eq. (53)). Interestingly this model predicts that the fracture energy Γ_0 will increase with the number of monomers between crosslinks.

$$\Gamma_0 \approx \Sigma\,U_{tot\,chain} \approx 2 * \Sigma\,N\,U_{C-C} \quad \text{Eq. (51)}$$

$$\Sigma = \frac{M_0\,N_A}{2 * a^2\sqrt{N}} \quad \text{Eq. (52)}$$

$$\Gamma_0 = \frac{M_0\,N_A\,\sqrt{N}\,U_{C-C}}{a^2} \quad \text{Eq. (53)}$$

This model has been first tested for different networks with different molar masses by Tobias and Gent [16] and more recently discussed by Creton and Ciccotti [17] and gives good agreement for simple randomly crosslinked networks of elastomers [18] or gels [19].

To return to the discussion of the weakness of simple polymer networks, Eq. (53) can explain the low fracture resistance of swollen polymer networks on their own, such as the first polyelectrolyte network in Gong's network. Indeed, the network is already highly swollen so it is close to the maximum elongation of its chains. If no other dissipative mechanism occurs, the failure will happen at a low deformation for a fracture test since the amount of energy needed to transmit to the network before reaching Γ_0 is very low and the chains are very dilute.

The Lake and Thomas model will be used in this work and it is necessary to note that it does not take into account any other dissipative mechanism that could happen during the fracture propagation and in particular no viscoelastic dissipation.

Regarding multiple networks, other models have been developed recently to understand the mechanism of DN hydrogels and will be presented in section II)2) in this chapter.

Now that a theoretical background has been presented for polymer chains and also for polymer networks, the next part will focus on the state of the art regarding multiple networks.

II) Double Networks (DN) hydrogels

1) Concept of Double Networks hydrogels: the work of Gong's group

Gels and especially hydrogels are the subject of a large amount of studies motivated by potential uses in biology. Indeed, most of the tissues in animals and plants can be either described as composites of mineral and polymer such as bones, nacres or as composite of polymer and polymer such as tendons or cell walls. In order to reproduce and use synthetic hydrogels to replace tissues such as tendons, a reinforcement mechanism had to be found to obtain as good mechanical properties as human tendons.

In 2003, to follow this perspective of creating artificial tissues for bioengineering, Gong and her group designed and characterized double networks hydrogels for the first time [1, 20]. They synthesised very tough gels made of interpenetrated networks swollen in water (around 90 wt % water). Those networks are synthesised in a two-step free radical polymerization. The synthesis begins with the highly crosslinked polyelectrolyte network with a UV-initiated polymerization. Then this network is swollen to equilibrium with a solution containing a small amount of crosslinker and a neutral monomer. Once the swelling is completed, another step of UV polymerization is performed to obtain a double network consisting of two interpenetrated networks. Finally, the sample is swollen in a bath of water to obtain a double network hydrogel containing 90 wt % water at equilibrium. To obtain interesting mechanical properties, the most important principle of those double networks is that they show an important asymmetry between the two networks; one has to be highly crosslinked and in a minority concentration while the other one is loosely crosslinked and is present in a high concentration.

In this particular example [1], the first network polyelectrolyte is made of a poly(2-acrylamido-2-methylpropanesulfonic acid) (called PAMPS) and the loosely crosslinked network of a poly(acrylamide) (called PAAm). In this seminal paper the group did some compression tests on each of the individual networks separately and on the double network as presented in Figure 4a). This figure illustrates the fact that the PAMPS gel is very brittle, as expected. On the other hand, PAAm is loosely crosslinked so it can be highly deformed but the stress at break is very low. Eventually, the double network displays both a high deformation and very strong hardening leading to a high stress at 90% of compression in comparison to the single networks. In Figure 4b), pictures are taken during this compression tests with the PAMPS on the left being destructed by the tests when the double network on the right shows no visible change after a compression up to 90 % despite the presence of 90 wt % of water.

The networks invented by Gong *et al.* [1] have shown very promising results in terms of enhancement of the mechanical properties. Since then, Gong's group has worked extensively

on those materials to develop their mechanical properties but also towards the understanding of the networks' structure and the mechanism behind this large reinforcement.

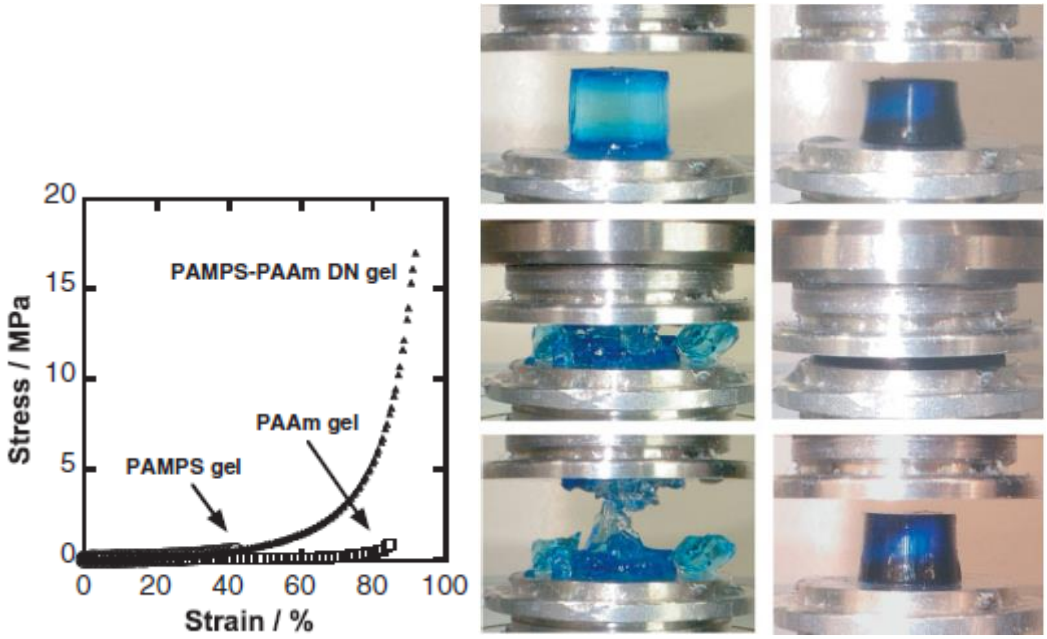

Figure 4: a) Stress-strain curve for hydrogel under uniaxial compression for each of the single networks (PAMPS and PAAm) and the double network made of the two networks (PAMPS-PAAm) b) Pictures: on the left of the compression of the network PAMPS and on the right compression of the double network PAMPS-PAAm[1]

Following the discovery of the principle of double network hydrogels, irreversible damage occurring in the DN hydrogels has been reported in 2007 by our group [21] using materials from Gong's group. Due to the high inhomogeneity of the crosslinking process, the samples presented a hysteresis between the loading cycle and unloading cycle even at a relatively low deformation. The large hysteresis, due to the breakage of some bonds inside the material, can be compared to the Mullins effect observed in elastomers [22]. The Mullins effect is usually defined as the fact that a material has softened after the first deformation to a given extension [23], showing a large hysteresis that can be explained by different dissipation mechanisms such as bond scission, cavitation or crystallisation.

For the material used by Webber et al.[21], it was the first time that the Mullins effect was observed for a polymer gel. This large hysteresis can be an explanation for the high values of toughness noted for DN gels. The reason for the dissipation of energy produced during the first loading is still not clear but it is guessed to be linked with some early bond breaking in the inhomogeneities of the first network.

At the same time, Gong and her research group have pursued their investigation to study the mechanical properties of these types of materials in uniaxial tension [24]. By reducing the amount of crosslinker in the rigid network, they could observe a necking phenomenon that was noticed for the first time in hydrogels as shown in Figure 5. The stress-strain curve starts with a linear increase, as presented in pictures a and b, until a critical stress is reached where the necking starts. This necking phenomenon starts at an elongation of 2.5, as shown in picture c, and then propagates to the un-necked region as described by picture d. Regarding the stress-strain curve, this macroscopic phenomenon is characterized by a plateau where the

strain increases at a constant nominal stress (constant force) until the un-necked region disappears and the uniform elongation of the sample continues. At the same time, they observed a large decrease in Young's modulus after the necking occurs, with a modulus starting at 0.1 MPa and decreasing to a value ten times lower of 0.015 MPa after the necking. This gave a much softer material and showed that irreversible structure changes had occurred in the double network during the propagation of the neck.

This decrease is linked with the breakage of the first network as observed by Webber *et al.* [21]. Due to their high prestretching, the chains of the first network are breaking early during elongation or compression. They act as a sacrificial network dissipating energy by breaking while the second network avoids the entire material to fail [25]. During the necking part, this breakage of the first network was observed by small angle neutron scattering, showing that the network might break into clusters with a periodicity of 1.5 µm [26]. The proposed hypothesis regarding the change of internal structure is that when the plateau stress is reached, large portions of the first network are breaking into pieces. This could create clusters of first network in the second network that might be considered as physical crosslinks of the second network.

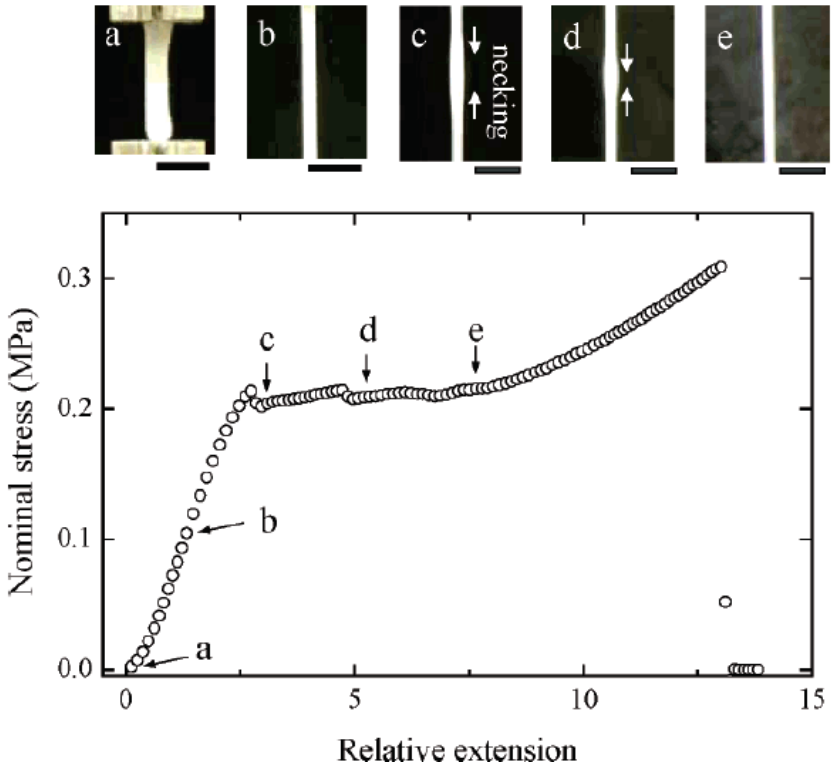

Figure 5: Uniaxial stress-strain curve of a double network hydrogel and pictures describing the macroscopic evolution of the sample and the necking progress[24].

The yielding is not the only peculiar mechanical behaviour shown by those hydrogels; the high fracture energy is also remarkable [27-29]. For their polymer volume fraction, the double network hydrogels described earlier display a fracture energy Γ that ranges from 10^2 to 10^3 J/m^2 when the PAAM alone has a value of $\Gamma \sim 10$ J/m^2 and PAMPS $\Gamma \sim 1$ J/m^2. This gives a fracture energy that is a 100 to 1000 times larger for double networks in comparison to single stiff networks [27]. During the study of this fracture toughness, they have observed with AFM

(atomic force microscopy) that around the crack tip, the modulus decreases sharply, showing the presence of a local damage near the crack tip [28]. This local yielding can be illustrated by Figure 6, showing a clear damage zone around the crack tip. They proposed that it is the presence of a local yielding and followed by a hardening at the crack tip that creates a large zone of influence of the crack that is responsible for the high fracture energy of those materials.

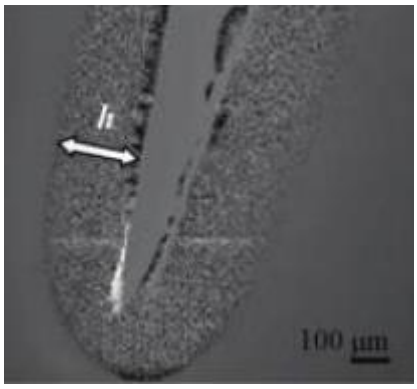

Figure 6: High-low image of the crack tip after tearing, captured using a colour 3D violet laser scanning microscope[29]

The breaking procedure of the double network (DN) gels has been studied in Gong's group [30]. By measuring the anisotropy of the swelling on samples after tensile tests, it has been shown that chains of the first network break preferentially in the tensile direction. This confirms the sacrificial nature of the first network. The exact structure of the network after macroscopic yielding remains however unknown.

After studying gels with PAMPS as first network, Gong and co-workers tried new compositions to expand the possibility of the DN gels concept. They observed that the reinforcement mechanism was not linked to a specific polymer chemistry, so that any kind of first network could be used. The first network could also be neutral or hydrophobic and not only a polyelectrolyte. In order to enhance the mechanical properties however, the prestretching of the first network appears to be necessary. To achieve this goal with neutral polymers in a single step, the idea was to use a polyelectrolyte as a molecular stent [31] that is trapped inside the first network. Therefore, since the molecular stent is a linear polyelectrolyte with a high molecular mass, in a good solvent, it will force the first neutral network to swell leading to the expected prestretching of the first network. The synthesis is schematically described in Figure 7. Two methods are described to obtain DN gels containing a molecular stent. The first option is to synthesize the first network from a solution of monomer containing the molecular stent that will be trapped inside the network. The second option is to disperse the monomer to create the stent in the neutral gel before starting the polymerization. The concentration of the stent is controlled, and leads to the ability to tune the swelling of the DN gels which could not be changed with polyelectrolytes swollen to equilibrium (except if the crosslink density was changed). Finally, in this paper, they showed that the obtained mechanical properties are similar to the standard DN hydrogels with PAMPS, the universality of the concept of double network being therefore demonstrated.

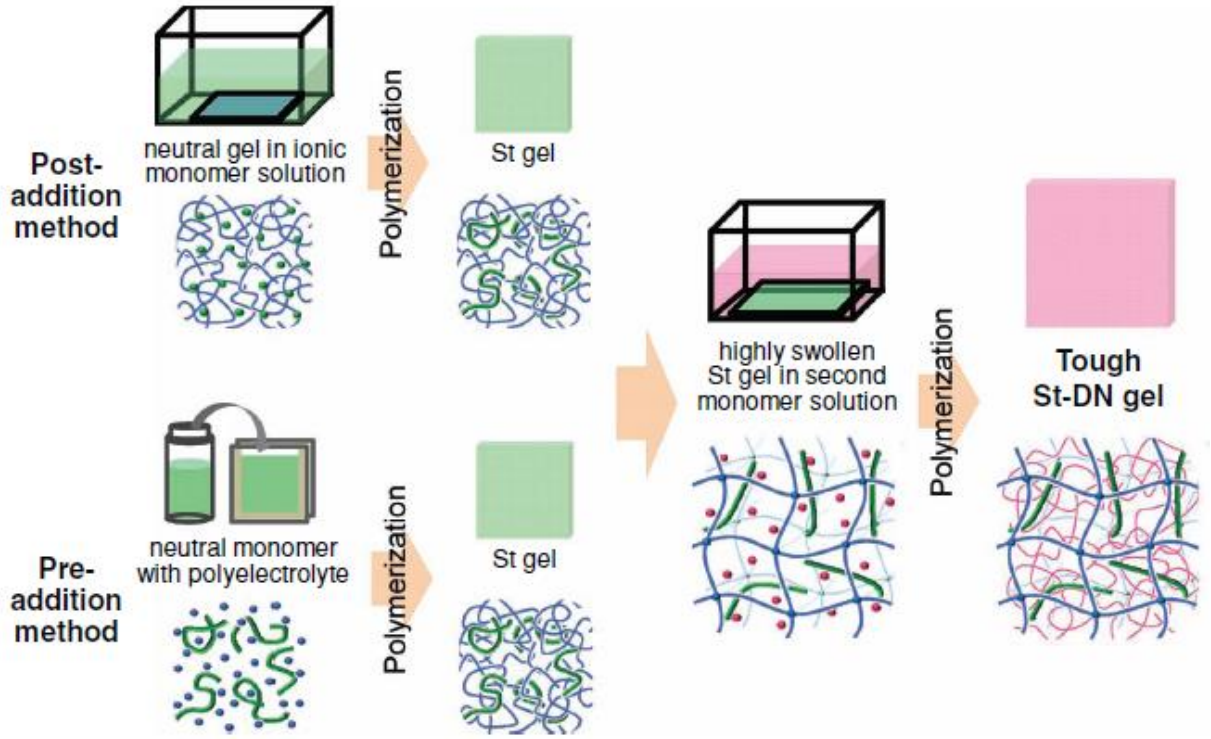

Figure 7: Schematic view of the principle of the synthesis of a DN hydrogel using a first network that is neutral and a molecular stent to force it to swell. Two methods are described, at the top (post-addition) the gel is synthesised and the molecular stent is created inside it, at the bottom (pre-addition) the stent is in solution and the first network is synthesised around it. [31]

After developing the concept of molecular stent they used it to create DN gels using the well-controlled tetra-PEG networks. In recent years, the tetra-PEG networks have been developed and studied [32-34] for their ability to be used as model gels due to their well-defined structure. The synthesis of those gels developed by *Sakai et al.* [34] leads to the creation of a "perfect network" with a well-controlled molecular weight between crosslinks. This control can be achieved by the use of two compatible tetrahedron (star polymer with four branches, giving the used name tetra-PEG) macromonomers of the same size. Ideally, each end of the branches will react with an opposite end of the other macromononer giving birth to a model network. The same procedure was used by Gong's group to create a first network [35, 36] that was then swollen by the molecular stent technique, as described in the schematic view of Figure 8.

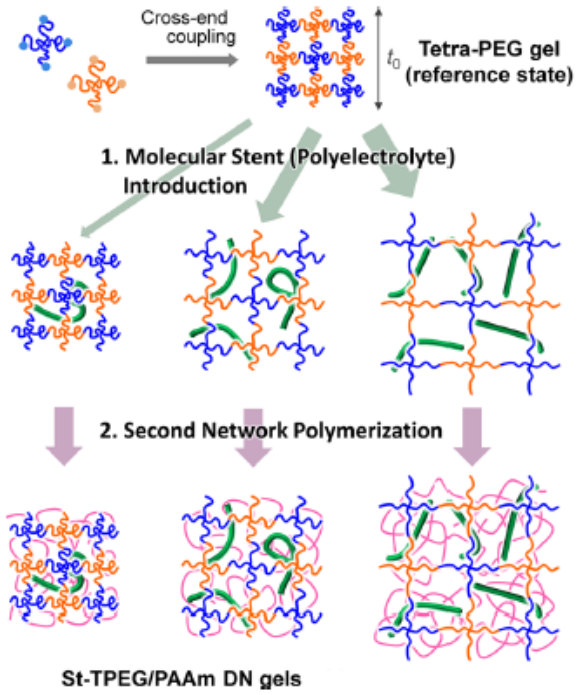

Figure 8: Synthesis procedure of a tetra-PEG DN gels using a molecular stent [35].

The creation of these model first networks was used to study the effect of the swelling on the yielding properties of the DN gels [35]. They observed that the yield stress decreases with the degree of swelling which in-turn increases when the prestretching ratio of the first network increases. Moreover, their experiments showed that the yield stress appears to be closely linked to the first network for two reasons. First, the yield stress increases with the areal density of the first network. Second, they make the assumption that the yield point is also the finite extensibility of the tetra-PEG network. This very recent paper focusing on the yielding phenomenon shows that the understanding of the DN enhancement mechanism is improving.

Gong and her group have created the promising concept of DN hydrogels. They have also developed many different systems stemming from the use of DN gels architecture that have inspired many groups in the world. Among those groups some have tried to come up with a theory regarding the principle of the reinforcement mechanism of the hydrogels. Those theories will be presented in the next part.

2) Double networks reinforcement mechanism

It is clear that DN hydrogels show outstanding properties but the reinforcement mechanism that is involved is not obvious. It is well understood that the good mechanical properties can only be achieved if the first network is highly crosslinked, prestretched and in a small concentration in comparison to the second loosely crosslinked network. Ahmed *et al.* [37] showed that a criteria regarding the ratio between the first and the second network could be found to separate brittle and ductile DN gels. To obtain a ductile network, the first network

will act as a sacrificial network that fractures at low stress while the second network can sustain a large extension and avoid the cracks propagations macroscopically. This allows good properties in tension, compression and fracture energy but the mechanism involved is not clear. Indeed, a hydrogel is normally very weak in terms of modulus but also in terms of elongation: it is a very brittle material that shows bad resistance to crack propagation. These undesirable properties regarding chemically crosslinked polymer networks that are highly swollen can be explained by the Lake and Thomas theory [15] that has been presented in the first section of this chapter. The outstanding properties of DN hydrogels must therefore come from the global architecture involving the two complementary networks. In this part, two models explaining the reinforced mechanical properties of DN gels are presented.

a) Brown's model

Since the appearance of double networks, some people, such has Brown [38], have tried to gather data to understand and propose a reinforcement mechanism. Brown's model [38] is based on the creation of micro-cracks in the DN gels to dissipate energy during deformation. This micro-crack propagation occurs in two steps. First, since the first highly crosslinked network is brittle, a micro-crack will initiate in the network. If there is not enough loose network to avoid this micro-crack propagation, then it will propagate and lead to the failure of the sample. Otherwise, if there is enough loose network to bridge the micro-crack, then the sample remains continuous despite micro-cracks occurring in the first network. The second step of the failure will then be reached with the micro-cracks propagating inside the second network and therefore leading to the macroscopic breakage of the sample.

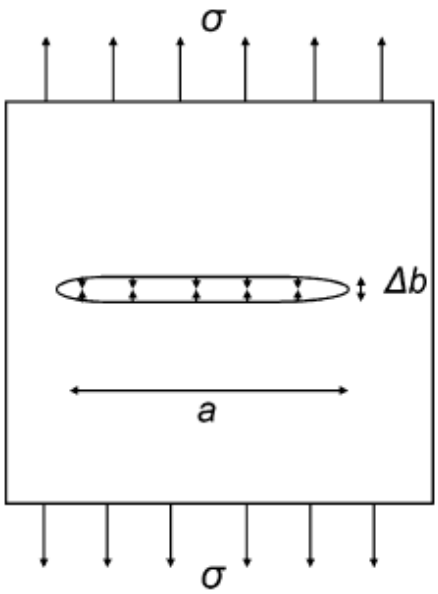

Figure 9: Schematic representation of a micro-crack in a DN gel [38]

The first step of the material failure, the micro-crack creation in the first network and the second network holding its propagation can be described schematically by Figure 9. In Figure 9, a is the length of the crack, σ is the external stress and Δb is the size of the crack held by

the second network. The maximum opening of the crack, Δb, is likely to be close to the contour length of the second network. From this, a strain energy release rate can be estimated as the energy per unit area required to close the crack as shown in Eq (54). For a contour length of 3 µm, which would be the case for a 10000 repeat unit chain, and a first network fracture toughness of G_c = 0.5 J/m², it gives a stress to create micro-cracks of 0.3 MPa. This value is of the order of the necking stress observed in Figure 5.

$$G_c = \frac{\Delta b\, \sigma}{2} \qquad \textbf{Eq. (54)}$$

Once this critical stress is reached, multiple micro-cracks are created in the first network located around inhomogeneities that are initiating them. To reach the failure of the whole sample, a zone of highly damaged first network will grow around the micro-crack. In this zone due to the high amount of damages, the elastic properties will be similar to those of the second network. As shown in Figure 10, the modulus E_1 in the undamaged zone is mainly controlled by the first network due to the stretch of the chains, but in the damaged area, the first network is partially broken leading to a sharply lower modulus E_2. From those assumptions Brown extracts a prediction of the global toughness of the DN gels (Eq. (55)). In Eq. (55), Γ_1 and Γ_2 are the toughness of each network taken individually, and λ_m is the maximal macroscopic elongation of the second network. This equation proposes a prediction of the toughness of the DN gels, in agreement with the results obtained by *Gong et al.* [24]. In this very insightful paper, Brown also gives a prediction of the reinforcement provided by the double network structure, which is around 40 times greater relative to the second network.

$$\Gamma_{global} = \frac{4 * \Gamma_1\, \Gamma_2}{(\lambda_m - 1) E_2\, \Delta b} \qquad \textbf{Eq. (55)}$$

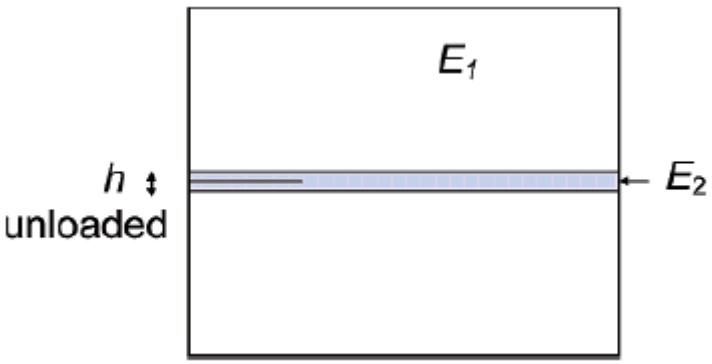

Figure 10: Elastic modulus around a micro-crack in a DN gel[38]

Brown's model provides a molecular picture to describe DN gels. It also creates the concept of micro-cracks occurring in the first network that are bridged by the second one to avoid the failure of the sample and create the reinforcement mechanism. The same year, Tanaka proposed a different but analogous model [39].

b) Tanaka's model

Tanaka's model [39] is based on the fact that DN gels are presenting a yielding phenomenon, macroscopically characterized by a necking in tension. It has been assumed that this necking is due to the breakage in fragments of the first network inside the second network, holding the sample together. Based on these observations, his hypothesis regarding the fracture toughness reinforcement is that a yielded area is created ahead of the crack tip. The formation of this yielded area dissipates a lot of energy leading to the enhancement of the overall fracture toughness of the DN gel. At the crack tip, yielding occurs when a critical stress σ_c is reached corresponding to the stress obtained when necking occurs in uniaxial tension. This results in the creation of a damaged zone ahead of the crack tip where this level of stress is effective, creating a soft and very elastic zone over a length *h* with a broken first network as described in Figure 11a), with a sharp transition between damaged and undamaged zones. This damage zone is characterized by the breakage of an important part of the first network that will be divided in clusters; those clusters will then act as crosslinkers for the loosely crosslinked network. This hypothesis can explain the enhancement of the toughness due to the dissipated energy observed when the first network breaks. The size of the damaged zone is then defined by Eq. (56) where Γ_0 is the fracture toughness of the soft zone and $U(\sigma_c)$ the elastic energy density (J/m3) for the uniform stretching to σ_c of a soft (crack tip type) unnotched sample. This sample's mechanical properties can be described by Figure 11b): the curve described by the points *OAC* is the first loading of the sample, creating a soft zone when reaching the point A and the critical stress σ_c. The material is then damaged and its stress-train curve now corresponds to the curve of points *OBC*. The area defined by points *OACB* is the irreversible work that has to be provided to the network to obtain the yielding. It can be approximated by the rectangle $\sigma_c * \varepsilon_c$. If we consider the fracture and the crack tip defined earlier, this rectangle has to be multiplied by the size of the damaged zone *h* to obtain the irreversible work of fracture. To propagate a crack, this irreversible work has to be provided to the material in addition to the energy needed to break the soft zone Γ_0, leading to Eq. (57) giving the fracture energy Γ.

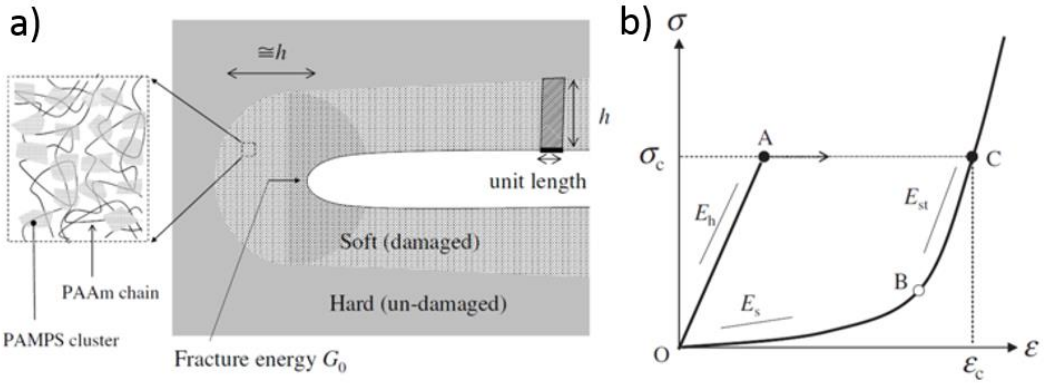

Figure 11: a) Description of the crack tip in a DN gel according to Tanaka's model. b) Prediction of the stress-strain curve according to the model.[39]

$$h = \frac{\Gamma_0}{U(\sigma_c)} \quad \text{Eq. (56)}$$

$$\Gamma = \Gamma_0 + \sigma_c \varepsilon_c h = \Gamma_0 * \frac{1 + \sigma_c \varepsilon_c}{U(\sigma_c)} \quad \text{Eq. (57)}$$

Eq. (57) is thus a correction of Γ_0 by an amplification factor. This equation is also in good agreement with the values obtained for DN gels, when taking the fracture energy of a single loosely network as an approximation of Γ_0. It does not however contain any molecular assumptions on what controls the parameters σ_c and ε_c.

Those two models are two different approaches to explain the enhanced fracture properties of DN gels. They both make the assumption that the soft area behaves like the second network on its own. On the other hand, the difference comes from the estimation of the energy needed to propagate the crack in the damaged network as is pointed out by Long and Hui [40]. In this paper, the two models described previously are compared and the differences are pointed out before an alternative calculation method of the energy needed to propagate a crack in the damaged network is proposed.

After describing the DN gels developed and studied by Gong's group, and the model that have been developed to describe their mechanical properties, we will focus on the recent developments in the field of DN gels in other groups around the world developing their own approach toward DN gels.

3) Development of different tough gels

One of the key aspects of DN hydrogels is that the reinforcement is based on the molecular architecture of the connected polymer chains, and not on the monomer chemistry of the different networks. Indeed, the reinforcement mechanism based on the difference of properties of each network can be applied to a wide range of polymer chemistries and does not involve the chemical nature of the monomers used in the different networks (except that the first network needs to be swollen for hydrogels). Based on Gong's DN hydrogels, the system needs a first network that can be stretched by the swelling of the solvent and a second network that can be mixed with the first one. Starting from this postulate, many different approaches have been developed [41, 42]. Some of them have pushed the concept further to create triple or even quadruple networks [43, 44] made of non-ionic polymers and sequential polymerizations. In this case the molecular stent technique was not used; the prestretching was only achieved by the multiple polymerisation steps.

In this part, we will describe some different promising techniques to obtain DN gels based on the architecture of DN hydrogels but also new properties discovered regarding those systems.

Partly recoverable tough hydrogels based on combination of physical and chemical crosslinking.

DN hydrogels dissipate energy due to the progressive breakage of the first network with increasing applied macroscopic strain. That approach requires the prestretching of the first network since all bonds have the same breakage force and some bonds should break first.

Another strategy that does not require prestretching is to work with weak and strong bonds or with intrinsically stiff and flexible networks with ionic [45-47], hydrophobic [48] or supramolecular interactions [49]. These are fundamentally different strategies that do not rely on out-of-equilibrium structures (such as those of DN gels) and are more appropriately called dual crosslinking gels.

The best example of a combination of a stiff and soft multiple network has been developed in Suo's group [46, 50], where they are using alginate gels as stiff network. Alginate gels are natural polymers that can be crosslinked with calcium ions Ca^{2+}, the crosslink points are made of several bonds occurring between calcium ions and the polymer chains as shown in Figure 12a). The extensible network (Figure 12b)) is a polyacrylamide gel with N,N-methylenebisacrylamide as crosslinker. Figure 12c) describes the DN gels formed by the two networks, the blue triangles are representing the eventual crosslinks that can occur between the amine groups of the polyacrylamide and the carboxyl groups of the alginate. This obtained DN gel is using water as solvent with a mass fraction of 86 %.

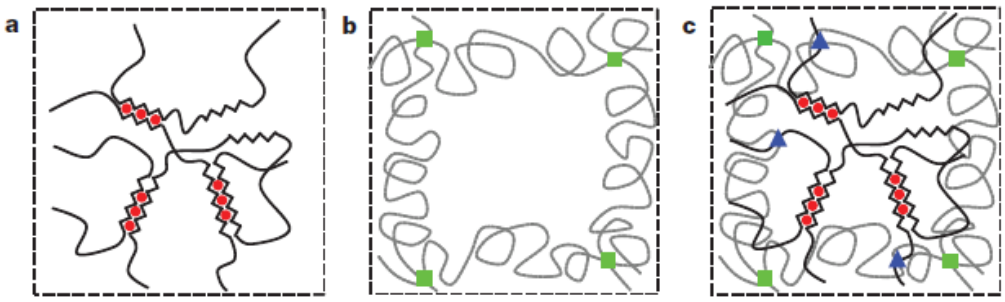

Figure 12: a) Alginate network with calcium ions represented as red circles. b) Second network chemically crosslinked (green square). c) DN gels combining both gels covalently linked (blue triangles)[46]

The networks formed by this process are showing very interesting mechanical properties. First, they can recover part of their initial mechanical behaviour within a few hours at high temperature to improve the diffusion of calcium ions (Figure 13a)). Secondly, the gel is showing remarkable extensibility up to λ = 21 in uniaxial tension, which represents a large improvement in comparison to a single alginate network ($\lambda \approx 1.2$ maximum elongation) and the polyacrylamide ($\lambda \approx 7$ maximum elongation). This increase in elongation is also accompanied by an increase of the Young's modulus and a large improvement of the stress at break that is multiplied tenfold. Finally, the fracture toughness is also largely improved by a factor of 100 reaching the value of 8700 J/m². This large improvement is attributed to the alginate network that can dissipate a lot of energy before the failure of the sample. Suo and his group suggest that while the second network avoids the crack propagation, it also allows

the alginate to unzip progressively, first around the crack tip but also in an extended damaged zone which dissipates energy and leads to this high value of fracture toughness.

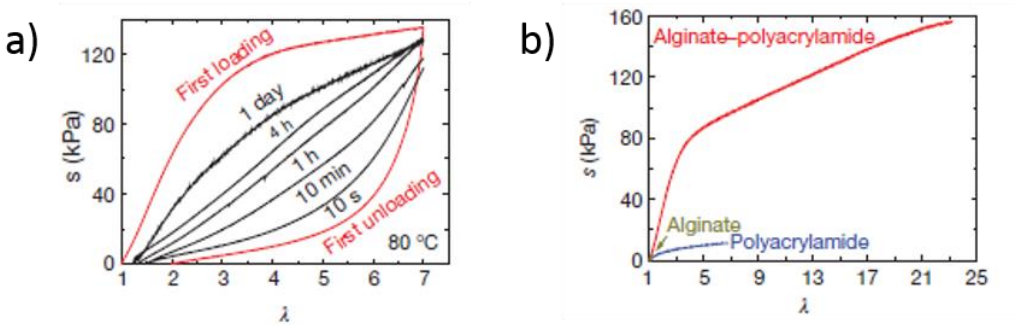

Figure 13: a) Cyclic uniaxial experiment showing the recovery of samples with different resting times. b) Uniaxial stress-train curve of the three types of gels[46].

Another approach is based on bonds with different dynamics. In this case, there is a single network but two types of bonds. An example of such dual crosslink gel has been developed in our group with the work of Mayumi *et al.* [47, 51]. The Dual crosslink hydrogels are here composed of a sparsely chemically crosslinked network which is also crosslinked physically with borate ions. The use of borate ions introduces transient crosslinks that are able to break and reform and that can therefore dissipate energy and influence on the fracture properties.

In Gong's group, some work has also been done on self-healing tough hydrogels [52, 53]. In those two papers they use either polyampholytes or polyion complexes. Polyampholytes are made of randomly dispersed cationic and anionic repeat units that will form electrostatic interactions. Macroscopically, the materials behave as if they had weak and strong bonds, but the molecular origin of the two populations of bonds is unclear. In any case, the existence of these two dynamics of bonds leads to tough gels that have significant viscoelasticity [52, 53]. The principle for polyions is similar; this time two polyelectrolytes are polymerized together, one charged positively and the other one negatively. Upon the removal of the counter ions, the two polyelectrolytes bond together to give birth to a wide distribution of crosslinks strength [52, 53]. The weak ones will act as sacrificial and the strong ones as permanent crosslinkers just as with the polyampholytes system. This type of bonds relies on electrostatic interactions and is therefore very dependent on ionic strength in the water phase. It is strongest in pure water and can fully dissolve in the presence of a high salt concentration.

This notion of sacrificial networks to dissipate energy as shown in this section is crucial to the concept of tough gels. The study of this dissipation mechanism can be done by analysing the hysteresis shown in tensile curve and is the object of the following part.

Towards biocompatible DN hydrogels

The first idea of Gong's group when they worked on DN hydrogels was to obtain tough hydrogels with mechanical properties comparable to human cartilage or tendons [1]. It may be nature that inspired the work on double networks, coming from the report that super

tough gels could be created by composites made of polymers only. Since the discovery of the DN architecture, the idea is to find a way to transpose the system to a biocompatible gel since the original networks cannot be applied as a clinical implant yet [54-56].

An idea to overcome the problem of biocompatibility is to use a polyzwitterion as first network. Polyzwitterions are polymers which present both anionic and cationic groups and have excellent anti-biofouling properties that make them interesting in the biomedical field. Gong's group successfully reproduced the DN architecture with those materials that can present good mechanical properties but also anti-biofouling properties [57]. Those materials are promising for the field of biomaterials. Also, the concept of the molecular stent has been used to make biocompatible materials [58]. In this paper they use a biopolymer as molecular stent. This technique was successful in making tough hydrogels that could be used for biomedical applications.

More recently, Nonoyama *et al.* have overcome the challenge of bonding hydrogels to defected bone [59]. The technique used to create osteointegration was to introduce calcium-phosphate-hydroxide salt hydroxyapatite nanospheres inside the DN gels. This procedure induces a spontaneous osteogenesis inside the gel with a hybrid layer of 40 µm formed at the interface.

Finally, a lot of people have tried to use bio-polymers such as polysaccharides to make interpenetrated networks toward their use in the biomedical field upon drug delivery or tissue engineering [60].

In this part, a lot of developments have been shown regarding the use of the DN concept to create new systems that all show interesting reinforced mechanical properties. Another field in physical-chemistry that uses polymer networks is the field of elastomers. Interpenetrated networks have also been used in this domain and it will be the subject of the next part.

III) Multiple networks in the field of elastomers

1) Bimodal polymer networks and interpenetrated polymer networks

Before the small revolution in the field of polymer networks caused by the arrival of the DN hydrogels, several groups tried to use different architecture strategies to enhance the mechanical properties of their systems. Starting from the observation that the ideal elastomer would present the high modulus of a highly crosslinked network and the important elongation of a loosely crosslinked one, two strategies have been tried: interpenetrated polymer networks (IPN) and bimodal networks.

Bimodal networks are composed of two types of chain length between crosslinks: short and long chains that are present inside a single polymer network as shown in the representation of Figure 14. Mark *et al.* [61] have worked on this system and detailed their mechanical properties.

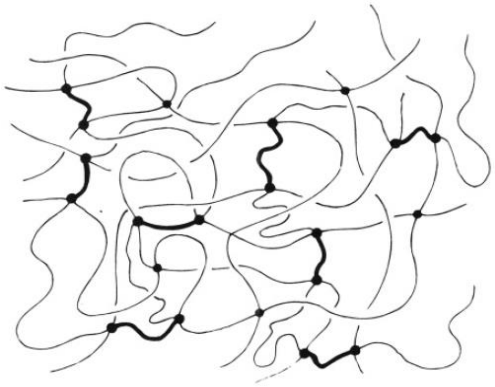

Figure 14: Schematic representation of a bimodal polymer network presenting long chains and short chains (thicker lines) [61].

The desired reinforcement strategy assumes that short chains reach their finite extensibility and create a stiffening before the long chains do. This will only work however if the short and long chains are somewhat bicontinuous which is rarely the case thermodynamically. In practice this lack of control of the structure has led to some improvements in stiffness (modulus) but the fracture toughness of such materials showed no significant improvement in comparison with the unimodal networks [62-64].

The other strategy to obtain reinforced mechanical properties is to use interpenetrated networks. This system is defined as a mix of two polymer networks or more, where at least one is polymerized in the presence of the other(s) [65], and the DN gels are part of this family. The strategy has been successfully used in different fields such as photodiodes [66] and solar cells [67]. Recently the use of supramolecular associations in IPN has led to high improvement of the tensile toughness [68]. In this case, the dramatic toughness enhancement was shown to be strain-rate dependent. This time dependence is due to dissociation/reassociation of the supramolecular associations.

The study of existing work on IPN in the elastomeric field and the discovery of the DN gels by Gong *et al.* [1] has led to the idea of translating the concept towards elastomer networks. This has been successfully done in our laboratory by Etienne Ducrot, his thesis work will be the subject of the following part.

2) Etienne Ducrot's PhD work

The properties of DN swollen hydrogels are very interesting but the question arises whether the same mechanism active in hydrogels would work for elastomers (without solvent). In the field of elastomers, the improvement of the mechanical properties is often achieved by the addition of nanofillers such as silica or carbon black. These nanofillers have been incorporated in elastomers to allow their use in the aeronautic and automobile fields, especially in tires. The fillers in elastomers have the ability to significantly increase the modulus, an expected effect because a hard particle is added to a soft matrix, but also to increase the elongation at

break [69]. Those two opposing properties can be obtained simultaneously by the addition of fillers, leading to the ability to use elastomers in different industrial applications.

The problem is that the use of fillers also changes the properties of the overall polymer matrix. It increases its density, changes significantly the viscosity for the processing part, and most noticeably the transparency is removed (at least for carbon black). The transparency can be useful and even necessary for some applications such as optical ones.

Knowing the reinforcement technique used for DN hydrogels, the project of Etienne Ducrot started in 2010 [25, 70-72]. The goal was to create reinforced elastomers with the same double network technique but without solvent.

To try to transfer the concept of DN hydrogels, the use of acrylate networks was chosen. These networks were used because the chemistry is simple, and they show a good resistance to UV and temperature. Also, acrylate networks are a good model system, simple acrylate networks show very poor mechanical properties to start with, and the reinforcement of those networks would thus be very noticeable. The principle of DN gels was partly based on the ability of the polyelectrolyte first network to swell very significantly in water due to the osmotic pressure of the counter-ions. A hydrophobic polymer cannot swell as much even in its own monomer. This time the stretching of the first network can only be obtained by the use of the second network. After the synthesis of a first network (SN), a bath of monomer was used to swell the first network before polymerization to obtain a double network (DN) (the details of this synthesis will be shown in chapter 2). This step can be repeated another time resulting in a triple network (TN). The reinforcement was then tested in uniaxial tension (technique developed in chapter 3) with a comparison to both networks on their own as it was done for DN hydrogels (Figure 15). The results of Ducrot et al. show an important reinforcement for double and triple networks in comparison to the two networks on their own. As expected, the well crosslinked first network is brittle with a macroscopic failure at 60 % of deformation while the nearly uncrosslinked second network alone is very soft and breaks around 600 % of deformation. The multiple networks show some hardening resulting in a higher stress at break and a better elongation than the first network, the triple network also shows some softening at high stress, suggesting that some damages occur inside the first network.

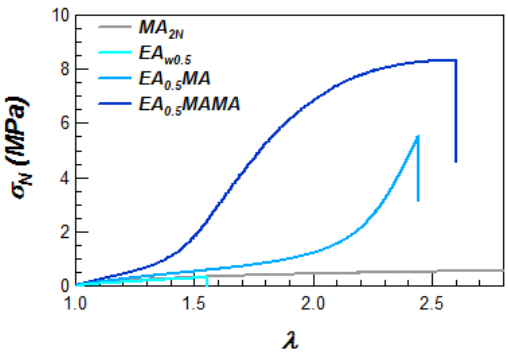

Figure 15: Stress-strain curves for different networks showing the concept of multiple networks elastomers. In grey the second network alone, the lightest blue is the first network alone, the two remaining curves are a double network and a triple network.

To investigate the damages occurring in the first network, Etienne Ducrot had the opportunity to collaborate with the group of Sijbesma to use the mechanoluminescence technique developed by their group [73, 74]. The principle is to use a molecule containing a dioxetane function, this four atom cycle has the ability to emit a photon when it breaks as shown in Figure 16.

Figure 16: schematic representation of the breakage of the dioxetane crosslinker resulting in a photon emission [25].

This dioxetane function can be introduced as a crosslinker in the first network of acrylates. Due to the fact that the energy to break a dioxetane cycle is less important than the energy needed to break a C-C bond but not greatly so, the mechanoluminescent molecule can be a good marker and have a probability of breakage similar to that of the C-C bond and be a good reporter molecule. This property will be then used to map the damages occurring inside the first network in the different multiple network elastomers, in uniaxial tension and also during the opening and propagation of a crack in a notched sample [25]. In Figure 17, it can be seen that the damaged area at the crack tip changes depending on the material, the SN showing a very small zone of light emission meaning that the dissipation occurs only at the very crack tip. On the other hand, the addition of the second network and the prestretching of the first network increases the affected area around the crack with a larger affected zone for DN than SN and an even larger one for the TN. The large area where damages can be observed confirms the improved fracture toughness observed for multiple networks elastomers. It also shows that the first network is able to dissipate some energy far from the crack tip, even hundreds of microns away some bonds are breaking inside the first network especially for the TN network. This mapping technique allowed Ducrot to confirm the presence of a damaged zone ahead of the crack tip as expected by Brown's and Tanaka's models. This mechanoluminescence molecule appears to be a great tool to use for the mapping of damages towards the improvement of material design, the group of Sijbesma has continued to use it in different applications [73, 75] among them the use of the dioxetane molecule has allowed to prove the contribution of bond scission in the Mullins effect of filled silicone elastomers.

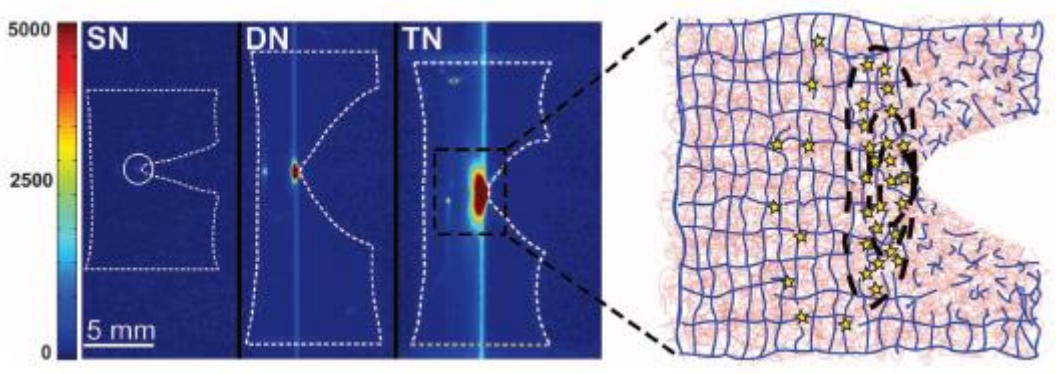

Figure 17: Intensity of the photon emission due to the breakage of the first network inside different multiple networks elastomers. (right) schematic representation of the bond breaking inside the first network (blue) while the second network is only deformed (red)[25]

In this part we have seen that the concept of DN hydrogels has been successfully transposed towards elastomers by Ducrot *et al.*. However, their structure and the details of their toughening mechanism is not yet fully and quantitatively understood, and this will be the subject of this manuscript.

Conclusion

In this chapter, the concept of DN hydrogels invented by Gong's group has been briefly exposed. A DN hydrogel needs two miscible networks; one of them is stretched, highly crosslinked and in minority while the other one is loosely crosslinked and in majority. This concept first published in 2003 has been developed by the same group and has inspired other groups around the world to propose variations and to increase the applicability of DN gels by changing the monomers but keeping the general concept of two interpenetrated networks with a sacrificial one dissipating energy and another one holding the macroscopic structure.

Another confirmation of the universality of this architecture has been added by Ducrot *et al.* [25].The PhD of Etienne Ducrot has led to the creation of new multiple network elastomers by proving that the concept of DN gels could be transposed to the field of elastomers. He was able to show the reinforcement of the mechanical properties that could be obtained for double and triple network elastomers. Also the use of mechanoluminescence has allowed him to map the damages occurring inside the samples and especially around the crack tip. This has helped prove the sacrificial nature of the first network. Still some questions remain on the details of the reinforcement mechanism: why are the double and triple networks so different? Can the concept be applied to any kind of elastomer? What is the molecular mechanism controlling the failure point?

To answer some of those questions a new PhD was undertaken, and will be the purpose of this manuscript.

References

1. Gong, J.P., et al., *Double-network hydrogels with extremely high mechanical strength.* Advanced Materials, 2003. **15**(14): p. 1155-1158.
2. Flory, P.J., *Principles of Polymer Chemistry.* Cornell University Press, 1953. **Book**.
3. Doi, M. and S.F. Edwards, *The theory of polymer dynamics*. 1986, Oxford: Oxford University Press. 391.
4. Rubinstein, M. and R.H. Colby, *Polymer Physics*. 1st ed. 2003, Oxford: Oxford University Press.
5. Kuhn, W., *Über die Gestalt fadenförmiger Moleküle in Lösungen.* Kolloid-Z, , 1934. **68**: p. 2-15.
6. Kuhn, W., *Beziehungen zwischen Molekülgröße, statistischer Molekülgestalt und elastischen Eigenschaften hochpolymerer Stoffe.* Kolloid-Z, 1936. **76**: p. 258-271.
7. Kuhn, W. and F. Grün, *Beziehungen zwischen elastischen Konstanten und Dehnungsdoppelbrechung hochelastischer Stoffe.* Kolloid-Z, 1942. **101**: p. 248-271.
8. Rivlin, R.S., *Large Elastic Deformations of Isotropic Materials .4. Further Developments of the General Theory.* Philosophical Transactions of the Royal Society of London Series a-Mathematical and Physical Sciences, 1948. **241**(835): p. 379-397.
9. Mooney, M., *A Theory of Large Elastic Deformation.* 1940.
10. Rubinstein, M. and S. Panyukov, *Elasticity of polymer networks.* Macromolecules, 2002. **35**: p. 6670-6886.
11. Rubinstein, M. and S. Panyukov, *Nonaffine deformation and elasticity of polymer networks.* Macromolecules, 1997. **30**: p. 8036-8044.
12. Gent, A.N., *A New constitutive relation for rubber.* Rubber Chemistry and Technology, 1996. **69**: p. 59-61.
13. Flory, P.J. and J. Rehner, *Statistical mechanics of cross-linked polymer networks II Swelling.* Journal of Chemical Physics, 1943. **11**(11): p. 521-526.
14. Guth, H.M.J. and Eugene, *Theory of the Increase in Rigidity of Rubber during Cure.* The Journal of Chemical Physics, 1947.
15. Lake, G.J. and A.G. Thomas, *The strength of highly elastic materials.* Proceedings of the Royal Society of London, series A: Mathematical and Physical Sciences, 1967. **A300**: p. 108-119.
16. Gent, A.N. and R.H. Tobias, *Threshold tear strength of elastomers.* Journal of Polymer Science: Polymer Physics Edition, 1982. **20**(11): p. 2051-2058.
17. Creton, C. and M. Ciccotti, *Fracture and Adhesion of Soft Materials.* Reports On Progress In Physics, 2016. **79**(4): p. 046601.
18. Bhowmick, A.K., A.N. Gent, and C.T.R. Pulford, *Tear Strength of elastomers under threshold conditions.* Rubber Chemistry and Technology, 1983. **56**: p. 226-232.
19. Akagi, Y., et al., *Fracture energy of polymer gels with controlled network structures.* The Journal of Chemical Physics, 2013. **139**(14): p. 144905.
20. Na, Y.H., et al., *Structural characteristics of double network gels with extremely high mechanical strength.* Macromolecules, 2004. **37**(14): p. 5370-5374.
21. Webber, R.E., et al., *Large Strain Hysteresis and Mullins effect of tough Double-Network Hydrogels.* Macromolecules, 2007. **40**(8): p. 2919-2927.
22. Mullins, L., *Softening of Rubber by Deformation.* Rubber Chemistry and Technology, 1969. **42**(1): p. 339-362.

23. Diani, J., B. Fayolle, and P. Gilormini, *A review on the Mullins effect.* European Polymer Journal, 2009. **45**(3): p. 601-612.
24. Na, Y.H., et al., *Necking phenomenon of double-network gels.* Macromolecules, 2006. **39**(14): p. 4641-4645.
25. Ducrot, E., et al., *Toughening Elastomers with Sacrificial Bonds and Watching them Break.* Science, 2014. **344**(6180): p. 186-189.
26. Tominaga, T., et al., *The molecular origin of enhanced toughness in double-network hydrogels: A neutron scattering study.* Polymer, 2007. **48**(26): p. 7449-7454.
27. Tanaka, Y., et al., *Determination of fracture energy of high strength double network hydrogels.* Journal of Physical Chemistry B, 2005. **109**(23): p. 11559-11562.
28. Tanaka, Y., et al., *Localized Yielding Around Crack Tips of Double-Network Gels.* Macromolecular Rapid Communications, 2008. **29**(18): p. 1514-1520.
29. Yu, Q.M., et al., *Direct Observation of Damage Zone around Crack Tips in Double-Network Gels.* Macromolecules, 2009. **42**(12): p. 3852-3855.
30. Nakajima, T., et al., *Characterization of internal fracture process of double network hydrogels under uniaxial elongation.* Soft Matter, 2013. **9**(6): p. 1955-1966.
31. Nakajima, T., et al., *A Universal Molecular Stent Method to Toughen any Hydrogels Based on Double Network Concept.* Advanced Functional Materials, 2012. **22**(21): p. 4426-4432.
32. Matsunaga, T., et al., *SANS Studies on Tetra-PEG Gel under Uniaxial Deformation.* Macromolecules, 2011. **44**(5): p. 1203-1210.
33. Matsunaga, T., et al., *Structure Characterization of Tetra-PEG Gel by Small-Angle Neutron Scattering.* Macromolecules, 2009. **42**(4): p. 1344-1351.
34. Sakai, T., et al., *Design and Fabrication of a High-Strength Hydrogel with Ideally Homogeneous Network Structure from Tetrahedron-like Macromonomers.* Macromolecules, 2008. **41**(14): p. 5379-5384.
35. Takahiro, M., et al., *Yielding Criteria of Double Network Hydrogels.* Macromolecules, 2016. **49**: p. 1865-1872.
36. Nakajima, T., et al., *Synthesis and Fracture Process Analysis of Double Network Hydrogels with a Well-Defined First Network.* ACS Macro Letters, 2013. **2**(6): p. 518-521.
37. Ahmed, S., et al., *Brittle–ductile transition of double network hydrogels: Mechanical balance of two networks as the key factor.* Polymer, 2014. **55**(3): p. 914-923.
38. Brown, H.R., *A model of the fracture of double network gels.* Macromolecules, 2007. **40**(10): p. 3815-3818.
39. Tanaka, Y., *A local damage model for anomalous high toughness of double-network gels.* Europhysics Letters, 2007. **78**(5): p. 56005.
40. Long, R. and C.Y. Hui, *Fracture toughness of hydrogels: measurement and interpretation.* Soft Matter, 2016. **12**: p. 8069-8086.
41. Peak, C., J. Wilker, and G. Schmidt, *A review on tough and sticky hydrogels.* Colloid and Polymer Science, 2013. **291**(9): p. 2031-2047.
42. Myung, D., et al., *Progress in the development of interpenetrating polymer network hydrogels.* Polymers for Advanced Technologies, 2008. **19**(6): p. 647-657.
43. Argun, A., et al., *Nonionic Double and Triple Network Hydrogels of High Mechanical Strength.* Macromolecules, 2014. **47**(18): p. 6430-6440.
44. S., S.E.h. and W. R. A., *Fabrication of Tough Hydrogels from Chemically Cross-Linked Multiple Neutral Networks.* Macromolecules, 2016. **49**: p. 8980-8987.

45. Henderson, K.J., et al., *Ionically Cross-Linked Triblock Copolymer Hydrogels with High Strength.* Macromolecules, 2010. **43**(14): p. 6193-6201.
46. Sun, J.-Y., et al., *Highly stretchable and tough hydrogels.* Nature, 2012. **489**(7414): p. 133-136.
47. Mayumi, K., et al., *Fracture of dual crosslink gels with permanent and transient crosslinks.* Extreme Mechanics Letters, 2016. **6**: p. 52-59.
48. Tuncaboylu, D.C., et al., *Tough and Self-Healing Hydrogels Formed via Hydrophobic Interactions.* Macromolecules, 2011. **44**(12): p. 4997-5005.
49. Huang, T., et al., *A novel hydrogel with high mechanical strength: A macromolecular microsphere composite hydrogel.* Advanced Materials, 2007. **19**(12): p. 1622-+.
50. Can Hui, Y., et al., *Strengthening Alginate/Polyacrylamide Hydrogels Using Various Multivalent Cations.* Acs Applied Materials & Interfaces, 2013. **5**: p. 10418-10422.
51. Mayumi, K., et al., *Stress–Strain Relationship of Highly Stretchable Dual Cross-Link Gels: Separability of Strain and Time Effect.* ACS Macro Letters, 2013. **2**(12): p. 1065-1068.
52. Luo, F., et al., *Oppositely Charged Polyelectrolytes Form Tough, Self‐Healing, and Rebuildable Hydrogels.* Advanced Materials, 2015. **27**(17): p. 2722-2727.
53. Gong, T.L.S., et al., *Physical hydrogels composed of polyampholytes demonstrate high toughness and viscoelasticity.* Nature Materials, 2013. **12**: p. 932-937.
54. Tanabe, Y., et al., *Biological responses of novel high-toughness double network hydrogels in muscle and the subcutaneous tissues* Materials in Medicine, 2007. **19**(3): p. 1379-1387.
55. Yasuda, K., et al., *Biomechanical properties of high-toughness double network hydrogels.* Biomaterials, 2005. **26**(21): p. 4468-4475.
56. Azuma, C., et al., *Biodegradation of high‐toughness double network hydrogels as potential materials for artificial cartilage.* Journal of Biomedical Materials Research Part A, 2006. **81A**(2): p. 373-380.
57. Haiyan, Y., et al., *Double network hydrogels from polyzwitterions: high mechanical strength and excellent anti-biofouling properties.* Journal of Materials Chemistry B, 2013. **1**: p. 3685-3693.
58. Zhao, Y., et al., *Proteoglycans and Glycosaminoglycans Improve Toughness of Biocompatible Double Network Hydrogels.* Advanced Materials, 2014. **26**(3): p. 436-442.
59. Nonoyama, T., et al., *Double-Network Hydrogels Strongly Bondable to Bones by Spontaneous Osteogenesis Penetration.* Advanced Materials, 2016. **28**: p. 6740-6745.
60. Matricardi, P., et al., *Interpenetrating Polymer Networks polysaccharide hydrogels for drug delivery and tissue engineering ☆.* Advanced Drug Delivery Reviews, 2013. **65**(9): p. 1172‐1187.
61. Mark, J.E., *Elastomeric Networks with Bimodal Chain-Length Distributions.* Accounts of Chemical Research, 1994. **27**(9): p. 271-278.
62. Genesky, G.D. and C. Cohen, *Toughness and fracture energy of PDMS bimodal and trimodal networks with widely separated precursor molar masses.* Polymer, 2010. **51**(18): p. 4152-4159.
63. Genesky, G.D., et al., *Experiments and Simulations: Enhanced Mechanical Properties of End-Linked Bimodal Elastomers.* Macromolecules, 2008. **41**(21): p. 8231-8241.
64. Cristiano, A., et al., *Fracture of Model Polyurethane Elastomeric Networks.* Journal of Polymer Science Part B-Polymer Physics, 2011. **49**(5): p. 355-367.

65. Sperling, L.H., et al., *The current status of interpenetrating polymer networks.* Polymers for Advanced Technologies, 1996. **7**(4): p. 197-208.
66. J. J. M., H., et al., *Efficient photodiodes from interpenetrating polymer networks.* Nature, 1995. **376**(6540): p. 498-500.
67. Ma, W., et al., *Thermally Stable, Efficient Polymer Solar Cells with Nanoscale Control of the Interpenetrating Network Morphology.* Advanced Functional Materials, 2005. **15**(10): p. 1617-1622.
68. Seyedali, M. and K. LaShanda, *Exploring the Role of Supramolecular Associations in Mechanical Toughening of Interpenetrating Polymer Networks.* Macromolecules, 2015. **48**: p. 7146-7155.
69. Mark, J.E., B. Erman, and F.R. Eirich, *Science and technology of RUBBER (3rd edition).* Elsevier Inc., 2005.
70. Ducrot, E., *Double Network Elastomers*. 2013, Université Pierre et Marie Curie: Paris.
71. Ducrot, E. and C. Creton, *Characterizing Large Strain Elasticity of Brittle Elastomeric Networks by Embedding Them in a Soft Extensible Matrix.* Advanced Functional Materials, 2016. **26**(15): p. 2482-2492.
72. Ducrot, E., H. Montes, and C. Creton, *Structure of tough multiple network elastomers by Small Angle Neutron Scattering.* Macromolecules, 2015. **48**(21): p. 7945-7952.
73. Chen, Y. and R.P. Sijbesma, *Dioxetanes as Mechanoluminescent Probes in Thermoplastic Elastomers.* Macromolecules, 2014. **47**(12): p. 3797-3805.
74. Chen, Y., et al., *Mechanically induced chemiluminescence from polymers incorporating a 1,2-dioxetane unit in the main chain.* Nat Chem, 2012. **4**(7): p. 559-562.
75. Clough, J.M., et al., *Covalent Bond Scission in the Mullins Effect of a Filled Elastomer: Real‐Time Visualization with Mechanoluminescence.* Advanced Functional Materials, 2016.

Chapter 2: Synthesis and Characterization Techniques of Multiple Network Elastomers.

Chapter 2: Synthesis and Characterization Techniques of Multiple Network Elastomers

Introduction

In the previous chapter, the theoretical background that will be used throughout this work has been presented along with the state of the art.

To complete this introduction, in this chapter, the synthesis of the materials will be described. Following the synthesis of the materials, their mechanical properties need to be tested. To do so, the different standard mechanical tests that have been used to characterize those materials are explained in detail. Then some general aspects of our materials are developed: the synthesis and its reproducibility and their viscoelastic properties.

I) Synthesis of multiple network elastomers

1) Standard synthesis of acrylate multiple networks elastomers

The preparation of multiple network elastomers is carried out through multiple steps of polymerization. Starting from monomers, a first network is synthesised, then multiple steps of swelling and polymerization will be conducted to create a multiple network. In this part we will first describe the chemicals we used and the detailed chemical mechanism of the synthesis. Then we will present the synthesis protocol of the set of materials that we investigated.

a) Chemicals

Solvents and reagents used during this work are commercial products purchased from Sigma Aldrich. The different monomers that were used are ethyl acrylate (EA, CAS: 140-88-5), methyl acrylate (MA, CAS: 96-33-3), butyl acrylate (BA, CAS: 141-32-2), hexyl acrylate (HA, CAS: 2499-95-8) and hexyl methacrylate (HMA, CAS: 142-09-6). 1.4-butanediol diacrylate (BDA, CAS: 1070-70-8) was used as a crosslinker and 2-hydroxy-2-metylpropiophenone (HMP, CAS: 7473-98-5) as initiator. The solvents that were used are ethyl acetate (CAS: 141-78-6), cyclohexane (CAS: 110-82-7), toluene (CAS: 108-88-3) and ethanol (CAS: 64-17-5). Table 1 shows the different chemicals that have been used with their molar mass, CAS number and formula.

Notation	Chemical name	Semi-developed formula	Molar mass ($g.mol^{-1}$)	Purity	Origin	CAS
MA	Methyl acrylate	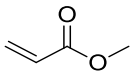	88.09	99 %	Aldrich	96-33-3
EA	Ethyl acrylate	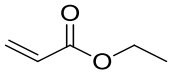	100.12	99 %	Aldrich	140-88-5
BA	Butyl acrylate	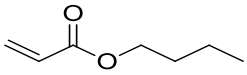	128.17	≥ 99 %	Aldrich	141-32-2
HA	Hexyl acrylate	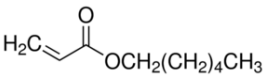	156.22	98 %	Aldrich	2499-95-8
HMA	Hexyl methacrylate	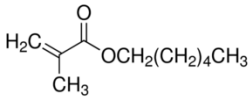	170.25	98 %	Aldrich	142-09-6

BDA	1,4-Butandiol diacrylate	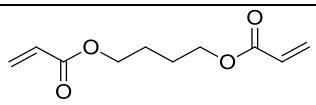	198.22	90 %	Aldrich	1070-70-8
HMP	2-hydroxyethyl-2-methylpropiophenone	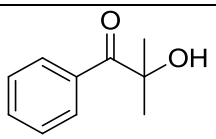	164.20	97 %	Aldrich	7473-98-5
Ethyl acetate	Ethyl acetate	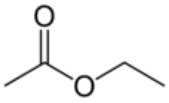	88.11	Technical	Aldrich	141-78-6
Cyclohexane	Cyclohexane		84.16	Technical	SDS	110-82-7
Toluene	Toluene	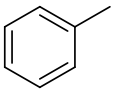	92.14	Technical	SDS	108-88-3
Ethanol	Ethanol		46.07	Technical	SDS	64-17-5

Table 1: Used chemicals

b) Principle of the free radical polymerization

The free radical polymerization is one of the main synthesis techniques used to create polymers. It is classified in the group of chain reactions using radicals. This technique has been chosen in this work because it is relatively simple to perform. The radicals are very reactive species that will react very quickly with surrounding molecules. For this reason, radical polymerization has to be done in a controlled atmosphere. Indeed, radicals have the capacity to react with oxygen from air. The radical polymerization is done in three main steps: initiation, propagation and termination. In this section we will present the detailed mechanism:

For our materials, the initiation is done using UV and HMP as initiator as described in Figure 1.

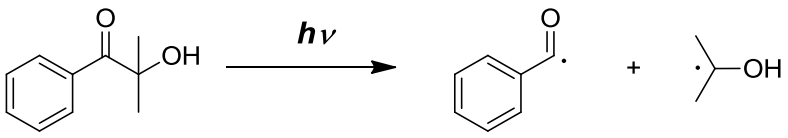

Figure 1: Decomposition of HMP under UV light

Following the initiation, the created radical ($R^{\cdot}$) combine with a monomer (M) to start a chain as shown in Figure 2. This chain will then grow by adding some monomers that are present in the solution. This step is called the propagation, an active chain (a chain that possesses a radical) keeps growing when reacting with monomer. At the end when not enough monomer is present in the solution, the termination step is more likely to occur. The termination step

by combination of two active chains can occur through two mechanisms displayed in Figure 2: combination and disproportionation. The termination removes active chains from the solution and therefore less reactions take place until no more active chains are present in the solution.

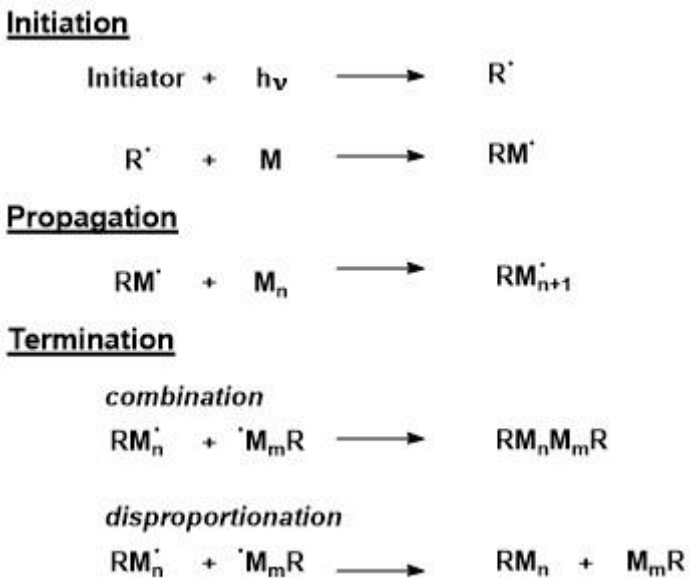

Figure 2: General mechanism of the free radical polymerisation

The free radical polymerization can also be subjected to chain transfer reactions. A chain transfer is observed when an active chain is having a reaction with another molecule resulting in the termination of the reaction for the chain involved. Those transfer reactions can happen with solvent molecules, monomers, initiator molecules and even polymer chains. This type of reaction will be encountered and detailed later in this work.

Now that the chemicals and the synthesis reaction has been developed, the following part be focusing on the actual synthesis of the materials.

c) Synthesis

The synthesis of the networks is carried out in a glove box (Mbraun Unilab) under nitrogen atmosphere to avoid side reactions with the oxygen of the air. Before the introduction in the glove box, every reagent and solvent was bubbled with nitrogen for 45 minutes to remove the dissolved oxygen. The reaction is a free radical polymerization of a solution of monomer under UV (UV light was produced by a Vilbert Lourmat lamp, model VL-215.L, focused on 365 nm). The UV power is kept low (10 µW/cm²) to create a slow polymerization, the goal is to decrease the number of simultaneous growing chains and the number of termination reactions. This has been inspired by Gong's procedure to prepare DN hydrogels [1], and will lead to a better homogeneity of the synthesised samples. Furthermore, to obtain a better homogeneity in the thickness of the samples, they are irradiated from both sides to avoid the presence of a gradient in initiation along the thickness of the sample.

The preparation of multiple networks starts with the synthesis of the first network, which is the more highly crosslinked one. The synthesis solution is prepared in the glove box before it is poured into a mold. The synthesis is carried out in the same mold that was used in a previous study [2] as shown on Figure 3. They are made of two glass plates with Dural spacers (precise thickness) and a Teflon tubing which is used to seal the mold. This setup is then tightened between metal frames to control precisely the final thickness of the samples.

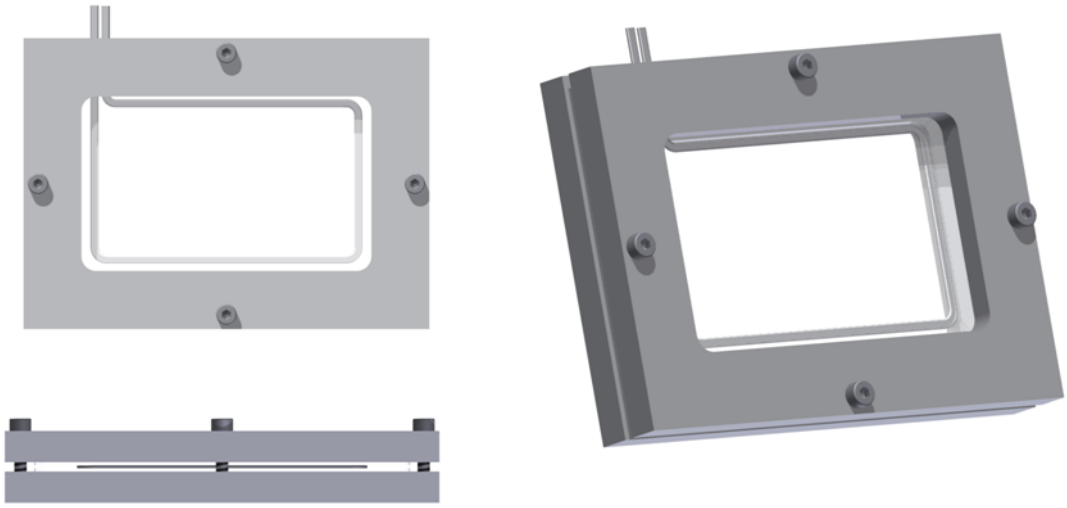

Figure 3: Glass mold used for polymerization (Image from Ducrot 2013)

The standard synthesis method of the first network is shown in Figure 4. The synthesis method is similar to that used by Ducrot, the amount of crosslinker of 1.45 mol% has been chosen as a reference since it is the one that displayed the best results in Ducrot's work. The synthesis is carried out in the presence of 50% of solvent. The solvent used is either toluene or ethyl acetate, which are both good solvents for ethyl acrylate and polyethylacrylate. The choice between the two solvents will be discussed in part III)1) of the current chapter. The goal of adding solvent during the synthesis step of the first network is to increase the final extensibility, to decrease the amount of trapped entanglements by creating slightly supercoiled chains while retaining the homogeneity of the crosslinking. As reported by Urayama et al. [3], this method of synthesis will allow us to obtain a higher degree of swelling at equilibrium.

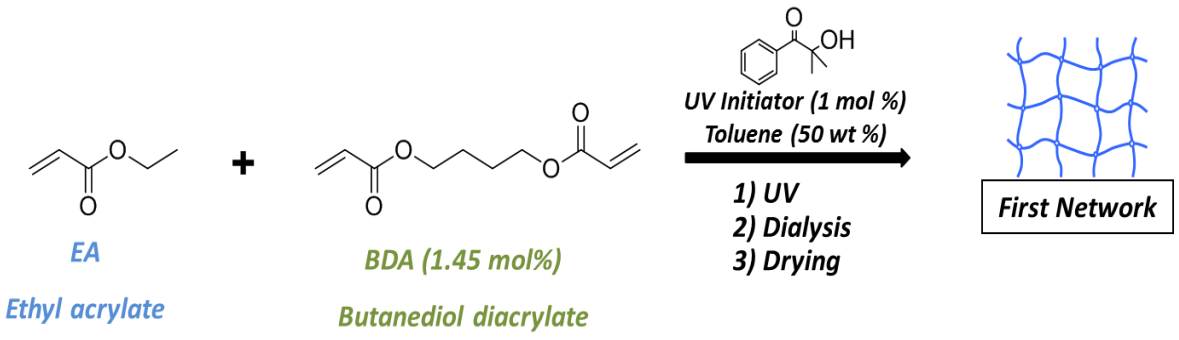

Figure 4: Standard synthesis of first network.

The mold containing the reactive solution is then exposed to UV radiation for two hours (10µW/cm²). After the synthesis, the sample is taken out of the mold and immersed in a bath of solvent containing 50 % of toluene and 50 % of cyclohexane. The bath will then be changed twice a day for three days. At the end of these three days the bath is changed to 25 % of toluene and 75 % of cyclohexane, this bath is also changed twice a day for two days. The goal of this step is to remove unreacted species and free chains, and to deswell the network progressively otherwise it will break with the evaporation of the solvent. After this step the network is dried under vacuum at 80 °C. In the end a simple network is obtained and these samples will be referred as SN.

To obtain a double network, a piece of first network is taken, the weight (m_{DN}) and the thickness (h_{SN}) of the first network sample are measured carefully. The piece of first network is swollen to equilibrium for two hours in a bath of monomer. The composition of the bath solution is shown in Figure 5. Once the swelling equilibrium is reached, the sample is taken out of the bath and placed between siliconized PET sheets and glass plates. The mold is then exposed to UV for two hours (10 µW/cm²). At the end the sample is dried overnight under vacuum at 80 °C.

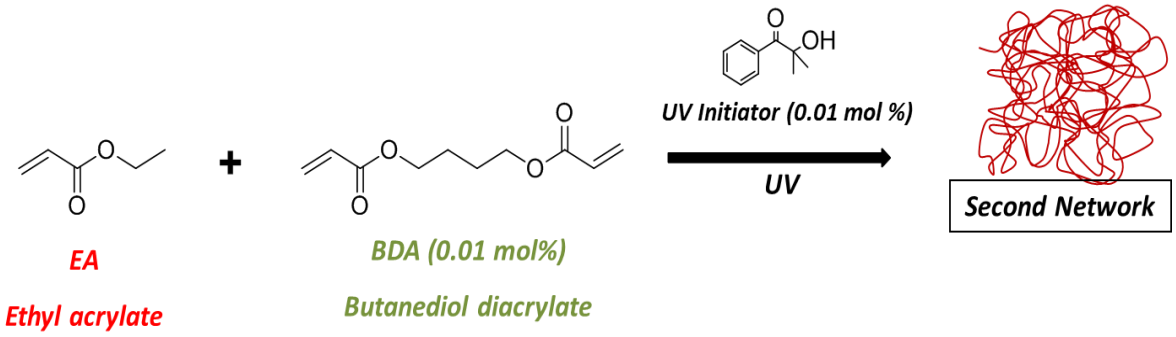

Figure 5: Composition of the monomer bath to perform the synthesis of the second network

After the overnight drying, the sample is collected, its weight and thickness are measured again, in order to determine the final composition of the double network. From the weight (m_{DN}) the ratio between the highly crosslinked network and the loosely crosslinked network can be deduced (ϕ_{SN} represents the mass fraction of first network in the total sample, its calculation is detailed in Eq. (1)). The prestretching of the chains of the first network is defined as λ_0, which is defined in Eq. (2). The two parameters presented in Eq. (1) and Eq. (2) are not independent, since an increase in the stretching of the first network corresponds to the decrease of its mass fraction as shown in Eq. (3). This relationship is valid as long as the network are made with the same monomers, a change of monomer in the second network would change its density and therefore the relation between the mass and the corresponding volume. In the case of two different monomers used with the first network having a volumetric mass ρ_{SN} and the second network a volumetric mass ρ_2. Then the previous three equations have to be changed into Eq. (4), (5) and (6) (m_2 is the mass of the second network only). It can be noted that Eq. (6) is transformed into Eq. (3) if the two monomers are identical.

$$\boldsymbol{\phi_{SN} = \frac{m_{SN}}{m_{DN}}} \qquad \textbf{Eq. (1)}$$

$$\lambda_0{}^3 = \frac{m_{DN}}{m_{SN}} \qquad \text{Eq. (2)}$$

$$\phi_{SN} = \frac{1}{\lambda_0{}^3} \qquad \text{Eq. (3)}$$

$$\phi_{SN} = \frac{m_{SN}}{m_{DN}} = \frac{m_{SN}}{m_{SN} + m_2} \qquad \text{Eq. (4)}$$

$$\lambda_0{}^3 = \frac{V_{DN}}{V_{SN}} = \frac{m_{SN} + m_2 \frac{\rho_{SN}}{\rho_2}}{m_{SN}} \qquad \text{Eq. (5)}$$

$$\phi_{SN} = \frac{1}{1 + (\lambda_0{}^3 - 1)\frac{\rho_2}{\rho_{SN}}} \qquad \text{Eq. (6)}$$

The swelling and polymerization steps shown to obtain a double network can be performed multiple times to increase the fraction of loosely crosslinked network in the prepared samples but also to further prestretch the initial highly crosslinked network. This procedure is used to obtain a double or a triple network. ϕ_{SN} decreases and λ_0 increases as the number of steps grows as shown in Figure 6.

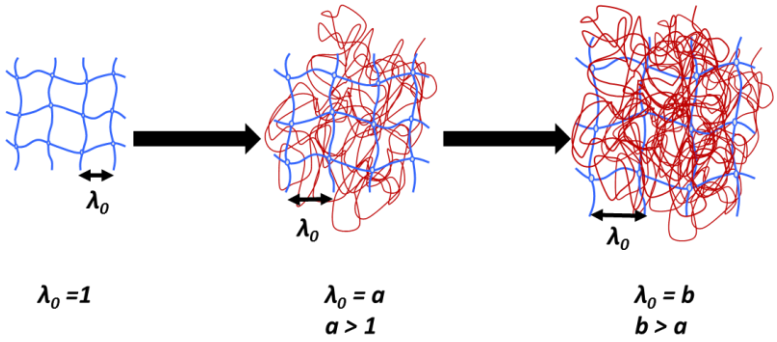

Figure 6: Evolution of λ_0 with the increase of loosely crosslinked network

The next part will show how the synthesis has been modified to obtain a wider range of materials than the one obtained in the previous study of Ducrot

2) Synthesis of a range of multiple network elastomers with added solvent to tune λ_0

In his thesis, Etienne Ducrot prepared and studied a limited number of networks. At an early stage of the current study we noted that the first network could be swollen even more than what had been done. Indeed, quadruple networks and even quintuple networks can also be synthesised. In Ducrot's thesis, the synthesis of the DN and TN was done by swelling the networks to equilibrium in a pure monomer bath before the polymerization was carried out. With this method, the ratio between the first network and the second is fixed by the equilibrium swelling ratio in monomer and can only be changed by changing the degree of crosslinking of the 1st network. This observation remains valid for a triple and a quadruple

network. As Ducrot has shown, the large strain mechanical properties are qualitatively different between double and triple networks. These differences seem to be mainly controlled by λ_0 which describes the average state of stretching of the first network after synthesis. In the following work, we will focus on λ_0 and study its influence on the uniaxial tension for a given first network.

To study the influence of this parameter λ_0, some samples with intermediate values of λ_0 need to be synthesised by modifying the composition of the swelling bath of the first network. The first network will still swell to equilibrium but this time the bath is composed of monomer and solvent. After the polymerization reaction, the solvent can be removed and the sample obtained will have a value of ϕ_{SN} and therefore λ_0 different from what would have been obtained by swelling in monomer only. The solvent that has been chosen is ethyl acetate which is a good solvent for poly(ethyl acrylate). Figure 7 shows the synthesis of an intermediate network starting from a simple network. This synthesis can be then repeated multiple times for several polymerizations allowing the creation, in several steps, of samples with different values of λ_0. By carrying out this synthesis in a mixture of solvent and monomer, we are conscious that we are creating a slightly different loose network in comparison with that done with monomer only. This difference might lead to less entanglements in our loose network and a slightly supercoiled network also.

Now that the synthesis has been described in general, the rest of the chapter will present the details of the materials actually synthesised.

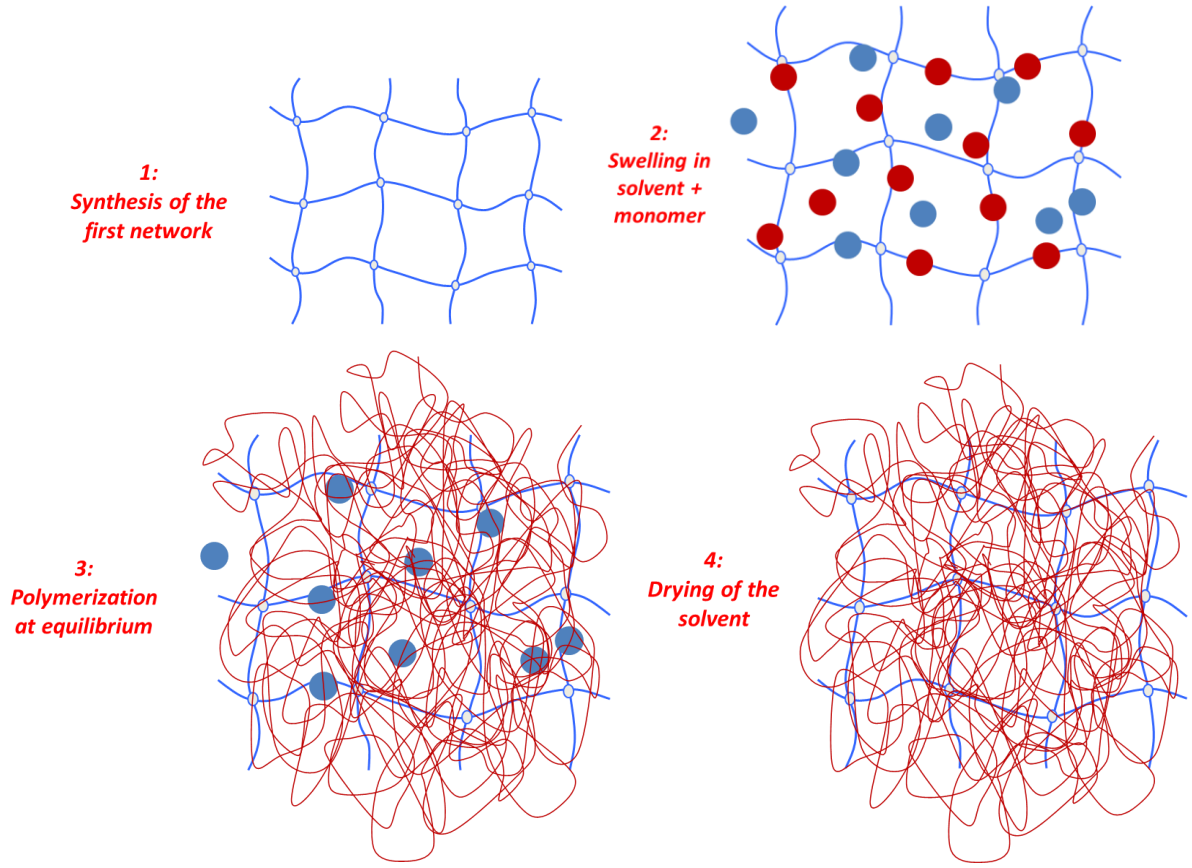

Figure 7: Synthesis of multiple networks with intermediate λ₀. Red dots = EA monomer, blue dots = ethyl acetate

Many samples with different compositions have been synthesised and we now need to define a general naming convention which will be used in the rest of the manuscript:

AbX(Y)C

A: Monomer of the first network
b: e or t represents the solvent (e = ethyl acetate, t= toluene), if solvent has been used in the synthesis of the first network
X: mol % of crosslinker
(Y): (λ_0) that represents the degree of prestretching of the first network chains
C: Monomer of second networks.

For example EAt1.45(1.68)EA has been synthesised with a first network of ethyl acrylate, synthesised in the presence of toluene as solvent with 1.45 mol% of BDA, it has been prestretched by a loosely crosslinked network of ethyl acrylate up to $\lambda_0 = 1.68$.

For the samples used in the mechanoluminescent experiments, in chapter 5 section II), the notation for the first network using different crosslinkers is the following: EA(d20)0.73(1) (the letter d refers to the use of dioxetane and 20 is for the 20 % of the mol % of crosslinker used that is dioxetane the remaining 80 % being BDA).

All the materials synthesised and used for this manuscript are listed in Table 2 and the notation for each network is detailed with the first network used, the number of polymerization steps and two important parameter that are λ_0 and the weight percent of simple network.

Sample name	First network	λ_0	SN wt%	Number of polymerization steps
EAe1.45(1)		**1**	**100**	**1**
EAe1.45(1.32)EA	**EAe1.45(1)**	**1.32**	**42.0**	**2**
EAe1.45(1.51)EA	**EAe1.45(1)**	**1.51**	**29.2**	**2**
EAe1.45(1.68)EA	**EAe1.45(1)**	**1.68**	**20.5**	**2**
EAe1.45(2.18)EA	**EAe1.45(1)**	**2.18**	**9.52**	**3**
EAe1.45(2.41)EA	**EAe1.45(1)**	**2.41**	**7.39**	**3**
EAe1.45(2.55)EA	**EAe1.45(1)**	**2.55**	**6.06**	**3**
EAe1.45(2.91)EA	**EAe1.45(1)**	**2.91**	**4.19**	**4**
EAe1.45(3.11)EA	**EAe1.45(1)**	**3.11**	**3.53**	**4**
EAe1.45(3.27)EA	**EAe1.45(1)**	**3.27**	**3.28**	**4**
EAe1.45(3.42)EA	**EAe1.45(1)**	**3.42**	**2.88**	**4**

EAe0.73(1)		**1**	**100**	**1**
EAe0.73(1.84)EA	**EAe0.73(1)**	**1.84**	**16**	**2**
EAe0.73(2.94)EA	**EAe0.73(1)**	**2.94**	**3.93**	**3**
EAe0.73(3.75)EA	**EAe0.73(1)**	**3.75**	**1.89**	**4**
EAe0.29(1)		**1**	**100**	**1**
EAe0.29(2.07)EA	**EAe0.29(1)**	**2.07**	**11.25**	**2**
EAe0.29(3.74)EA	**EAe0.29(1)**	**3.74**	**1.9**	**3**
EAe0.29(5.39)EA	**EAe0.29(1)**	**5.39**	**0.64**	**4**
EAe0.15(1)			**100**	**1**
EAe0.15(2.19)EA	**EAe0.15(1)**	**2.19**	**9.4**	**2**
EAe0.15(3.65)EA	**EAe0.15(1)**	**3.65**	**2.05**	**3**
EA1.45(1)				**1**
EA1.45(1.39)EA	**EA1.45(1)**	**1.39**	**32.6**	**2**
EA1.45(1.92)EA	**EA1.45(1)**	**1.92**	**13.5**	**3**
EA1.45(2.34)EA	**EA1.45(1)**	**2.34**	**7.9**	**4**
EA0.73(1)				**1**
EA0.73(1.51)EA	**EA0.73(1)**	**1.51**	**26.6**	**2**
EA0.73(2.19)EA	**EA0.73(1)**	**2.19**	**10.8**	**3**
EA0.73(2.73)EA	**EA0.73(1)**	**2.73**	**4.9**	**4**
BAe1.86(1)				**1**
BAe1.86(1.59)EA	**BAe1.86(1)**	**1.59**	**20.8**	**2**
BAe1.86(2.41)EA	**BAe1.86(1)**	**2.41**	**6.3**	**3**
BAe1.86(3.21)EA	**BAe1.86(1)**	**3.21**	**3.3**	**4**
BAe1.86(1.64)BA	**BAe1.86(1)**	**1.61**	**22.6**	**2**
BAe1.86(2.28)BA	**BAe1.86(1)**	**2.28**	**8.4**	**3**
BAe1.86(2.88)BA	**BAe1.86(1)**	**2.88**	**4.2**	**4**
EAe1.45(1.41)HA	**EAe1.45(1)**	**1.41**	**33.3**	**2**
EAe1.45(2)HA	**EAe1.45(1)**	**2**	**11.8**	**3**
EAe1.45(2.62)HA	**EAe1.45(1)**	**2.62**	**5.5**	**4**
HMA1.24(1)				**1**
HMA1.24(1.43)EA	**HMA1.24(1)**	**1.43**	**28.7**	**2**
HMA1.24(2.14)EA	**HMA1.24(1)**	**2.14**	**9.7**	**3**
HMA1.24(2.68)EA	**HMA1.24(1)**	**2.68**	**5.5**	**4**

EA(d20)0.73(1)		**1**	**100**	**1**
EA(d20)0.73(1.43)EA	**EA(d20)0.73(1)**	**1.43**	**26.2**	**2**
EA(d20)0.73(1.88)EA	**EA(d20)0.73(1)**	**1.88**	**15.1**	**3**
EA(d20)0.73(2.19)EA	**EA(d20)0.73(1)**	**2.19**	**7.5**	**3**
EA(d20)0.73(2.67)EA	**EA(d20)0.73(1)**	**2.67**	**5.2**	**4**
EA(d20)0.73(2.94)EA	**EA(d20)0.73(1)**	**2.94**	**3.6**	**4**

Table 2: Description of all the different materials used in this manuscript.

II) Characterizing mechanical properties in uniaxial extension

Before discussing the details of the tests carried out, some preliminary remarks need to be made. Mechanical tests have been performed with an Instron tensile tester, model 5565, fitted with a 100 N load cell and a video extensometer. The extensometer is able to track during the uniaxial deformation, two markers placed around 10 mm apart on the sample. This provides an accurate value of the local strain in the region of interest of the sample without having to consider any slip that might occur in the clamps. The load cell is accurate at ±0.1 % in the range of 0 to 100 N, and the extensometer is accurate at ±0.11 % for the full scale up to 120 mm. The crosshead speed is calibrated to be used between 0.001 mm/s to 1 mm/s.

Samples were clamped to the tensile frame with homemade pneumatic clamps (Figure 8) with an adjustable pressure to reduce slippage or damage in the clamping area. For the toughest samples that could experience slippage in the clamps, some sandpaper was used. The use of an oven was also necessary for certain experiments, the temperature being limited to 120 °C for our system because of plastic components inside the clamps, the range that was used starts at 20 °C up to 120 °C.

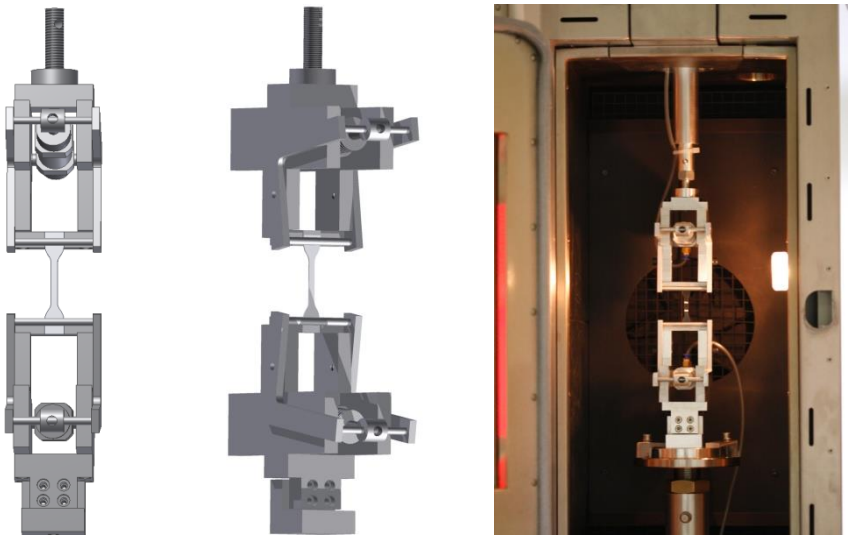

Figure 8: Homemade pneumatic clamps for mechanical testing, scheme and picture once in the oven (Ducrot 2014)

1) Tensile tests

Samples were first characterized in simple uniaxial tension to rupture. This test provides a good fingerprint of the type of large strain mechanical behaviour and several parameters can be extracted for each test: the Young's modulus, the stress at break and the strain at break. Every sample was cut in a dumbbell shape using a punch (Figure 9). The gauge length of the central part used for the strain measurement is fixed at 20 mm. The cross-section is 4 mm in width (w) and has a thickness (h) fixed by the sample itself between 0.5 and 2.5 mm. As mentioned earlier two white spots of paint were printed in the central zone to allow a precise measurement of the deformation via the video extensometer. Uniaxial tensile tests were performed at a constant crosshead velocity of 500 µm.s^{-1}µ. With the extensometer signal, one can calculate the initial strain rate by using the initial slope of the curve showing the deformation as a function of the time. For most of our experiments, the initial strain rate is approximately 0.020 s^{-1}.

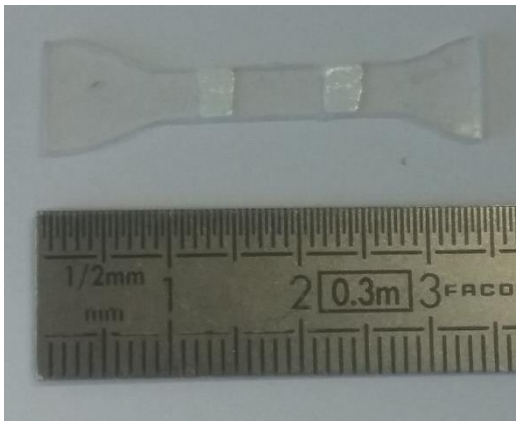

Figure 9: Typical sample used for tensile tests

The force F and the stretch ($\lambda = L/L_0$), were recorded all along the experiment. Using these quantities, the nominal stress σ_N which is the force divided by the initial cross-section $w_0 * h_0$ (Eq. (7)) and the true stress σ_T; which is the force divided by the instantaneous cross-section $w * h$ (Eq. (8)), can be calculated by assuming that these materials are incompressible. True and nominal stress in uniaxial tension are also related by Eq. (9).

$$\sigma_N = \frac{F}{w_0 * h_0} \quad \textbf{Eq. (7)}$$

$$\sigma_T = \frac{F}{w * h} \quad \textbf{Eq. (8)}$$

$$\sigma_T = \sigma_N * \lambda \quad \textbf{Eq. (9)}$$

$$\sigma_N = E * \varepsilon \quad \textbf{Eq. (10)}$$

The Young's Modulus (E), can be estimated from the small strain regime at the beginning of the tensile curve by using Eq. (10).

2) Step-cycle extension

In order to characterize the energy dissipation in the samples with increasing deformation, step-strain cyclic experiments were also carried out. The principle of this experiment is to increase step by step the maximum value of lambda (λ_{max}). Each cycle was done between λ = 1 and $\lambda = \lambda_{max}$. Between each increase of λ_{max}, the sample is unloaded to a force of 0.1 N before being loaded again twice to the same λ_{max}. The value of λ_{max} was then increased progressively until failure of the sample as shown in Figure 10.The reason for carrying out three cycles at the same maximum deformation is to separate the first cycle hysteresis (due to structural damage) from the subsequent cycles hysteresis (due to the viscoelastic properties of the sample). This separation leads to the separation between some irreversible damages and some reversible ones. For example, in some materials where viscoelastic dissipation occurs, this dissipation is partially recovered during the second cycle when some bond scissions are not. The shape of the sample used for this test is the same that is used for uniaxial tensile tests.

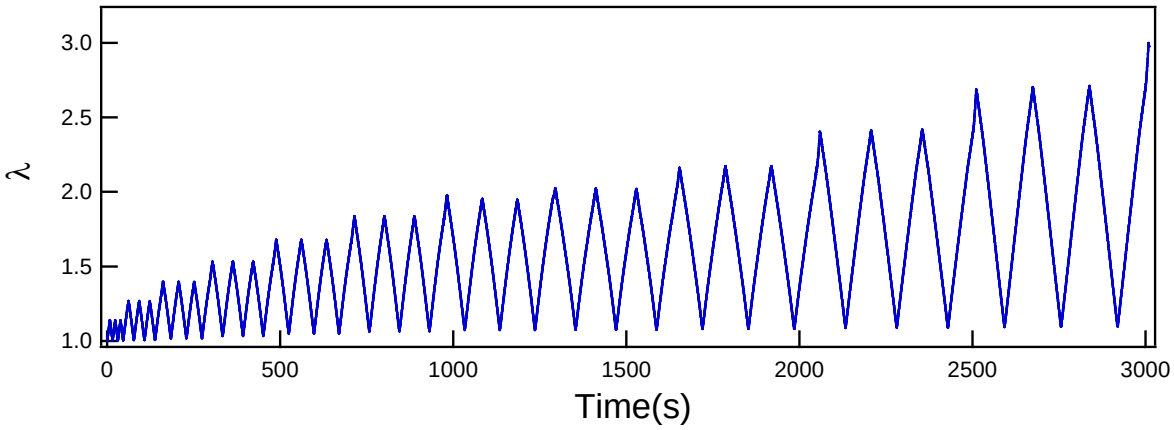

Figure 10: Evolution of lambda with time during a cyclic experiment

3) Fracture in single edge notch tests

Fracture tests were also performed on the Instron machine. This time a rectangular piece of material is used with a length kept around 20 mm, w_0 = 5 mm in width and the thickness h ranging from 0.7 mm to 2.5 mm. A notch of approximately a_0 = 1 mm was made with a scalpel (Figure 11). The actual length of the initial crack was measured from microscope pictures of the sample with a ruler using ImageJ. In order to use the extensometer to record the deformation, two white dots were made, one on each side of the crack located each at 5 mm from the initial crack. The sample was fixed in the pneumatic clamps already presented with a spacing around 20 mm between clamps. Force and strain were measured until failure of the sample. During typical experiments, the deformation of the sample was applied by moving the

crosshead at 100 µm.s^{-1}, which gives an initial strain rate around 0.005 s^{-1} at the beginning of the experiment.

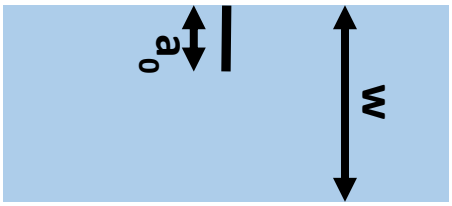

Figure 11: Scheme of a sample used for single edge notch test with a_0 the size of the initial crack and w the width of the sample

III) Preliminary study of the materials

1) Study of the impact of solvent used for the synthesis of the first network

As described in the experimental section, solvent was used during the synthesis to decrease the entanglement density in the first network and create slightly supercoiled chains to favour swelling during the later polymerization steps. In the previous study from Ducrot *et al.*[2] the solvent used for the synthesis of the first network was always toluene. The problem is that this solvent can be subjected to transfer reactions with hydrogens from the methyl group as shown by Mayo [4]. This leads to shorter chains since a transfer leads to the termination of the propagating chain reaction and to the initiation of a new one from the solvent molecule. Indeed, as shown in Figure 12 the hydrogen located in alpha position of the toluene can be attacked by the radical to create a new radical. This radical can then grow as a new chain, ending simultaneously the previously growing chain.

Figure 12: Scheme showing the transfer reaction from a growing chain to a solvent molecule of toluene

Transfer reactions during our synthesis could reduce the kinetic chain length and the homogeneity of our samples. For these reasons, ethyl acetate has been selected in this study to avoid transfer reactions to the solvent since it is less likely to react with any radical during the synthesis. If there is less transfer during the creation of the first network, the first network synthesised should be more homogeneous which means that in principle the average length of the elastic strands between crosslinks should be shorter than what is obtained with a synthesis in toluene. Note however that the most likely transfer reaction is that to the polymer and acrylates are notorious to lead to transfer and hence additional crosslink points [5].

To investigate the influence of the solvent nature, two types of first networks have been synthesised using either 50 wt% of toluene or 50 wt% of ethyl acetate as solvent, while the

precursor composition was kept unchanged. The two solvents have slightly different swelling properties. According to the theory of equilibrium polymer swelling by Rehner and Flory [6] presented in chapter 1, the crosslink density of the polymer network but also on the mixing parameter χ_{12} between the solvent and the polymer have an influence on the swelling. The higher the value of χ_{12} is, the less soluble are the two components. This mixing parameter can be estimated using the Hildebrand solubility parameters δa and δb of the solvent as shown in Eq. (11). The values of the solubility parameters for ethyl acrylate: 9.50, ethyl acetate: 9.10 and toluene: 8.91 can be found in the Polymer Handbook [7]. The values are quite close for both solvents but suggest that the ethyl acetate gives a higher swelling ratio of poly(ethyl acrylate).

$$\chi_{12} \approx \frac{V_s}{RT} (\delta_a - \delta_b)^2 \qquad \textbf{Eq. (11)}$$

Table 3 shows the content of the solution used to carry out the synthesis. The amount of 1.45 mol% of BDA will be the standard amount used mainly in this work. As it can be calculated using Eq. (13), this amount of BDA corresponds to a theoretical molar mass between entanglements of 3400 g.mol^{-1} (M_{Xth}). Since the theoretical value for the average molecular weight between entanglements M_e of the polyethyl acrylate homopolymer is around 13000 g.mol^{-1}, our standard first network should be essentially unentangled. Also because solvent is used during the synthesis, it is less likely to have entanglements as shown in the previous part.

Sample	[BDA] (mol %)	Monomer (g)	Solvent (g)	BDA (µL)	HMP (µL)	E (MPa)	$M_{x\,exp}$ (kg.mol^{-1})
Eat1.45(1)	1.45	8.6	8.6 of toluene	236	152.5	0.80	10.6
EAe1.45(1)	1.45	8.6	8.6 of ethyl acetate	236	152.5	0.90	8.7

Table 3: Characteristics of the first networks synthesised in different solvents

After the synthesis, samples were prepared to perform a uniaxial tensile test. The results are shown on Figure 13. The only significant difference that can be observed is the value of the modulus E which is slightly higher for the network created in ethyl acetate. Since there are no entanglements in either simple network due to a high amount of crosslinker, the difference in modulus value must come from a difference in elastic chains density. This elastic chains density is linked to the average molecular weight of the chain between crosslink point, and this can be calculated using the affine model of rubber elasticity Eq. (12).

$$E = \frac{3\,n\,k_B\,T}{V} = \frac{3\,\rho\,R\,T}{M_x} \qquad \textbf{Eq. (12)}$$

$$M_{x\,th} = \frac{M_{monomer} n_{monomer}}{2\,n_{BDA}} \qquad \textbf{Eq. (13)}$$

In Eq. (12), ρ is the density of the polymer, here for PEA ρ = 1.13, R is the ideal gas constant and T is the temperature taken for this work at 293 K. The calculated values show that the difference between the experimental value and the theoretical mass between crosslinks: 3400 g.mol^{-1} (calculated using Eq. (13)) is nearly three times larger. This discrepancy can be attributed to the transfer reactions that create more dangling chains and more inefficient crosslinks, leading to a lower modulus and a less homogeneous network.

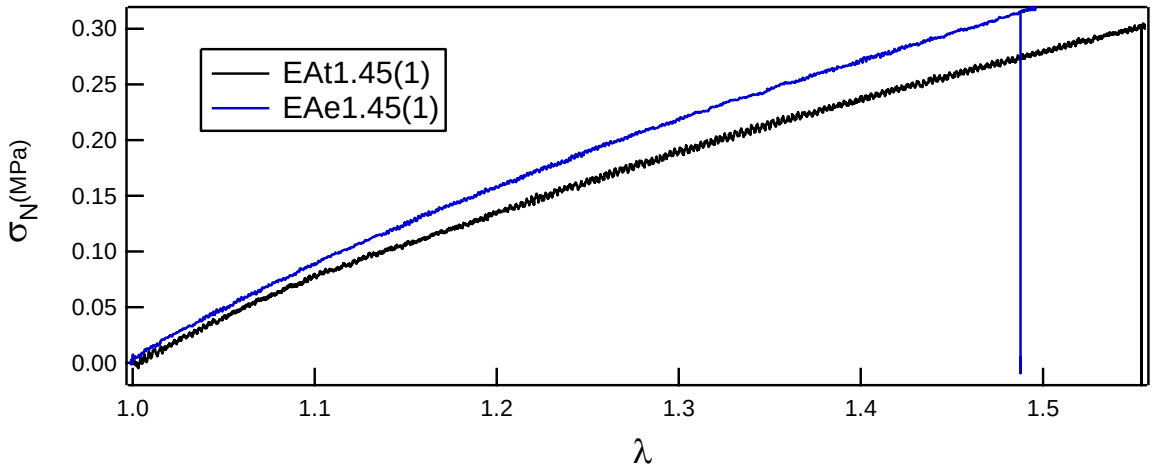

Figure 13: Tensile curves for first networks synthesised in different solvents

The two first networks synthesised in different solvents seem to have a small difference in their modulus. To confirm that we could obtain the same type of reinforcement that Ducrot et al. found for DN and TN, some multiple networks were prepared using the first network EAe1.45(1) and MA as monomer for the second networks. To reproduce the previous synthesis method, each type of network was synthesised three times. After the synthesis, the equilibrium swelling and the results of uniaxial tension tests were compared for both types of networks. Table 4 summarizes the differences observed between the materials and the influence of the two solvents used in the polymerization of the first network. As shown in Table 3, the value of $M_{x\ exp}$ is slightly higher for the network created in toluene. The ability for a network to swell is linked to the average length of the elastic chains, from a competition between the restoring elastic stress of the network chains and the osmotic pressure to swell the network. Those calculations have been developed by Flory and Rehner and have been shown in chapter 1 section I)5. The polymer concentration at equilibrium swelling can be extracted from equation (43) of chapter 1 and can lead for small values of ϕ_2 to Eq. (14) [6] where ϕ_2 is the volume fraction of the polymer, V_s is the molar volume of the solvent and B is a constant depending on the components. This equation shows that if M_x increases (so the crosslink density decreases), then the volume fraction of the polymer is smaller, meaning that the swelling is more important.

$$\boldsymbol{\phi_2 = \left(\frac{2\,\rho\,V_s}{M_x\,(1 - 2\,B\,\frac{V_s}{RT})} \right)^{3/5}} \qquad \textbf{Eq. (14)}$$

Table 4 shows the value of λ_0 and of the weight percentage of the first network (wt% (SN)) for a DN and a TN synthesised with a first network created in toluene or ethyl acetate. It can be seen that the prestretching λ_0 are slightly higher when the first network is made in toluene, consistent with the difference in M_x observed from the Young's modulus and in agreement with Eq. (14).

Sample	Type of network	λ_0	SN (wt%)	E
EAt1.45(1.73)MA	**DN**	**1.73**	**17.5**	**1.23**
EAt1.45(2.67)MA	**TN**	**2.67**	**5.1**	**1.82**
EAe1.45(1.68)EA	**DN**	**1.68**	**19.6**	**1.24**
EAe1.45(2.56)EA	**TN**	**2.56**	**6.1**	**1.91**

Table 4: Comparison of the impact of the solvent on multiple networks, values are calculated upon the synthesis of three samples for each type.

To continue the comparison between toluene and ethyl acetate, uniaxial tensile tests were carried out on this set of samples. The results of the comparison are shown on Figure 14.

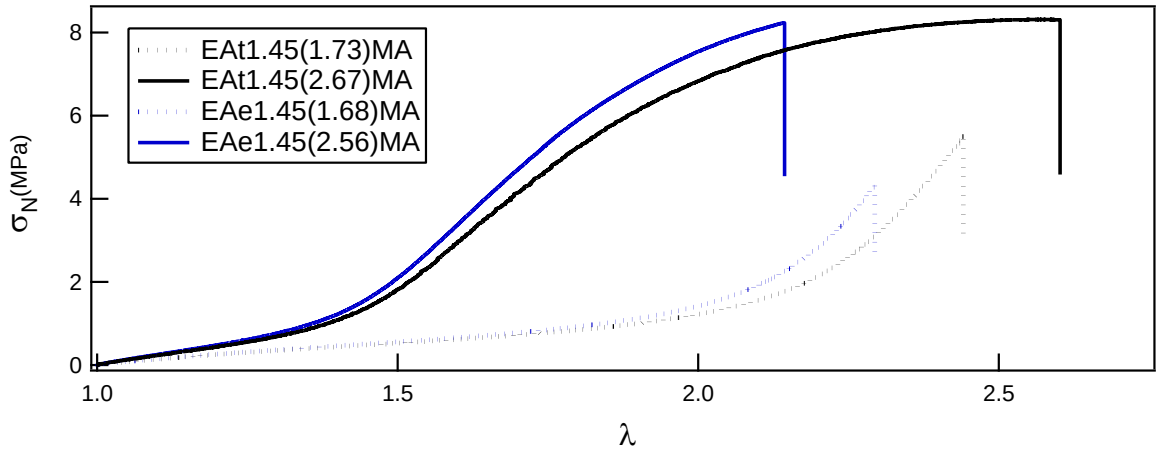

Figure 14: Uniaxial tension of DN and TN using different first networks

It can be observed in Figure 14 and Table 4, that E does not significantly change and the main difference stems from the hardening region, which corresponds to the final extensibility of the chains of the first network. This hardening is characterized by an increase of the stress slope starting at a certain value of extension called λ_h. Since the chains of the PEA network prepared in ethyl acetate are shorter on average than those prepared in toluene, this hardening at lower values of λ was expected. To study more precisely the difference in hardening, a strain hardening model can be used like the model proposed by Gent [8]. This model has been presented in chapter 1 section I)4) and the prediction of the stress in uniaxial extension is recalled in Eq. (15). In this equation, J_1 is the first invariant in uniaxial extension and J_m is the limiting value of this invariant. This model will be used to fit each of the stress-strain curves of the prepared samples. To obtain the best fit, first the parameter J_1 is fixed and

a fit to obtain the modulus is carried out at small deformations (up to λ = 1.1) then this value of E is fixed and the fit is done on the rest of the stress-strain curve to obtain the value of J_m. Gent's model is designed to describe the hardening appearing as the chains reach their limit of extensibility, and therefore no damages are taken into consideration. For this reason, for the samples that soften before breaking, the fit is only carried out up to the inflexion point and before the softening takes place. The quality of the fit is shown in Figure 15, with the red curves being the corresponding Gent fit of the stress-strain curves displayed in Figure 14.

$$\sigma_N = \frac{E\,(\lambda^2 - \frac{1}{\lambda})}{3\,(1 - \frac{J_1}{J_m})} \qquad \text{Eq. (15)}$$

$$J_m = \lambda_h{}^2 + \frac{2}{\lambda_h} - 3 \qquad \text{Eq. (16)}$$

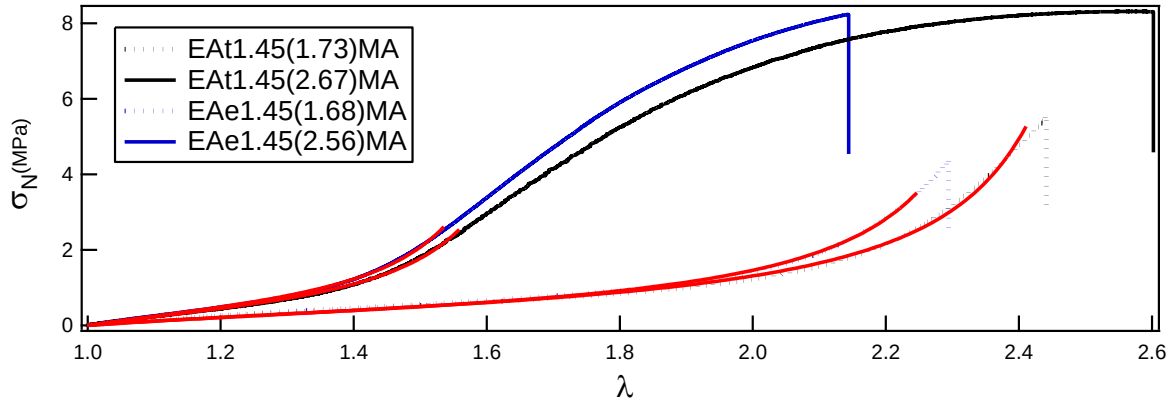

Figure 15: The same stress-stress curves presented in Figure 14 are shown with the Gent fit to show the quality of the fit (red curves)

The fits shown in Figure 15 provide a value of J_m for each sample and by solving Eq. (16), λ_h can be deduced. The limiting elongation found is 2.58 for the DN made using a toluene based first network and 2.45 for the one using ethyl acetate. For the TN, the value are respectively 1.72 and 1.69. The values are quite close but still show an earlier hardening occurring for the networks using the first network made in ethyl acetate. This means that the maximum extensibility of the first network synthesised in ethyl acetate is lower than the one of the first network made in toluene.

Figure 14 shows also that the elongation at break is lower for EAe1.45(1) but as will be discussed later, this discrepancy might also come from the difference in prestretching of the chains of the first network.

The uniaxial tensile tests of multiple networks confirm what has been seen in simple networks: the synthesis in toluene appears to result in less homogeneous networks and is less efficient in terms of crosslink density.

This result has also been confirmed by NMR, through a collaboration with a laboratory in Radboud university in Nijmegen (Holland) with Walter Chassé and Arno Kentgens. The NMR stands for Nuclear Magnetic Resonance, and here we focus on the carbon 13 NMR, where 13

stands for the number of the isotope used for its nonzero spin, its abundance is around 1.1 %. The principle of NMR is to put a sample in a constant magnetic field to align the spins. Then a perpendicular magnetic field with a range of frequencies is employed to change the alignment of those spins. The relaxation of the spins to get back to the original alignment is recorded. The signal returned for each different atom depends on their surrounding environment. In our particular case the NMR has a constant field frequency of 300 MHz, the typical frequency used to solicit carbon 13 is 25.1 MHz.

Carbon NMR spectra have been acquired on both first networks to detect the presence of unreacted double bonds. Figure 16 shows the 13C NMR spectrum of EAt1.45(1). The peaks observed at 144 ppm are attributed to carbon double bonds, resulting from unreacted crosslinking sites. The intensity of the peak seen on Figure 16 b) corresponds to 3-5% of crosslinker molecules. The spectrum of EAe1.45(1) does not show any remaining double bond. The fact that double bonds are present can be an explanation of the observed difference in elastic chain length but more importantly it offers a site where a growing chain can attach during the next polymerization step.

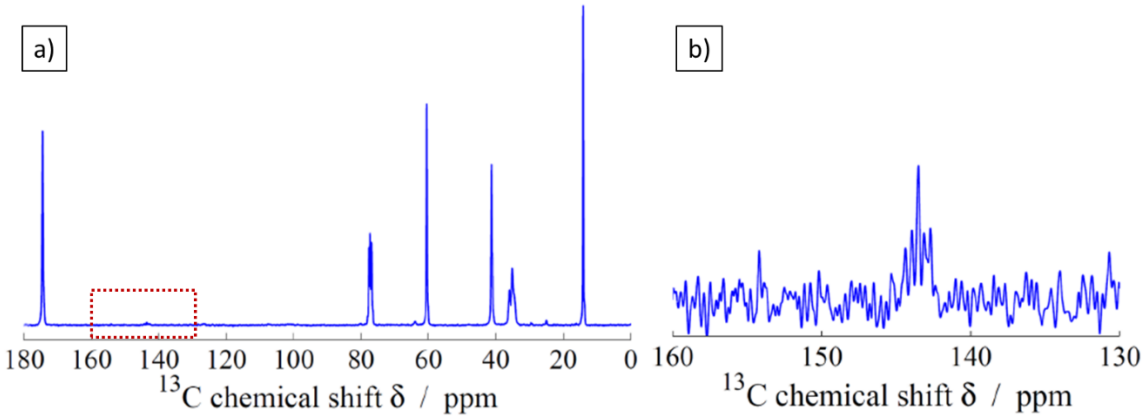

Figure 16: a) ^{13}C NMR spectrum of EAt1.45(1) b) zoom on the area corresponding to unreacted double bonds

NMR shows that the synthesis of the first network in toluene results in some transfer reactions that can lead to longer effective elastic chains. Also the fact that unreacted double bonds remain in the first network creates an opportunity for the later synthesised networks to chemically bond to the first network, which means that a less controlled system is created, even though during the synthesis of the second network some bonds can still be created with the first network by chain transfer to the labile H in acrylate molecules, and this will be developed in this study.

For those reasons, in this work, every first network synthesised in solvent will be prepared in ethyl acetate to obtain a more homogenous and a better controlled reaction for the first network. The structure of the first network is a key parameter, as will be shown in the next chapter.

2) Variability observed during the synthesis of the first network

It is important to first discuss the variability of the network properties. Indeed, the radical UV initiated synthesis was chosen because it is very efficient and simple. However we faced an issue that we were not initially aware of: the relatively poor reproducibility of the synthesis of the first network under UV light. As it will be shown in details later, the first network structure is responsible for a major part of the mechanical properties of the multiple networks. The synthesis as reported at the beginning of this chapter, is done in a glove box, the atmosphere is kept the same so are the reactants. Despite this, the resulting first networks can show significant differences: change of the initial modulus, of the elongation at break and therefore of the equilibrium swelling properties of the first network. Those differences could be caused by several things, first the change of temperature inside the room that could not be controlled. The room can be very hot in the summer due to the extra heat generated by the pumps in the room up to 30°C, while quite cold in the winter down to 15°C. Those temperature changes can lead to some variations in the evaporation of the solvent and of the monomer. The polymerization could also be affected by the power of the UV lamp that we tried to keep around 10 mW/cm² but could fluctuate. Finally, the gloves box is efficient to avoid oxygen inside but as a small amount of oxygen can act as an inhibitor therefore radicals can be stopped.

All those experimental conditions have led to the synthesis of some different networks over the three years despite the use of the same reactants and the same composition. In this section we will present the properties of samples synthesised with the first network composition mainly used in this study: EAe1.45(1). Starting with this family of first networks many DN and TN have been created.

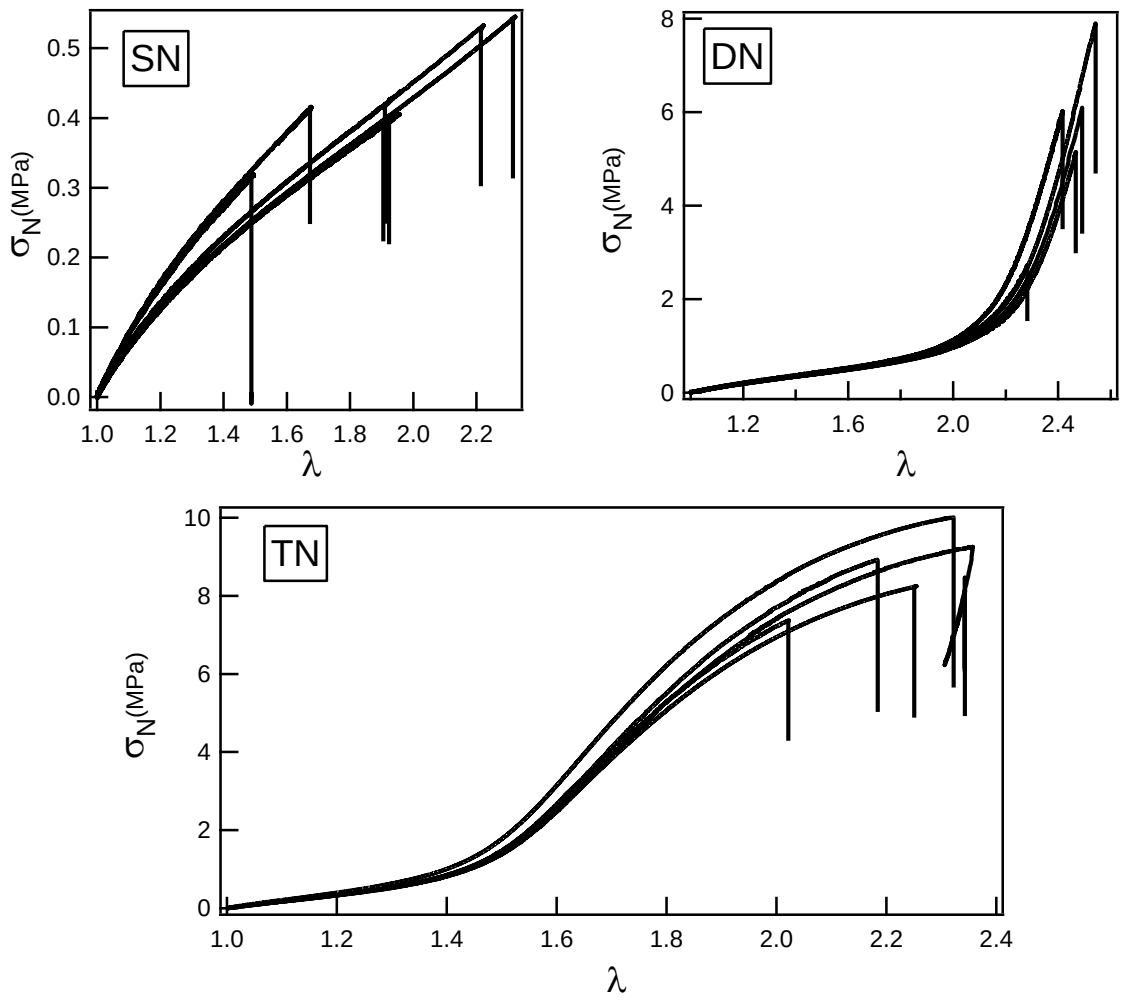

Figure 17: Stress-strain curves of SN, DN and TN samples done with an identical precursor solution for the first network SN EAe1.45(1).

Figure 17 shows the stress-strain behaviour of those SN, DN and TN. The graph showing the SN curves shows the problem of reproducibility described earlier with quite a broad range of modulus and elongation at break. The Young's modulus values are included between 0.86 MPa and 1.03 MPa and the stress at break can go from 1.5 to 2.3.

Despite these differences in the stress-strain curves, when the DN are synthesised, the swelling obtained and the prestretching of the first network are very similar as shown in Figure 18 . Indeed, the equilibrium swelling and therefore the wt % of the first network is very similar and most of the time comprised between 20.5 and 22 %. Figure 17 shows also that the mechanical properties obtained for the DN are more reproducible with a similar modulus and a similar strain hardening. The same observation can be made for TN samples. To confirm this observation on the hardening, the Gent model (described in this chapter section III)1)) can also be used for the curves presented in Figure 17. The obtained range of λ_h for the different DN starts at 2.50 and stops at 2.56 when for TN the range is 1.70 to 1.73. The different values of λ_h are very close for DN and TN showing that despite the observed differences in the moduli of the SN , the DN and TN have still very similar properties.

DN and TN still show some differences in elongation and stress at break but we think that those differences are also related to sample to sample variation. Indeed some samples done at the exact same time from the exact same batch can have different elongation and stress at break, this comes from the presence or not of defects in the sample that can lead to an earlier failure.

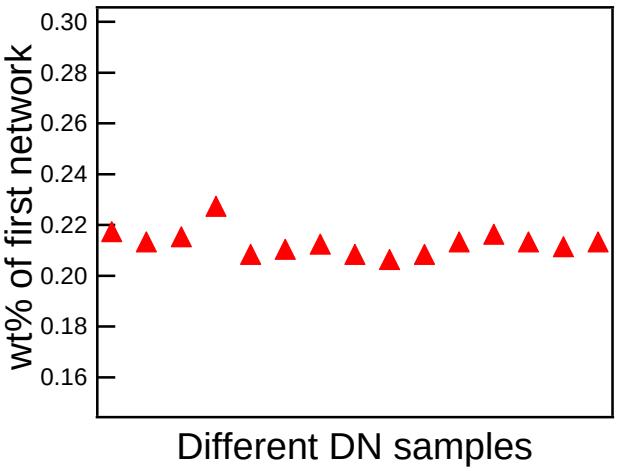

Figure 18: wt% of first network in similar DN samples synthesised with different samples of first network created from the same reactants

In this part, it has been shown that the synthesis of the first network is not as highly reproducible as I would have wanted (but my advisor says it is OK) but that the resulting mechanical properties for the multiple networks are not very affected by those differences. Thus suggests that the strain hardening may have an importance on the equilibrium swelling as well. The hypothesis can be made that those initial differences in modulus like very short chains or inhomogeneously crosslinked zones could be smoothed by swelling the samples and adding another polymer inside them.

3) Linear viscoelastic properties of standard multiple networks

In order to characterize the linear viscoelastic properties of our networks and their temperature and frequency dependence, a set of samples has been made to be tested on a rheometer. The samples used in this part are those described in section I.1.a. This family of samples uses EA as monomer for both networks and 1.45 mol% of BDA. The first network is EAe1.45(1) and its synthesis is shown in Table 3. From this first network, multiple networks were prepared following the procedure shown in Figure 5 to obtain a DN and a TN. Table 5 shows the resulting properties of the multiple networks. This family of networks with EAe1.45(1) as first network will be used as our reference for future work. It is the standard family of samples created with only EA and the standard amount of BDA (1.45 mol%).

Sample name	Type of network	First network	Second networks monomer	SN wt%	λ_0
EAe1.45(1)	**SN**			**100**	**1**
EAe1.45(1.68)EA	**DN**	**EAe1.45(1)**	**EA**	**20.6**	**1.68**
EAe1.45(2.55)EA	**TN**	**EAe1.45(1)**	**EA**	**6.07**	**2.55**

Table 5:Multiple networks created from EAe1.45(1)

Once the samples have been synthesised, the frequency dependence small strain behaviour was investigated with an RDAII parallel plate rheometer (Rheometrics). The samples were cut in small disks of 8 mm in diameter, which were then glued (with Loctite 407 used for high temperature) to a parallel plate geometry. The limits of the linear regime were first investigated by performing a deformation sweep as shown on Figure 19a). The linear regime for the sample of Figure 19a) goes from 0.05% to 0.4% of deformation. To stay in the linear regime, the strain was kept at 0.1 % during frequency sweeps from 0.063 to 63 rad.s^{-1} with a temperature range from -20 °C to 70 °C. During the experiment the following parameters are recorded by the device: the temperature, the frequency, G', $G''$and $tan\ \delta$. The data were then used to construct a master curve using the principle of time temperature superposition. Once a reference temperature was chosen (here 19 °C, 292 K), the $tan\ \delta$ (defined as shown in Eq.(17)) data obtained at different temperatures were shifted horizontally one by one with a factor a_T to superpose on the reference curve on the frequency range. To improve the resulting corrected curve, a vertical correction with a factor b_T needs to be applied due to the temperature and density dependence of the entropic modulus as shown in Eq. (18). Applying this vertical shift leads to a clear improvement in the elastic plateau region. A correction on G' and $G''$is applied for each range of temperature with a factor b_T calculated from Eq. (19).

$$tan\ \delta = \frac{G''}{G'} \qquad \textbf{Eq. (17)}$$

$$G' = \frac{\rho RT}{Mx} \qquad \textbf{Eq. (18)}$$

$$G' b_T = G' \frac{T}{T_0} \qquad \textbf{Eq. (19)}$$

$$E = 3 * G' \qquad \textbf{Eq. (20)}$$

Figure 19b) shows the master curve for the simple network EAe1.45(1). This graph shows the evolution of $G'$and G''over a large range of frequencies. It can be observed that G'presents a plateau for a range of frequencies going from 10^{-3} to 5 Hz. The value of G'at the plateau modulus is approximately $G' \approx$ 0,22 MPa, which for incompressible materials leads a Young's modulus of 0.66 MPa (Eq. (20)). This value of Young's modulus is in the range of the values that are obtained for first networks during tensile test with the Instron device. Figure 19b) shows the absence of crossover between $G'$and G''on the entire frequency range. For the

lower values of frequencies, it is normal because the sample is highly crosslinked meaning the sample cannot flow. There is also no crossover at high frequencies with values of G'' always smaller than G' meaning that the viscoelastic dissipation that could occur will always be rather low during tensile tests.

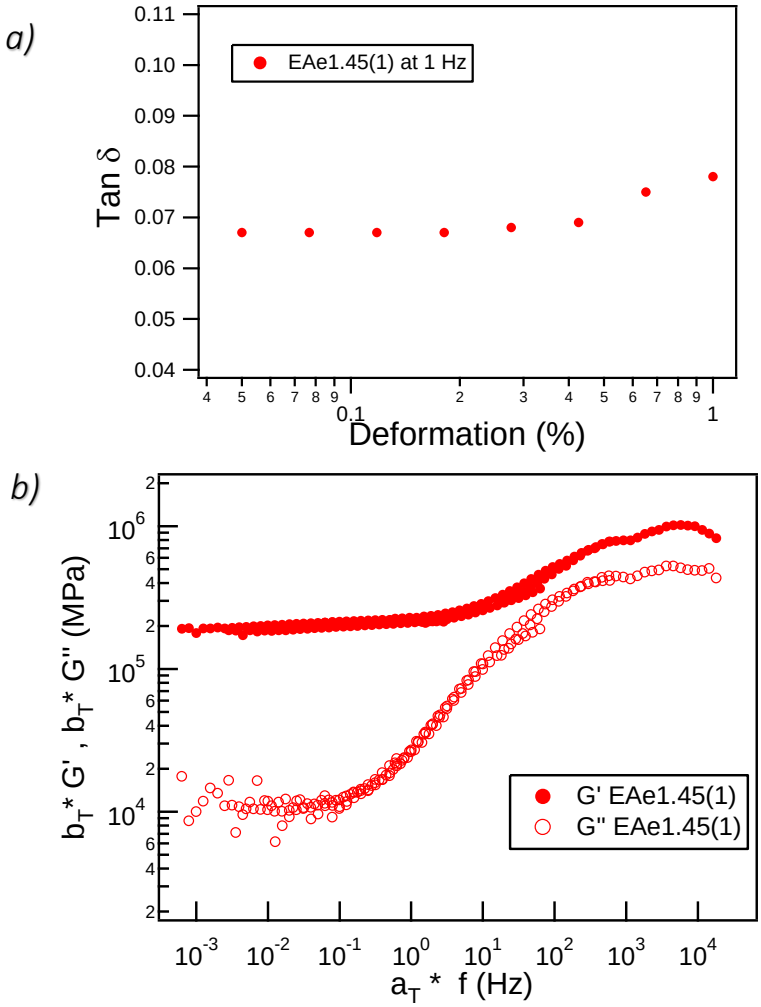

Figure 19: a) Tan δ as a function of the deformation showing a linear regime for EAe1.45(1). b) master curve of G' and G'' for EAe1.45(1) as a function of frequency

After studying the first network alone, the same experiments were carried out for the multiple networks DN and TN. Figure 20 shows the same G', G'' and $tan\ \delta$ for the standard samples SN, DN and TN described previously. The experiment has been carried out over the same range of frequencies and temperatures, then the master curve is constructed and shown for G' and G'' in Figure 20a). This figure shows a difference of plateau modulus of G' with a higher modulus when the number of polymerization steps is increased as it was observed in section III)2). This graph also shows a stable frequency region where G' and G'' are constant, from 10^{-3} to 10^{-1} Hz, this range of frequency has helped us define the strain rate used in uniaxial tension, indeed to avoid viscoelastic dissipation we have decided to use an initial strain rate of 0.025 s^{-1}. From this graph, we can observe that the samples DN and TN show crossover points between G' and G'' at high frequencies which was not the case for the first network SN. These crossover points can be clearly observed on Figure 20b) where the crossing point corresponds to the value of 1 of $tan\ \delta$. Since this only occurs for the multiple networks samples, some additional

viscoelastic dissipation mechanism is present in the multiple networks samples due to a higher value of G'' in comparison to G'. This result will have to be taken into account during our future analysis.

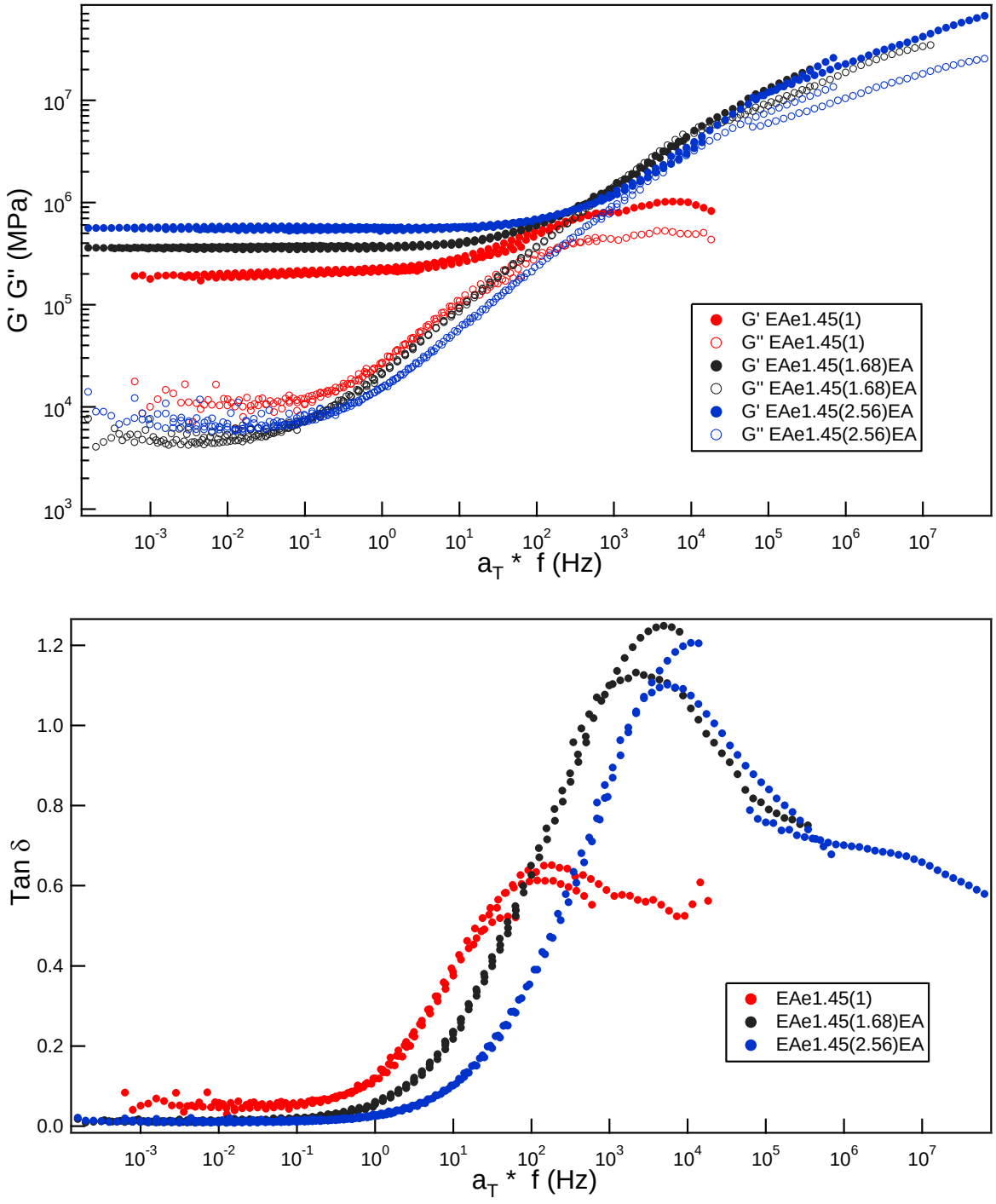

Figure 20a) G' and G'' as a function of the frequency for four different samples. b) Tan δ as a function of the frequency

Performing the small strain study through the rheology of the standard ethyl acrylate samples has led to the definition of a range of strain rates where the uniaxial tensile tests could be carried out and where the samples behave, very elastically in small strain as would conventional elastomers.

Outside of this range where a plateau of G' and G'' have been observed, the value of tan δ is increasing at high frequency meaning that some additional viscoelastic dissipation will occur for those systems at higher strain rates or lower temperatures.

Conclusion

In this chapter, the synthesis technique of the multiple networks has been described. This synthesis permits to create many different multiple network elastomers. We have also seen why the standard synthesis method has been slightly changed from that used by Ducrot [2] by using ethyl acetate for the first network synthesis.

After the synthesis, those networks will be mechanically characterized on different tests that have also been presented in this chapter. The mechanical analysis has been started in this chapter with the display of the viscoelastic properties of the standard multiple network elastomers.

Now that the synthesis and the mechanical tests have been introduced, the following chapters will be presenting the mechanical results for different type of networks.

References

1. Gong, J.P., et al., *Double-network hydrogels with extremely high mechanical strength.* Advanced Materials, 2003. **15**(14): p. 1155-1158.
2. Ducrot, E., *Double Network Elastomers*. 2013, Université Pierre et Marie Curie: Paris.
3. Urayama Kenji, K.S., *Uniaxial elongation of deswollen polydimethylsiloxane networks with supercoiled structure* Polymer, 1997. **38**(4): p. 955-962.
4. Mayo, F.R., *Chain Transfer in the Polymerization of Styrene: The Reaction of Solvents with Free Radicals1.* Journal of The American Chemical Society, 1943.
5. Plessis, C., et al., *Intramolecular Chain Transfer to Polymer in the Emulsion Polymerization of 2-Ethylhexyl Acrylate.* Macromolecules, 2001. **34**(17): p. 6138-6143.
6. Flory, P.J. and J. Rehner, *Statistical mechanics of cross-linked polymer networks II Swelling.* Journal of Chemical Physics, 1943. **11**(11): p. 521-526.
7. Brandrup, J. and E. Immergut, H., *Polymer Handbook*. 1999, New York: Wiley.
8. Gent, A.N., *A New constitutive relation for rubber.* Rubber Chemistry and Technology, 1996. **69**: p. 59-61.

Chapter 3: Mechanical Behaviour in Uniaxial Tension of the Reference Sample Family EAe(1.45)

Chapter 3: Mechanical behaviour in Uniaxial Tension of the Reference Sample Family EAe(1.45)

Introduction

In chapter 2 we have seen the details on how the multiple network elastomers were synthesised. They are made of two types of networks which are interpenetrated, a minority network that is highly crosslinked and prestretched and a majority loosely crosslinked network. Since their physical properties and small strain rheology have been reported in Chapter 2, we now logically turn to their mechanical properties in large strain which need to be characterized in detail. The goal of this chapter is to understand how the structure of the networks controls the non-linear elastic properties, the internal damage in the network and ultimately the strain and stress at break.

A specific set of materials based on the first network EAe1.45(1) and the multiple networks made from swelling it, is used as reference in this work. We first focus on the uniaxial tensile properties of those materials. Then a detailed analysis of the results is carried out to obtain a master curve in uniaxial tension to characterize the mechanical behaviour of every multiple network.

I) Mechanical properties of standard ethyl acrylate networks

It is useful to start with the end point of the previous study and reproduce the methodology of sequential swelling and polymerization developed by Etienne Ducrot [1-3] on a very simple case. Three networks, fully based on the ethyl acrylate monomer and with a crosslinker and initiator compositions of 1.45 mol% and 1.16 mol% were synthesised in one to four steps. Their mechanical properties were tested in uniaxial tension following the protocol described in the previous chapter and the resulting stress-strain curves are shown in Figure 1. The curves obtained are very similar to those shown in Ducrot's thesis [3] by using methyl acrylate as a second network. A large increase in both stress and stretch at break can be observed by comparing the SN and the DN. This increase is also observed with the TN, the difference being that the network appears to soften after the hardening stage (inflexion point in nominal stress) but reaches a higher stress at break than the DN.

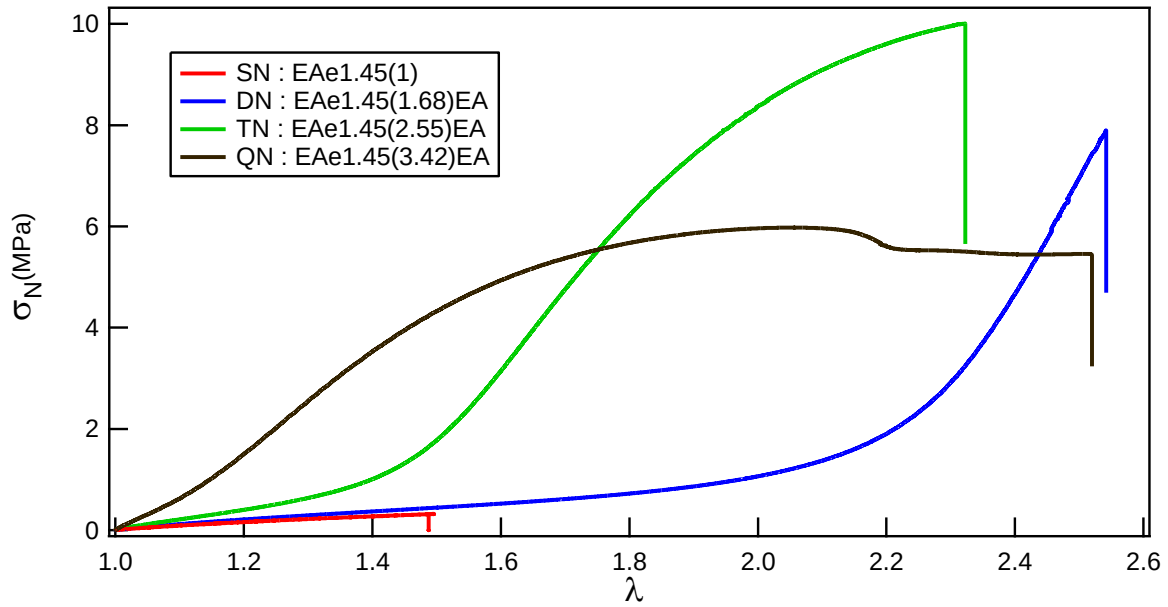

Figure 1: Stress-strain curve of standard ethyl acrylate multiple networks (SN DN TN) and a quadruple network. $\dot{\lambda} = 0.021\ s^{-1}$

These sequential swelling and polymerisation steps change dramatically the mechanical properties of the networks suggesting that further polymerisation steps might lead to further (positive) changes. Therefore, a quadruple network (QN) was synthesised with another step of swelling and polymerizing on a TN, as described in chapter 2. After the synthesis, the sample is dried and its weight and thickness are measured, the stress-strain curve shown in black in Figure 1 corresponds to the QN. This QN stress-strain curve shows a qualitatively different behaviour from the other multiple networks: first the initial modulus keeps increasing to around 6 MPa for the QN while the modulus of the TN was around 2.8 MPa. Then the hardening appears at a lower stretch than the TN, in agreement with the work of Ducrot [1] where the hardening phenomenon is linked with the prestretching, the more prestretched the first network is, the earlier it will reach its maximum elongation. The hardening is, like for the TN, followed by a softening of the material. The main difference comes from the fact that this

time when the material softens, it does not break but leads to a stress maximum that will be called yield stress, following this, a plateau of nominal stress is observed before the failure of the sample. The reason for the occurrence of this plateau of nominal stress can be observed macroscopically on Figure 2. Before the yield stress region, the material deforms homogeneously. This homogeneity is lost after the yield stress and a necked region is created. The necked region is located between the two white arrows, it is characterized on the picture by a reduced width in comparison of the rest of the sample. The two fronts of the necked zone that are delimited by the white arrows on figure 2, move towards the clamps and are expanding the necked zone at constant nominal stress.

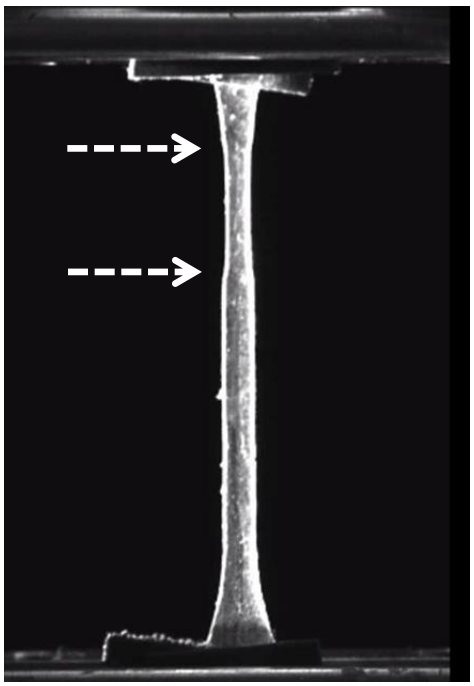

Figure 2: Photo of a sample presenting a necking part (between the two arrows) and two necking fronts (at the white dashed lines) propagating through the entire sample

Figure 1 shows four very different stress-strain curves with significantly different mechanical properties. Since the same first network is used, this change in mechanical behaviour can either be simply explained by the differences in composition (relative amount of stretched first network vs unstretched networks defined in chapter 2 section I)1)c)) or by the experimental protocol, i.e. the different number of swelling polymerisation steps. This last hypothesis can be tested by synthesizing the networks in the presence of added solvent as described in chapter 2 section I)2). The use of a solvent/monomer mix in the swelling step will allow us to compare two multiple networks having the same ratio between second and first networks therefore with the same prestretching λ_0 but made with a different number of polymerization steps. To check this hypothesis, two multiple networks with identical values of λ_0 were synthesised from the same initial first network: a standard double network in two steps and a triple network in three steps. After the synthesis, a uniaxial tensile test was carried out on both samples and the resulting stress-strain curves are shown in Figure 3. This graph shows that the mechanical behaviour in uniaxial tension of both samples is very similar, the only difference being in the strain hardening possibly due to a small difference in prestretching. Figure 3 shows that, with our synthesis strategy and experimental system, the

number of polymerization steps does not appear to be an essential parameter, the prestretching of the first network seems to be more important for a given first network.

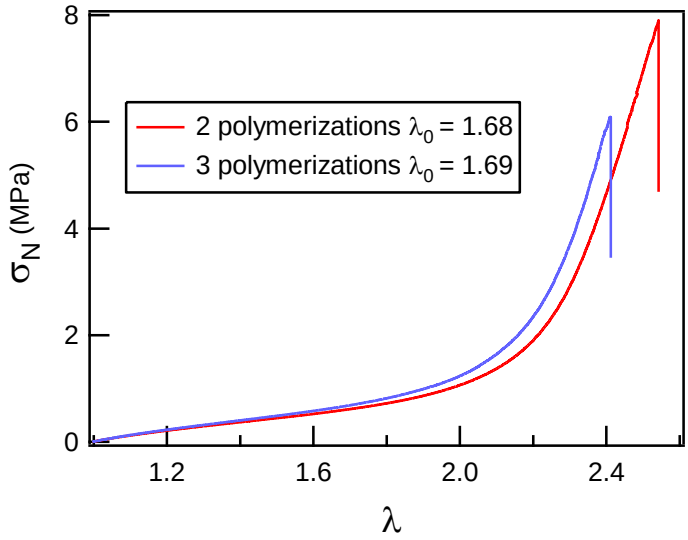

Figure 3: Stress-strain curve of two samples presenting the same prestretching of the first network but a different synthesis path. $\dot{\lambda}$ = 0.021 s^{-1}

To study the influence of this parameter λ_0, a systematic study has been carried out on a set of samples showing a larger range of prestretching levels.

II) Influence of the degree of prestretching λ_0 of the first network in uniaxial tension

1) Set of materials

Following the synthesis procedure described in chapter 2, a family of materials has been synthesised to study the influence of λ_0 for an identical first network. Table 1 summarizes the main characteristics of the multiple networks. When the prestretching of the first network λ_0 changes, so does the percentage of first network. Those two parameters are related by the relationship shown in Eq. (1) as explained in chapter 2 section I)1)c).

$$\lambda_0^{\,3} = \frac{1}{\phi_{SN}} \qquad \textbf{Eq. (1)}$$

Sample name	λ_0	**SN wt% (=100*ϕ_{SN})**	**Type of network**	**Number of polymerization steps**
EAe1.45(1)	**1**	**100**	**SN**	**1**
EAe1.45(1.32)EA	**1.32**	**42.0**	**DN**	**2**

EAe1.45(1.51)EA	**1.51**	**29.2**	**DN**	**2**
EAe1.45(1.68)EA	**1.68**	**20.5**	**DN**	**2**
EAe1.45(2.18)EA	**2.18**	**9.52**	**TN**	**3**
EAe1.45(2.41)EA	**2.41**	**7.39**	**TN**	**3**
EAe1.45(2.55)EA	**2.55**	**6.06**	**TN**	**3**
EAe1.45(2.91)EA	**2.91**	**4.19**	**QN**	**4**
EAe1.45(3.11)EA	**3.11**	**3.53**	**QN**	**4**
EAe1.45(3.27)EA	**3.27**	**3.28**	**QN**	**4**
EAe1.45(3.42)EA	**3.42**	**2.88**	**QN**	**4**

Table 1: Set of samples synthesised with intermediate λ_0 and its influence on the mechanical behaviour domain in uniaxial tension

The synthesis of eleven different samples with values of λ_0 varying from 1 to 3.42 will now highlight the specific role played by λ_0 in controlling the mechanical properties of the material. In Table 1, highlighted lines correspond to the materials of Figure 1 while white lines represent multiple networks with intermediate values of λ_0 relative to the materials shown in figure 1.

2) Uniaxial tensile tests

Every sample was cut in a dumbbell shape and the uniaxial tensile test was performed as described in chapter 2. The results of the uniaxial tests at a constant stretch rate of 0.020 s^{-1} are displayed in Figure 4. The prestretching varies from a starting value of 1 for the SN alone to 3.42 for a highly stretched first network.

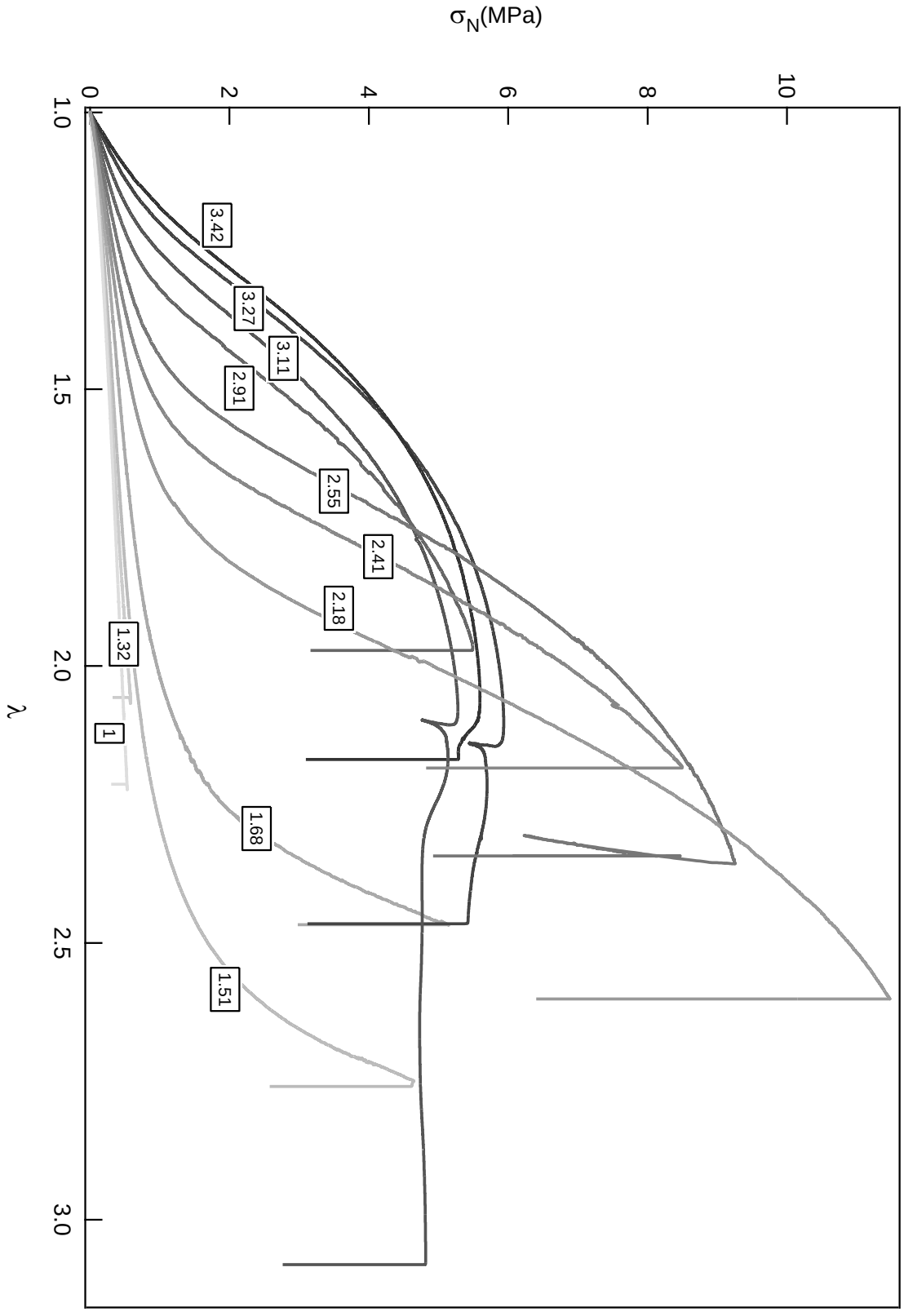

Figure 4: Stress-strain curves of different samples with different values of λ_0. The value of λ_0 is shown in the labels attached to each curve. The gray level increases with the degree of prestretching of the first network Starting from a very light gray for the unstretched simple first network to black for the sample EAe1.45(3.42)EA. $\dot{\lambda} = 0.021\ s^{-1}$

The first observation that can be made on Figure 4 is that as the degree of prestretching of the first network λ_0 increases and its volume fraction decreases, the Young's modulus of the material, i.e. the initial slope of the stress-strain curve keeps increasing as shown in Figure 5. However, the Young's modulus increases non-linearly with λ_0. For that specific first network, a sharp increase in *E* is observed approximatively when λ_0 reaches the value of 2.5-3.

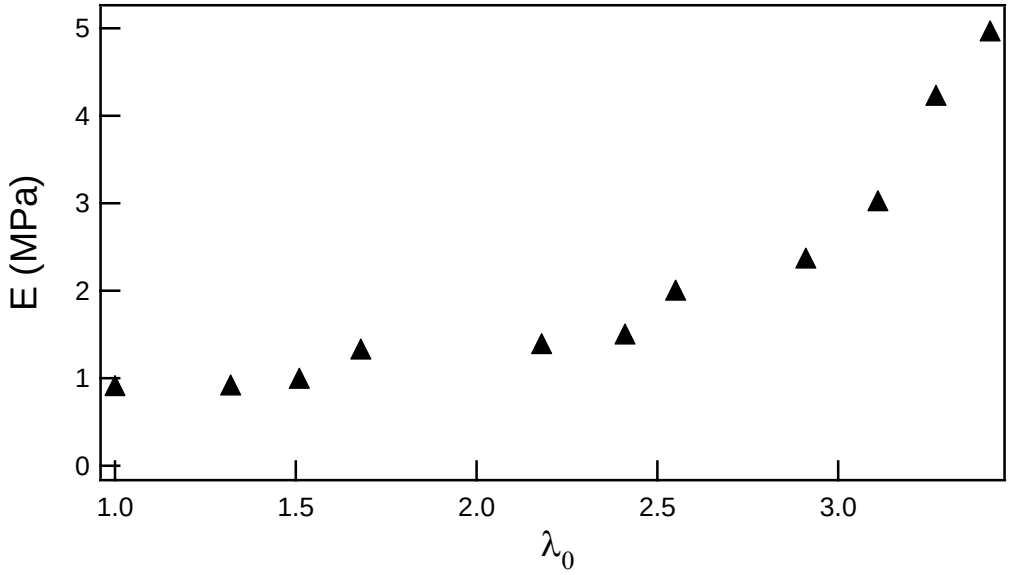

Figure 5: Evolution of the Young's modulus as a function of the degree of prestretching of the first network λ_0

It is worthwhile to discuss the stress-strain curves of Figure 4 in somewhat more detail. The first network on its own EAe1.45(1) has a low modulus and low stress at break with no hardening observed before fracture. This behaviour is normal for a well crosslinked, unentangled and unfilled elastomer. When λ_0 is increased to a value of 1.32 by the addition of a second network it can be observed that the only noticeable difference with the first network alone is coming from the small increase in modulus. However, upon increasing λ_0 to higher values, the modulus keeps increasing and a hardening phenomenon before fracture can be observed for all samples with $\lambda_0 > 1.4$. This hardening is characterized by an increase of the stress slope starting at a certain value of strain called λ_h, different for every value of λ_0. Following this hardening phenomenon, the samples having a $\lambda_0 > 2$ present also a softening in their stress-strain curve, i.e. a decrease of the slope after the hardening with an inflection point. When λ_0 is above 3, a "yield" stress is observed followed by a plateau where the increase in strain occurs at a constant nominal stress as described above.

3) Analysis of the hardening phenomenon

If we focus on the hardening phenomenon, it is clear that the value of λ_0 has an influence on the value of λ_h at which the phenomenon occurs. An increase in λ_0 results in a smaller value of λ_h. This λ_h can be identified more precisely using a strain hardening model and we use here the model proposed by Gent [4]. Gent's model introduces the finite extensibility of the polymer chains and his physical picture is that the hardening corresponds to the deformation

reaching the maximum extensibility of the chains λ_h. This parameter controls mainly the stress and the strain at high deformation as shown in Eq. (2). In this equation, J_1 is the first invariant for uniaxial extension and J_m is the maximum admissible value of this invariant. In essence λ_h corresponds to the elongation where strain hardening kicks in for each multiple network, and is different from but related to the maximum extensibility of the first network itself (which is unknown). This model will be used to fit each of the stress-strain curves of the prepared samples in the same way shown in chapter 2 section III)1). Figure 6 shows an example of the quality of the fit for three different networks.

$$\sigma_N = \frac{E\,(\lambda^2 - \frac{1}{\lambda})}{3\,(1 - \frac{J_1}{J_m})} \qquad \textbf{Eq. (2)}$$

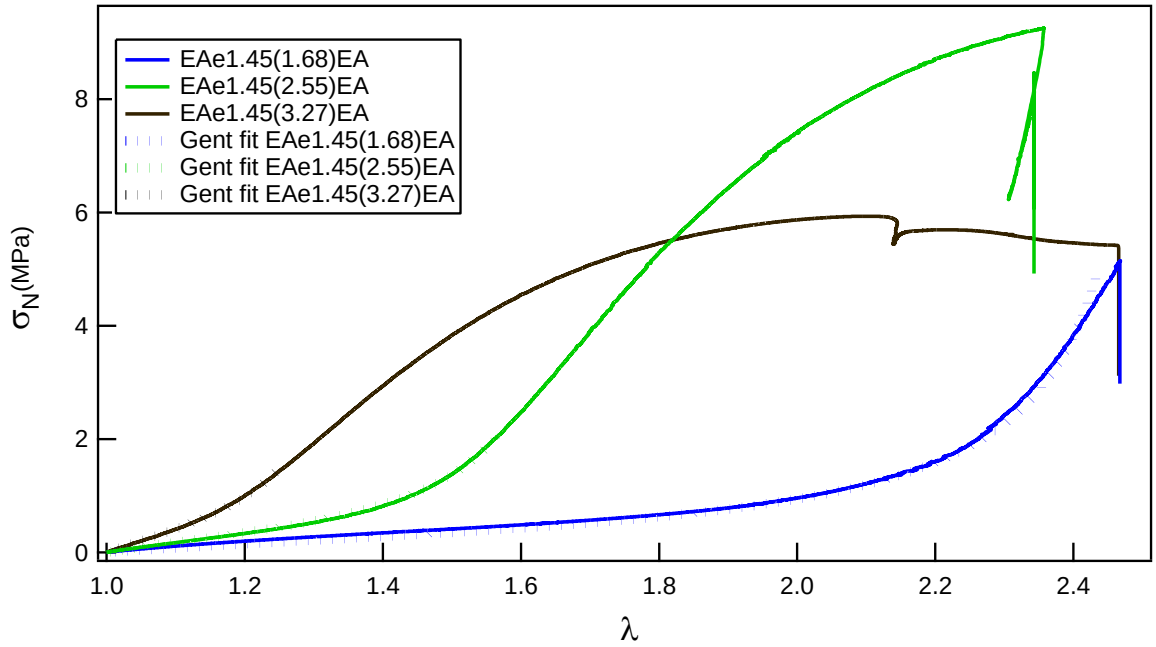

Figure 6: Stress-strain curves of different multiple networks to show the quality of the fit by Gent's model. $\dot{\lambda}$ = 0.021 s^{-1}

Fitting the curve using the Gent model provides a value of J_m corresponding to the maximum value of J_1 that can be observed in our network. The fit was done for each curve shown in Figure 4 and this value was then used to obtain the specific hardening strain of each network λ_h as shown in Figure 7. This graph shows clearly the expected behaviour with J_m decreasing with increasing prestretching of the first network. This demonstrates that the hardening elongation is a decreasing function of λ_0 meaning that as the degree of swelling of the first network increases the hardening occurs at lower strains.

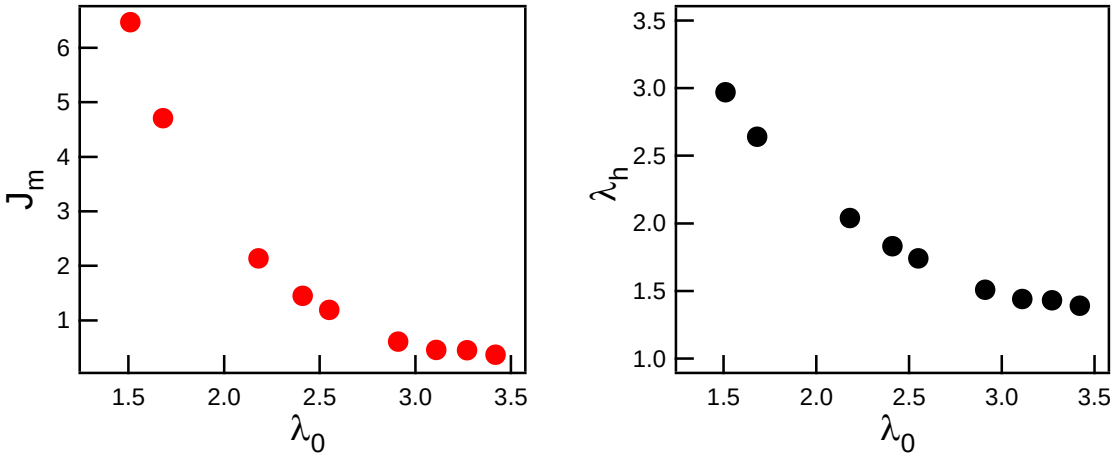

Figure 7: Left: Evolution of J_m with λ_0, right: evolution of λ_h solution of Eq. (4) with λ_0.

For this set of samples, the first network has been kept strictly identical, which means that the first network should have an intrinsic maximum elongation that is constant for every multiple network. The value of this maximum elongation can be theoretically calculated as described in chapter 1 section I)1) by using the maximum extension of a Gaussian chain. The experimental value of the modulus of the first network (0.87 MPa) can be converted to an experimental value of the average molar mass between crosslinks (9.5 kg/mol), leading, for poly(ethyl acrylate), to the number of carbon bonds between crosslinks ≈ 189. The characteristic ratio C_∞ for a poly(ethyl acrylate) network being around 9.67, the estimate of the maximum elongation λ_{limit} gives a value of 3.98. This theoretical value can be compared with the values obtained with Gent's model that measures macroscopic strain hardening.

Since the first network is much more crosslinked than the second network, the assumption can be made that the onset of hardening in multiple networks is controlled by the first network only. If this is true, the maximum elongation of the first network λ_m should be the same in each multiple network with no influence of the degree of prestretching. To verify this assumption, we can use the following procedure: we define the true stretch of the first network chains in the multiple network with Eq. (3) and define it as λ_{cor}. This corrected elongation is obtained by taking as a reference the unstretched chains of the first network in their initial state and assuming that upon swelling, the chains deform isotropically. To obtain the maximal elongation of the first network λ_m in each multiple network, λ in eq (3) is replaced by the value of λ_h obtained from Figure 7 (Eq. (4)). If the first network is responsible for the hardening, the product $\lambda_0 * \lambda_h$ in Eq. (4) should be constant. Figure 8 shows the result for each multiple network. Within 5 % dispersion, the value of λ_m is constant for each multiple network. Also this value is very close to the theoretical value calculated in the previous paragraph.

The result of Figure 8 confirms our hypothesis that, in multiple networks, the elongation where hardening appears, is mainly or even exclusively controlled by the first network. In other words, for the same first network, it will occur at the same value of λ_{cor}. Note that for highly swollen networks (high values of λ_0) the fitting procedure cannot separate modulus and strain hardening very well because the latter appears at relatively low elongation. This could

explain the small deviation from the average for a high level of prestretching as shown in Figure 8.

$$\boldsymbol{\lambda_{cor} = \lambda_0 * \lambda} \qquad \textbf{Eq. (3)}$$

$$\boldsymbol{\lambda_m = \lambda_0 * \lambda_h} \qquad \textbf{Eq. (4)}$$

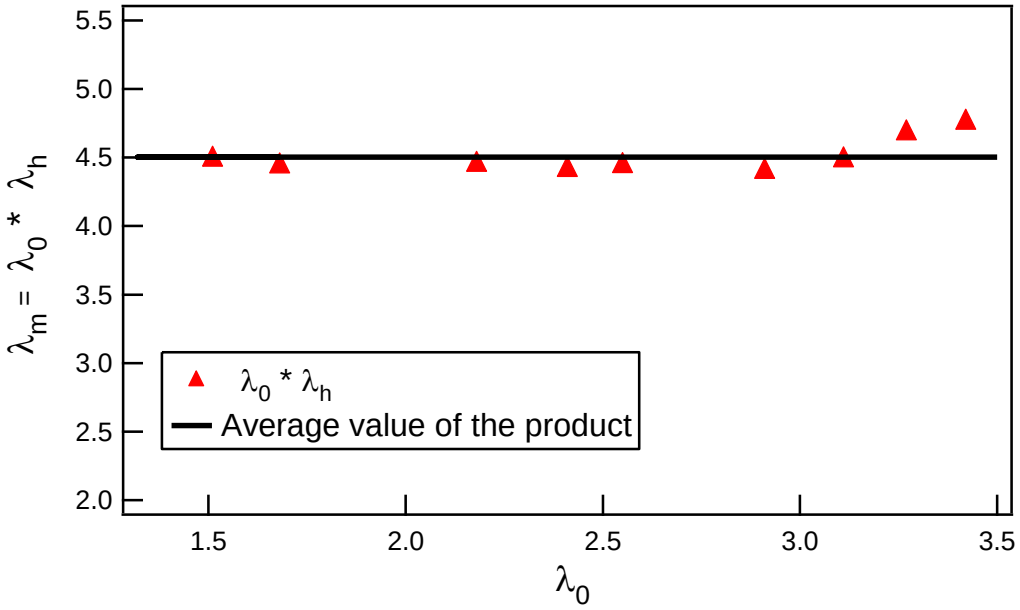

Figure 8: Maximum elongation of the first network λ_m as function of the prestretching of the first network λ_0 showing no dependence on λ_0. The continuous black line is the average value of λ_m

This representation of the maximum extensibility of the first network is based on a fit to Gent's model, and is slightly different from that used by Ducrot[1, 3] but leads to the same conclusion: That the strain hardening is mainly controlled by the structure of the first network. Given that conclusion, it is in principle possible to create a master curve by plotting the nominal stress as a function of λ_{cor} (horizontal shift). This has been done in Figure 9, where the nominal stress is displayed as a function of the true elongation of the first network.

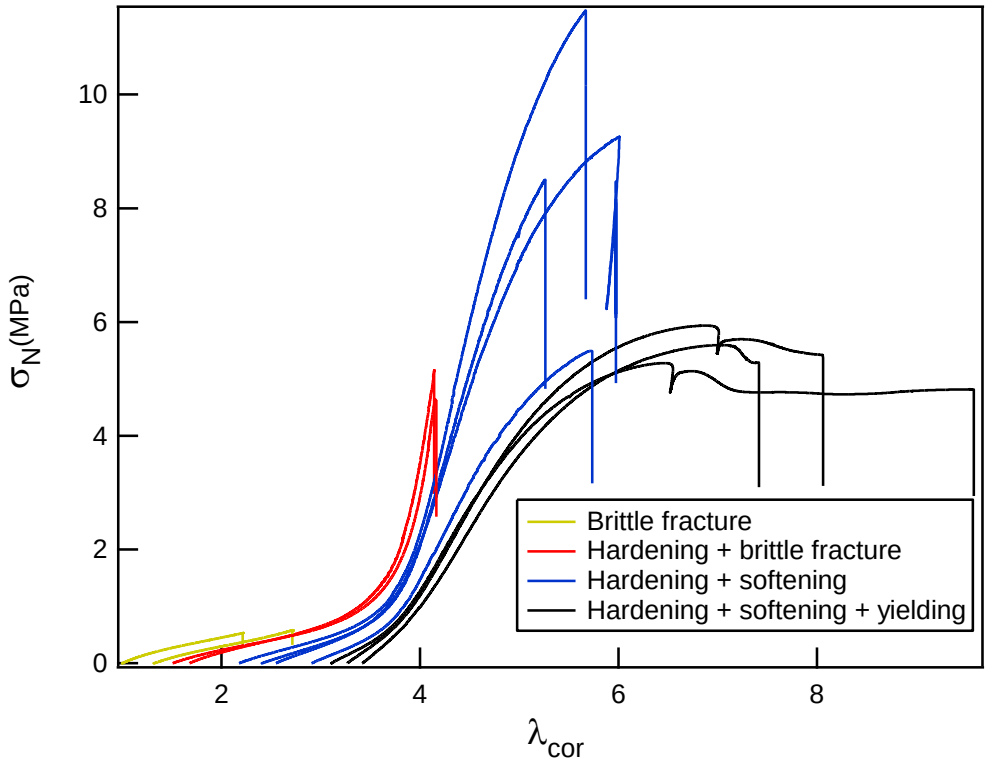

Figure 9: Nominal stress as a function of the corrected strain of the first network showing a hardening area common to every sample made with the same first network. The legend describes the different mechanical behaviours that can be observed depending on the prestretching of the first network. $\dot{\lambda}$ = 0.021 s^{-1}

Figure 9 shows that the hardening kicks in at a common λ_{cor}. This figure also shows a large difference of nominal stress at small strain, this can be changed by empirically applying a vertical shift in order to obtain the best match with the initial part of the first network stress-strain curve. The stress correction that is applied by this shift of the curves is justified by the increase in modulus due to their higher pre-extension but also to the increase in crosslink and entanglement density. The master curve for the materials of Figure 4 is then plotted on Figure 10.

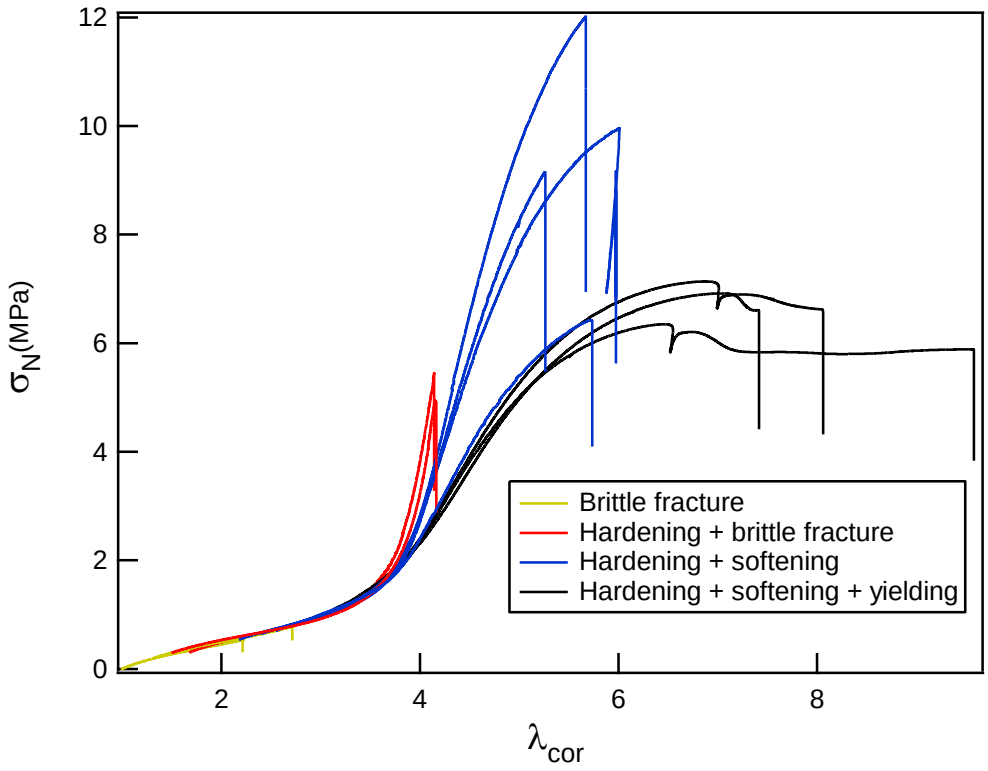

Figure 10: Master curve of the nominal stress as a function of the corrected strain of the first network showing a hardening area common to every sample made with the same first network. The legend describes the different mechanical behaviours that can be observed depending on the prestretching of the first network and an empirical vertical shift has been applied to the data to match the initial part of the curve. $\dot{\lambda} = 0.021\ s^{-1}$

The graph in Figure 10 shows that the first part of the curve appears to correspond to a master curve with all the samples collapsing on the same curve up to the onset of the strain hardening which appears for all the curves around $\lambda_{cor} = 3.8$. However, while all the samples display some hardening, the slope of the strain hardening is not similar for all samples suggesting that something is missing in the analysis.

The preceding section focused on the influence of λ_0 on the uniaxial mechanical properties to fracture. We observed some major differences in mechanical behaviour in uniaxial extension and our materials can be classified into four different categories based on these tests shown in figures 4 and 9: for low λ_0 brittle fracture at relatively low strain is observed, then for $1.5 < \lambda_0 < 2$ a hardening phenomenon is observed in large strain leading to a much higher stress at break. The third class of materials for $2 < \lambda_0 < 3$, are those showing a hardening followed by a softening and finally for $\lambda_0 > 3$ the materials display a yield stress with a necking appearing macroscopically. Those different types of material behaviours are highlighted in different colors in Figure 10. To understand what is happening at a molecular scale during the different steps of hardening, softening and necking, the hysteresis of the different samples has to be investigated through cyclic load/unload experiments. This will allow us to quantify the level of damages occurring during the increase in strain in the different types of samples and will help us to refine the interpretation of the differences observed.

4) Behaviour of the samples under cyclic tensile tests

While monotonic uniaxial tensile experiments to rupture are useful to determine the materials strength and modulus, they cannot distinguish between reversible and irreversible deformations and between elasticity and dissipation. Such a distinction requires cyclic tests. For many complex soft solids, hysteresis can be divided between the first cycle and the stabilized cycle. The previous work of Ducrot showed that the stabilized cycle hysteresis (due to viscoelasticity) is extremely low for these well crosslinked and unfilled elastomers. However the first cycle hysteresis, corresponds to a permanent damage or change in structure in the material. This damage can be recoverable or not over long times or annealing procedures but again previous work [2, 3] has shown that for multiple networks made with covalent bonds only, the damage is irrecoverable and due to bond breakage. The purpose of the next section is to quantify this irrecoverable damage observed in the materials with variable λ_0 as a function of applied stretch.

This requires step-strain cyclic experiments (presented in chapter 2 section II)2)) that can be used to quantify the extent of damage occurring in the multiple networks during the deformation in large strain through the quantification of the hysteresis. This hysteresis is measured between the first loading curve and the third unloading curve. The set of materials with different λ_0 that have been studied through uniaxial tests behave differently in cyclic experiments.

Steps cycle tests are carried out on the different samples used in the previous part. Figure 11a) shows the cyclic experiment done on a network EAe1.45(1.68): the loading-unloading curve is very similar to the monotonous uniaxial tension curve meaning that no hysteresis is observed during the entire experiment. The absence of hysteresis between loadings and unloadings at different maximal elongations strongly suggests that the material undergoes minimal damage in the bulk before a crack propagates and macroscopic breakage occurs. For materials displaying some softening in uniaxial tension, the corresponding cyclic experiment is shown in Figure 11b). A large difference can be observed with Figure 11a), i.e. starting at an elongation of 1.6, hysteresis is observed for every new cycle to a higher value of λ while no hysteresis is observed in subsequent cycles, to the same λ suggesting some damage. Despite the presence of some damage inside the material, the modulus does not appear to decrease significantly with increasing stretch.

Finally, Figure 11c) shows a cyclic experiment for a sample with a macroscopic yield stress: this sample displays a very different behaviour. First the hysteresis starts to appear at a low value of λ around 1.3. Then the hysteresis continues to increase after the yield point (λ = 2.2) quantifying the increasing damage as the necked region propagates along the sample. Finally, the nominal stress increases again as the necked region has fully propagated through the sample. This second hardening at very large strain was not observed in standard uniaxial tension (breakage during the propagation of the necked area) but can be observed if the experiment is carried out at a very low stretch rate suggesting that some time-dependent effects may be active in the damage process itself.

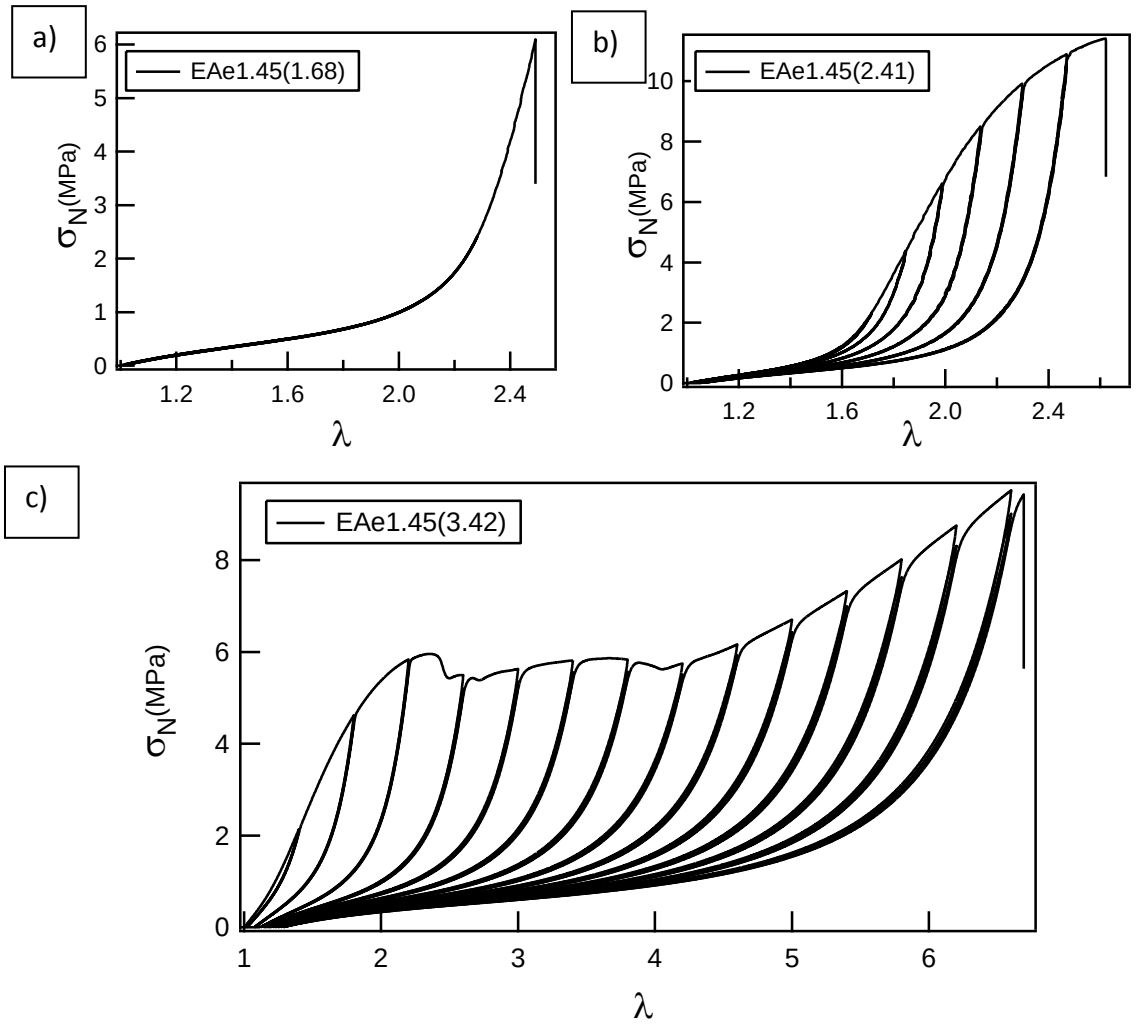

Figure 11: Cyclic experiment done on a) a sample from domain 2 presenting no hysteresis b) a sample from domain 3 presenting some softening resulting in some hysteresisc) a sample from domain 3 showing large hysteresis and a second hardening. $\dot{\lambda} = 0.020\ s^{-1}$

Another noticeable phenomenon observable in Figure 11c) is the evolution of the Young's modulus as the maximum deformation applied λ_{max} increases. After damage starts and in particular when necking kicks in, the modulus clearly decreases dramatically with increasing λ_{max}, something which is not observed for multiple networks with lower values of λ_0. A 20% decrease in modulus was also noticed by Ducrot [3] in his TN, corresponding roughly to the sample shown in Figure 11b) but for sample EAe1.45(3.42) the decrease appears to be more of the order of 80% (Figure 12).

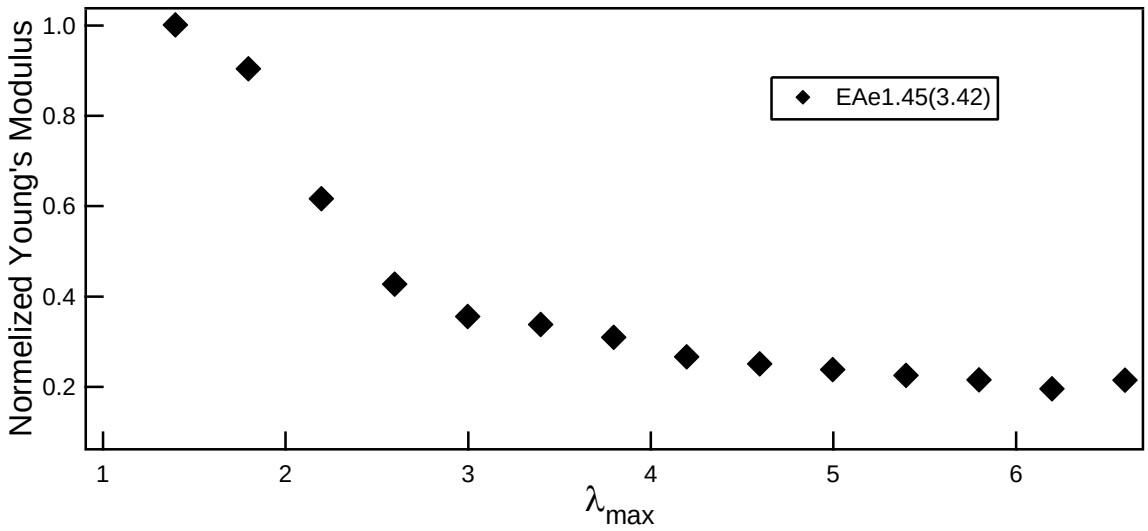

Figure 12: Evolution of the normalized Young's modulus with the maximum deformation

Figure 12 shows that the modulus evolves in a nonlinear way with λ_{max}. As discussed in Figure 5, for this high level of λ_0 the initial modulus is expected to be linked with the degree of prestretching of the first network. Therefore, we can assume that this decrease in modulus observed in parallel with a large hysteresis must be due to some chain breaking in the first network. Ducrot et al. [2] proposed a method to study quantitatively the chain breakage by making the hypothesis that the Lake-Thomas mechanisms of energy dissipation is active for every broken strand of the first network. Note that after the breakage of some bonds of the first network, locally, the stress needs to be carried by the second network. This second network needs to be present in a sufficient amount to prevent the propagation of a macroscopic crack. Since the hysteresis is observed at low stretch in comparison to the deformation needed to break the second network on its own (around $\lambda = 6$), we assume that the bonds that break before the failure of the entire sample belong to the first network. . Another point to reinforce that hypothesis is that due to the nature of the architecture of multiple networks, if the second network starts to break the entire sample fails.

5) Analysis of the damage occurring in the first network

The hysteresis energy per cycle $U_{hyst}(n)$ can be measured for each cycle by measuring the area located between the loading curve of the 1st cycle up to a certain λ_{max} and the loading of the third cycle to that same λ_{max} as described in Eq. (5). This procedure is used to subtract viscoelastic dissipation from the overall dissipation during the first cycle and take into consideration only permanent dissipation as explained in chapter 2. The value of energy dissipation obtained from the use of Eq. (5) on each increment of stretch is shown as a function of λ_{max} in Figure 13. From this figure, it can be seen that the hysteresis increases for each cycle until reaching a plateau corresponding to the yield stress and the necking. Then a second increase of hysteresis is observed showing that some more damages are occurring after the necking process.

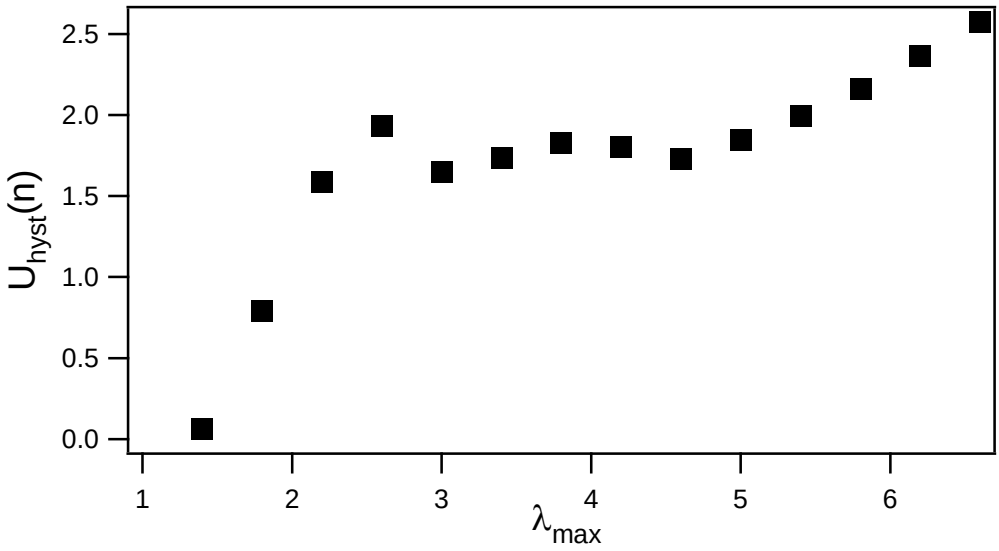

Figure 13: Hysteresis per cycle as a function of the maximal elongation reached λ_{max} for the sample EAe1.45(3.42)EA.

With the values shown in Figure 13, Eq. (6) gives the cumulative hysteresis $U_{hyst\ total}(n)$ for a given number of cycles n. Then, if the breakage of the chains of the first network is uniquely responsible for the dissipated energy of each cycle it is possible to estimate an amount of broken chains corresponding to the energy dissipated during each cycle. To do so, the energy released by a broken chain of the first network has to be estimated. This estimate is based on the Lake and Thomas theory presented in chapter 1 section I)6), with the energy dissipated by the scission of a bond in a stretched chain corresponding to the bond energy of each carbon bond of the chain (one C-C bond dissipates 360 kJ/mol) being stretched and broken. Using this assumption the energy that can be released by the breakage of every bond of the chains of the first network can be estimated (see Eq.(7)) and therefore an average percentage of broken chains $\phi_{first\ netwwork}$ can be calculated for each value of λ_{max} as shown in Eq. (8). Of course this will only be a rough estimate and shorter chains are likely to break first so that this value will probably be a lower bound.

$$\boldsymbol{U_{hyst}(n) = \int_{1}^{\lambda(n)} \sigma_N(1st\ cycle)d\lambda - \int_{1}^{\lambda(n)} \sigma_N(3rd\ cycle)d\lambda} \qquad \textbf{Eq. (5)}$$

$$\boldsymbol{U_{hyst\ total}(n) = \sum_{i=1}^{n} U_{hyst}(n)} \qquad \textbf{Eq. (6)}$$

$$\boldsymbol{U_{tot\ 1^{st}\ network} = \frac{\phi_{1^{st}} * \rho_{PEA} * 2 * U_{C-C}}{M_{EA}}} \qquad \textbf{Eq. (7)}$$

$$\boldsymbol{\phi_{first\ network}(n) = \frac{U_{hyst\ total}(n)}{U_{tot\ 1^{st}\ network}} * 100} \qquad \textbf{Eq. (8)}$$

To compare the different percentages of broken chains, the calculation is carried out for different multiple networks with different values of λ_0 and the results are shown in Figure 14. Obviously, the networks that did not show any detectable softening and hysteresis, do not show any amount of broken chains. This means that no or few bonds are broken in the bulk

before a macroscopic crack propagates. On the other hand, networks that soften in uniaxial tension show some bond scission up to about 1 % of the first network when the macroscopic failure of the sample occurs. This low amount of broken chains can explain the small decrease in modulus observed for those samples. Finally, samples that display a yield stress and a very large hysteresis are showing a high amount of broken chains, up to 10 % when the sample reaches failure after the second hardening. With the assumptions discussed above, Figure 14 shows the percentage of the first network chains that break before macroscopic failure of the sample. Note that the samples with $\lambda_0 > 3$, necking is observed and the increase in broken bonds corresponds (during the propagation of the neck) to the increase in volume of the necked part of the sample and not to the density of broken bonds. For λ_0=3.42 the neck has finished propagating for λ=4.3 and this corresponds to about 4.5% of broken bonds and is the critical value of broken bonds necessary for necking.

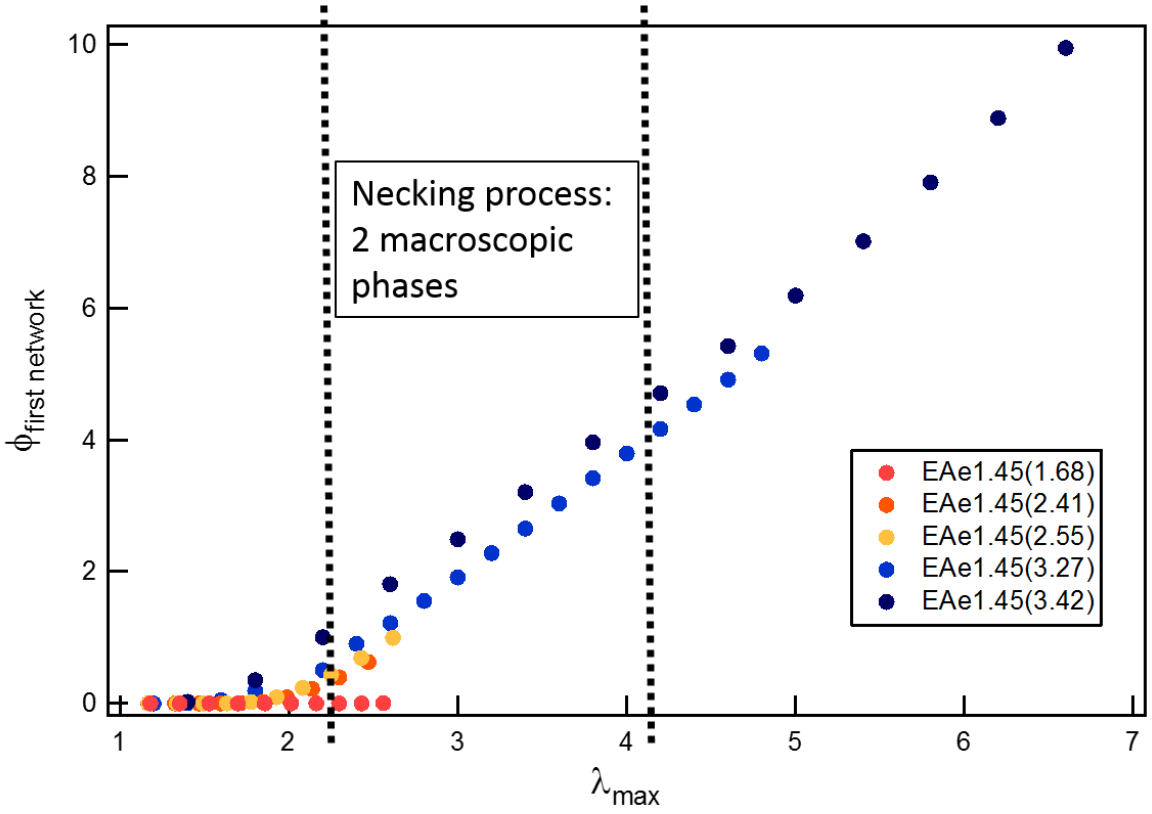

Figure 14: Fraction of broken chains in the first network as a function of the maximal deformation. The two black dashed lines are delimiting the necked region, in this area two phases are observed.

This estimate illustrates the importance of the necking (or widespread damage) phenomenon in order to dissipate the maximal amount of energy through broken chains. This necking phenomenon is only observed when the first network is highly prestretched in the multiple network elastomer.

In summary, the systematic study of the hysteresis has shown that a large fraction of chains can be broken in the first network (up to 10 %) before the sample fails macroscopically. This fraction of broken bonds at failure is however highly dependent on the level of prestretching of the first network and appears to greatly influence the strain and stress at break suggesting that it plays a major role in controlling crack nucleation and propagation.

6) Master curve using the damages and the dilution of the 1st network

In the previous step cycles experiments, we have seen that the damages observed in the different multiple networks change largely with the prestretching. The damages start after the hardening during the softening part and it is at the onset of the softening part that the master curve in Figure 10 fails to capture the mechanical behaviour. The correction done to the stress in Figure 10 was relevant only for the small strain part of the curve up to the hardening. From the study of the hysteresis due to chain breakages in the 1st network, we can assume that the damages of the first network have a role in the slope of the softening. Those damages are occurring in the plane normal to the tensile direction, therefore we expect the areal density of the 1st network in that plane to have an impact on the level of softening. The surface density of the first network for each network $\Sigma_{SN(Multiple\ Network)}$ can be approximately calculated from that of the initial 1st network using Eq. (9) and using the fraction of the first network ϕ_{SN}. Therefore, if we assume that the stress is fully carried by the first network chains in the strain hardening and softening region, a correction of the nominal stress by ${\phi_{SN}}^{2/3}$ would take into account the dilution of the first network chains for each multiple network. If such corrected stress per fractional area of first networks chains is plotted as a function of the stretch of first network chains λ_{cor} as defined in equation 5, one obtains Figure 15.

$$\boldsymbol{\Sigma_{SN(Multiple\ Network)} = \Sigma_{SN}{\phi_{SN}}^{2/3}} \qquad \textbf{Eq. (9)}$$

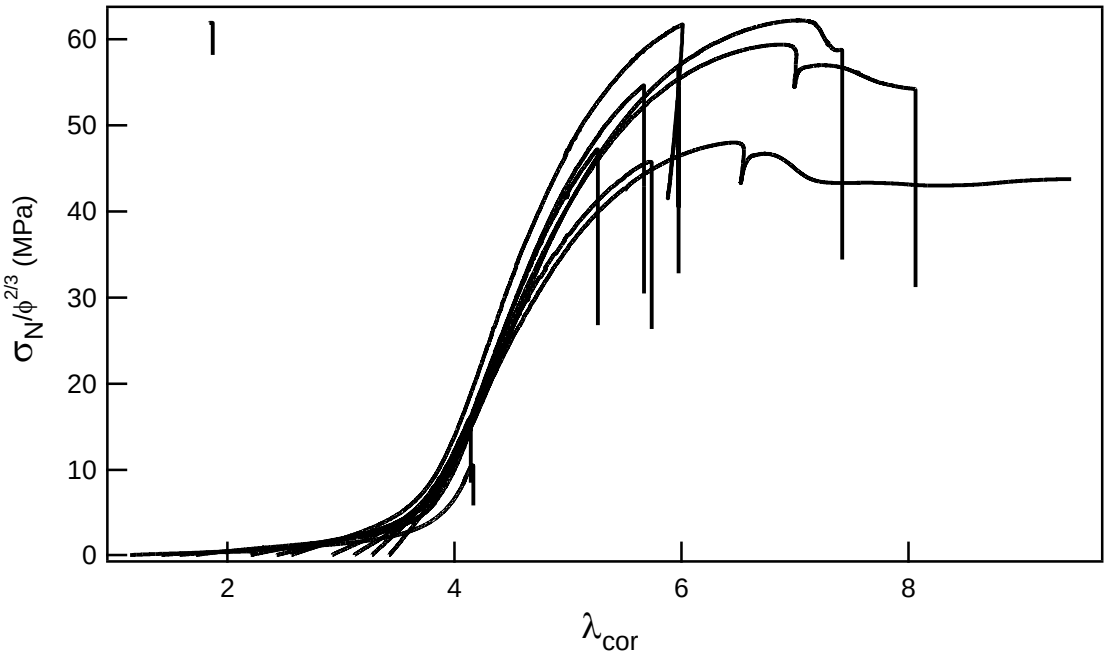

Figure 15: Corrected nominal stress as a function of the corrected elongation λ_{cor}. $\dot{\lambda}$ = 0.021 s^{-1}

In Figure 15, it can be seen that the correction of the nominal stress by the dilution in the plane normal to the tension gives a master curve. On the other hand, this correction is only valid for the large strain part of the curves, the small strain part is clearly controlled by the complete network and the necking stress is not described by the dilution factor alone.

7) Summary

In uniaxial and cyclic experiments, this series of multiple networks displays important differences of mechanical behaviour with increasing λ_0. The different materials can be classified into four types of mechanical behaviours delimited by precise values of λ_0 for a given crosslink density.

- For λ_0 between 1 and 1.4, there is no improvement of the elongation at break or of the stress at break. We define this regime as Type 1.
- For $1.4 < \lambda_0 < 2$, we start to observe a strain hardening phenomenon followed by a brittle fracture, the fracture occurs before any damage is observed in the bulk sample as shown through cyclic experiments. The presence of hardening results in a very significant increase of the stress at break. This type of behaviour will be referred to as Type 2.
- For $2 < \lambda_0 < 3$, we reach a mechanical behaviour (referred to as Type 3) where the hardening is followed by a softening and the cyclic experiments, show that some permanent damages occurs in the bulk before failure leading to even higher stresses and elongations at break.
- Finally, if $\lambda_0 > 3$ a very early hardening, followed by a softening up to a yield point where the elongation keeps increasing at a constant nominal stress and a necking is observed. This Type 4 behaviour is characterized by extensive damage occurring in the necked region (up to 10 % of the first network chains can be broken) and a significant decrease of the Young's modulus.

Some interpretation can be now tentatively provided. The key point to understand is that the change in λ_0 modifies both the level of macroscopic stretch where chains break (from Figure 7) but also their volume fraction and hence the stress that can be carried by the other networks when the first network chains are broken.

The transition from Type 1 to Type 2 is probably triggered by the progressive decrease in the volume fraction of the first network. Making it possible for the 2nd network chain to accommodate the transfer of stress between the broken chains of the first network and the yet unstretched ones of the second. However, breakage of these moderately prestretched chains only occurs at high values of lambda, and hence at the crack tip but not in the bulk.

The transition from Type 2 to Type 3 occurs when the first network chains start to break in the bulk before fracture occurs and finally type 4 correspond to widespread damage in the bulk and the stress and strain at break are now controlled by a second network filled with fragments of the broken first one. Such complex behaviour suggests strongly that the breakage is not uniform as suggested by Brown [5] in his very insightful model and will be discussed in a later section.

The careful investigation of the effect of the degree of prestretching λ_0 has shown the importance of this parameter, which appears to be determinant for a given first network. The knowledge of the value of λ_0 controls the mechanical behaviour observed in uniaxial tension.

Table 2 shows that the number of polymerization steps does not describe well the mechanical behaviour, but the value of λ_0 only has to be considered for a given first network.

However, λ_0 is not the only parameter needed to fully describe our material, indeed we can expect a change in mechanical properties also

- when the amount of crosslinker in the first network is changed influencing therefore the value of λ_{max} (that would be changed in Figure 8) and
- when the volume fraction of the second network is changed, which can be done by replacing polymer with solvent in the third and fourth steps of swelling polymerization.

Sample name	λ_0	SN wt%	Type of network	Number of polymerization steps	Type of behaviour
EAe1.45(1)	**1**	**100**	**SN**	**1**	**1**
EAe1.45(1.32)EA	**1.32**	**42.0**	**DN**	**2**	**1**
EAe1.45(1.51)EA	**1.51**	**29.2**	**DN**	**2**	**2**
EAe1.45(1.68)EA	**1.68**	**20.5**	**DN**	**2**	**2**
EAe1.45(2.18)EA	**2.18**	**9.52**	**TN**	**3**	**3**
EAe1.45(2.41)EA	**2.41**	**7.39**	**TN**	**3**	**3**
EAe1.45(2.55)EA	**2.55**	**6.06**	**TN**	**3**	**3**
EAe1.45(2.91)EA	**2.91**	**4.19**	**QN**	**4**	**3**
EAe1.45(3.11)EA	**3.11**	**3.53**	**QN**	**4**	**4**
EAe1.45(3.27)EA	**3.27**	**3.28**	**QN**	**4**	**4**
EAe1.45(3.42)EA	**3.42**	**2.88**	**QN**	**4**	**4**

Table 2 : Description of the studied samples, addition of the notion of mechanical domain

III) Mechanics of solvent swollen multiple networks: Decorrelation between λ_0 and ϕ.

1) Experimental method

In DN gels, the degree of prestretching of the first network and the ratio of first to second network can be easily separated either by using a stent [6] to change the stretching of the first network or a change in the pH or the ionic fraction to change the degree of swelling of certain polyelectrolytes. In elastomers, this change cannot be done in the same way. To separate the influence of λ_0 and ϕ_1 (the mass fraction of the first network), it has been chosen to use different solvents to swell the networks. The goal was to stretch the first network but at the same time to dilute the second network in comparison to the samples studied at the beginning of this chapter.

To avoid the evaporation of the solvent during the mechanical tests, all solvents used have a relatively high boiling point. Three solvents have been selected: dimethylsulfoxyde (DMSO), 1-methyl-2-pyrrolidone (MPD) and acetophenone (ATP). Two networks were synthesised for this experiment: one of type 2: EAe1.45(1.68)EA and one of type 3: EAe1.45(2.53)EA. Samples of those two materials were swollen to equilibrium into the different solvents. Once the equilibrium is reached the dimensions of the samples were measured and a uniaxial tension test was carried out. Table 3 displays the different swelling ratios that could be obtained with those three particular solvents, with λ_s being the chain stretching due to the swelling of the elastomer by the solvent only. As expected the degree of prestretching imposed by the swelling is smaller with similar solvents for the type 3 sample that is already more prestretched. It can be seen that the sample EAe1.45(2.53)EA swollen in ATP can reach a swelling close to that of EAe1.45(3.42)EA.

Materials	**Solvent**	**Stretching due to solvent (λ_s)**	**Total λ_0 of first network chains**	**Young's modulus (MPa)**
EAe1.45(1.68)EA	**None**		**1.68**	**1.21**
EAe1.45(1.68)EA	**DMSO**	**1.32**	**2.22**	**1.02**
EAe1.45(1.68)EA	**MPD**	**1.49**	**2.5**	**1.09**
EAe1.45(1.68)EA	**ATP**	**1.6**	**2.69**	**1.36**
EAe1.45(2.53)EA	**None**		**2.53**	**1.58**
EAe1.45(2.53)EA	**DMSO**	**1.24**	**3.14**	**3.62**
EAe1.45(2.53)EA	**MPD**	**1.31**	**3.31**	**4.37**
EAe1.45(2.53)EA	**ATP**	**1.37**	**3.47**	**6.48**
EAe1.45(3.42)EA	**None**		**3.42**	**4.93**

Table 3: Samples used to separate the influence of λ_0 and ϕ

The stress-strain curves of these solvent swollen samples are shown in Figure 16. Note that the first test carried out on the sample EAe1.45(2.53)EA swollen in DMSO slipped in the clamps. Figure 16 shows the second test on the same sample which explains the different shape of the second light blue curve.

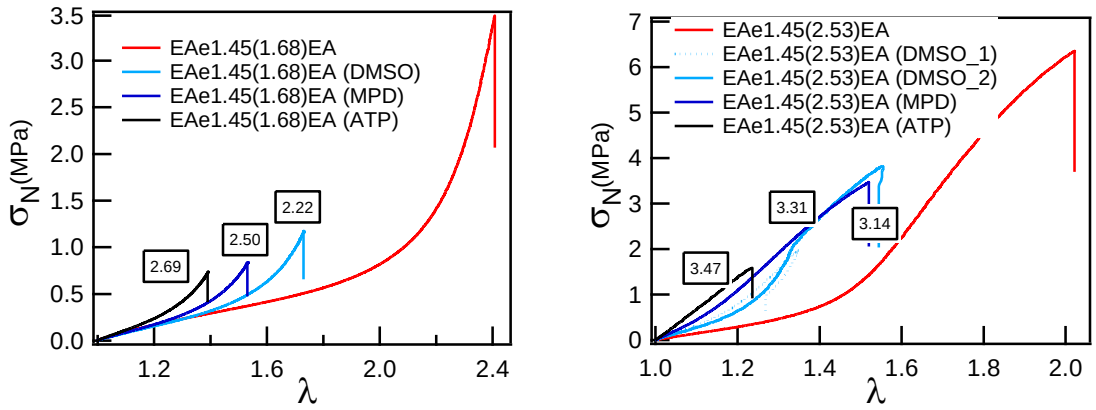

Figure 16: Stress-strain curves of multiple networks swollen in different solvents. Left starting from the sample EAe1.45(1.68)EA and right starting from the sample EAe1.45(2.53)EA. $\dot{\lambda}$ = 0.020 s^{-1}. Values on the graph correspond to the final values of λ_0.

The first result from Figure 16 is that the swelling of both samples in solvent dramatically weakens the mechanical properties. Indeed a sharp decrease in elongation and stress at break can be observed especially for the sample EAe1.45(1.68)EA. The second more interesting result concerns the Young's modulus, the different values of E were measured and compared to those shown in Figure 5 obtained after polymerization of ethyl acrylate monomer and plotted as a function of λ_0.

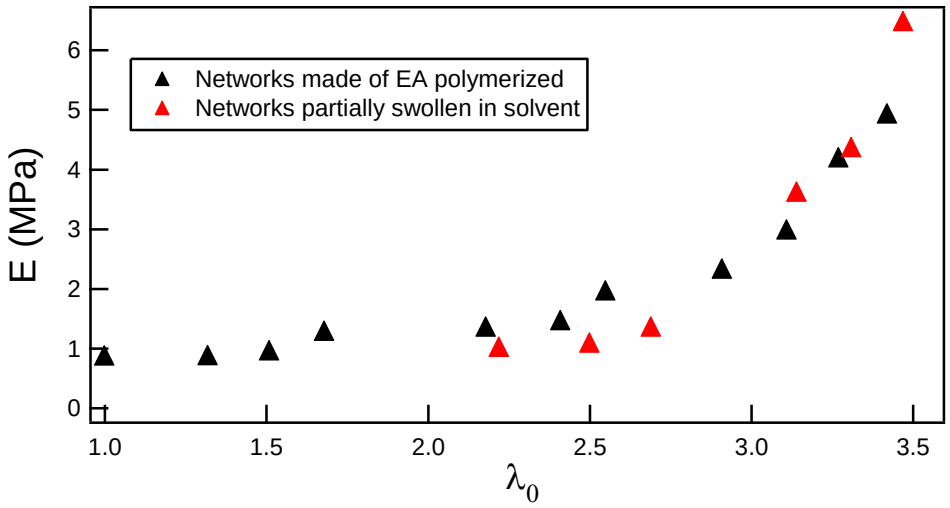

Figure 17: Evolution of the modulus as a function of the total λ_0 for standard samples and for samples partially swollen in solvent.

Figure 17 shows that for values of prestretching between 2 and 3, the samples swollen with solvent have lower moduli than those swollen with polymer. This effect was expected, since the solvent dilutes the elastic chains by swelling the network and does not add any entanglements. This dilution leads to a decrease of the concentration of the elastic chains that

is linked to the Young's modulus as seen in chapter 1 section I)5). Therefore, a dilution by solvent normally reduces the Young's modulus but this was not observed for values of prestretching above 3. Indeed, Figure 17 shows that at high values of λ_0, above 3, the values with or without solvent don't change. It can be assumed that the effect of the dilution is negligible and the modulus is mainly driven by the nonlinear behaviour of the prestretched chains of the first network than by the unswollen chains of the second or third network which lead to similar values for the two types of samples.

2) Comparison between samples with similar λ_0

Considering the degree of stretching of the first network that can be obtained for those swollen samples, it is interesting to compare those stress-strain curves with some classic multiple network samples with similar values of λ_0. The results are presented in Figure 18. Interestingly the onset of the hardening still occurs at roughly the same elongation and at very similar stress levels for every sample despite the presence of solvent. However, the elongation at break and stress at break are much lower for the samples swollen in solvent. The difference with the samples containing polymer instead of solvent is particularly significant for the samples with a λ_0 smaller than 3 where fracture occurs at the onset of the hardening.

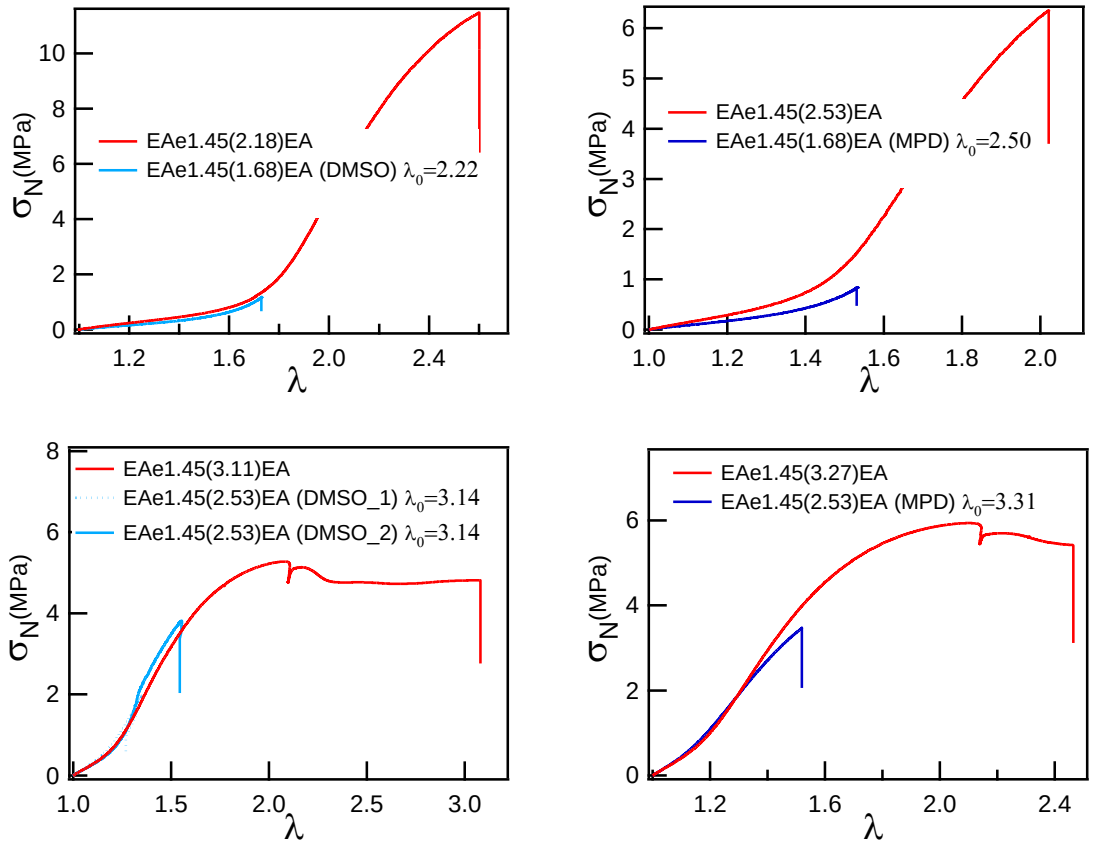

Figure 18: Stress-strain curves of swollen solvent in comparison with samples showing a similar prestretching. $\dot{\lambda}$ = 0.021 s^{-1}

In summary, the influence of the solvent on the Young's modulus appears to be negligible at high values of λ_0, suggesting that in this regime the modulus is controlled by the highly diluted stretched chains alone. At smaller λ_0 the change in modulus is due to the combined effect of a dilution of the elastic chains and the increased stretching of the first network chains.

To complete the characterization of this set of samples, hardening is studied. The same methodology used in chapter 2 section III)1) can be applied here: uniaxial tensile curves can be fitted to the Gent model, and J_m and λ_h can be extracted. It should be noted that since no hardening is detectable for EAe1.45(2.53)EA swollen in acetophenone (Figure 16), the fit could not be applied to this sample. Results of the maximum extensibility of the first network chains is shown in Figure 19 alongside results of Figure 8 for classic multiple networks. The average value of the blue triangles (swollen samples) is slightly smaller than that of the red triangles, but this might be due to the fact that the first networks used for the different sets of data are not exactly the same which could lead to small changes as explained in chapter 2. Nevertheless, the tendency is very similar for both sets of data with a constant value of λ_m controlling the onset of the hardening according to Gent's model.

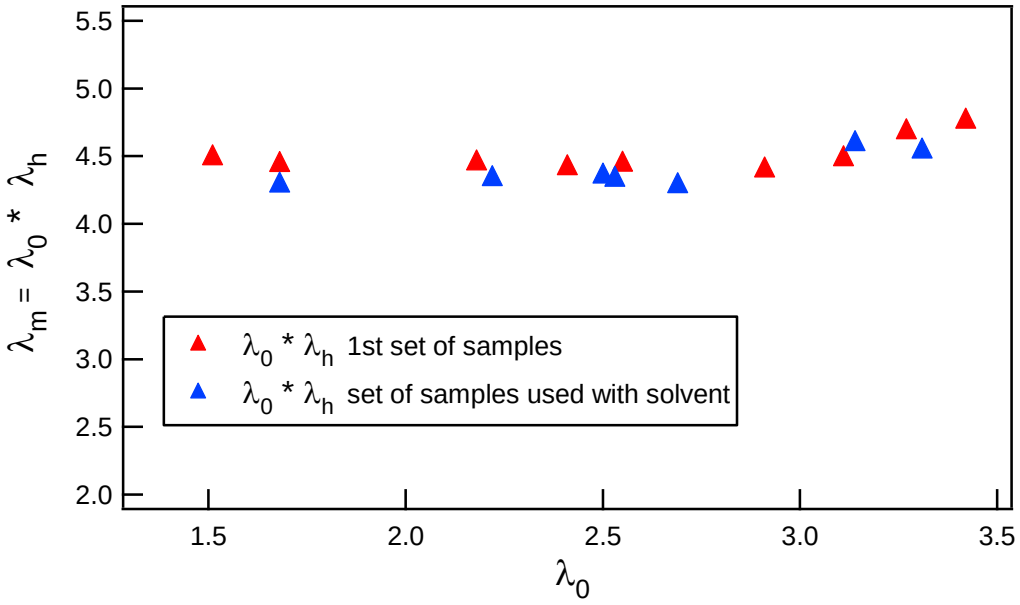

Figure 19: Maximum elongation of the first network λ_m as function of the prestretching of the first network λ_0 to investigate the influence of the swelling by solvent

Figure 19 is a further proof that the hardening phenomenon is governed by the first network, and that the dilution of the polymer by the solvent does not affect this phenomenon. On the other hand, the dilution influences the stress at break and the elongation at break significantly, i.e. it influences crack propagation. Indeed, Figure 16 clearly shows a decrease in stress at break when the samples are swollen. Another way to represent it is to plot the true stress at break as a function of λ_0 for samples swollen in solvent and samples from this chapter part II) as shown in Figure 20. This graph illustrates the influence of the prestretching on the true stress at break. Despite having the same limiting elongation of the first network, the samples swollen in solvent display a much worse true stress at break. This is especially true when $2 < \lambda_0 < 2.5$ whereas the difference becomes less important when $\lambda_0 > 3$.Figure 20 is a clear proof of the role played by the 2nd network. It should be noted that we did not test

mechanically any network with low value of λ_0 swollen with solvent since they become too brittle.

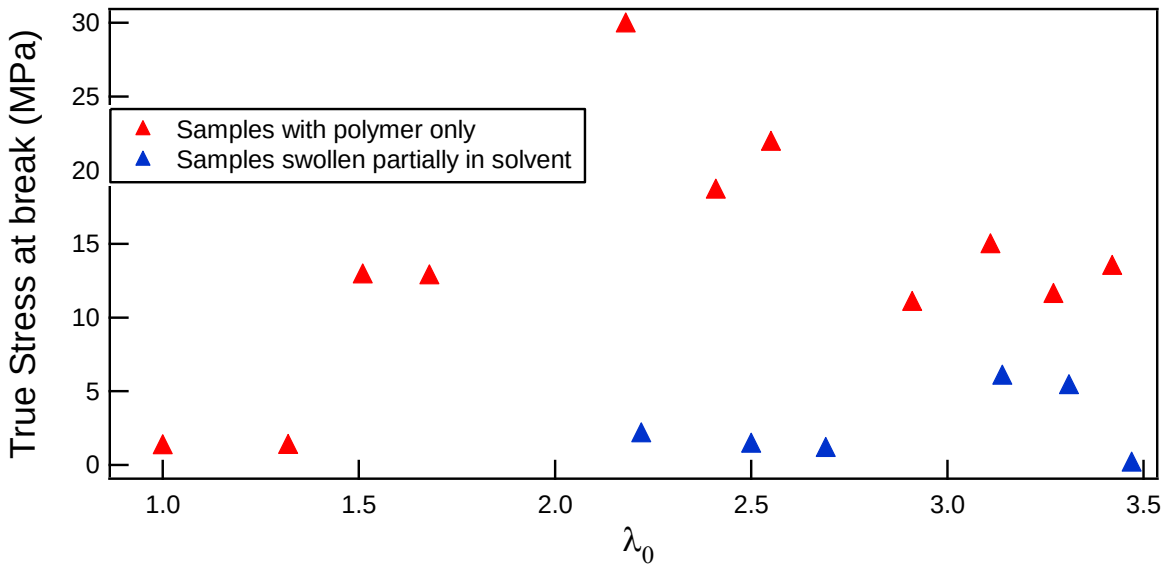

Figure 20: True stress as a function of the prestretching of the first network

Indeed, this experimental procedure of comparing the mechanical properties of multiple networks swollen in solvent with those made of polymer with the same λ_0 results in materials where the fraction of 2nd network changes while the proportion of the stiff 1st network stays the same. Due to the differences observed on Figure 20 it can be said that the amount of 2nd network plays a crucial role, and the dilution of the 2nd network with solvent leads to the early failure of the sample.

After studying the impact of the dilution of the second network in multiple networks elastomers, we will return to an interesting novel result that we reported: the case of extreme dilution of the first network leading to a macroscopic yielding and necking.

IV) Discussion around a new phenomenon: the yield stress

1) Description of the necking process

One of the most interesting results obtained during this work is the behaviour that has been observed for samples of type 4 with a yield stress and a necking phenomenon appearing. This specific behaviour is interesting because it is fundamentally different from what is observed for example in semi-crystalline polymers such as polyethylene: despite damages occurring in the sample, the material remains very elastic. This has been seen from the step-strain experiments shown in Figure 11c). This figure shows also that, once the damage is done in the network, the multiple networks elastomers are still extremely elastic and show little hysteresis during the following cycles to the same maximal elongation.

The yield process can only be observed for a highly prestretched first network or similarly for a highly diluted first network (dilution in polymer). Since it seems that the yield stress is linked to the first network, we think that this yield stress is linked to the large amount of damage occurring in the first network. At the yield stress, this high amount of damage is localized at a specific spot in the sample nucleating the actual necking process where two domains of the sample coexist with different states of true stress and elongation as shown in Figure 21. At the beginning of the tensile test, the nominal stress increases with elongation and the sample is homogeneous as shown on pictures a and b. Starting from the yield stress occurring at 4.6 MPa, the necking process begins with a nucleation point that is creating two fronts. Those two fronts propagate through the entire sample as shown in picture c until the complete sample has been necked (picture d). Afterwards a second hardening will start until the failure of the material. During the propagation of the necking, the sample is separated into two regions, the first region is unnecked and the elongation λ_1 remains the same as that reached at the yield stress. The second region is the highly damaged portion where the elongation is λ_2. Both of course extend at the same level of nominal stress, i.e. the same force. Between the two values of macroscopic elongation, the necking front moves along the sample until all the volume of sample reaches λ_2.

This process corresponds to a large dissipation of energy at the two necking fronts that has been attributed to the comprehensive breakage of first network's chains. At first sight, it seems that the first network is at least partially responsible for the occurrence of the necking (high prestretching and high dilution needed) and it undergoes an important structural change during the necking. This last hypothesis can also be found in Gong's work regarding the change in structure occurring during the necking [7, 8] in hydrogels where ultra-low volume fractions of first network are easy to obtain. In her review paper of 2010 [8], Gong proposes that during the necking process the first network breaks into clusters and those clusters will then play the role of crosslinkers of the second network. In the next part, some hypothesis will be made to try to explain the origin and the mechanism behind the necking process.

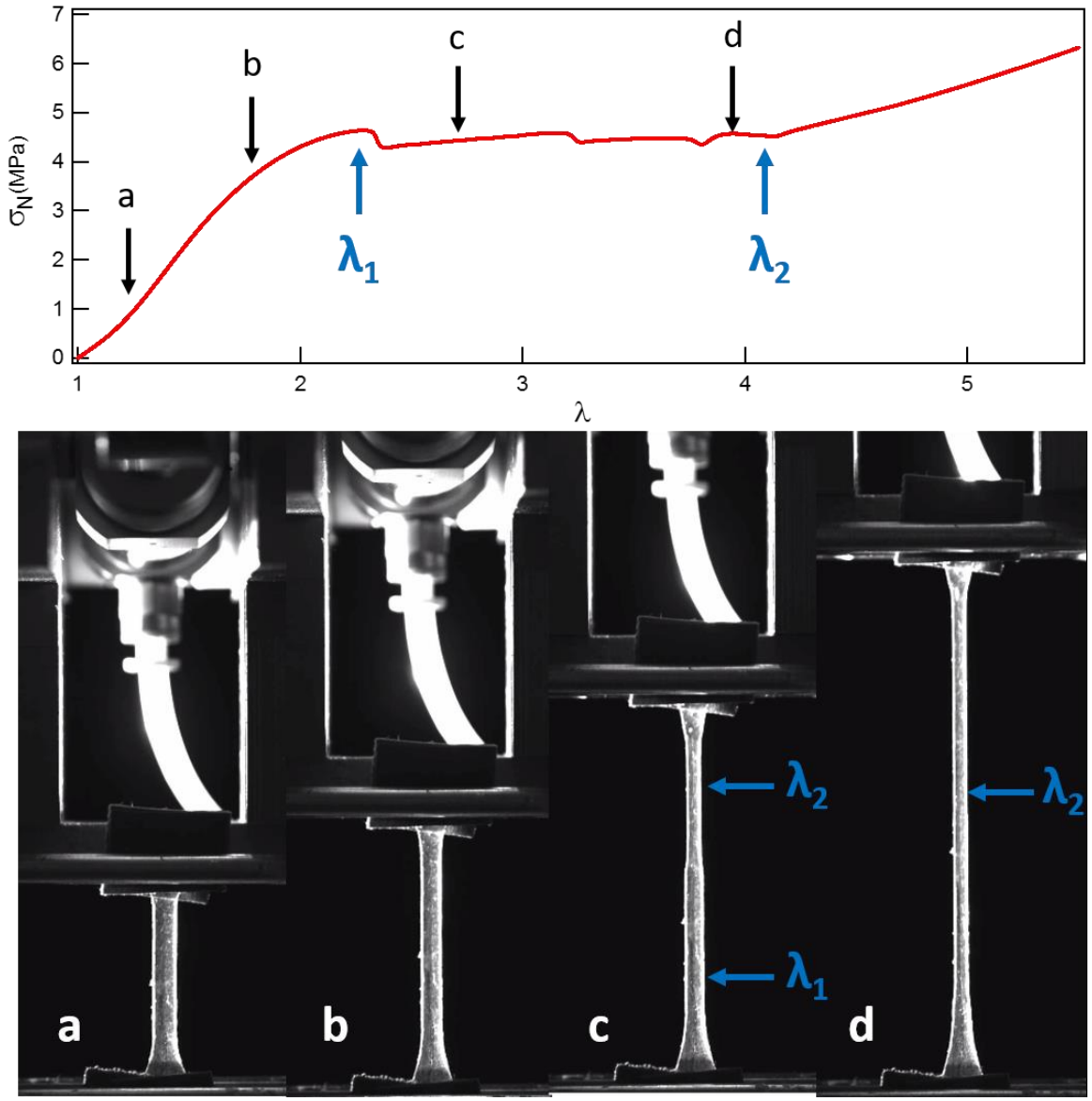

Figure 21: Stress-strain curve of a sample presenting a yield stress and recorded pictures describing the macroscopic state of the sample as the elongation increase. $\dot{\lambda}$ = 0.0039 s^{-1}

2) Discussion on the origin of the yield stress

From those experimental observations, we can try to link the measured value of the yield stress for a given λ_0, to the underlying molecular structure. If we assume that the yield stress is controlled by the first network, it is logical to link it to the areal density of first network strands crossing a plane normal to the tensile direction. The estimate of the areal chain density inside the simple network can be calculated by assuming Gaussian chain statistics as done previously by Guillaume Miquelard during his PhD [9, 10]. The areal chain density of the first network can be estimated using Eq. (10) if the crosslinking is random and has a functionality of four, with ν the number of crosslinking points per unit volume and $\langle {R_0}^2 \rangle$ the average distance between crosslinks. Knowing the expression of $\langle {R_0}^2 \rangle$ developed in chapter 2, we can

obtain Eq. (11), with l_0 the length of a C-C bond (1.54 Å), E_{SN} the modulus of the first network, C_∞ the polymer structure factor and N_c the number of carbon bonds between crosslink points. When the first network is swollen with monomer during the multiple steps of polymerization, the surface chain density is diluted as described in Eq. (12), so that the first network areal chain density can be estimated for our entire set of samples.

$$\Sigma_{SN} = \frac{\nu * \langle R_0^2 \rangle}{2} \qquad \text{Eq. (10)}$$

$$\Sigma_{SN} = \frac{l_0 E_{SN} \sqrt{C_\infty N_c}}{6\,R\,T} \qquad \text{Eq. (11)}$$

$$\Sigma_{SN(Multiple\ Network)} = \Sigma_{SN} \phi^{2/3} \qquad \text{Eq. (12)}$$

To obtain more values of the yield stress, especially for type 3 samples that fail before yielding, we extrapolated the value of the yield stress based on the shape of the curves that show an actual yielding as shown in Figure 22.

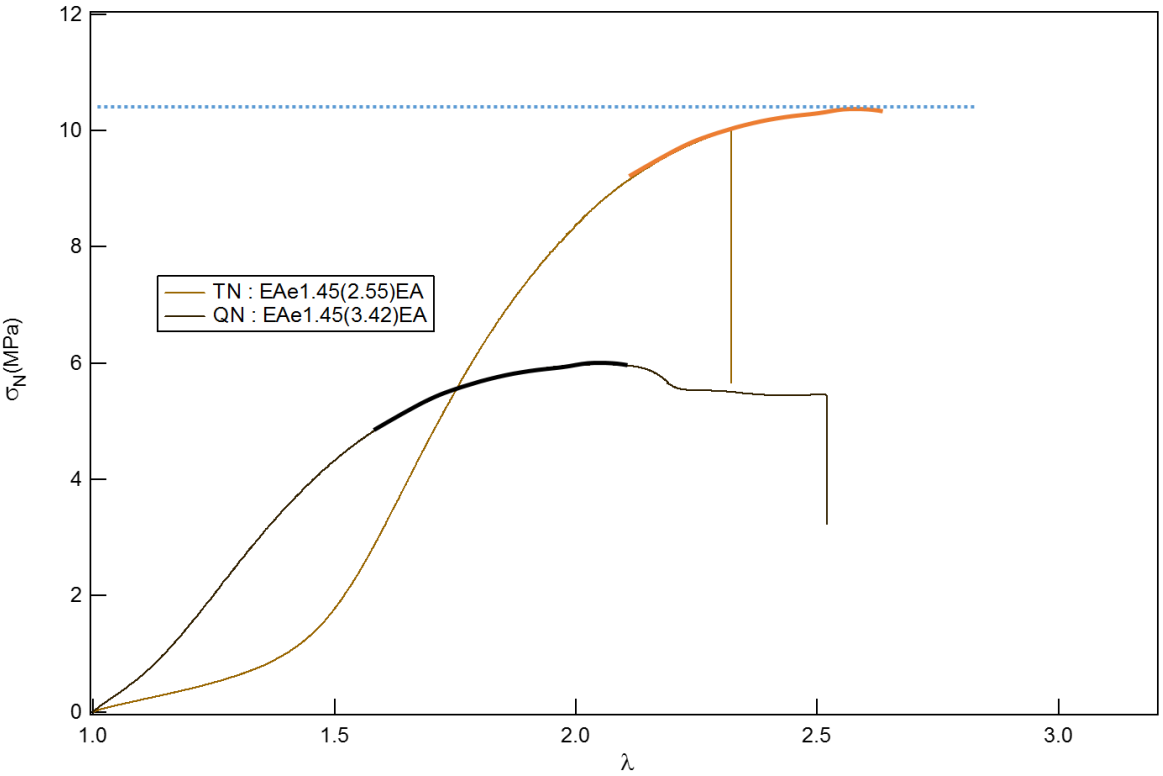

Figure 22: Stress-strain curve to show how an estimated value of the yield stress can be obtained for type 3 materials

The values of the yield stress for type 3 and 4 networks are plotted as a function of the first network's surface chain density (Figure 23) calculated based on the dilution of the first network.

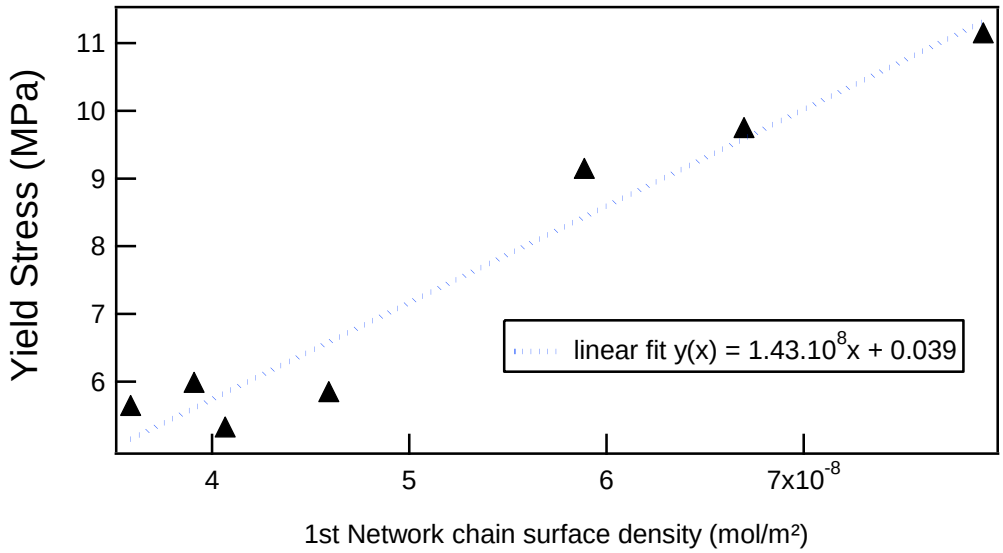

Figure 23: Evolution of the yield stress as a function of the 1st network's chain surface density

Figure 23 shows that the yield stress is an increasing linear function of the surface chain density of the first network. The best fit of the experimental points shows that the intercept is very close to the origin. The slope of the curve can in principle be converted in N/molecule which gives $1.43 \times 10^{14} / 6.023 \times 10^{23}$ = 0.2 nN/chain, which is roughly a tenth of the breakage strength of a C-C bond. This suggests clearly that there are some stress concentrations in the material leading to collective failure of bonds such as the microcracks proposed by Brown.

This experimental observation agrees with the results observed by Gong *et al.* for the hydrogels [7]. Indeed, the yield stress decreases with the swelling of the first network and the prestretching of its chains. At the yield point, starting in an area presenting some defects in the first network, like shorter chains or higher crosslink's density, a nucleation point is created leading to the local breakage of a large number of bonds in the first network and to this necking phenomenon. We think that at the yield stress some large portions of the first network are breaking in the necked area. Then the denser the first network is, the more strain energy is necessary to obtain this large breakage which leads to a higher yield stress for the network with less diluted first network.

In summary, the yield stress appears to be dependent on the details of the structure of the first network and especially on its areal density of strands normal to the tensile direction. It seems to be a spontaneous phenomenon that appears locally and then propagates to the entire sample through two necking fronts. The energy per unit volume dissipated during this necking process is very high and leads to very interesting properties for the multiple networks elastomers with a high modulus but also a large elongation at break.

Conclusion

In this chapter, a reference set of multiple networks were synthesised and tensile tests were carried out. Those tests have led to the observation of four different types of mechanical behaviour for the different multiple networks depending on their respective value of prestretching of the 1st network chains λ_0. Type 1 does not present any improvement in comparison to the first network. Type 2 shows a higher stress and elongation at break due to a hardening phenomenon but no dissipation in the bulk. Type 3 presents a hardening followed by a softening phenomenon that occurs with damages in the bulk before failure. Finally, type 4 presents the same behaviour as type 3 plus the occurrence of a yielding followed by a necking process.

Despite the differences of mechanical behaviour observed, some parameters have been used in order to create a master curve. We have not succeeded yet to obtain a global master curve but different parts of the curve are relatively well understood. We have seen that the onset of strain hardening is controlled by the first network chains and therefore their prestretching in the different multiple networks. The softening part appears to be dependent on the areal density of first network chains in a plane normal to the tensile direction. Finally, the yield stress increases linearly with the areal chain density of the first network.

In this section, we have investigated in detail a particular set of materials using only the same first network. In the next chapter, we will try to generalize those findings to the use of different first networks and different monomers.

References

1. Ducrot, E. and C. Creton, *Characterizing Large Strain Elasticity of Brittle Elastomeric Networks by Embedding Them in a Soft Extensible Matrix.* Advanced Functional Materials, 2016. **26**(15): p. 2482-2492.
2. Ducrot, E., et al., *Toughening Elastomers with Sacrificial Bonds and Watching them Break.* Science, 2014. **344**(6180): p. 186-189.
3. Ducrot, E., *Double Network Elastomers*. 2013, Université Pierre et Marie Curie: Paris.
4. Gent, A.N., *A New constitutive relation for rubber.* Rubber Chemistry and Technology, 1996. **69**: p. 59-61.
5. Brown, H.R., *A model of the fracture of double network gels.* Macromolecules, 2007. **40**(10): p. 3815-3818.
6. Nakajima, T., et al., *A Universal Molecular Stent Method to Toughen any Hydrogels Based on Double Network Concept.* Advanced Functional Materials, 2012. **22**(21): p. 4426-4432.
7. Takahiro, M., et al., *Yielding Criteria of Double Network Hydrogels.* Macromolecules, 2016. **49**: p. 1865-1872.
8. Gong, J.P., *Why are double network hydrogels so tough?* Soft Matter, 2010. **6**(12): p. 2583-2590.
9. Miquelard-Garnier, G., *Synthese et propriétés mécaniques d'hydrogels polyélectrolytes modifiés par des groupements hydrophobes.* archives-ouvertes, 2008.
10. Miquelard-Garnier, G., D. Hourdet, and C. Creton, *Large strain behaviour of new hydrophobically modified hydrogels.* Polymer, 2009. **50**: p. 481-490.

Chapter 4: Mechanical Behaviour in Uniaxial Tension: influence of Changes in the First Network

Chapter 4: Mechanical Behaviour in Uniaxial Tension: influence of Changes in the First Network

Introduction

The focus of the previous chapter was the study of a set of samples with the same first network to investigate the effect of its prestretching. It was shown that the prestretching λ_0 is a critical parameter to understand the mechanical behaviour of the materials. However, it is not the only factor. Ducrot *et al.* [1] introduced some differences in the design of the first networks that led to different mechanical behaviours of the related multiple networks. For example, by increasing the amount of crosslinker to create stiffer first networks, they observed a corresponding difference in the onset of the hardening of the multiple networks.

This result has led us to investigate the influence of different synthesis parameters of the first network. After studying the level of prestretching, we will focus in this chapter on the effect of the amount of crosslinker and of the nature of the used monomer. Ducrot *et al.* [1] studied more densely crosslinked first networks than the one used in chapter 3. In comparison to this reference of 1.45 mol % of BDA, in this chapter the crosslink density will be decreased and its influence studied in uniaxial tension. The study of the first network will be pushed further with the investigation of the effect of the nature of the monomer with the use of different acrylate and methacrylate monomers.

I) Modification of the first network: change in crosslink density

1) Synthesis and study of the first networks

a) Synthesis

The reference first networks used in chapter 3 had a crosslink density of 1.45 mol%. In this part a decrease in the crosslink density will be investigated. Therefore, three new first networks were synthesised, with a decreasing amount of crosslinker, up to ten times less than the reference. The synthesis is done as described in chapter 2 with 50 % of ethyl acetate and 50 % of ethyl acrylate as monomer. The amount of HMP is unchanged (1.16 mol %). This means that the number of radicals created during the synthesis of the first network is kept identical for every first network. Therefore, the same number of chains should be growing simultaneously during the synthesis. However, in the three different syntheses the amount of crosslinker is decreased to 0.725 mol %, 0.29 mol % and 0.145 mol % respectively. Table 1 summarises the characteristics of the different reactants of the three new first networks in comparison to the reference EAe1.45(1). The last column of Table 1 describes the theoretical mass between crosslinks $M_{x\,th}$ that was calculated based on Eq. (13) from chapter 2. Note that some theoretical values of the mass between crosslinks are above the characteristic mass between entanglements of the poly(ethyl acrylate) (13 kg/mol).

Sample	[BDA] (mol %)	Monomer (g)	Ethyl acetate (g)	BDA (µL)	HMP (µL)	$M_{x\,th}$ ($kg.mol^{-1}$)
EAe1.45(1)	**1.45**	**8.6**	**8.6**	**236**	**152.5**	**3.5**
EAe0.73(1)	**0.725**	**8.6**	**8.6**	**118**	**152.5**	**6.9**
EAe0.29(1)	**0.29**	**8.6**	**8.6**	**47**	**152.5**	**17**
EAe0.15(1)	**0.145**	**8.6**	**8.6**	**23.6**	**152.5**	**34**

Table 1: Chemical reactants used during the synthesis of various first networks

Once the synthesis is completed, the same procedure as described in chapter 2 is used to obtain the dried first networks. Then, the mechanical tensile tests are carried out and will be the object of the following part.

b) Uniaxial tensile test

The synthesised samples are cut into a dumbbell shape and tested in uniaxial tension as described in chapter 2. The corresponding stress-strain curves are shown in Figure 1.

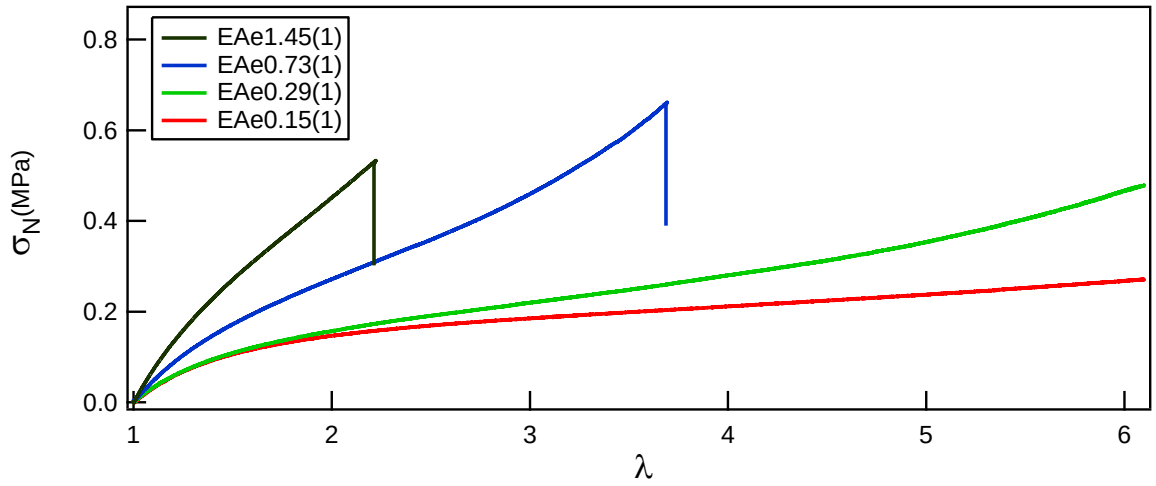

Figure 1: Stress-strain curve of the different first networks

Figure 1 shows the effect of the amount of crosslinker with a wide difference in mechanical properties. Depending on the amount of crosslinker, a simple polymer network can be tuned from soft and deformable towards a stiff and brittle material. The first noticeable change is the modulus, which is expected to be different due to the change in the amount of crosslinker. As described in Figure 2, the modulus increases with the amount of BDA but it does not increase as predicted by Eq. (12) and (13) in chapter 2. The increase should in principle be linear with the amount of BDA and intercept the origin. This difference with the theory is due to the fact that entanglements are always present in the less crosslinked samples.

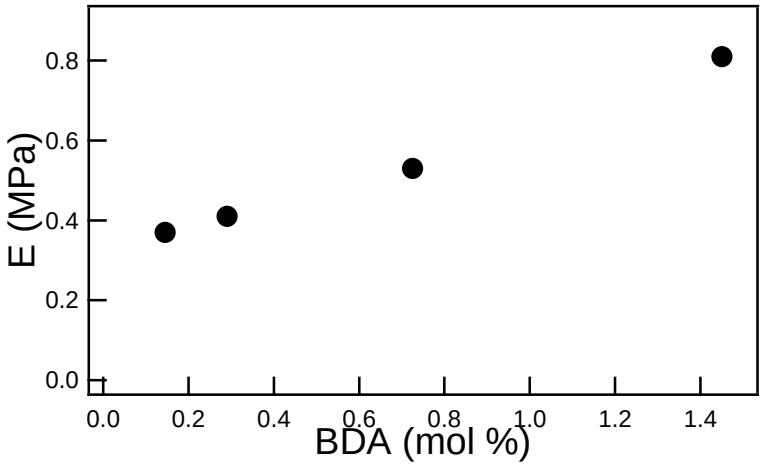

Figure 2: Evolution of the modulus as a function of the amount of crosslinker in the first networks.

To evaluate the respective contributions of the entanglements and crosslinks, the Mooney Rivlin model shown in chapter 1 section I)3) can be used [2, 3]. In this approach, Mooney and Rivlin proposed a general expression for the free energy leading to a relation between the

Mooney stress (defined in Eq. (1)) and the stretch lambda as shown in Eq. (2) for uniaxial tension This model can be applied to our materials, and the Mooney stress can be plotted as a function of lambda as shown in Figure 3.

$$\sigma_{Mooney} = \frac{\sigma_N}{\lambda - \frac{1}{\lambda^2}} \qquad \textbf{Eq. (1)}$$

$$\sigma_{Mooney} = 2\,C_1 + \frac{2\,C_2}{\lambda} \qquad \textbf{Eq. (2)}$$

In Figure 3, softening is only observed for the two less crosslinked networks EAe0.29(1) and EAe0.15(1). This significant decrease in Mooney stress shows the presence of entanglements. For the sample EAe0.73(1), a moderate softening is followed by a stiffening meaning that a few entanglements may be present, but also that the chains are quickly reaching their limit of extensibility. Finally, the Mooney stress of EAe1.45(1) is nearly constant, meaning a small amount of entanglements could be present but the limit of extensibility is quickly reached.

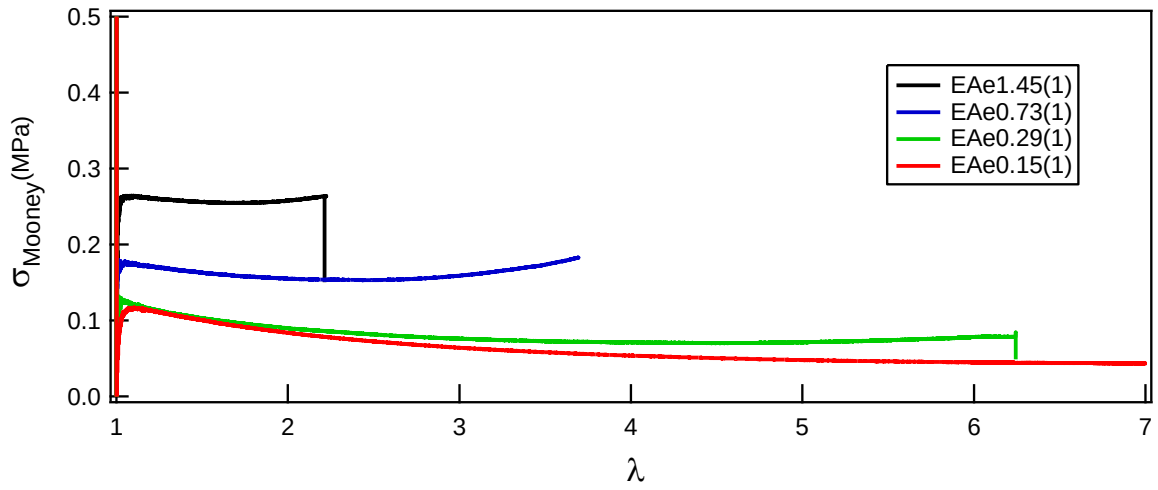

Figure 3: Mooney stress as a function of the elongation for the different first networks

To explore in more detail the different contributions to the modulus, the molecular model proposed by Rubinstein and Panyukov can be used as described in chapter 1 section I)3). Due to the presence of a clear stiffening (as seen in Figure 3) for EAe1.45(1) and EAe0.73(1), the model cannot be applied to those samples. For the two other samples, the best fits are obtained for the part with no stiffening, i.e. from 1/λ = 0.3 to 0.9, and the result is shown in Figure 4.

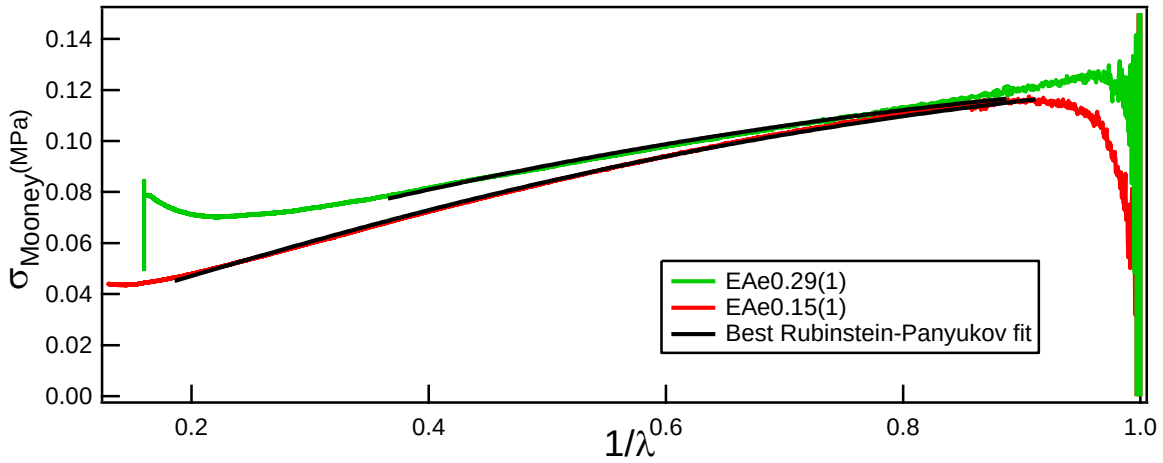

Figure 4: Mooney Stress as a function of the inverse of the elongation and in black the best Rubinstein-Panyukov fit.

This model fits the data well, as seen in Figure 4 separating in fact the respective contributions to the Young's modulus for those two samples as shown in Table 2. It can be seen that the contribution of the entanglements to the modulus E_e is close for both samples at around 0.3 MPa, and the amount of crosslinks is increasing. The values found for E_e are different from those found for the second network alone. This difference comes from the fact that the latter is synthesised in bulk conditions leading to a higher value of entanglements ($E_e \approx 0.5$ MPa). This result is a clear evidence that the synthesis in the presence of solvent helps reduce the density of entanglements as described by Urayama [4].

Samples	**Young's modulus E (MPa)**	**E_x (MPa)**	**E_e (MPa)**
EAe0.29(1)	**0.37**	**0.11**	**0.26**
EAe0.15(1)	**0.41**	**0.06**	**0.30**

Table 2: Different contribution to the Young's modulus for the less crosslinked samples

After studying the first networks and the different contribution on their modulus, multiple networks materials are synthesised.

2) Multiple network from first networks with variable crosslinker concentrations

a) Synthesis and materials

Once the first network is obtained, the standard procedure to create multiple networks is followed as described in chapter 2. The multiple networks synthesised were obtained with a solution of monomer (ethyl acrylate) only and 0.01 mol % of BDA and 0.01 mol % of HMP as described in chapter 2. After the drying phase, the weight of the sample was measured to obtain their characteristic parameters λ_0 and φ_1. Table 3 shows those parameters for each

synthesised multiple network. The greyed boxes correspond to the reference set of samples made from EAe1.45(1), shown as a comparison.

Sample name	First network	λ_0	SN wt %	Number of polymerization steps
EAe1.45(1)		1	100	1
EAe1.45(1.68)EA	EAe1.45(1)	1.68	20.5	2
EAe1.45(2.55)EA	EAe1.45(1)	2.55	6.06	3
EAe1.45(3.42)EA	EAe1.45(1)	3.42	2.88	4
EAe0.73(1)		1	100	1
EAe0.73(1.84)EA	EAe0.73(1)	1.84	16	2
EAe0.73(2.94)EA	EAe0.73(1)	2.94	3.93	3
EAe0.73(3.75)EA	EAe0.73(1)	3.75	1.89	4
EAe0.29(1)		1	100	1
EAe0.29(2.07)EA	EAe0.29(1)	2.07	11.25	2
EAe0.29(3.74)EA	EAe0.29(1)	3.74	1.9	3
EAe0.29(5.39)EA	EAe0.29(1)	5.39	0.64	4
EAe0.15(1)		1	100	1
EAe0.15(2.19)EA	EAe0.15(1)	2.19	9.4	2
EAe0.15(3.65)EA	EAe0.15(1)	3.65	2.05	3

Table 3: Summary of the different elastomer networks synthesised starting with various first networks

Once the synthesis is completed the mechanical tensile tests are carried out and will be the object of the following section.

b) Uniaxial tension

The synthesised samples are cut into a dumbbell shape, and tensile tests are carried out as described in chapter 2. Figure 5 presents stress-strain curves for multiple networks, grouped by corresponding first network as indicated in the legend.

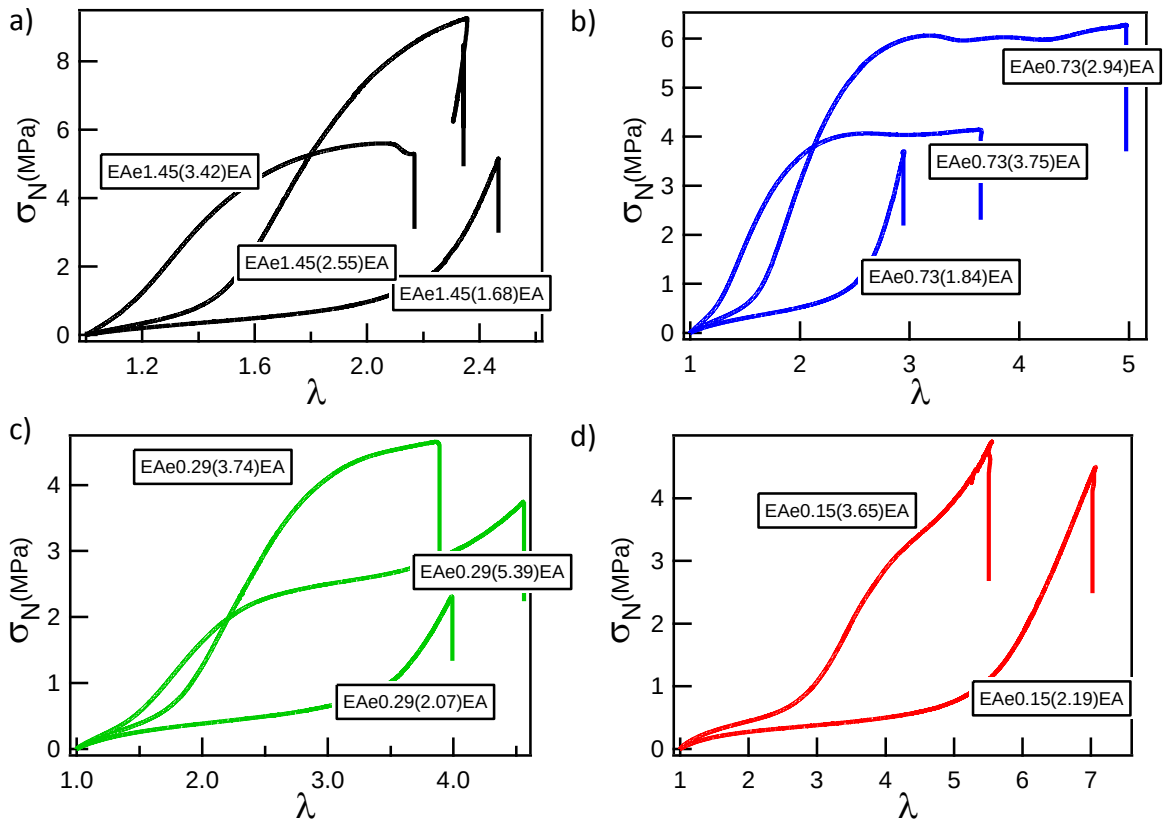

Figure 5: Stress-strain curves of multiple networks elastomers made from different initial first networks. a): EAe1.45(1), b): EAe0.73(1), c): EAe0.29(1), d): EAe0.15(1)

Figure 5a) shows the reference samples studied in chapter 3 (EAe1.45(1),black curves). To comment the curves obtained in Figure 5 we will use the classification described in chapter 3 section II). It is notable that the samples created using EAe0.73(1) (Figure 5b), blue curves) show a qualitatively similar behaviour to EAe1.45(1). This family of samples shows hardening, softening and a necking phenomenon but the synthesis to equilibrium leads to only one type 2 curve (the DN) and two type 4 curves. It can also be seen that the hardening sets in at higher deformation in comparison to the reference.

Multiple networks made from EAe0.29(1) as first network present a new type of mechanical behaviour. Figure 5c) shows that the type 2 and 3 behaviour can be obtained but no necking plateau is observed. When the yield stress is reached, instead of a plateau, a second hardening appears until breakage of the sample. This type of mechanical behaviour will now be referred to as type 5.

Only two samples were synthesised from EAe0.15(1) as shown in Figure 5d): the DN presents a type 2 behaviour with hardening and breakage before softening. The TN presents a type 5 behaviour with what could be interpreted as a yield stress immediately followed by the second hardening.

Extracting selected data from Figure 5, we can now compare different samples with only two steps of polymerization as shown in Figure 6.

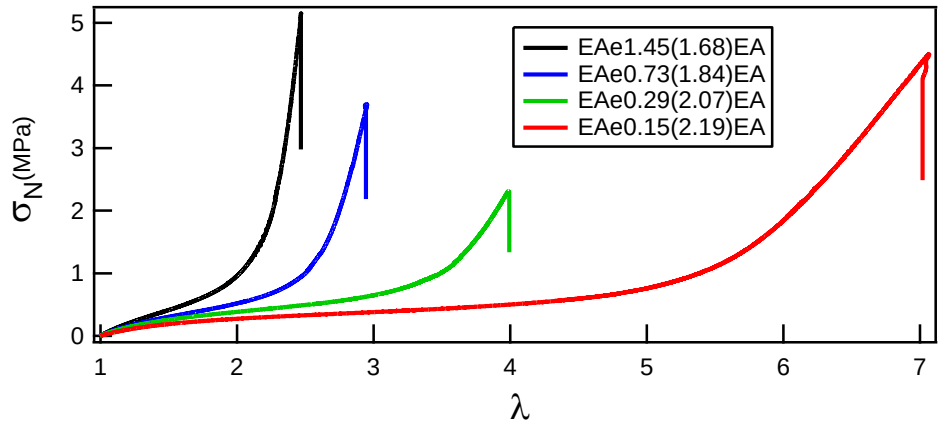

Figure 6: Comparison of four samples made with different first networks and two polymerisations steps.

In Figure 6, we can see that the onset of strain hardening occurs at different deformations for the four samples. Indeed, the more crosslinked is the first network the earlier the onset of the hardening. Note also that the *true* stress at break increases as these DN become more extensible. The EAe1.45(1.68) breaks at a true stress of 12.5 MPa while the EAe0.15(2.19) breaks around 32 MPa.

To have a better grasp of the importance of the crosslink density on the hardening phenomenon, a comparison can be done between samples with the same λ_0.

3) Influence of the crosslink density at similar λ_0

From the set of materials shown in Table 3 and from those presented in chapter 3 Table 1, we can extract some samples with similar prestretching values of the first network and directly compare them to each other. Three values of λ_0 have been selected: 2.2, 2.9 and 3.75. The comparison at similar prestretching will lead to the direct study of the impact of the amount of crosslinker in the first network. The selected stress-strain curves are plotted in Figure 7.

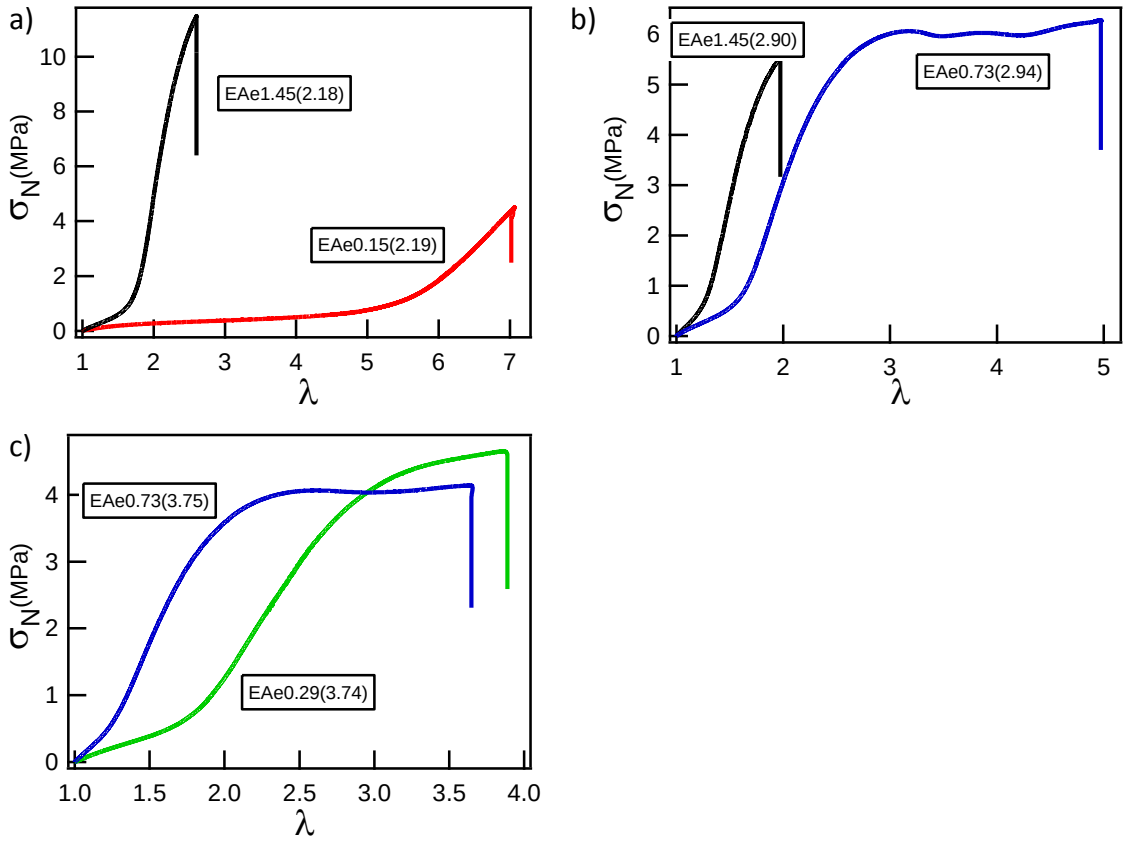

Figure 7: Comparison of different multiple networks presenting the same prestretching of their first network.

From the observation of Figure 7, the first aspect to note is the difference in the onset of the hardening process. In chapter 3, we showed that the onset of the hardening phenomenon was governed entirely by the level of prestretching of the first network for an identical first network. However, Figure 7a), compares two multiple networks where λ_0 = 2.2 but there is 10 times more crosslinker in EAe1.45(2.18) than EAe0.15(2.19), and the onset of the hardening occurs at approximately λ =1.7 and 5.5 respectively. This shows that the elongation where the hardening occurs depends on the intrinsic stretchability of the first network.

Another noticeable aspect from Figure 7 is that despite having the same value of λ_0, the type of mechanical behaviour is different. At λ_0 = 2.9, EAe1.45(2.9) presents a mechanical behaviour of type 3 when EAe0.73(2.94) has a type 4 behaviour.

The behaviour seen in Figure 7 shows that the amount of crosslinker in the first network is a second important parameter to describe the properties of the multiple networks. To continue the analysis of this parameter, the following part will be focusing on the use of the Gent model and the study of the yield stress for the networks shown in Table 3, Figure 6 and Figure 7.

4) Analysis

a) Gent model

The constitutive model proposed by Gent [5] has been successfully used in chapter 3 to fit the uniaxial extension behaviour of the samples leading to the determination of the limiting elongation of the first network and its link with the prestretching factor λ_0. Since we just saw that the hardening also depends on the crosslinker density in the first network, the fit described in chapter 3 was carried out for the different multiple networks of Table 3.

The values of J_m can be obtained by fitting the data of figure 6 for each material. Then, using Eq. (4) in chapter 3, the maximal elongation λ_m of the first network chains within the multiple networks can be deduced. These results are presented in Figure 8. The average of the maximum elongation for each network is also shown in Figure 8 (corresponding dashed lines).

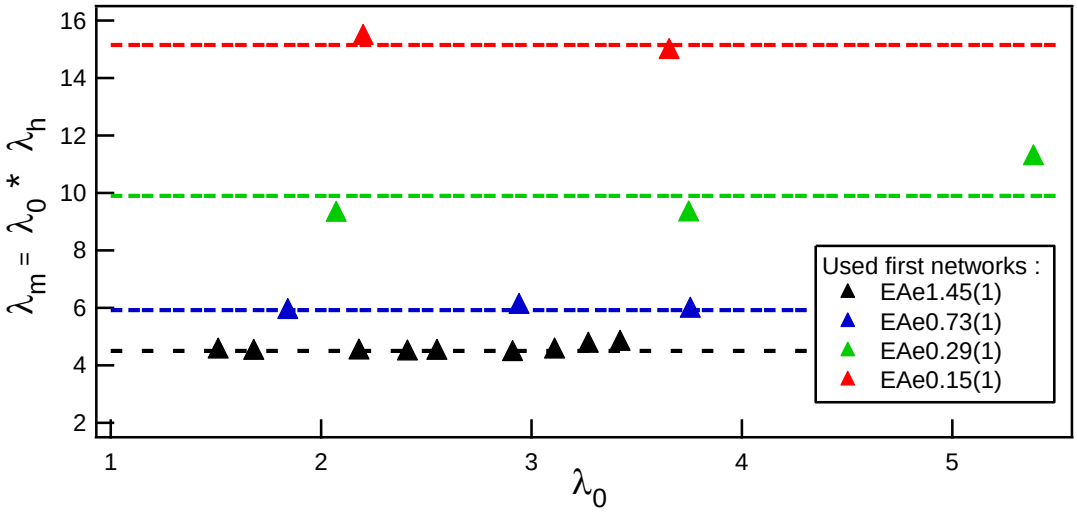

Figure 8: Representation of the maximum elongation for different multiple networks depending on their first network. The dashed lines correspond to the respective average of λ_m for each first network.

Figure 8 shows that λ_m is nearly constant, independent of λ_0. This means that, λ_m is a material constant of the first network. That is to say that for a given $\lambda_m$and a given λ_0 the onset of the hardening can be predicted.

It is now interesting to compare these values of λ_m with theoretical predictions. As shown in chapter 3, the maximum extensibility of the chains can be estimated from the contribution of the crosslinks to the small strain modulus by using Eq. (27) from chapter 1. The results are presented in Table 4. We can observe that the measured and calculated maximal elongation of the chains (λ_m Gent and λ_m calculated from E_x) of the first network are in reasonable agreement. This suggests that the estimate of the density of crosslinks with the Rubinstein-Panyukov model is correct and also that the limiting extensibility measured in the material is nearly identical to that predicted for single chains, which rather surprisingly suggests that the entanglements play a relatively minor role in the maximum extensibility of these multiple networks.

First network	E_x	$M_{x\ exp}$ (kg/mol)	N_{C-C}	λ_m Gent	λ_m calculated
EAe1.45(1)	**0.81**	**10**	**203**	**4.502**	**4.1**
EAe0.73(1)	**0.53**	**16**	**310**	**5.93**	**5.1**
EAe0.29(1)	**0.11**	**75**	**1499**	**9.90**	**11.2**
EAe0.15(1)	**0.06**	**138**	**2748**	**15.15**	**15.1**

Table 4: Characteristics of the different first networks.

From the use of the Gent fit in Figure 8 and of Table 4, the two parameters (λ_m and λ_0) governing the hardening phenomenon of our system can be identified. As shown in chapter 3, the degree of prestretching of a given first network governs the onset of the hardening but the crosslink density of the first network is the key parameter that governs the maximum intrinsic extensibility in multiple networks elastomers.

b) The yield stress

The amount of crosslinker in the first network having clearly an influence on the hardening, it is interesting to focus on the yield stress which was found to be linked to the areal density of first network strands in chapter 3.

Figure 5 (above) shows that the yield stress can be reached for a large number of multiple networks. Therefore, it is interesting to compare this yield stress with the values measured in chapter 3 for the reference material family. To do so, the areal density of elastic chains of the first network has to be calculated for each network. In the calculation of the density of elastic chains, E_x is used for the samples based on EAe0.29(1). The results of those calculations are added to those obtained in chapter 3 and shown in Figure 9.

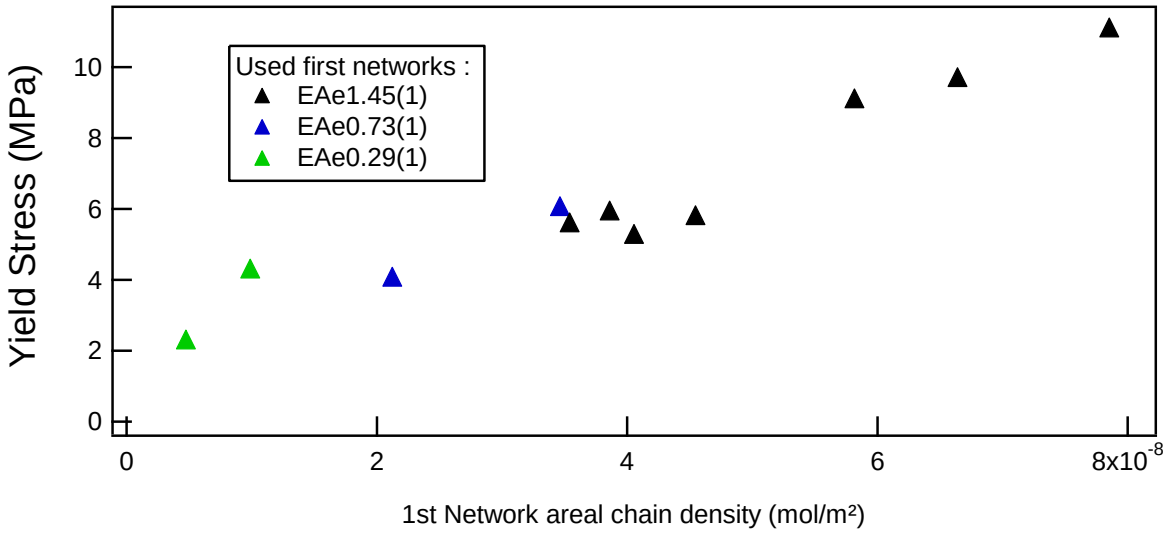

Figure 9: Yield stress as a function of the 1st network areal chain density for three different types of first networks

Figure 9 shows the yield stress points for samples prepared from different first networks and seems to confirm the result obtained in chapter 3. The yield stress is an increasing function of the areal chain density of the first network. Since some entanglements are present in EAe0.29(1), some more points would be necessary to be sure that they do not have an impact on the yield stress. If this is confirmed, by looking at Figure 9, we can see that a master curve for the yield stress can be obtained, meaning that the crucial parameter controlling the strain hardening and breakup of the first network is the first networks' areal chain density.

In chapter 3, a master curve has also been constructed in section II)6) for the stress-strain curve. In the next section, the same procedure will be applied on the networks with different crosslink densities.

c) Master curve

In chapter 3, the master curve of the stress-strain curves is obtained by correcting the stress by the dilution of the areal chain density and the elongation by the prestretching. This procedure has led to a good master curve shown in chapter 3 Figure 15. In this chapter since the first networks are different the true first network elongation will in addition be normalized by the maximum intrinsic elongation of the first network λ_m. The resulting curve for the set of samples EAe1.45 and EAe0.73 are shown in Figure 10.

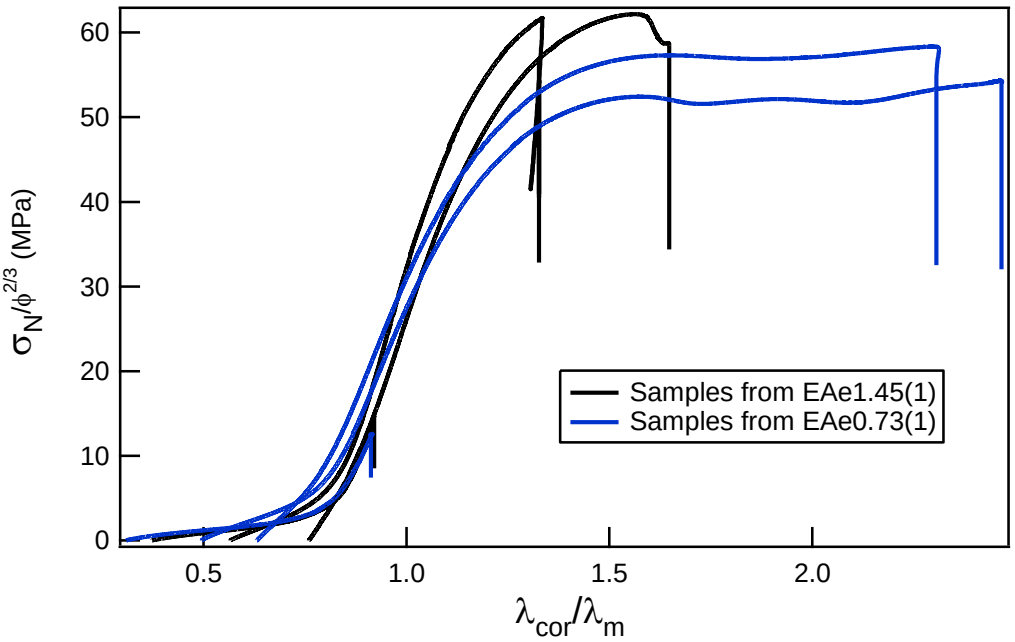

Figure 10: Corrected master curve for the samples from EAe1.45(1) and EAe0.73(1).

In Figure 10, it can be seen that the master curve, obtained from the family of elastomers obtained with the two most crosslinked first networks, is quite good with an onset of hardening appearing at approximately the same ratio of λ_{cor}/λ_m (equivalent to λ/λ_h). Both the hardening and the softening are in good agreement for both families of networks. On the other hand, it is difficult to conclude on the values of the yield stress and the slope around the

hardening might be corrected differently. A similar normalization can be applied to the EAe0.29 and EAe0.15 families of materials and the curves are shown in Figure 11.

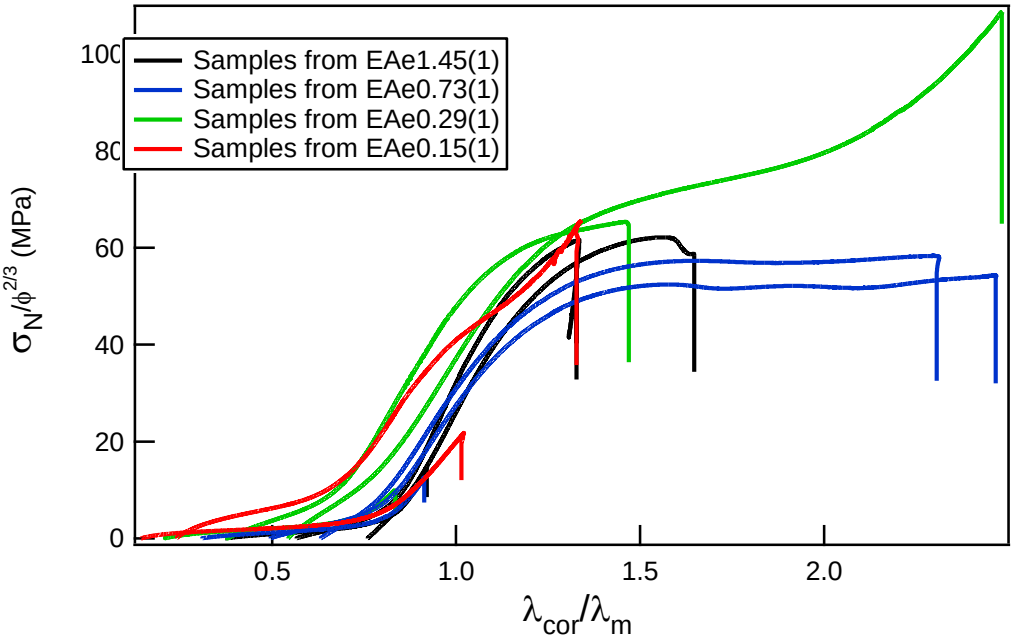

Figure 11: Corrected master curve for the samples from EAe1.45(1), EAe0.73(1), EAe0.29(1) and EAe0.15(1).

The addition of the two less crosslinked master curves in Figure 11, shows that the strain hardening occurs at a much lower extension ratio relative to the intrinsic extensibility of the first network. This could be due to the dominant presence of entanglements in the first network or to the transfer reactions between networks that could lead to a more progressive hardening. It should be noted however that the normalization by the areal density of chains leads to a fairly good superposition of the yield stresses as surmised from Figure 9.

In summary the amount of crosslinker changes the mechanical properties of the multiple networks by changing the intrinsic finite extensibility of the first polymer network. While, the behaviour for relatively highly crosslinked first networks appears to be quite well understood and the renormalization of the stress and elongation are giving a good master curves to describe the mechanical behaviour of the system, using less crosslinked first networks leads to more complex network structures.

Another parameter that can be changed is the use of solvent or not during the synthesis of the first network and this will be the subject of the following section.

II) Modification of the first network: synthesis without solvent

1) Synthesis of first networks without solvent

As shown in chapter 2, the synthesis of the first network in the presence of solvent is used to separate the growing chains from each other and therefore to decrease the density of entanglements in comparison with the synthesis in the bulk as described by Urayama [4].

The synthesis without solvent is not described in chapter 2. The only difference is that, after the polymerization, the dialysis phase is no longer needed so the sample is dried directly under vacuum overnight. Two different first networks have been synthesised to analyse the effect of the solvent: one with 1.45 mol % of BDA and the other one with 0.725 mol % of BDA. The amount of initiator (HMP) was kept unchanged at the value of 1.16 mol %. A summary of the reactants used for each network is shown in Table 5. Also, as a comparison, Table 5 presents the same networks made with solvent.

Sample	[BDA] (mol %)	Monomer (g)	Ethyl acetate (g)	BDA (µL)	HMP (µL)	E (MPa)
EAe1.45(1)	**1.45**	**8.6**	**8.6**	**236**	**152.5**	**0.81**
EAe0.73(1)	**0.725**	**8.6**	**8.6**	**118**	**152.5**	**0.53**
EA1.45(1)	**1.45**	**8.6**		**236**	**152.5**	**1.42**
EA0.73(1)	**0.725**	**8.6**		**118**	**152.5**	**0.94**

Table 5: Chemical reactants used during the synthesis of first networks, with or without solvent.

To evaluate the impact of the solvent on the properties of the first network, a tensile test is carried out on each new system to compare them with the reference material (chapter 3 and beginning of this chapter). The result is shown in Figure 12 and the Young's moduli are measured and tabulated in the last column of Table 5. As expected, the values of E are much lower when solvent is used. The hypothesis is that the higher chain concentration during the bulk synthesis will lead to a more efficient crosslinking procedure and the synthesis in the bulk leads also to a higher concentration of entanglements. Indeed, chains that are far away from each other are more likely to bond only from one side to crosslinkers or to create loops, leading to non-effective crosslinks. Also, more transfer reactions could take place in the bulk synthesis. Those reasons could explain the difference in modulus between the two types of synthesis.

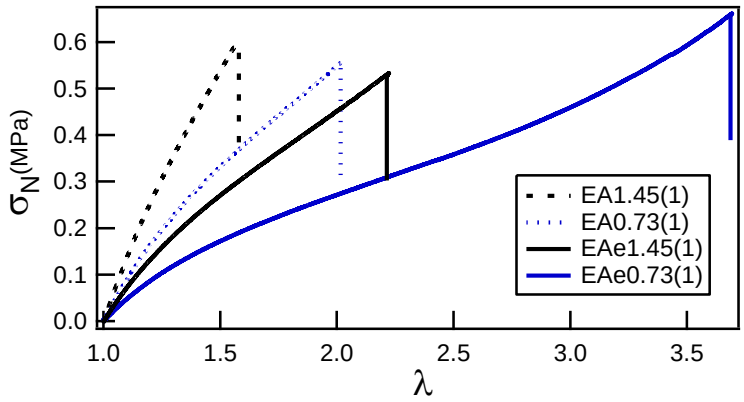

Figure 12: Stress-strain curves of different first networks showing the influence of the solvent in the synthesis of the first network

In Figure 12, the strain at break is also higher for samples made in the presence of solvent than for those made in the bulk. If a more effective crosslinking process occurs in the bulk then it leads to a smaller elongation at break of the first networks alone as predicted by the Lake-Thomas model. For those reasons, we expect that the samples created with a first network made from the bulk swell less at equilibrium than the other set of samples. The study of the multiple networks will now be the object of the following part.

2) Multiple networks made from first networks synthesised in the bulk

After the synthesis of the first networks, multiple networks were made using a combination of both bulk and solvent-synthesised networks. Three steps of swelling in monomer only (0.01 mol % of BDA and HMP) and polymerizing where done to obtain 4 different networks (as shown in chapter 2). The properties of those networks are shown in Table 6.

Sample name	First network	λ_0	SN wt%	Number of polymerization steps
EA1.45(1)				**1**
EA1.45(1.39)EA	**EA1.45(1)**	**1.39**	**32.6**	**2**
EA1.45(1.92)EA	**EA1.45(1)**	**1.92**	**13.5**	**3**
EA1.45(2.34)EA	**EA1.45(1)**	**2.34**	**7.9**	**4**
EA0.73(1)				**1**
EA0.73(1.51)EA	**EA0.73(1)**	**1.51**	**26.6**	**2**
EA0.73(2.19)EA	**EA0.73(1)**	**2.19**	**10.8**	**3**
EA0.73(2.73)EA	**EA0.73(1)**	**2.73**	**4.9**	**4**

Table 6: Characteristics of multiple networks made from bulk first networks

In Table 6, all samples are made from first networks synthesised without solvent. By comparing the fraction of first network in Table 3 and Table 6, one can note that while the same molar ratio of crosslinker relative to monomer was used in the solution for the first network, the equilibrium swelling is affected by the synthesis procedure, with or without solvent. Because the samples synthesised in the presence of solvent are then dried, the chains are slightly supercoiled, i.e. they are more compact and less entangled than when they are synthesised in the bulk. Therefore, the swelling is greater for those networks synthesised in the presence of solvent. For the two sets of samples synthesised with 1.45 mol % of BDA, the swelling leads to a fraction of first network of 32.6, 13.5 and 7.89 without solvent whereas the values are 20.5, 6.06 and 2.88 with solvent. The poorer swelling ability of the first network made in the bulk confirms the hypothesis that first networks made in the bulk are more efficiently crosslinked. This means that the extensibility limit of the networks synthesised in the bulk is lower and, from what has been seen in the current chapter part I), this should also lead to a hardening phenomenon occurring at lower extensions. This last statement can be verified by performing tensile tests on each sample of Table 6. The result of those tests are shown in two different graphs in Figure 13, one for each amount of crosslinker.

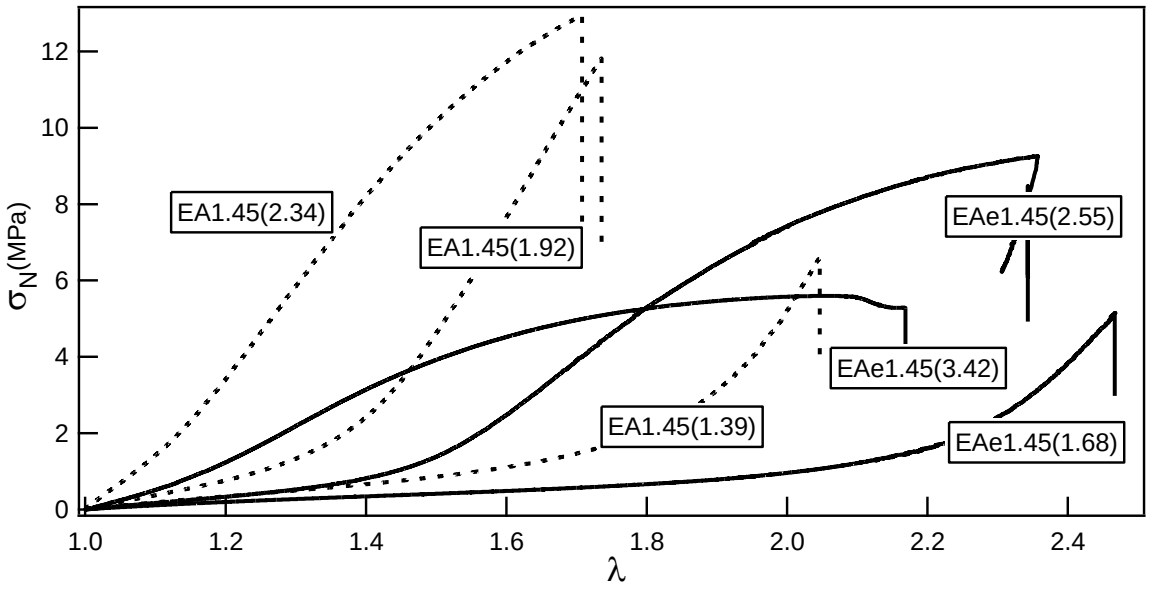

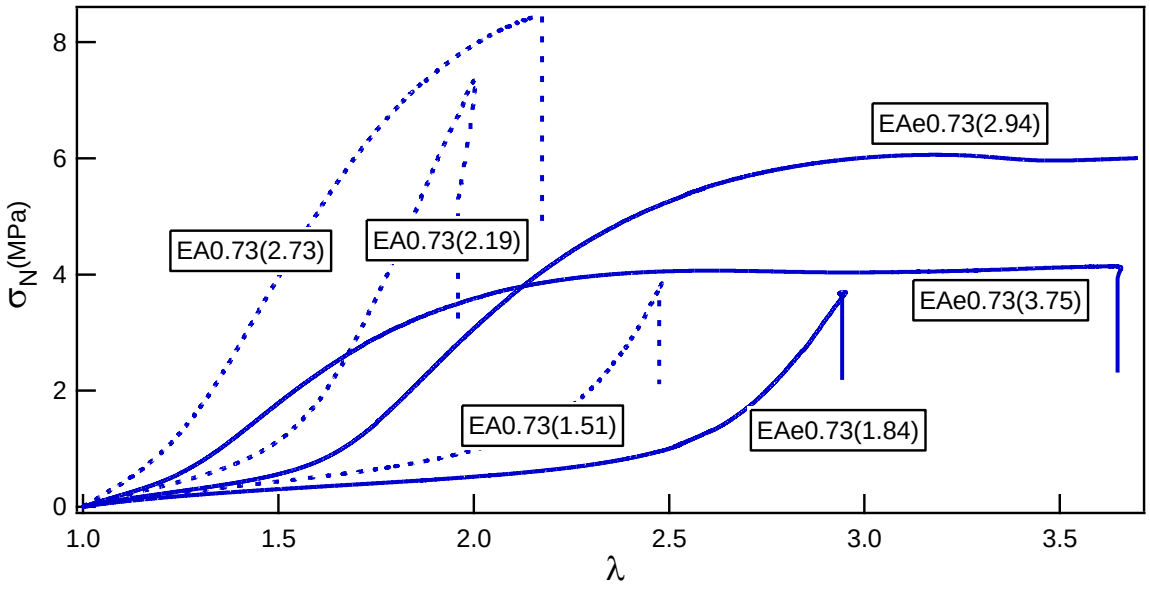

Figure 13: Stress-strain curves of multiple networks synthesised from first networks made in the bulk (dashed lines) or made in solvent (full lines). First networks are made with at the top 1.45 mol% of BDA and at the bottom with 0.725 mol% of BDA.

In Figure 13, we compare samples that have been made with the same number of polymerization steps. It is notable that samples with a first network made in the bulk always have a higher modulus value than the corresponding ones made with a first network synthesised in solvent. This is true for both amounts of BDA that have been used. The values of the Young's modulus can reach the highest point of 15 MPa for the sample EA1.45(2.34)EA.

If we compare samples at close levels of prestretching (the ones with the same steps of polymerizations), it can be seen that all samples made from the bulk first network show an earlier stiffening despite a smaller value of the first network prestretching. On the other hand, no samples made from the bulk show any necking phenomenon. Indeed, those samples display only type 2 (EA1.45(1.39)EA, EA1.45(1.92)EA, EA0.73(1.51)EA and EA0.73(2.19)EA) or type 3 (EA1.45(2.34)EA and EA0.73(2.73)EA) mechanical behaviour. To confirm the type 2 mechanical behaviour of EA1.45(1.39)EA and EA1.45(1.92)EA, step cycles experiment have been carried out. Those results are presented in Annex 1. Those stress-strain curves show nearly no dissipation confirming that those samples undergo a brittle fracture with a hardening followed by a macroscopic failure of the samples.

Another difference observed in Figure 13 is the elongation at break that is always smaller for samples synthesised from the first network made in the bulk, especially when samples showing some necking are compared to equivalent bulk ones. However, the stress at break systematically increases when the first network is made in the bulk. Indeed, the highest values that could be obtained in chapter 3 Figure 4 are around 10 MPa in nominal stress when here a stress at break of 13 MPa was measured for EA1.45(2.34)EA.

3) Analysis

In Figure 13, a higher modulus and an earlier hardening are observed for every sample prepared from a first network synthesised in bulk. Those two differences from the standard multiple networks are further evidence of the higher efficiency of the crosslink procedure in the bulk synthesis. The earlier stiffening is related to the presence of less C-C backbone bonds between crosslinks leading to a higher density of effective crosslinks. For further evidence of this difference, a fit to the Gent model as previously described in part 1 of this chapter can be carried out. From best fit values, the maximal elongation λ_m can be found for the two types of first networks made in bulk. The results are plotted in Figure 14. It can be seen first that the Gent model again works well to describe the hardening (refer to Annex 2). As expected, the materials made from first networks synthesised with the same proportion of BDA are clearly different depending on whether solvent is used or not during the synthesis of the first network. Indeed, for samples with 0.725 mol % of BDA, the average value of the maximal elongation of the first network λ_m changes from 5.9 for the series synthesised in the presence of solvent to 4.1 for that synthesised in the bulk. For the samples with 1.45 mol % of BDA, λ_m goes from 4.5 to 3.1 for solvent and bulk respectively.

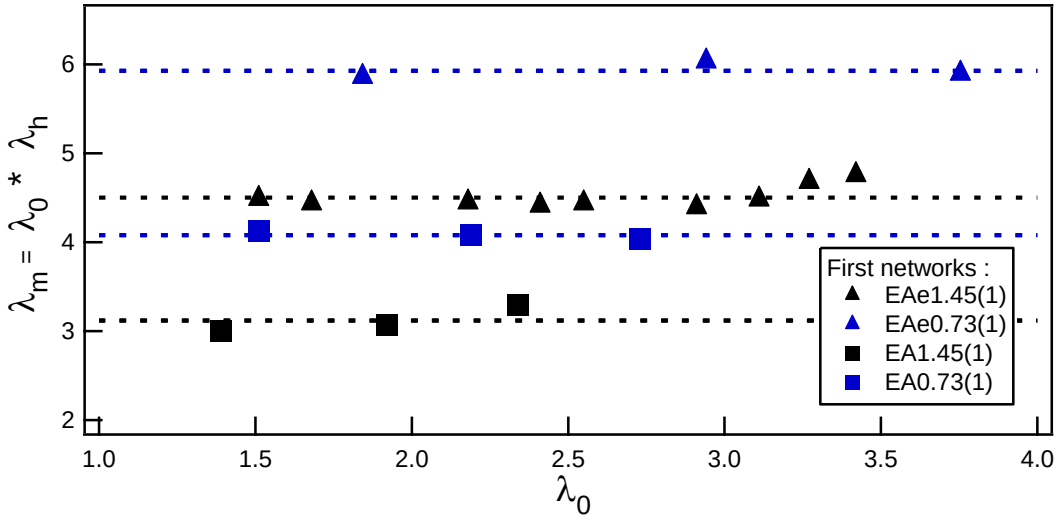

Figure 14: Representation of the maximum elongation for different multiple networks depending I the first network is made in solvent or not. The dashed lines correspond to the respective average of λ_m for each first network.

Assuming that there are no or few entanglements in our first networks, and using Figure 14, a comparison can be made in Table 7 between λ_m obtained from the average molecular weight between crosslinks obtained from the modulus of simple networks, and λ_m obtained from the Gent fits. As shown in Table 7 the two values of λ_m are in reasonable agreement. More importantly, Table 7 shows the difference in crosslinker efficiency when the synthesis is carried out in the bulk or in the presence of solvent. Indeed, the calculation of the average number of carbons between crosslinks shows directly the difference in efficiency. For 1.45 mol % of BDA, an average of 125 carbon bonds are obtained between crosslinks in the bulk compared to an average of 203 with a synthesis in 50 % solvent.

First network	E_x	$M_{x\ exp}$ (kg/mol)	N_{C-C}	λ_m Gent	λ_m calculated
EAe1.45(1)	0.81	10	203	4.502	4.1
EAe0.73(1)	0.53	16	310	5.93	5.1
EA1.45(1)	1.31	6.3	125	3.1	3.2
EA0.73(1)	0.93	8.9	176	4.1	3.8

Table 7: Characteristics of the different first networks showing the effect of the synthesis in solvent.

As an interim conclusion, we can see that the synthesis conditions of the first network are important. As shown in the part I of the current chapter, the concentration of entanglements decreases with the use of solvent during the synthesis. On the other hand, the synthesis in bulk conditions creates also a network with a higher efficiency of the crosslinking process. This leads to higher modulus values and earlier stiffening, but a smaller elongation at break and less swelling in monomer. Bulk conditions are useful to obtain stiff multiple networks (Young's moduli up to 15 MPa) that have a high nominal stress at break (up to 13 MPa).

It has therefore been shown that the use of solvent or not in the synthesis procedure of the first network is another way to tune the mechanical properties of the multiple network. A further possibility to tune the first network properties is to change the monomer used, which will be the object of the following section.

III) Modification of the multiple networks: influence of the nature of the monomers.

In this part the use of different monomers to make multiple networks is studied and this work was done with the collaboration of Elisa Deloffre during her master's degree. The goal is to prove the universality of the concept and to investigate the effect of the details of the chemistry of the monomers on the mechanical properties. To do so two types of monomers are used: acrylate monomers and methacrylate monomers.

The monomers that will be used in this part and some of the properties of the corresponding homopolymers are presented in Table 8.

Monomer	M_0 (g/mol)	Polymer T_g	M_e	ρ	C_∞
EA	100.212	-24	13000	1.13	9.76
BA	128.17	-54	25000	1.087	
HA	156.22	-57	27000	1.04	

HMA	**170.25**	**-5**	**33100**	**0.96**	**10.1**

Table 8: Different properties of used monomers. M_e represents the average molecular weight between entanglements ρ the density and C_∞ the structure factor.

1) Use of different acrylate monomers

a) Butyl acrylate networks

In his PhD work [1, 6], Ducrot used three types of monomers to synthesize his first networks: methyl acrylate, ethyl acrylate and butyl acrylate. The first networks were synthesised to obtain the same average theoretical molecular weight between crosslinks: 1700 g/mol. Since the monomers have different molar masses, by keeping the same average molecular weight between crosslinks, the number of backbone C-C bonds in elastic chains changes with the molar mass of the monomer. The butyl acrylate first network will have the smallest number of backbone bonds between crosslinks (13), followed by ethyl acrylate (17) and methyl acrylate (19). After the synthesis, tensile tests were performed on simple networks and it appeared that the butyl acrylate network was the most brittle. However, upon swelling the three simple networks in methyl acrylate and polymerizing them, the best DN was obtained with BA as first network. The study of the glass transition temperature of the DN BA1.45[MA] by DSC showed that a phase separation occurs in the sample [1, 6]. Since the sample is transparent, it must be a micro phase separation that takes place at the local scale in the sample. Because the BAe1.45[MA] has interesting properties, we decided to investigate the effect of the phase separation and therefore to study different monomers from ethyl acrylate.

Butyl acrylate first network

Due to the results obtained by Ducrot [6], butyl acrylate was used to create multiple networks with BA as first network and EA as second network (BAe1.86[EA]). The first network was synthesised to obtain the same molecular weight between crosslinks as EAe1.45(1). Since the molar mass of BA is 128.17, the amount of BDA used was 1.86 mol % to create BAe1.86(1). The synthesis of a first network with BA implies also a change in the dialysis procedure shown in chapter 2 where cyclohexane is replaced by ethanol.

After the synthesis of the first network, the same standard protocol was used to create multiple networks: a bath of monomer made of EA with 0.01 mol % of BDA and 0.01 mol % of HMP. The synthesised samples are listed in Table 9 which shows that the samples BAe1.86[EA] swell slightly less than EAe1.45[EA], leading to a smaller prestretching of the first network.

Sample name	First network	λ_0	SN wt%	Number of polymerization steps
EA1.45(1)				**1**
EAe1.45(1.68)EA	**EAe1.45(1)**	**1.68**	**20.5**	**2**
EAe1.45(2.55)EA	**EAe1.45(1)**	**2.55**	**6.06**	**3**
EAe1.45(3.42)EA	**EAe1.45(1)**	**3.42**	**2.88**	**4**
BAe1.86(1)				**1**
BAe1.86(1.59)EA	**BAe1.86(1)**	**1.59**	**20.8**	**2**
BAe1.86(2.41)EA	**BAe1.86(1)**	**2.41**	**6.3**	**3**
BAe1.86(3.21)EA	**BAe1.86(1)**	**3.21**	**3.3**	**4**

Table 9: Characteristics of the multiple networks made EAe1.45[EA] and BAe1.45[EA]

Once the samples are created, a DSC experiment was carried out on the different samples to investigate the presence of a phase separation. The DSC stands for Differential Scanning Calorimetry. The principle of this experiment is to analyse the heat flow needed to increase the temperature of a sample as a function of the temperature and to compare the heat flow needed to a reference. For those experiments, the temperature ranged from -80°C to 80°C, with a temperature increase set at 20°C per minute. For samples BAe1.86[EA], no phase separation was observed meaning that only one glass transition temperature (T_g) was observed as can be seen in Annex 3.

A series of tensile tests was performed at room temperature and the results are displayed in Figure 15. Because room temperature is far away from both T_g we did not adjust the temperature. The samples from the family BAe1.86[EA] have the same qualitative mechanical behaviour than those made of only ethyl acrylate. This graph also shows that an earlier onset of the hardening can be observed for every sample from the set BAe1.86[EA] in comparison to the equivalent set fully made from ethyl acrylate.

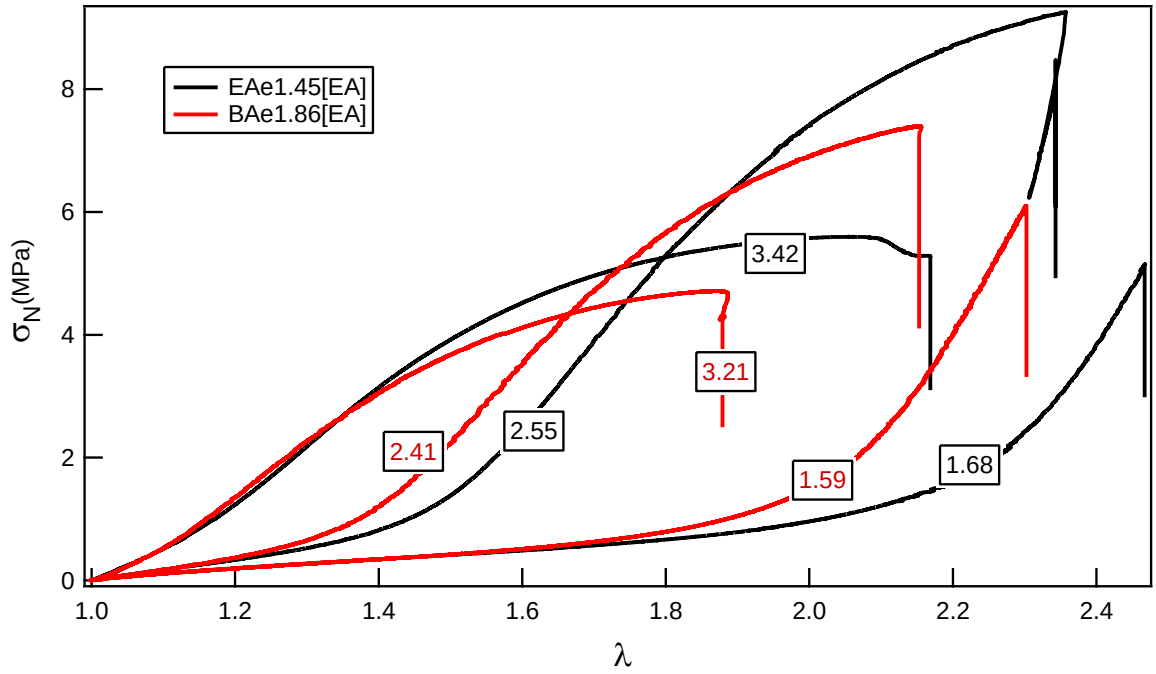

Figure 15: Stress-strain curves to compare the two sets of samples EAe1.45[EA] (black) and BAe1.86[EA] (red). The values on each curves are the respective value of λ_0 for each network.

It has been seen earlier in this chapter and in chapter 3 that the onset of the hardening is linked to the intrinsic extensibility of the chains of the first network. In Figure 15, an earlier stiffening for BAe1.86[EA], for samples showing a smaller prestretching, clearly shows that the finite extensibility of the first network is reached at lower deformations. This was expected because the synthesis is designed to conserve the molecular weight between crosslinks. Therefore, when monomers with larger side chains are used, shorter chains between crosslinks are created leading to a lower maximum extensibility.

The differences between first networks do not seem to have an important impact on the mechanical properties of the multiple networks. To go one step further, we also modify the second network leading to networks composed of only BA.

Multiple networks of butyl acrylate

This time, the second network was also made from butyl acrylate to create the set of samples BAe1.86[BA]. For the second polymerization, the bath of monomer is made of BA with 0.01 mol % of BDA and 0.01 mol % of HMP. Three different multiple networks were synthesised with such a bath. The details of those networks are shown in Table 10, in comparison to the family shown in the previous part BAe1.86[EA].

Sample name	First network	λ_0	SN wt%	Number of polymerization steps
BAe1.86(1)				**1**
BAe1.86(1.59)EA	**BAe1.86(1)**	**1.59**	**20.8**	**2**
BAe1.86(2.41)EA	**BAe1.86(1)**	**2.41**	**6.3**	**3**
BAe1.86(3.21)EA	**BAe1.86(1)**	**3.21**	**3.3**	**4**
BAe1.86(1.64)BA	**BAe1.86(1)**	**1.57**	**22.6**	**2**
BAe1.86(2.28)BA	**BAe1.86(1)**	**2.28**	**8.4**	**3**
BAe1.86(2.88)BA	**BAe1.86(1)**	**2.88**	**4.2**	**4**

Table 10: Characteristics of the multiple networks BAe1.86[EA] and BAe1.86[BA]

Table 10 shows a small difference in equilibrium swelling, the equilibrium degree of swelling with ethyl acrylate being higher than when swelling is done with butyl acrylate, suggesting that the molar volume of the swelling monomer is here more important than the χ parameter. This leads to a small difference in prestretching between the two sets of samples. Once the samples have been dried, tensile tests are performed to study their mechanical properties. Stress-train curves are shown in Figure 16.

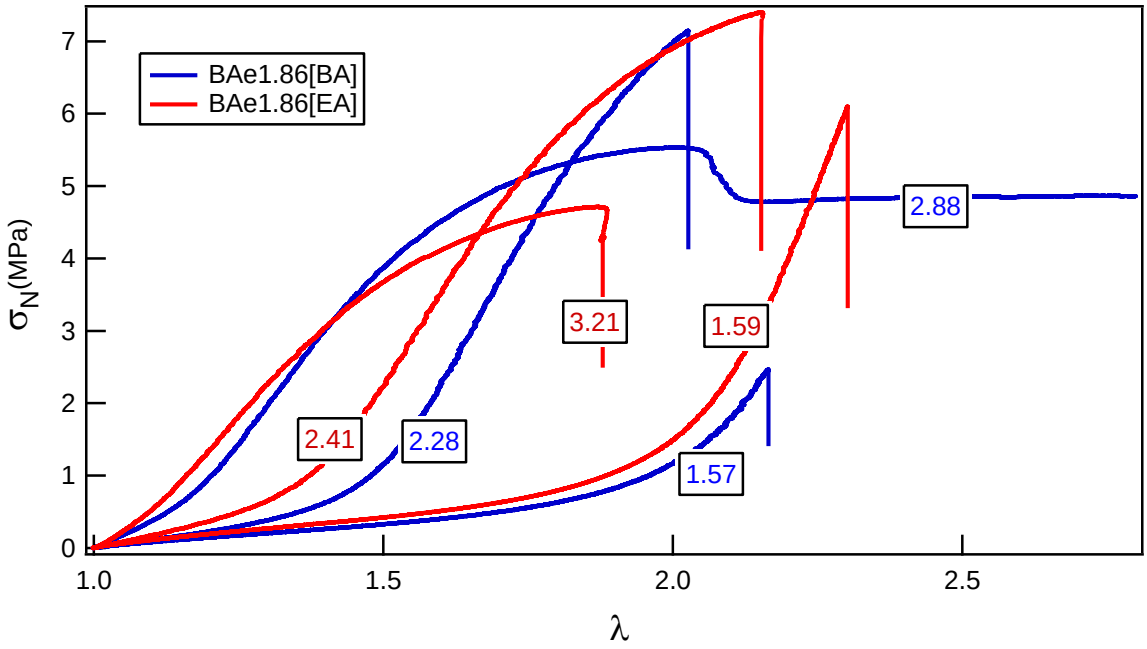

Figure 16: Stress-strain curves of multiple networks elastomers presented in Table 10. Blue curves correspond to BAe1.86[BA] samples and red curves to BAe1.86[EA] samples.

In Figure 16, the same observation can be made as for Figure 15: the mechanical behaviour is similar. The onset of the hardening is controlled by the prestretching of the first network. Since the same first network is used for both families of samples, this result was expected. The use

of EA or BA as second network does not appear to create any difference, only the equilibrium swelling of the first network is changed.

The use of BA as first or second network does not have a large impact on the mechanical properties. The same properties are obtained with networks done with BA, even if four polymerizations are carried out. This result confirms the architecture universality of the multiple networks. Phase separation has not been obtained so its impact has not been studied, to do so, a monomer with a longer side chain is used.

b) Hexyl acrylate to force the phase separation

In order to obtain the clear phase separation that Ducrot observed [1] for networks BA[MA], a monomer with a longer side chain has been chosen. Indeed, a longer side chain implies a more hydrophobic monomer that should be more likely to phase separate with ethyl acrylate. The chosen monomer is hexyl acrylate HA. It was difficult to obtain homogeneous first networks with the HA monomer alone so hexyl acrylate will only be used as a swelling monomer to create second networks within a first network made of EA. The solution to make second networks is kept similar as the standard procedure but with HA as monomer, 0.01 mol % of BDA and HMP. Three multiple networks are synthesised and their characteristics are in Table 11 and show a clear difference in equilibrium swelling where samples EAe1.45[HA] swell noticeably less than EAe1.45[EA].

Sample name	First network	λ_0	SN wt%	Number of polymerization steps
EA1.45(1)				**1**
EAe1.45(1.68)EA	**EAe1.45(1)**	**1.68**	**20.5**	**2**
EAe1.45(2.55)EA	**EAe1.45(1)**	**2.55**	**6.06**	**3**
EAe1.45(3.42)EA	**EAe1.45(1)**	**3.42**	**2.88**	**4**
EAe1.45(1.41)HA	**EAe1.45(1)**	**1.41**	**33.3**	**2**
EAe1.45(2)HA	**EAe1.45(1)**	**2**	**11.8**	**3**
EAe1.45(2.62)HA	**EAe1.45(1)**	**2.62**	**5.5**	**4**

Table 11: Characteristics of the multiple networks EA[EA] and EA[HA]

Once the samples were synthesised, DSC experiments as described earlier were performed. The heat-flow as a function of the temperature for the sample EAe1.45(1.41)HA is shown in Figure 17. It seems that, despite being macroscopically transparent, the sample EAe1.45(1.41)HA presents a micro-phase separation. Indeed, in Figure 17, two T_g can be observed one at -48°C (corresponding to the T_g of the poly(hexyl acrylate) and the other one

at -14°C (corresponding to the T_g of the poly(ethyl acrylate). Those two T_g prove the non-miscibility of the two polymers. Regarding the two other samples EAe1.45(2)HA and EAe1.45(2.62)HA, no double T_g could be clearly observed. Only one T_g could be observed as shown in Annex 4. The absence of a double T_g might be due to the high dilution of the ethyl acrylate first network that only represent 12 and 6 wt% in those samples.

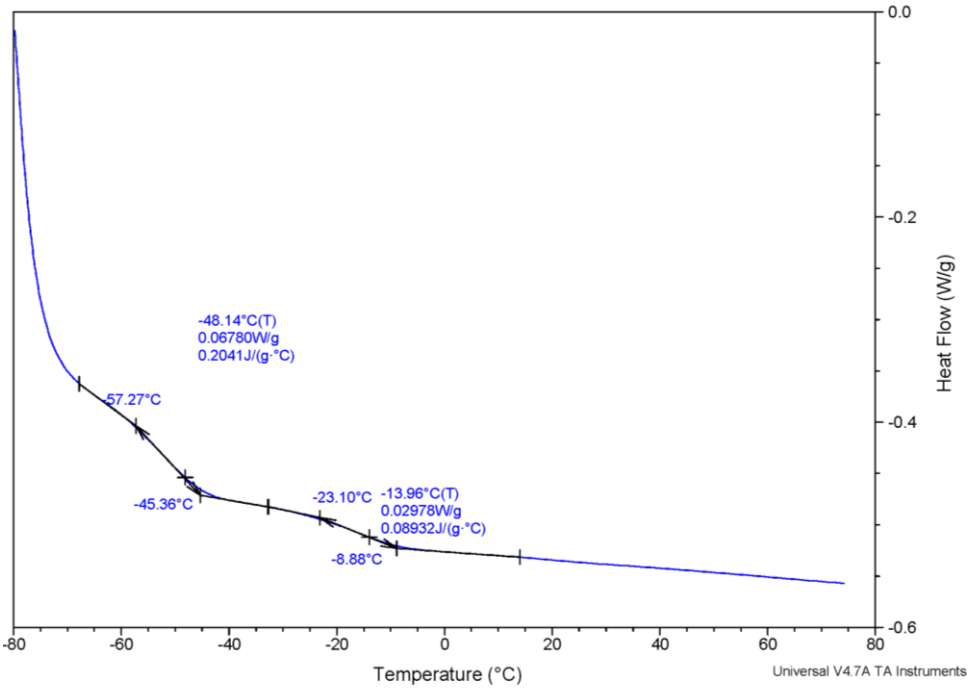

Figure 17: Heat flow versus temperature for the sample EAe1.45(1.41)HA

Once the micro-phase separation was identified, tensile tests were carried out to see if this phenomenon affects the mechanical properties. The results are presented in Figure 18. The sample EAe1.45(2)HA slipped in the clamps so a second test was done on the same sample as it can be seen with the two different curves.

Figure 18 shows that, considering the difference in prestretching obtained, the mechanical properties are quite similar in comparison to the reference EAe1.45[EA]. Indeed for example, EAe1.45(1.41)HA contains only 66 wt% of second network. From Figure 18, no reinforcement is observed for that sample. The micro-phase separation does not seem to have an impact on the mechanical properties. For the more swollen sample of EAe1.45[HA] the mechanical behaviour corresponds to that obtained with the first network EAe1.45 at this degree of prestretching.

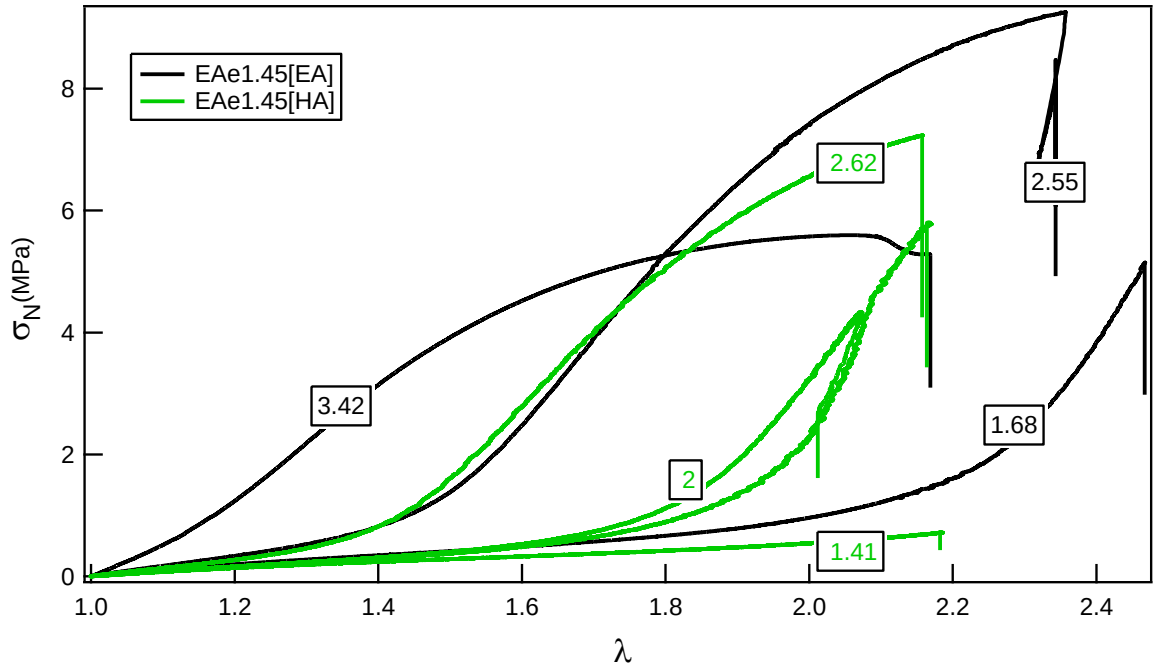

Figure 18: Stress-strain curves of multiple networks elastomers presented in Table 11. Black curves correspond to EA[EA] samples and red curves to EA[HA] ones.

At this point, there is no clear evidence of the impact of the change of monomer, to investigate further this change, some more in-depth analyses of the data are needed.

c) Analysis

Young's modulus

As it can be seen in Table 8, the average molecular weight between entanglements changes for the homopolymers made from different monomers. Those changes did not show any qualitative influence on the maximal stress and strain for a given prestretching but could have an impact on the Young's modulus. To investigate the evolution of the modulus, a comparison is made between EAe1.45[EA] and EAe1.45[HA] and between BAe1.86[EA] and BAe1.86[BA]. The modulus measured on the stress-strain curves is plotted in Figure 19 as a function of the degree of prestretching of the first network.

Figure 19a) shows the Young's moduli as function of λ_0 for samples made from the same first network EAe1.45(1) but two different monomers as second networks. It shows that the modulus of the set of samples EAe1.45[EA] is slightly higher than that of EAe1.45[HA] but differences are small and the increase in modulus is continuous. Figure 19b) shows the same moduli for a first network BAe1.86(1) and two different monomers used for the second network: BA and EA. Figure 19b) tends to show a small increase in the Young's modulus of BAe1.86[EA] relative to the set of samples BAe1.86[BA].

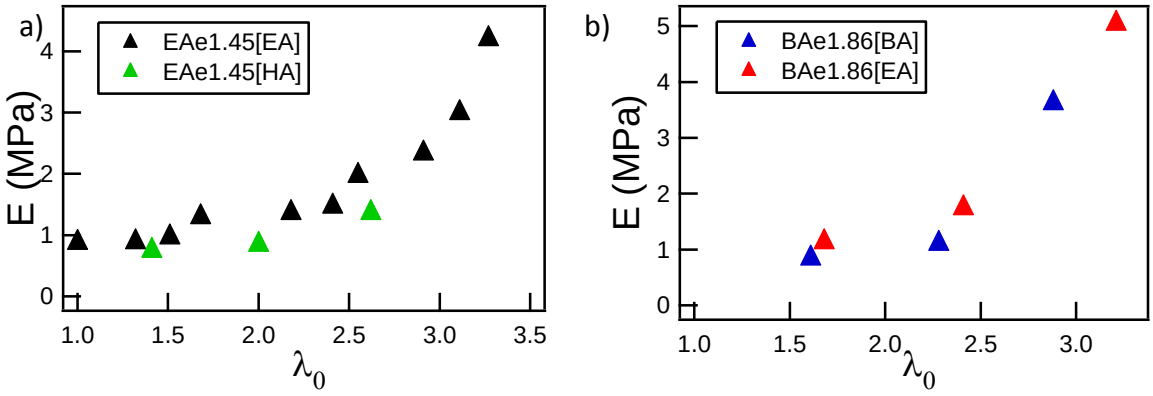

Figure 19: Evolution of the modulus of multiple networks elastomers as a function of λ_0 depending on the monomer used for the second network. a) EAe1.45 is the first network, b) BAe1.86 is the first network

The only difference in those samples comes from the monomers used for the second network. Table 8 shows that the homopolymers made from those monomers do not have the same molecular weight between entanglements and our data shows that the modulus is slightly lower when the monomer of the second network has a lower entanglement density.

The results of Figure 19 confirm that the modulus of multiple networks elastomers is also controlled by the density of entanglements in the second network. A higher entanglement density in the second network leads to a higher modulus. Another analysis that can be made on this set of data is how Gent's model describes the strain hardening of those multiple networks.

Strain hardening

As used in chapter 3 and in the current chapter, the Gent model was used to characterize the strain hardening of the samples using different acrylate monomers as second network. The goal of using Gent's model here is to see if the nature of the second network has an influence on the hardening of the first network. As in the previous section, the objective will be to compare the samples with the exact same first network: EAe1.45[EA] with EAe1.45[HA] and BAe1.86[EA] with BAe1.86[BA]. The fit is done as described in chapter 3 section II)3). λ_m can be then calculated for each multiple network from the best fit of J_m and the results are shown in Figure 20.

For the multiple networks made with BAe1.86(1), the values obtained for λ_m are relatively constant around an average value of 3.9. However, for the samples made with EAe1.45(1), a small difference is observed with λ_m being a bit higher for the samples using EA as second network than the networks using HA. This change of limiting extensibility could indicate a difference of interaction taking place between the two types of networks. Only two points have been obtained here and more experiments should probably be made to confirm this tendency. More experiments would be also useful to understand if the micro-phase separation has an influence on the onset of the hardening as it might be seen in Figure 20.

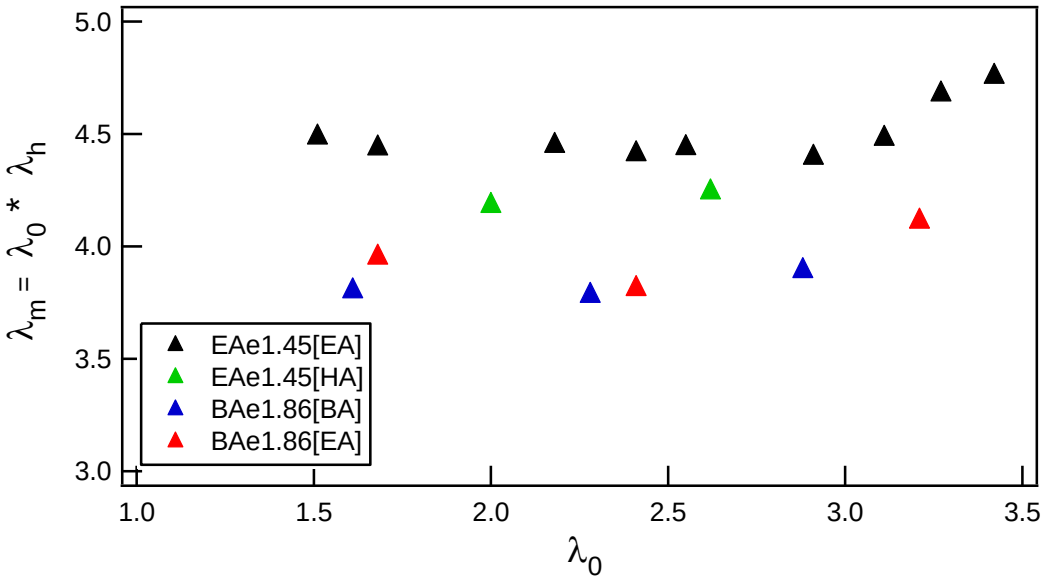

Figure 20: Evolution of λ_m as a function of λ_0 to investigate the influence of the nature of the second network.

The values of λ_m obtained in Figure 20, are in good agreement with the difference in moduli observed in Figure 19. Indeed, the smaller value of λ_m obtained for BA1.86 can explain the earlier onset of the modulus increase observed in Figure 19b in comparison to the samples made with EAe1.45.

Master curve

As it was done in the previous section, a stress-stretch master curve can now be plotted for the samples with different monomers. As discussed earlier, the comparison can be effectively done for similar first networks with the same λ_m . Therefore, two master curves are shown in Figure 21, one with the first network being EAe1.45 and the other one Bae1.86.

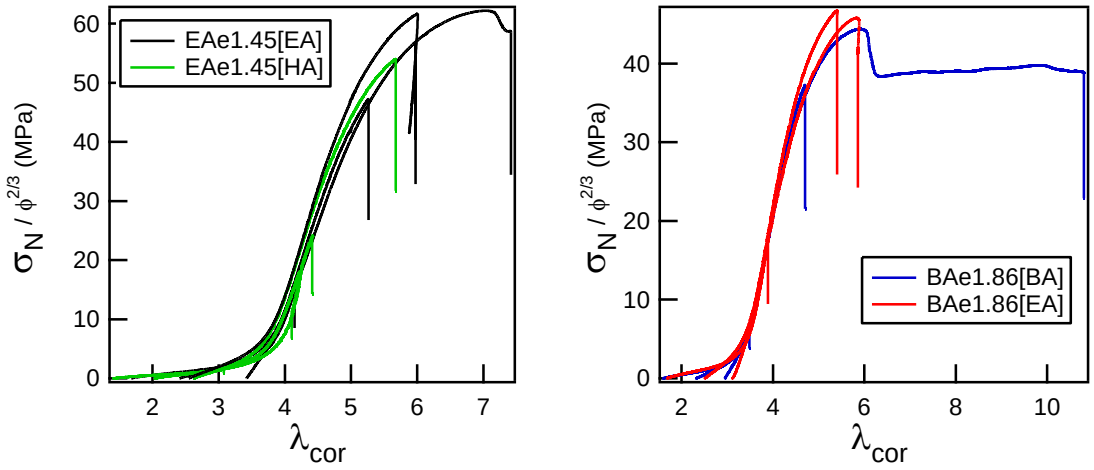

Figure 21: Corrected master curves for the samples made from on the left EAe1.45 and on the right BAe1.86 using different monomers as second network.

Figure 21 clearly shows two good master curves that seem to be rather independent of the choice of the second monomer as long as the data is rescaled by the equilibrium swelling. The hardening and the softening are both well described by the correction by respectively the prestretching and the dilution in the cross-sectional plane. Regarding the yield stress, few samples present a clear necking but from the curve here we expect that the renormalization of the stress is valid.

However if all the data points are plotted on a single graph by performing a normalization of λ_{cor} by the maximum elongation λ_m, a clear difference in yielding values can be observed for the two types of first networks in Figure 22.

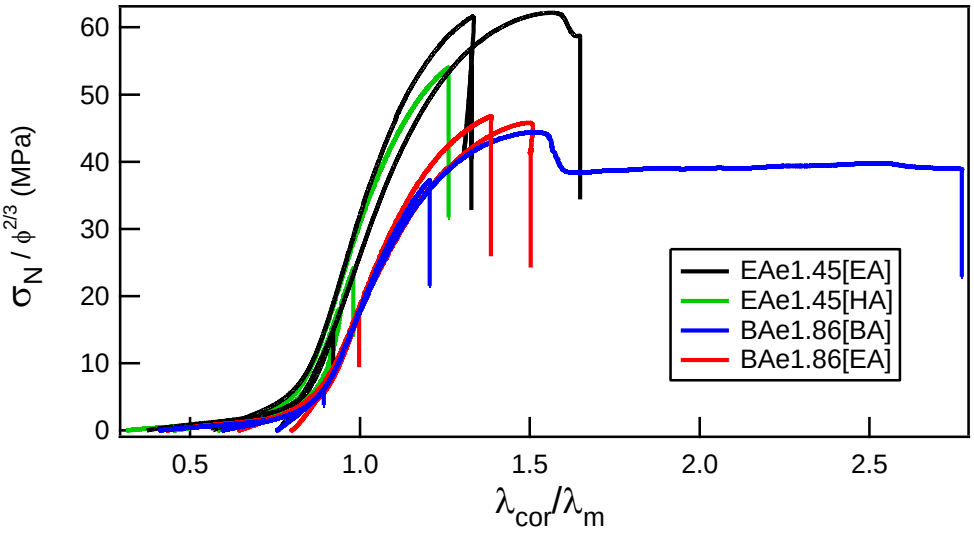

Figure 22: Overall master curves for the samples made from EAe1.45 and BAe1.86.

Two observations can be made from the analysis of Figure 22. First the slope of the hardening is slightly different, even if the inflexion point occurs at the same ratio of λ_0/λ_m. This might be due to a different distribution of chain lengths in the network. The second point concerns the values of the yield stress that are significantly smaller for the samples using BAe1.86(1) than for those using EAe1.45(1). This is an intriguing difference that suggests that the PBA first network is intrinsically easier to break than the PEA network. This discrepancy points to the fact that while the stress of the unbroken network might scale with the areal density of the chains, the yield process of the first network may be more complex. Following the molecular fracture model of Brown and the Lake-Thomas model one would expect a more brittle PBA network (lower number of C-C bonds that need to be broken), but this remains a hypothesis.

As a conclusion to this part, there is no clear evidence of any impact on the mechanical properties of a micro-phase separation. This section helped to confirm the universality of the multiple network concept that works with different chemistries.

However, the nature of the second monomer used has a clear impact on the equilibrium swelling properties of the first network and a larger monomer tends to decrease the level of swelling of the first network as expected from theory. However the impact of the nature of the second monomer on the mechanical properties is not clear. Despite having different T_g

the mechanical behaviours of the multiple networks are essentially controlled by the nature of the first network and its level of prestretching.

The main impact of larger monomers comes from their use as first network. First using the same molar mass between crosslinks with a larger monomer naturally decreases the maximal elongation but it seems that it has also an impact on the damages occurring in the network. Indeed, Figure 22 shows a difference in the softening and in the necking values for different monomers in the first network with a bigger monomer and shorter chains leading to more softening and an earlier yield.

In order to introduce a more pronounced chemical change to our system methacrylate monomers have been tested and are the subject of the following part.

2) Use of methacrylate monomers

a) Structure and interest of methacrylate monomers

In chapter 2, a change of solvent from toluene to ethyl acetate has been done to suppress the transfer reactions to the solvent during the synthesis of the first network. But the solvent is not the only source of transfer reactions. Indeed, acrylate networks themselves are subject to chain transfer since the H in alpha of the acrylate function is labile (Figure 23: (a)). This means that during the synthesis of the second or subsequent networks, a radical could bond to a chain by replacing the H shown in red in Figure 23: (a). This could lead to more coupling between the networks. To avoid this phenomenon, methacrylate monomers can be used. As shown in Figure 23: (b), methacrylate molecules present a methyl group instead of the labile H. This methyl group cannot be replaced by a radical, therefore the amount of transfer reactions is dramatically reduced.

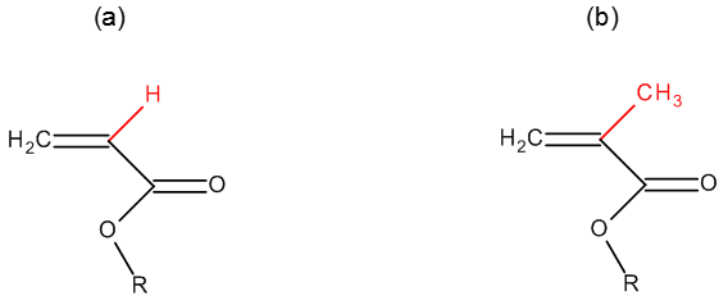

Figure 23: Structure difference between acrylate (a) and methacrylate monomers (b)

In this section, HMA will be used to try to see the potential influence of the transfer reactions on the properties of multiple networks. HMA was chosen for its quite low T_g (-5°C) in comparison to other methacrylate polymers. It is a monomer with a long side chain in comparison to ethyl acrylate. The first experiment that was done with HMA was to use it as a second network with a first network of EA. Double, triple and quadruple networks were made. The reactivity of methacrylates is known to be less good than that of acrylates. For this reason, the polymerization time was increased from 2 hours to 6 hours. In Annex 5, the stress-strain

curves are shown. Those networks did not show good mechanical properties certainly due to the fact that the swelling with HMA was poor and not homogeneous.

b) HMA as first network

The real interest of the use of HMA is to use it as a first network. Indeed, as first network, during the other polymerisation steps, no second network will be able to react onto the first network. This will lead to a first network that is separated from the other networks and that can rearrange more freely.

The synthesis of HMA first networks was difficult, with the standard procedure. We had to increase the polymerization time to 6 hours. Nevertheless, that did not lead to a good first network so the UV initiator HMP amount was also increased 10 times. This increase of the HMP was efficient to obtain a first network after 6 hours of polymerization. On the other hand, the synthesis in solvent resulted in some breakage during the dialysis process. It is possible that the ideal deswelling solvent has not yet been found. In order to obtain a first network made of HMA it was then decided to create one without solvent and with the equivalent molecular weight between crosslinks as EA0.73(1). This means 1.24 mol % of BDA was used. This synthesis was successful and the networks made from it will be compared to those made from EA0.73(1) presented in section II)1).

Following the synthesis of a HMA first network, multiple networks were created using the same procedure shown in chapter 2 but with a 6 hours long polymerization. Table 12 shows the characteristics of the obtained multiple networks. From Table 12, it can be seen that the swelling properties are similar and that the multiple networks have similar levels of first network prestretching and can easily be compared.

Sample name	First network	λ_0	SN wt%	Number of polymerization steps
EA0.73(1)				**1**
EA0.73(1.51)EA	**EA0.73(1)**	**1.51**	**26.6**	**2**
EA0.73(2.19)EA	**EA0.73(1)**	**2.19**	**10.8**	**3**
EA0.73(2.73)EA	**EA0.73(1)**	**2.73**	**4.9**	**4**
HMA1.24(1)				**1**
HMA1.24(1.43)EA	**HMA1.24(1)**	**1.43**	**28.7**	**2**
HMA1.24(2.14)EA	**HMA1.24(1)**	**2.14**	**9.7**	**3**
HMA1.24(2.68)EA	**HMA1.24(1)**	**2.68**	**5.5**	**4**

Table 12: Comparison of multiple network characteristics between HMA0.73[EA] and EA0.73[EA]

Once the synthesis is completed, the tensile tests were performed on each multiple network. It has to be mentioned that since the glass transition temperature of HMA is around -5 °C, the tensile test were carried out at 30 °C instead of 20 °C for a better comparison with EA. The results are presented in Figure 24 and some interesting differences are immediately clear. Note that the stress-strain curve of the sample HMA1.24(2.14)EA has a slightly different shape due to early slippage in the clamps during the first test, the tensile test has been done again on the same sample, which was already slightly damaged.

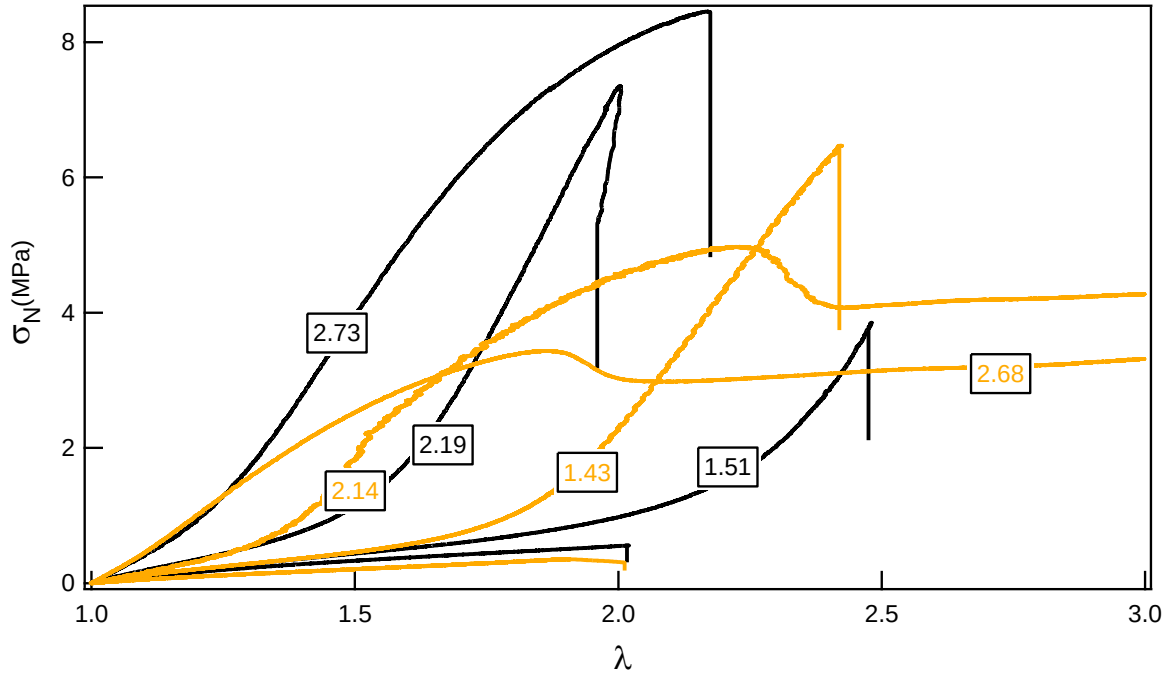

Figure 24: Stress-strain curves of multiple networks elastomers presented in Table 12. Black curves correspond to EA0.73[EA] samples and red curves to EA0.73[HMA] ones.

First the onset of hardening appears somewhat earlier with the first network HMA1.24(1): this was expected as explained earlier due to the fact that the monomer HMA has a higher molecular weight and fewer C-C bonds are present between crosslinks. This is confirmed by the measurement of the Young's modulus that is lower for the respective samples EA0.73[EA] in comparison to HMA1.24[EA].

Secondly, the yield stress observed for HMA1.24(2.14)EA and HMA1.24(2.68)EA at the same prestretching level is much lower than for the EA0.73[EA] set of samples. In comparison, the value expected for EA0.73(2.73)EA would be around 9 MPa when HMA1.24(2.68)EA necks at 3.4 MPa.

The Young's modulus is plotted as a function of the prestretching in Figure 25 for both systems and differences are small. The smaller values obtained for the samples made with HMA as first network could be due to a smaller efficiency of the synthesis leading to less crosslink points than expected.

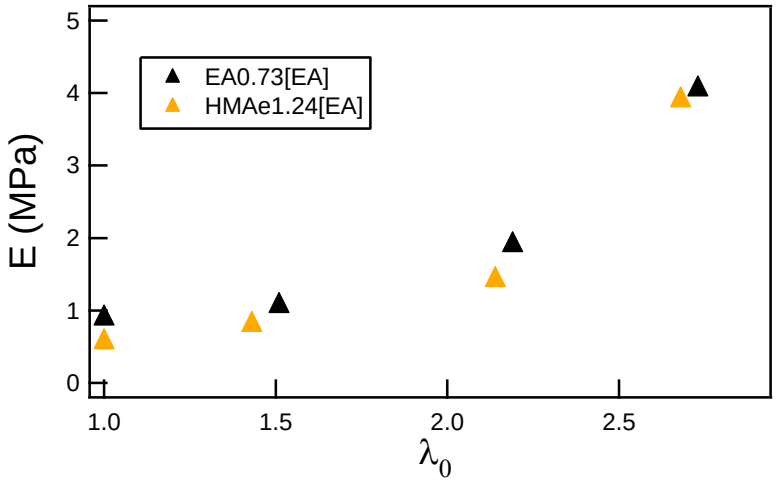

Figure 25: Young's modulus as a function of the prestretching for samples using EA or HMA as first network's monomers.

Next, the Gent fit has been applied to the set of samples with HMA as first network. From this operation, the extrapolated value of the maximal elongation can be obtained from the fit as done in chapter 3 section II)3) and the results are shown in Figure 26.

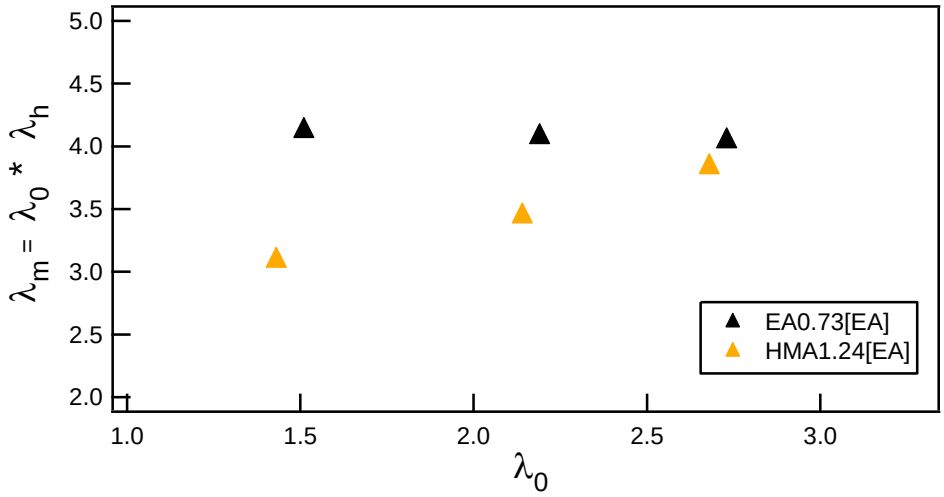

Figure 26: Evolution of λ_m as a function of λ_0 for samples with EA0.73(1) (in black) or HMA1.24(1) (in orange) as first network.

Figure 26 shows that the obtained values for λ_m for the samples of the family HMA1.24[EA] are not constant. Nevertheless, the average gives a value of maximal elongation of 3.4, as expected because of the monomer size, this value is below that found for EA0.73 which is around 4.1. Using the value of the Gent fit, a master curve can be plotted. To do so we normalize the nominal stress by the areal density of chains and the stretch by the prestretching divided by the maximum elongation obtained with the Gent fit. The result is shown in Figure 27.

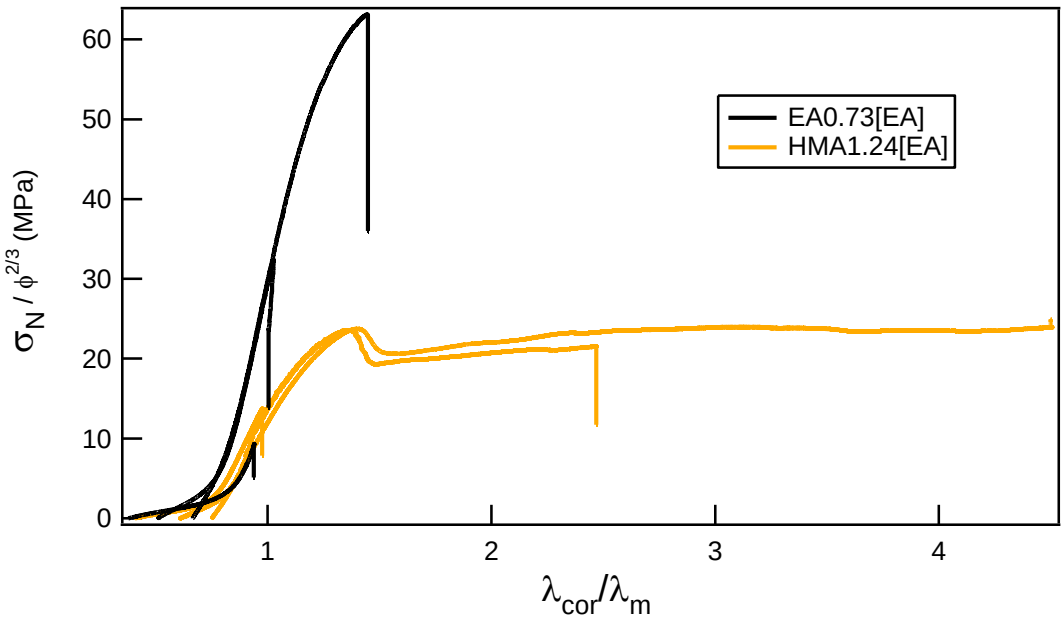

Figure 27: Stress-strain master curve for multiple networks elastomers presented in Table 12. Black curves correspond to EA0.73[EA] samples and red curves to EA0.73[HMA] ones.

Figure 27 shows that for each type of network, a relatively good master curve is obtained. Those two master curves are however quite different in terms of slope of the hardening that is much higher for EA0.73[EA] than HMA1.24[EA]. Also, the yield stress values per chain appears to be quite different as observed in Figure 24. This Figure 27 gives a clear evidence that the change of first network monomer has a great impact. The observed difference is even more significant than with BA as shown in Figure 22 and might be due to the difference in synthesis due to the presence of a methacrylate monomer.

This difference suggests that the transfer reactions may be important to transfer the stress from a highly stretched network to the other less stretched one. More systematic experiments without transfer may be needed to elucidate this point.

Conclusion

In this chapter, the influence of different parameters of the first network has been studied through tensile tests. First, the change in crosslinker density has been investigated. It has shown that a decrease of crosslinker will logically lead to a higher swelling ratio of the network but also to a higher finite extensibility of the first network. The construction of a master curve has shown that the corrections applied to the strain and stress do not appear to be valid if entanglements are largely present in the first network.

Secondly, the synthesis of the first network without solvent has been tried leading to a higher efficiency of the crosslinker. A higher crosslink density leads to less swelling and a smaller lambda max.

Finally, different monomers have been tried. It has been observed that the use of larger monomers in the second network leads to less swelling, and that has been attributed to the molecular size. Also, as expected, the extensibility of the first network is less when larger monomers are used with an unchanged molecular weight between crosslinks. This confirms the link between the final extensibility of the first network and the number of monomers in the chain. The use of methacrylate monomers is another way to change the first network configuration. Indeed, its use avoids the creation of covalent bonds between the first network and the networks polymerized afterwards due to the absence of any labile hydrogen in the first network. It is not clear yet but it seems that this absence of connections between the loosely networks and the prestretched network leads to interesting mechanical properties. It has been observed that a yield stress can be obtained for less prestretched samples with a higher weight fraction of first network and the necking observed for those samples appeared to be very stable and did not show any early breakage. This last result suggest that the extent of coupling between the networks plays a crucial role in controlling the stress transfer and the breakup process of the first network.

Conclusion on tensile tests

The use of tensile tests coupled with step cycle experiments has led to the classification of the different multiple network elastomers based on their mechanical behaviour. Those networks have been shown in chapter 3 to present four types of stress-strain curves which can be renormalized to approximately fall on the same master curve. The stress can be corrected by the prestretching of the first network defined as λ_0. At large strain, this correction can be coupled by a correction of the stress by the dilution of the surface chain density in the cross-section plan. This correction has been shown to give reasonably good master curves even between samples with different types first networks. However, this correction can be applied only where the stretching of the first network governs the mechanical behaviour of the sample. This is not the case at small strain where the stress is carried also by the entanglements of the second networks. The resulting master curve gives good results between the hardening up to the yield stress where it is not clear yet which parameters control this behaviour.

Following the analysis done in chapter 3, different properties of the first network have been tuned in chapter 4. As expected, it has been confirmed that the crosslink density affects the hardening phenomenon by changing the maximal elongation. Then by removing the solvent in the synthesis it has been shown that wider mechanical properties can be obtained with networks showing very high modulus and high stress at break. Finally the effect of the monomer has been studied. The change of monomer in the second network did not show any interest but the best effects where observed with a change of 1st network monomer. It was shown that it has an impact on the slope after the hardening and on the values of the yield stress. Those results are not understand yet and more experiments should be done to do so but the methacrylate as a first network shows some promising properties that could be linked with the absence of connections with the second networks.

The results obtained in tensile test have led to a better understanding of the link between the molecular structure of the networks and their mechanical properties. With that knowledge one can now decide how to create a multiple network depending on which stress-strain curve is targeted. However, the tensile tests are not sufficient to fully characterize some materials, in order to do that, the impact of cracks has to be evaluated. To do so, the following chapter will be discussing of fracture experiments on some of the materials presented in chapter 3 and 4 in order to link the properties in tensile tests to the fracture toughness that will be measured.

References

1. Ducrot, E. and C. Creton, *Characterizing Large Strain Elasticity of Brittle Elastomeric Networks by Embedding Them in a Soft Extensible Matrix.* Advanced Functional Materials, 2016. **26**(15): p. 2482-2492.
2. Rivlin, R.S., *Large Elastic Deformations of Isotropic Materials .4. Further Developments of the General Theory.* Philosophical Transactions of the Royal Society of London Series a-Mathematical and Physical Sciences, 1948. **241**(835): p. 379-397.
3. Mooney, M., *A Theory of Large Elastic Deformation.* 1940.
4. Urayama Kenji, K.S., *Uniaxial elongation of deswollen polydimethylsiloxane networks with supercoiled structure* Polymer, 1997. **38**(4): p. 955-962.
5. Gent, A.N., *A New constitutive relation for rubber.* Rubber Chemistry and Technology, 1996. **69**: p. 59-61.
6. Ducrot, E., *Double Network Elastomers*. 2013, Université Pierre et Marie Curie: Paris.

Chapter 5: Fracture properties of multiple network elastomers and visualisation of the crack tip deformation

Chapter 5: Fracture properties of multiple network elastomers and visualisation of the crack tip deformation

Introduction

Tensile tests characterize the mechanical properties of a sample in terms of Young's modulus, stress at break and elongation at break. Cyclic experiments also lead to the knowledge of the viscoelastic, damage and recovery properties of a sample. Yet, when a material is used for industrial applications, often a crack can appear during its lifecycle or during its preparation, the ability of the material to avoid crack propagation is crucial for its lifetime use. In practice, the fracture energy gives the information of the ability of a material to resist crack opening and propagation.

For simple polymer networks, we saw in chapter 1 with the Lake and Thomas theory [1], that the fracture energy can be linked to the length of the elastic chain between crosslinks. This theory predicts that for a given chemistry of the polymer, the fracture energy of a crosslinked network scales with the inverse square root of the density of crosslinks. This result has been confirmed experimentally [2].

In chapter 3 and 4, our multiple network elastomers have been characterized with uniaxial tensile tests. Those tests have resulted in a clear understanding of their general mechanical behaviour as a function of their composition and synthesis steps. In this part, we will focus on the study of the fracture energy of the same materials.

I) Fracture energy of multiple networks elastomers

1) Measurement of the fracture energy

In the study of the mechanical behaviour of materials, one of the important properties is the ability of the material to avoid the propagation of an existing crack. This property is commonly referred to as fracture toughness (Γ) and is characterized with fracture mechanics experiments. More specifically, the fracture energy is the energy necessary to propagate a crack per unit area and is expressed in J/m².

For elastomers, the evaluation of the fracture energy has given rise to many experimental approaches. In this work, we follow the energy approach developed by Rivlin and Thomas [3] and the approximation proposed and checked experimentally by Greensmith for single edge notch samples [4]. The simple expression proposed by Greensmith to quantify the fracture energy for this geometry is shown in Eq. (1).

$$\Gamma = 2\,C * W(\lambda_c) * a \qquad \textbf{Eq. (1)}$$

In Eq. (1), C is a strain dependent empirical correction associated to the lateral contraction of the sample in extension, a is the initial length of the crack, $W(\lambda_c)$ is the strain energy density and λ_c the elongation at which the crack starts to propagate.

The strain energy density $W(\lambda_c)$ is calculated from the stress-strain curve obtained during the tensile test of the un-notched sample. To do so, λ_c is obtained by performing a tensile test on a notched sample as described in chapter 2 section II)2). Then this λ_c is reported on the stress-strain curve of the un-notched sample and the integration up to this value leads to $W(\lambda_c)$ as described in Figure 1.

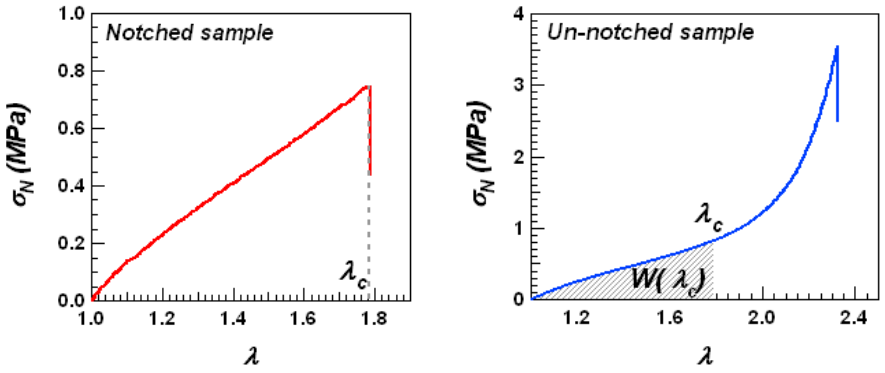

Figure 1: Procedure to measure $W(\lambda_c)$ by performing a single edge notch test (on the left, red curve) and doing the integration of the stress-strain curve of the un-notched sample (on the right, blue curve) up to λ_c.

Regarding the strain dependence correction C, it has been experimentally determined by Greensmith for single-edge notch samples for different elastomers and its expression is shown in Eq. (2). Combining Eq. (1) and Eq. (2), the Fracture toughness is given by Eq. (3).

$$C = \frac{3}{\sqrt{\lambda_c}} \qquad \textbf{Eq. (2)}$$

$$\Gamma = \frac{6 * a * W(\lambda_c)}{\sqrt{\lambda_c}} \qquad \textbf{Eq. (3)}$$

Eq. (3) is the equation that will be used in this chapter to experimentally obtain values of the fracture energy. The single edge notch tests are performed as described in chapter 2. The maximum of the stress for the notched sample is taken to obtain the value of the elongation at break λ_c, it corresponds to the initiation of crack propagation.

For each single edge notch test, the experiments were performed multiple times when enough material was available. The reproducibility of this test is not perfect as can be seen in Figure 2. The elongation at which the crack propagates (corresponding to the maximal stress) varies a bit even for the same material.

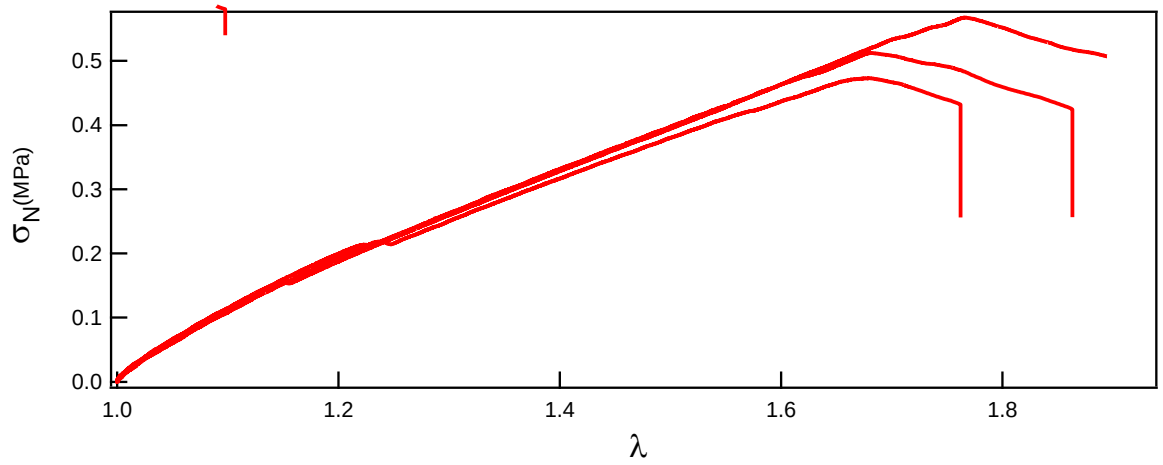

Figure 2: Stress-strain curves obtained for three samples of EAe1.45(1.68)EA. $\dot{\lambda} = 4.10^{-3}$ s^{-1}.

The relatively poor reproducibility shown in Figure 2 can be explained by multiple reasons. First the geometry chosen is limited, with a sample of 5 mm width and a crack of 1 mm length, the ratio of the two is not as large as wanted. This specific geometry was chosen because it uses a relatively small amount of material that is precious due to the long to prepare it. Another reason that can cause dispersion in the results is the fact that the notch is performed by hand with a razor. Therefore, the initial crack is not identical for every sample. Finally, between two samples from the same material, some inhomogeneities can be present leading to different results.

Now that the test and the method to obtain the fracture energy have been described, the next section will focus on the standard family of samples EAe1.45[EA].

2) Fracture energy as a function of degree of prestretching of the first network

a) Single edge notch test results for EAe1.45[EA] samples

To investigate systematically the influence of the degree of prestretching of the first network on the fracture energy, the same set of samples studied in chapter 3 section II) was used. Samples are cut in rectangular pieces and an initial crack of approximately 1 mm is created

with a razor blade. The initial length of the crack *a* is measured carefully for each sample before the test. The tensile test on the notched sample is then performed at least twice per material. Representative stress-strain curves obtained are then plotted in Figure 3.

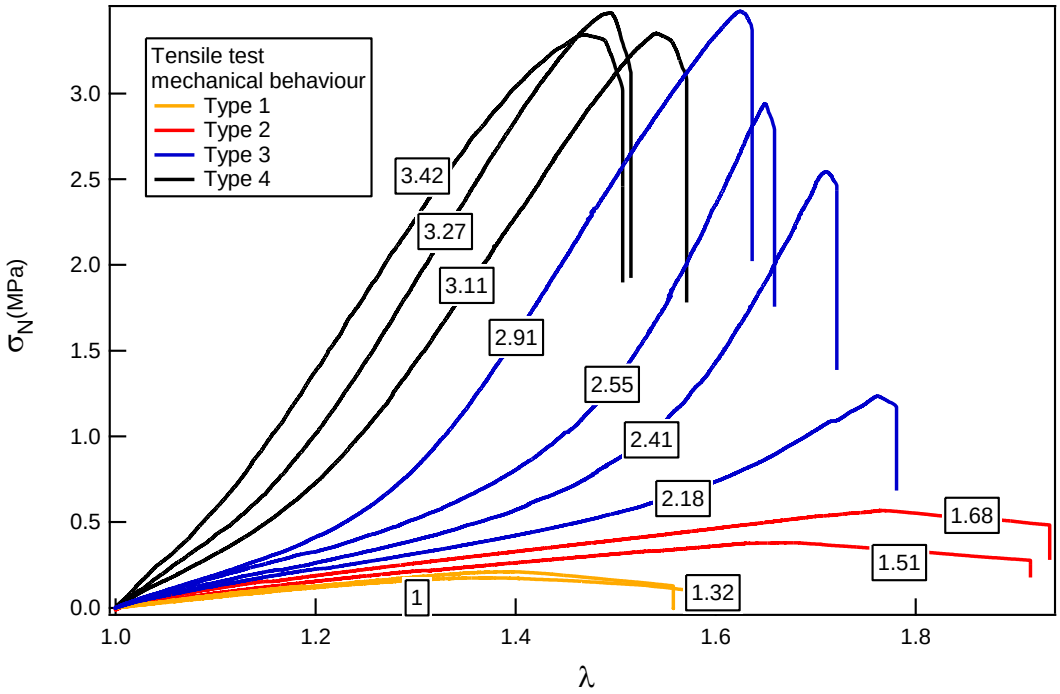

Figure 3: Stress-strain curves of notched samples (Table 1 in chapter 3) during a tensile test. The colours used for the different curves describe the type of mechanical behaviour that was obtained for standard tensile tests in chapter 3 figure 4. $\dot{\lambda} = 4.10^{-3}s^{-1}$.

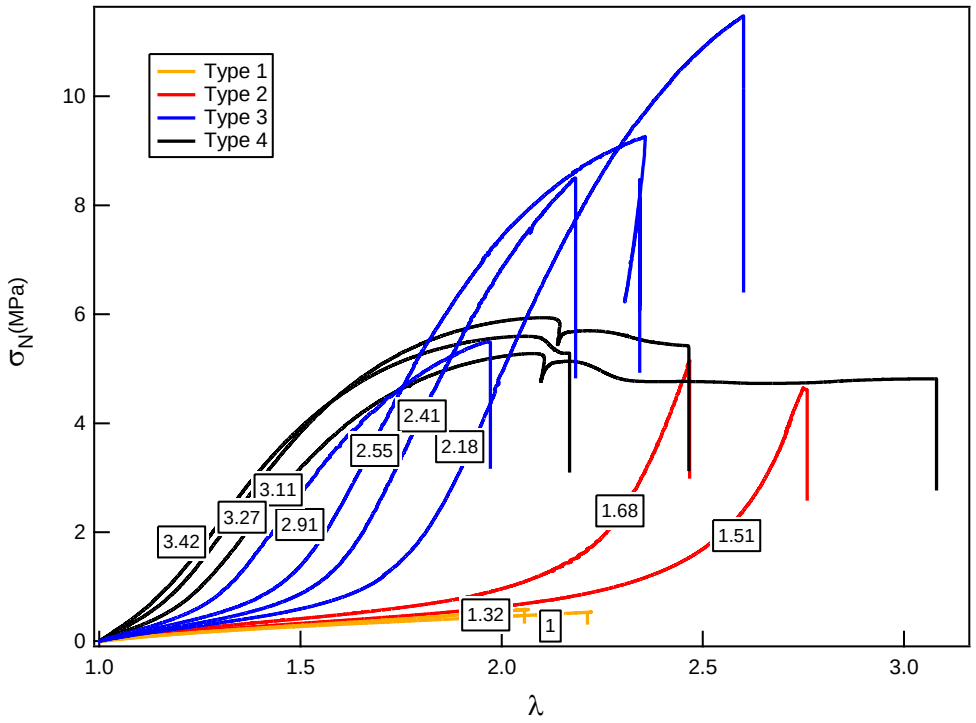

Figure 4:Stress-strain curve of the unnotched samples in uniaxial tension for the same samples displayed in Figure 3. . $\dot{\lambda} = 2.10^{-2}$

Figure 3 corresponds to the fracture tests of the same notched samples on which a tensile test has been performed (chapter 3) and the resulting stress-strain curves of unnotched samples are shown again in Figure 4. The colours that are used represent the different types of mechanical behaviours that were obtained for the tensile tests. The comparison between those two figures clearly highlights the role played by the presence of the crack. The stress at break and elongation at break are drastically reduced by the presence of a crack. The critical elongation at crack propagation ranges from λ = 1.5 to 1.8 when the maximum elongation was 2 to 3 in simple tensile tests. Therefore, the nominal stress at break also decrease in comparison to the un-notched samples. Also while four different types of behaviour are observed in Figure 4, only two types can be observed in Figure 3: an early brittle propagation of the fracture and a hardening followed by a brittle fracture.

From Figure 3, one can evaluate the fracture energy corresponding to the stress-strain curves. Once the critical elongation λ_c is determined for each sample at the maximal nominal stress, $W(\lambda_c)$ can be determined. Then, using Eq. (3), the fracture energy Γ is obtained for each sample of each material and plotted in Figure 5 as a function of the prestretching of the first network λ_0.

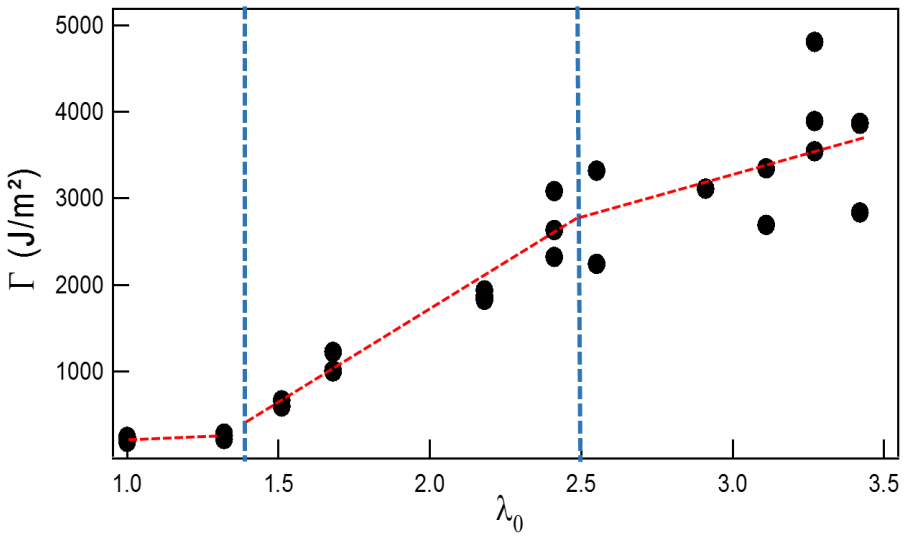

Figure 5: Fracture energy as a function of the prestretching of the first network.

Figure 5, shows that the fracture energy is an increasing function of λ_0 and one can distinguish three different regimes:

- For very low values of λ_0, the increase in fracture energy is very small between EAe1.45(1) and EAe1.45(1.32)EA.
- Then for 1.4 < λ_0 < 2.5, a linear increase in Γ with a steep slope occurs.
- Finally, for λ_0 > 2.5 the fracture energy increases more slowly or tends to saturate.

Figure 5 shows that at high prestretching levels, despite very different mechanical behaviours for the reference un-notched samples, the values of the fracture energy are of the same order of magnitude. Type 4 samples present some necking in uniaxial extension while type 3 do not. However, this difference is not observed in terms of fracture energy and samples of type 3

with a prestretching of 2.41, 2.55 and 2.9 have similar values than those of type 4: with a λ_0 of 3.11, 3.27 and 3.42.

Because the Lake and Thomas theory [1] predicts a decreasing fracture energy with increasing modulus, it is interesting to represent Γ as a function of the Young's modulus. For simple polymer networks, Γ indeed decreases with increasing modulus. However, our system is not a simple polymer network and since an increasing λ_0 increases the modulus, the fracture energy increases with the modulus as seen in Figure 6. From this figure, we can observe that the fracture energy and the modulus can both be increased analogously to what occurs with elastomers filled with nanoparticles. Figure 6 shows a large increase in Γ in the modulus range of 0.9 MPa to 2 MPa. For higher moduli, the fracture energy increases more moderately with the modulus.

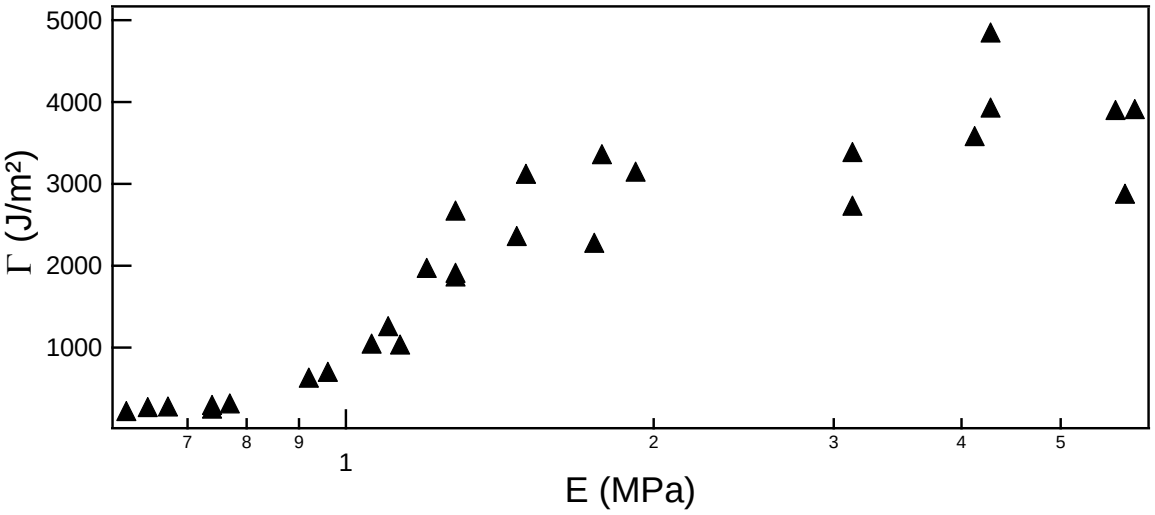

Figure 6: Evolution of the fracture energy as a function of the Young's modulus for the set of samples EAe1.45[EA].

From Figure 3, one can also note that after reaching the maximal stress, corresponding to the onset of the propagation (i.e. crack initiation), the decrease of the nominal stress as the crack grows, is not similar for all samples although the loading rate is. This means that once the fracture propagates, the time taken to break the sample is not constant. In order to compare the time taken to propagate the crack for each sample, the maximal stress is normalized for each sample. Also, starting from the maximal nominal stress, the time is set at zero to be able to compare easily the different samples. The result of those data treatments can be observed in Figure 7.

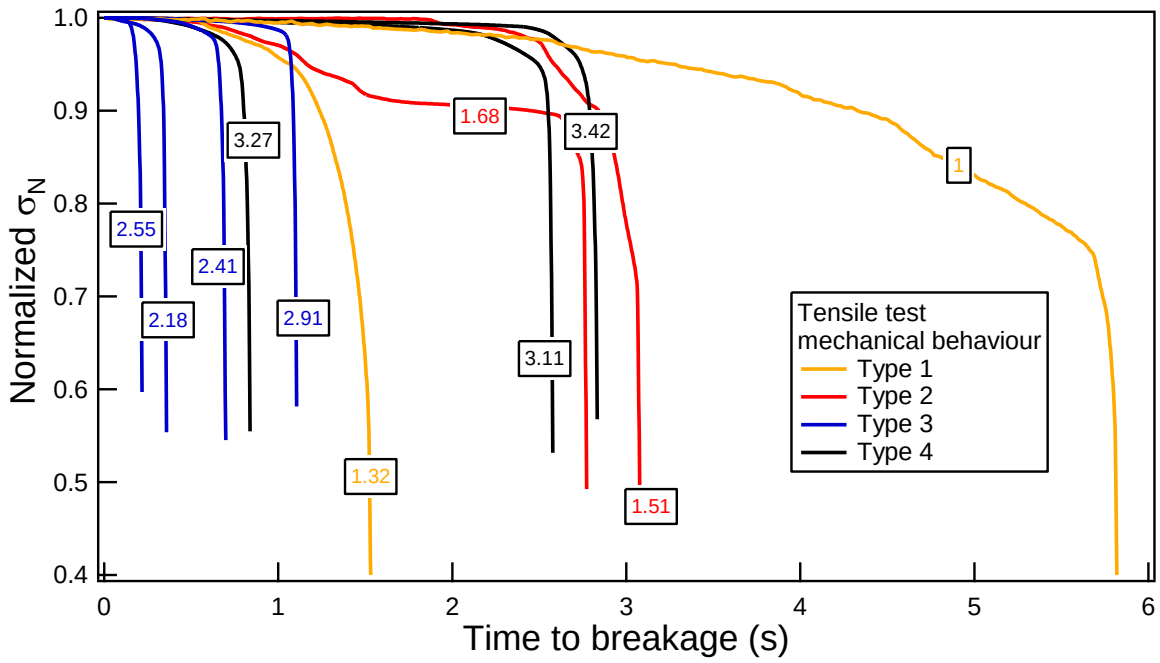

Figure 7: Difference of time for the crack to propagate through the samples EAe1.45[EA].

Figure 7 represents the time taken for the crack to propagate after reaching its initiation energy at the maximal stress. It can be seen that this time is clearly dependent on the sample and on λ_0. At low values of λ_0 below 2, the time to propagate goes from 1.5 s to 6 s. This propagation time then decreases to values between 0.2 s to 1 s for λ_0 between 2 and 3. Finally, for λ_0 superior to 3, the propagation time seems to increase again to over 1 s.

To have a better idea of the differences observed in Figure 7, an average propagation speed can be estimated. This estimate assumes that the crack has to propagate through the sample for approximately 4 mm. Therefore, dividing this distance by the time to propagate obtained from Figure 7, the average crack propagation velocity can be calculated. The results are shown in Figure 8.

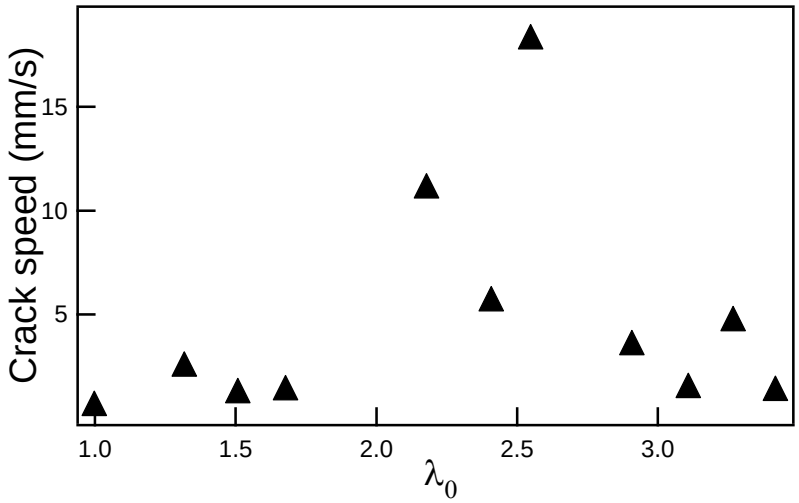

Figure 8: Speed of the crack propagation as a function of the prestretching of the first network for the samples from the set EAe1.45[EA]

In Figure 8, the differences observed earlier are clearer. The crack speed as a function of the prestretching of the first network goes through a maximal value of ~ 19 mm/s for λ_0 = 2.55. For values of λ_0 < 2 and λ_0 > 2.8, the speed remains at least three times slower under 5 mm/s.

This change in crack propagation speed depending on the nature of the multiple networks suggests that time and temperature effects should be present. In the following part, strain rate and temperature of the experiments will be changed to have an insight at their effect on the fracture energy. This data can be used to obtain some information on the propagation of the crack as opposed to the initiation. Interestingly it seems that when going from type 3 to type 4 samples, the fracture energy at initiation is rather similar but once propagation sets in, the crack is slower for type 4 materials suggesting a higher toughness in steady-state crack propagation mode.

b) Influence of changing temperature and strain rate on the fracture energy

In the previous part, the single edge notch tests have been carried out at the same loading rate (crosshead velocity v = 100 µm/s corresponding approximately to a stretch rate $\dot{\lambda} = 4.10^{-3}$ s^{-1}) and at a temperature T = 20 °C. Therefore, the influence of those parameters needs to be studied to investigate the effect of viscoelastic dissipation, another possible mechanism of dissipation at the crack tip. In this section, the stretch rate and the temperature will be changed. The samples will be tested at room temperature and $\dot{\lambda}$ varying from $1.9.10^{-6}$ s^{-1} up to $4.7\ 10^{-2}$ s^{-1} and at $\dot{\lambda} = 4.10^{-3}$ s^{-1} and temperature varying from 20 °C up to 120 °C. The rest of the test procedure is kept identical.

To conduct those experiments some samples already presented in chapter 3, table 1 have been synthesised. The samples tested are: EAe1.45(1), EAe1.45(1.68)EA, EAe1.45(2.55)EA and EAe1.45(3.42)EA. To investigate the effect of stretch rate and temperature, the set of samples will be compared to a reference elastomer sample. This elastomer SBR is a random copolymer of styrene and butadiene graciously provided by Michelin. This SBR is crosslinked with a low amount of crosslinker (around 1.5 wt%) and 5 wt% of carbon black. This low amount of carbon black is not added for reinforcement but for processing reasons. In a standard elastomer, the viscoelastic dissipation is an important dissipation mechanism. The viscoelastic dissipation is maximal at temperatures above but near the glass transition and decreases as the temperature increases. On the other hand, high strain rates create more viscoelastic dissipation which decreases with decreasing rate [5].

The different strain rates are first applied to the described 5 samples. The loading curves of the notched samples are presented in Figure 9. Figure 9a shows that the elongation at break of the SBR sample increases with strain rate as expected [6]. Figure 9b shows that the simple network EAe1.45(1) evolves identically with an even bigger increase of elongation at break with strain rate. However, Figure 9c and Figure 9d show a different behaviour for EAe1.45(2.55) and EAe1.45(3.42) with no clear difference in elongation at break with increasing stretch rate.

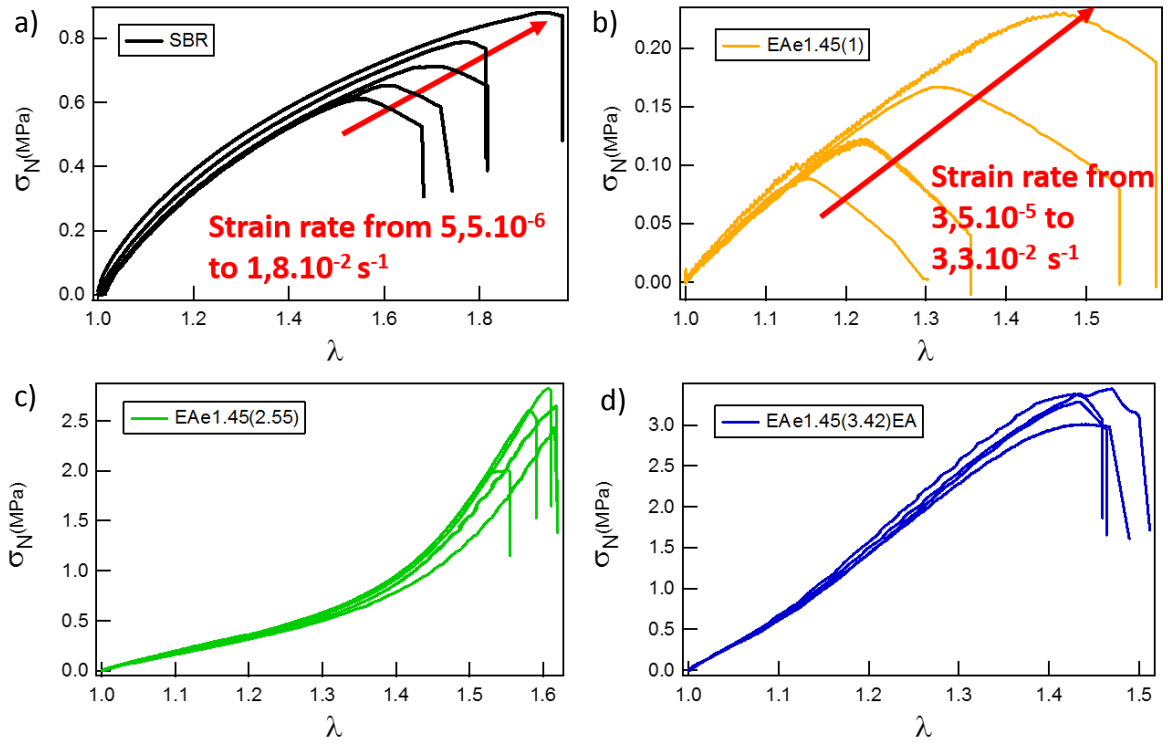

Figure 9: Stress-strain curves for different samples during single edge notch tests at different stretch rates.

The resulting fracture energy is then plotted as a function of the stretch rate for each sample in Figure 10 and the following observations can be made:

- For SBR and EAe1.45(1), Γ increases with strain rate. Those two samples being simple elastomers, this result was expected. In particular, the fracture energy of EAe1.45(1) is increasing sharply gaining around an order of magnitude between $3.5.10^{-5}$ s^{-1} up to $3.3\ 10^{-2}$ s^{-1}.
- For the three other samples that are multiple networks, the strain rate does not show any obvious effect. The fracture energy values are approximately constant or slightly decreasing over this range of strain rates.

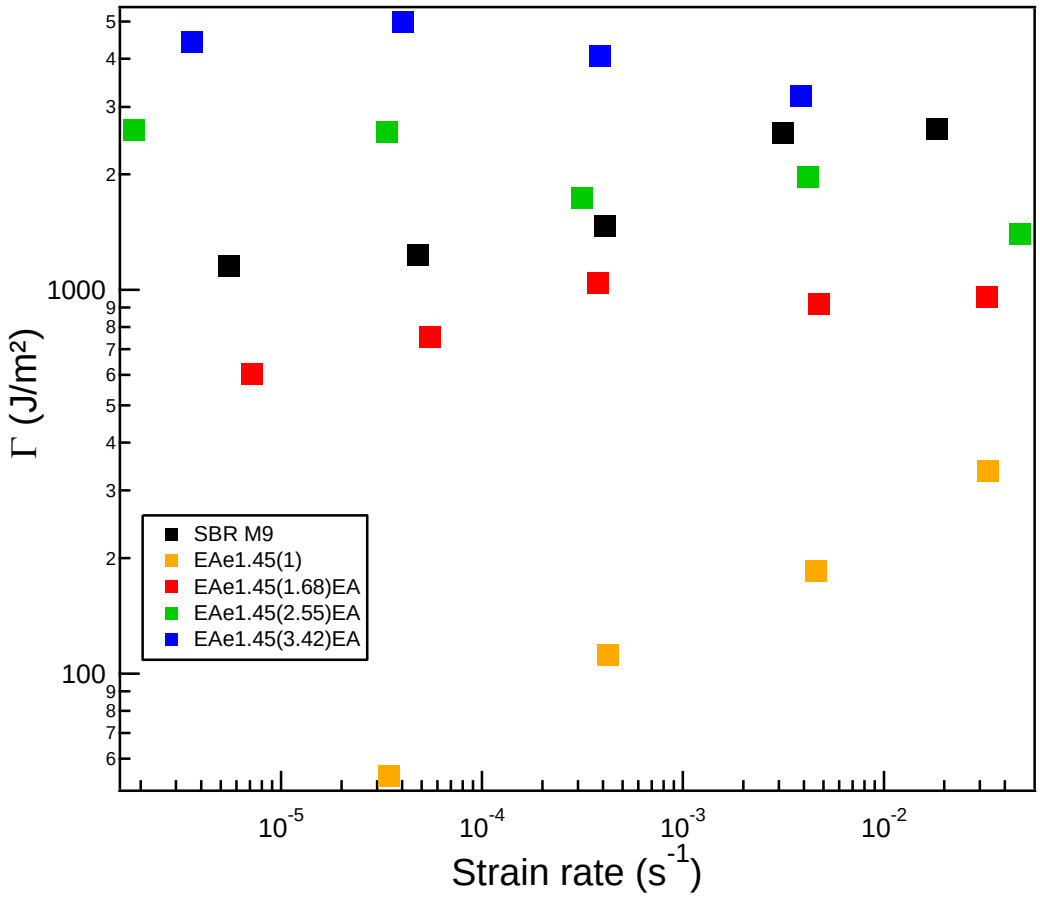

Figure 10: Evolution of the fracture energy as a function of the strain rate.

The single edge notch tests have shown that the multiple networks have a qualitatively different behaviour from the standard elastomers that are unfilled SBR and EAe1.45(1). In order to confirm this behaviour, the same tests are now carried out at different temperatures. The temperature range goes from 20 °C to 120 °C. The stress-strain curves for some of the sample used are shown in Figure 11. The elongation at break decreases significantly for SBR and EAe1.45(1). However, the decrease is less important for the two other samples EAe1.45(2.55)EA and EAe1.45(3.42)EA. Another result that can be noted is that the Young's modulus increases with temperature for every sample as expected due to entropic elasticity as discussed in chapter 1 Eq. (27).

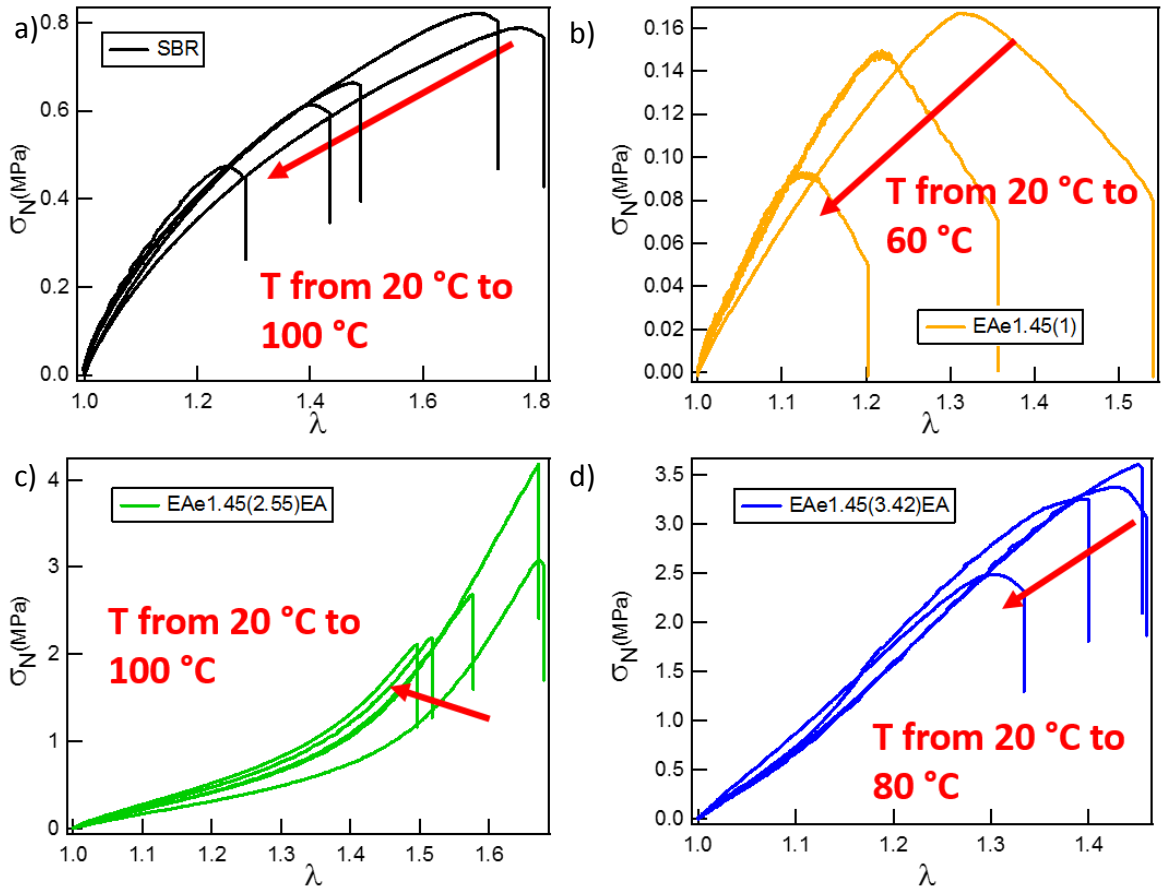

Figure 11: Stress-strain curves for different samples during single edge notch tests at different temperature. . $\dot{\lambda} = 3.10^{-3}\ s^{-1}$.

From the curves shown in Figure 11, the fracture energy is then extracted and the results are plotted in Figure 12. The fracture energy Γ of the single network decreases sharply with temperature with a loss in fracture energy of one decade over 40 °C. At higher temperatures, the sample cannot be tested and breaks immediately in the clamps. For SBR, the expected behaviour is also observed with a decrease in fracture energy of nearly one decade when the temperature goes from 20 °C to 120 °C. For the multiple networks, Figure 12 shows a qualitatively similar behaviour for the three of them but with a relatively smaller decrease in Γ than for SBR. It appears that the decrease is less important with values of fracture energy only divided by two or three over a change of 100 °C in temperature.

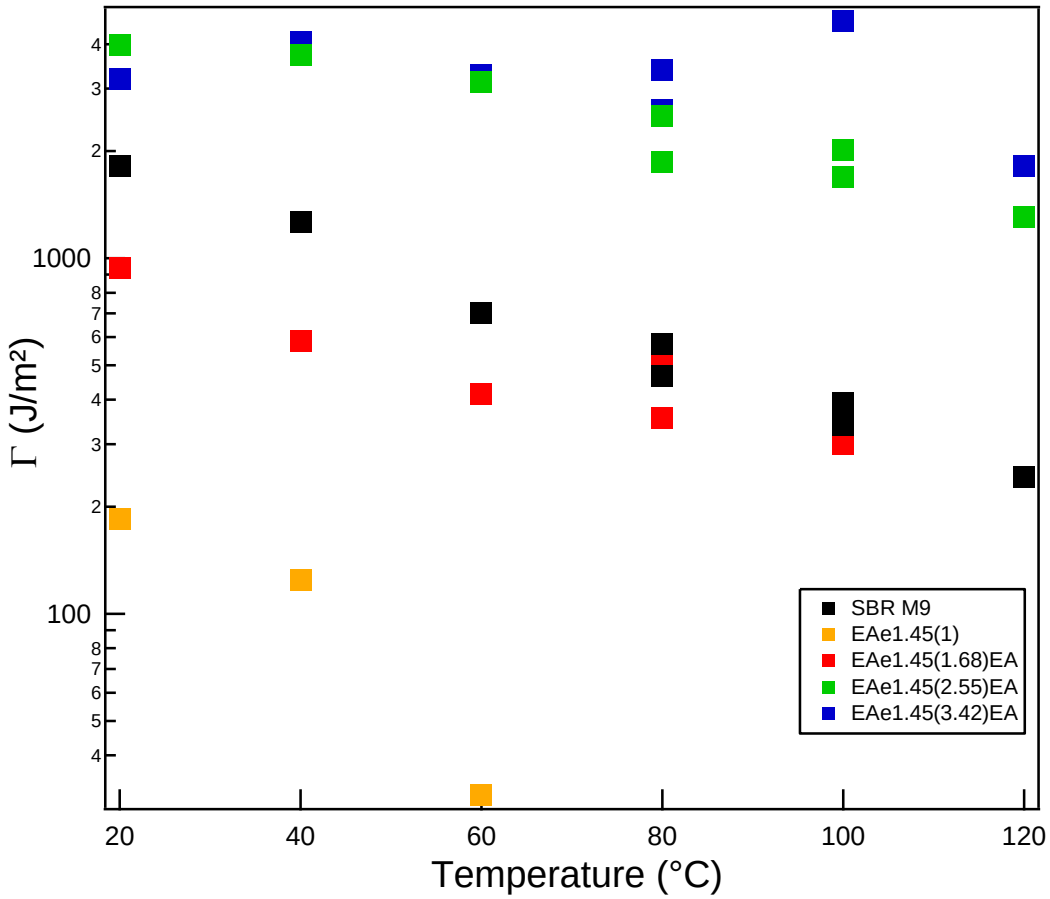

Figure 12: Evolution of the fracture energy as a function of the temperature.

In this part, we investigated the effect of the viscoelastic dissipation occurring at the crack tip in multiple network elastomers. By combining the results shown in Figure 10 and Figure 12, some general trends can be extracted. The fact that the fracture energy decreases with temperature suggests that some viscoelastic dissipation still occurs in our samples. However, the comparison between the evolution of the fracture energy for multiple networks and that of the simple network or that of SBR shows that the effect of the viscoelasticity is much smaller. The large difference with EAe1.45(1) clearly shows that the multiple networks have drastically decreased their viscoelastic dissipation occurring at the crack tip in comparison to the simple network.

Now that we have studied the sensitivity to temperature and stretch rate, we will try to evaluate the flaw sensitivity of our materials using the flaw criteria proposed by Suo [7].

c) Suo's criteria for flaw sensitivity

Very recently, Suo and his group discussed the flaw sensitivity of a wide range of materials [7]. The flaw sensitivity of a material is related to the applicability of fracture mechanics. When existing defects are smaller than a critical value (intrinsic to that material), the energy to fracture (and the strain at break) are not affected by the presence of the flaw. When the defect

is larger, the strain at break is a function of the defect size. In their paper inspired by the work done in metallurgy, they propose a criterion to define the flaw sensitivity. This criterion is a characteristic length of the material that can be obtained by dividing the fracture energy Γ in J/m² by the energy per unit volume needed to break a sample in the absence of flaw W which is the area under the stress-strain curve in uniaxial tension in J/m^3. This ratio is homogeneous to a length and gives a rough idea of the average thickness of the damage zone which experiences strains of the order of the fracture strain and is qualitatively similar to the criterion Γ/W which estimates the size of a zone where the strain of the order of 100%. It can be calculated by using the values obtained in part I) of the current chapter and the curves from chapter 3 figure 4. The values of W are obtained for all the networks from the family EAe1.45[EA] and plotted in Figure 13 as a function of λ_0. It can be seen that W is an overall increasing function of λ_0 however the dispersion of the values is quite large. The relatively high dispersion of W could be sample dependant, any defect in some sample would create an earlier breakage and led to a significantly lower value of W.

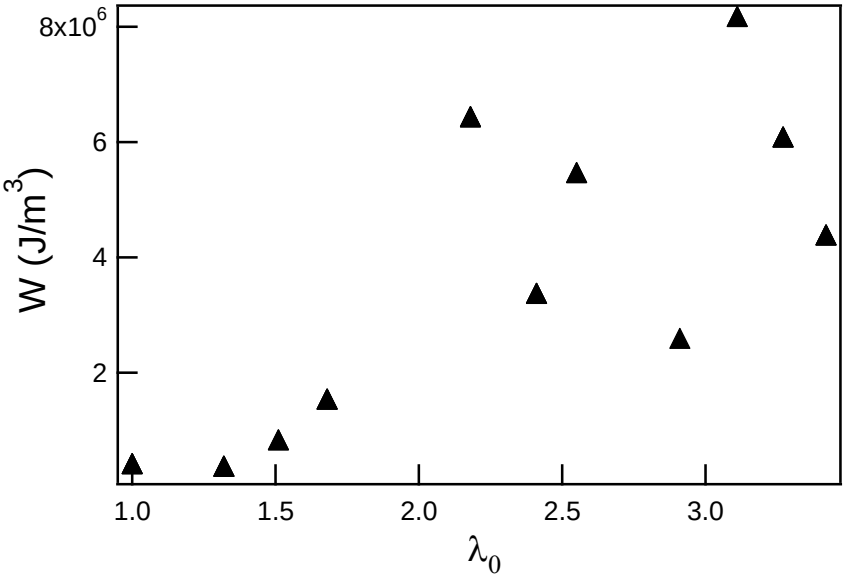

Figure 13: W as a function of λ_0 for the set of samples EAe1.45[EA]

The values of W presented in Figure 13 are used to calculate the ratio of Γ/W as function of λ_0, the result is shown in Figure 14 for the standard family of materials. Interestingly the critical flaw length goes through two minima for λ_0 = 2.2 and 3.2 corresponding to the onset of widespread damage and of yielding. Values vary from 0.3 to 1.2 mm. The two minima are observed for the materials that are showing the best uniaxial properties EAe1.45(2.18)EA has the highest nominal stress at break and EAe1.45(3.11)EA has the highest elongation at break. Therefore the value of W is very high for those two networks leading to a minima of the ratio Γ/W.

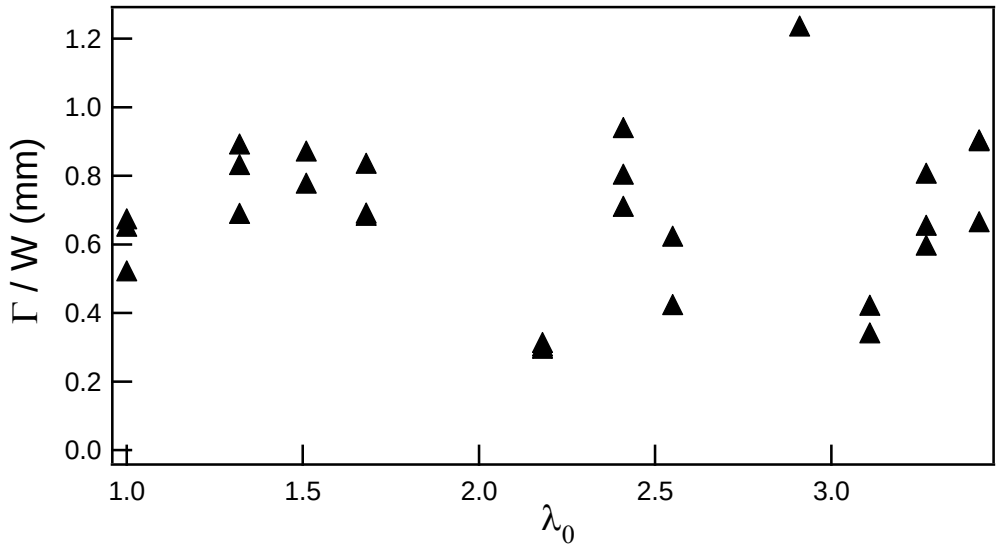

Figure 14: Flaw criteria as a function of λ_0 for the set of samples EAe1.45[EA]

Suo's group proposed a classification for a wide range of very different materials in their paper [7]. This classification is illustrated by plotting Γ as a function of W. As an example, the flaw sensitivity of silica glass is around 1 nm when the bone is around 30 mm. The results obtained for our system can be added to this universal representation as shown in Figure 15. It shows that the elastomers created have a flaw sensitivity that is in the overall range of the elastomeric family. Interestingly while the multiple networks are significantly tougher than the single networks, their flaw sensitivity does not change all that much, i.e. it is really the intrinsic toughness of the material that changes.

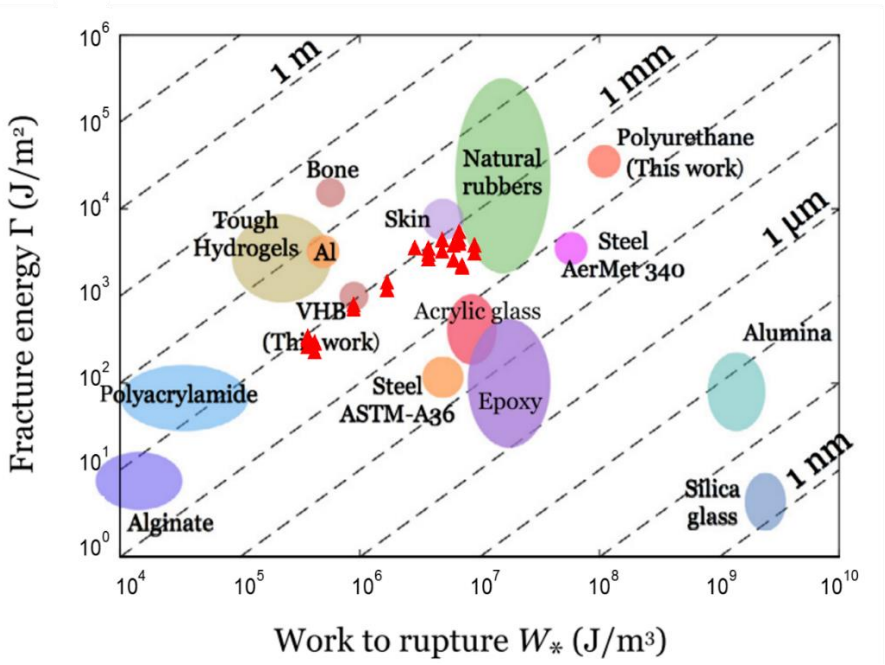

Figure 15: Γ as a function of W for a wide range of materials calculated by Suo's team [7] and the added point of the samples EAe1.45[EA] (red triangles)

So far we have discussed the fracture energy of the set of samples EAe1.45[EA] i.e. with equally densely crosslinked first network. It is now interesting to discuss the multiple networks based on first networks with less crosslinker.

d) Analysis: Impact of the elasticity of the multiple networks

We showed that the dissipation due to viscoelasticity of the multiple networks was lower than for simple networks. However, Γ is largely much higher for multiple networks than for the single network suggesting that another mechanism of dissipation is involved. In his work, Ducrot [8] showed that covalent bonds (belonging to the first network) break inside the material before macroscopic fracture occurs. In this fracture experiment, the bond breaking mechanism occurs at the crack tip and the magnitude of the fracture energy appears to be qualitatively linked to the amount of broken chains in the bulk before the crack propagates. The ability of the network to break chains irreversibly in the bulk before the crack propagates should be dependent on λ_h (the hardening elongation) which corresponds approximately to the onset of the mechanical hysteresis in the multiple networks. To check the influence of λ_h on the fracture energy, Γ is plotted against λ_h in Figure 16.

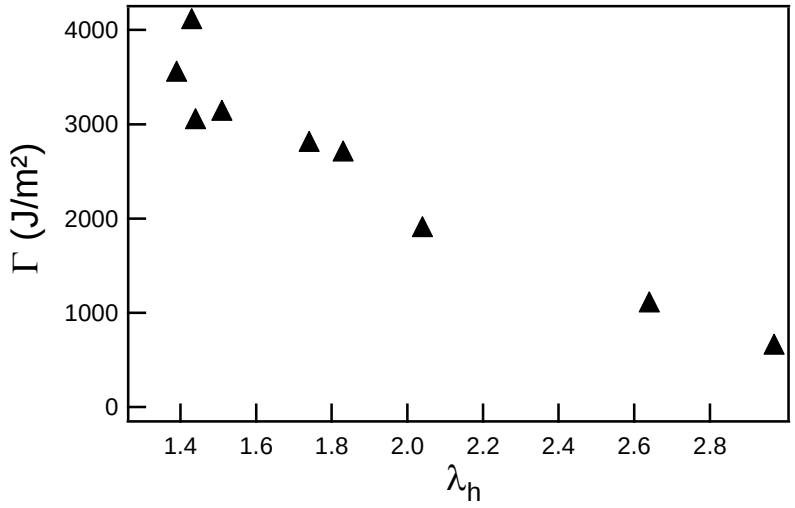

Figure 16: Fracture energy as a function of the strain hardening stretch λ_h calculated with the Gent model as shown in chapter 3 for samples made with EAe1.45 as first network.

Figure 16 shows that Γ is a decreasing function of λ_h. This result means qualitatively that the earlier (in terms of strain) a multiple network experiences damages, the higher its fracture energy will be, suggesting that the dissipation at the crack tip is linked to the amount of damages that can occur in this area. However, the size of the dissipating volume should be taken into account and cannot be estimated from those experiments.

From this set of fracture experiments conducted on the standard series of samples EAe1.45[EA], the following main results can be summarized:

- The fracture energy Γ increases globally with λ_0 but a sharper increase is observed for values of λ_0 between 1.4 and 2.5.
- Γ is an increasing function of the modulus which is different from what is observed for standard polymer networks.
- The dependence of Γ on strain rate and temperature is much less pronounced that for standard elastomers suggesting that viscoelastic dissipation is a less important dissipation mechanism for interpenetrated networks.
- The average velocity of crack propagation, after initiation appears to depend non-monotonously on λ_0 with an increase until a maximal value for λ_0 = 2.55 and then a decrease.
- There is a trade-off between reversible elasticity and fracture energy. The more elastic a multiple network, the more brittle it is.

3) Evolution of the fracture energy with a different crosslink density in the first network

The samples shown in chapter 4, table 3 are used to perform similar fracture energy tests and the results are compared in Figure 17 to the results obtained with the EAe1.45[EA] series presented in Figure 5.

Figure 17 shows that the samples EAe0.73[EA] and EAe0.29[EA] have similar values of fracture energy than the reference set of samples EAe1.45[EA]. Also the overall behaviour appears to be similar with a global increase in Γ with prestretching of the first network. However, the samples using the least crosslinked EAe0.15(1) first network show a different evolution. In this case the first network alone has a reasonably high fracture energy due to its softness and extensibility. This fracture energy decreases then slightly for the samples swollen and polymerised once and then increases again for the sample swollen and polymerised twice. The high value of fracture energy for the simple network was expected because the network is poorly crosslinked. On the other hand, the fracture energy decreasing for the sample with λ_0 = 2.2 is more difficult to explain. It could be due to the fact that adding the second network leads to a higher amount of trapped entanglements that could act as crosslink points and therefore decrease the fracture energy.

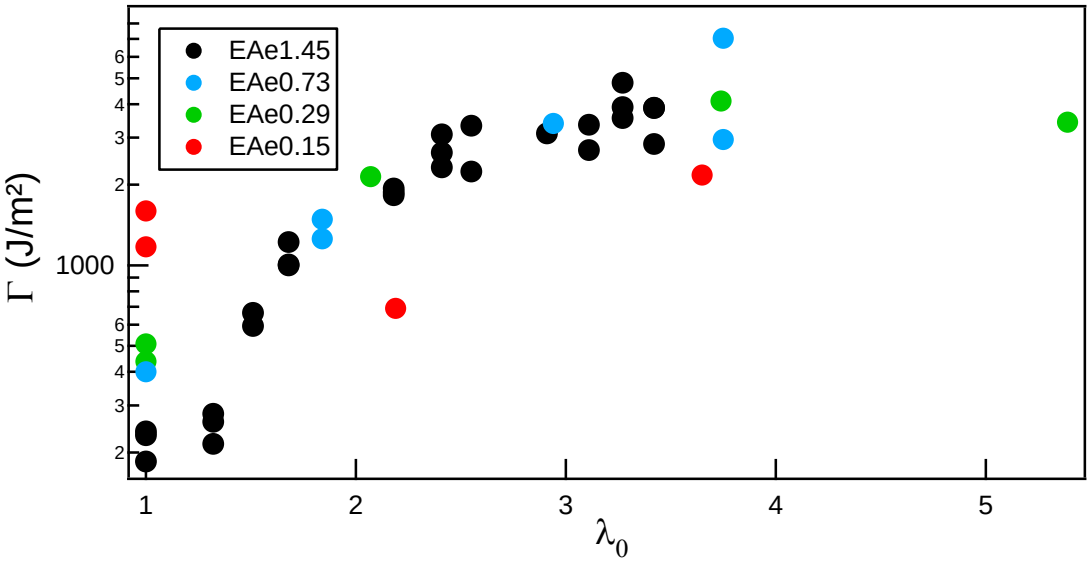

Figure 17: Fracture energy as a function of λ_0 for multiple networks made of different first networks

Figure 17 shows a similar trend for the fracture energy as a function of the prestretching of the first network. However, the maximal potential elongation of each first network is very different for different crosslinking densities. A renormalization by this maximal elongation (obtained with the Gent model in chapter 3 section II)3)) is done by dividing λ_0 by this limit of extensibility. Then the fracture energy can be replotted in Figure 18 as a function of this normalized prestretching for each set of samples. In this figure, it can be observed that the fracture energy behaviour is now different for every set of samples. More points are needed to conclude on the behaviour of the set of samples EAe0.73[EA] and EAe0.29[EA] but it seems that the increase of the fracture energy is appearing at much earlier ratio between λ_0 and λ_m than for the samples EAe1.45[EA]. This result suggests that the dilution of the first network chains in the plane normal to the tensile direction (determined by λ_0) and the unstretched network properties control the value of Γ while the extensibility of the first network chains before they break has no influence.

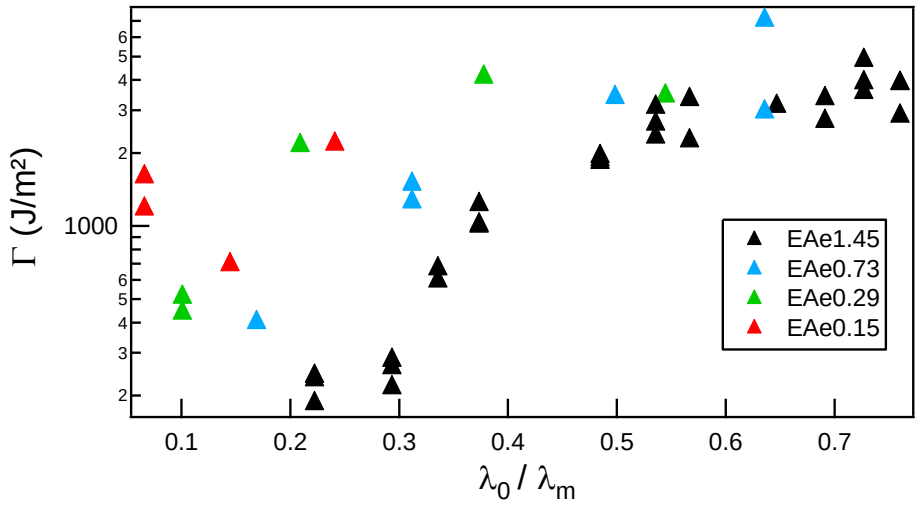

Figure 18: Fracture energy as a function of the ratio between the prestretching of the first network and its maximal extensibility.

The use of different first networks in multiple networks shows that it can have an impact on the fracture energy. The fracture energy depends chiefly on λ_0 rather than on its normalized value λ_0/λ_m (= 1/ λ_h). To obtain clear answer on the behaviour of the fracture energy for those samples, more systematic experiments should be carried out.

The fracture energy has been studied in this section from a macroscopic point of view. However, to obtain more information on the mechanisms active at the crack tip, the local deformation and the local damage must now be investigated.

II) Local deformation at the crack tip

1) Mechanoluminescence to visualise molecular bond scission occurring at the crack tip

a) Synthesis of the materials and principle of the technique

The mechanoluminescence technique used in this work has been developed by the Sijbesma's group in Eindhoven [9, 10]. It has been used in our laboratory by Ducrot in previous work [8, 11]. The principle of the mechanoluminescence is to trigger light emission in response to a specific bond scission inside the material. This light emission upon bond scission can be achieved by the use of a dioxetane group. The dioxetane is a cycle of four atoms made with two atoms of oxygen and two atoms of carbon as shown in Figure 19.

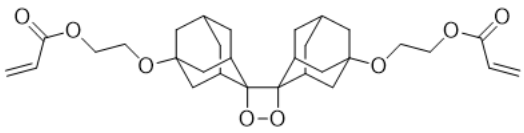

Figure 19: Representation of the used divinyl crosslinker containing the dioxetane cycle.

The four atoms cycle shown in Figure 19 has the ability to break upon the application of a mechanical force leading to the creation of two ketones. One of those two functions is in the excited state so that when it returns to its equilibrium state it will emit a photon. This principle is shown in a scheme in Figure 20. The emitted photon has a wavelength of 420 nm.

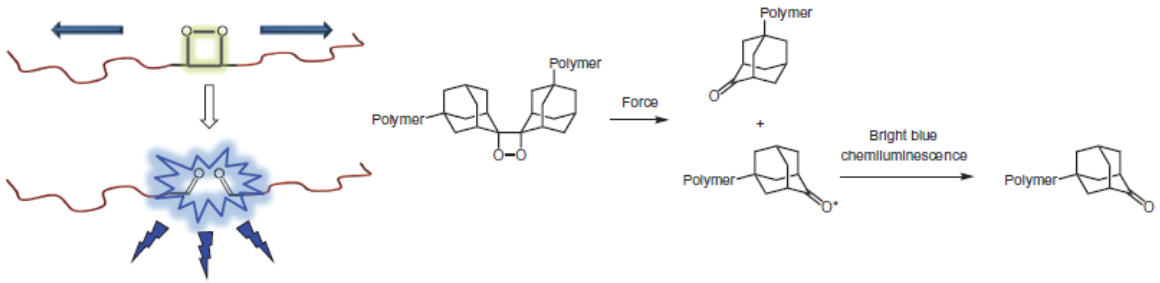

Figure 20: Schematic description of the principle of the luminescence emitted by the dioxetane molecule.

In the previous work of Ducrot *et al.* [8] the dioxetane crosslinker shown in Figure 19, was successfully incorporated as a crosslinker in the first network of a DN and a TN. Using those

functionalized networks, it has been shown that some damages occur in the bulk for the triple network as mechanical hysteresis is observed. During the observation of the propagation of a crack in those same materials, it was qualitatively observed that the sample volume emitting light in front of the crack during crack propagation increased in size when going from a simple network, where fracture involves very localized bond breaking, to DN and TN where significant bond scission in a large volume was observed.

Following the work of Ducrot, the objective was for us to perform some fracture experiments with the goal to do some quantification of the amount of bond scission and to correlate it with the amount of dissipated energy at the crack tip. The collaboration is still undergoing with Sijbesma and her PhD student Jessica Clough who synthesised the molecule.

The synthesis described by Ducrot in his PhD work [11] was carried out in the presence of toluene with the dioxetane molecule instead of the BDA as crosslinker. The only difference from the standard synthesis was that the polymerisation was carried out overnight for approximately 16 hours due to the fact that the solution appeared to be still liquid after the normal 2 hours of UV illumination.

During the present work, several difficulties have been encountered during the synthesis step. The first network synthesis was tried three times unsuccessfully. The inhibitor may not have been removed efficiently enough or some solvent may have been still present with the dioxetane molecule resulting in incorrect stoichiometry. Alternatively, the explanation could be the replacement of toluene with ethyl acetate as solvent. Indeed, the last try that was carried out without any solvent, led to a first network with dioxetane incorporated in it. Ducrot used toluene and could obtain some dioxetane crosslinked networks but we did not succeed in reproducing this synthesis in the presence of ethyl acetate. Sadly, we did not have time and material to verify the influence of the different solvents on the synthesis. The idea that the failure of the synthesis may be linked to the solvent used did not come up until after our last set of synthesis, therefore we could not verify by using toluene instead.

The only first network that was then successfully synthesised was EA(d20)0.73(1) (the letter d refers to the use of dioxetane and 20 is for the 20 mol % of the total amount of crosslinker used that is dioxetane the remaining 80 % being BDA). After the first network was obtained, multiple networks were synthesised at different degrees of prestretching and the properties of those networks are shown in Table 1.

Sample name	First network	λ_0	SN wt %	Number of polymerization steps
EA(d20)0.73(1)		**1**	**100**	**1**
EA(d20)0.73(1.43)EA	**EA(d20)0.73(1)**	**1.43**	**26.2**	**2**
EA(d20)0.73(1.88)EA	**EA(d20)0.73(1)**	**1.88**	**15.1**	**3**

EA(d20)0.73(2.19)EA	**EA(d20)0.73(1)**	**2.19**	**7.5**	**3**
EA(d20)0.73(2.67)EA	**EA(d20)0.73(1)**	**2.67**	**5.2**	**4**
EA(d20)0.73(2.94)EA	**EA(d20)0.73(1)**	**2.94**	**3.6**	**4**

Table 1: Description of the studied samples.

It should be noted first that the amount of incorporated dioxetane molecules in the first network is not precisely known with this method. Since the respective reactivity of both crosslinkers is not known, mixing two crosslinkers like BDA and the dioxetane, results in uncertainties in the amount of dioxetane incorporated in each network. The use of a blend of crosslinkers was decided in order to save the precious mechanoluminescent crosslinker. Unfortunately we realized later that this introduces also an uncertainty on the real amount of dioxetane crosslinker present in the material.

The experiments that will be conducted with the samples shown in Table 1 are fracture experiments. The propagation of the crack and the part before the propagation will be studied and compared.

Camera setup

Once those samples have been synthesised, mechanical tests are performed and a film is made with an EMCCD Andor ultra-sensitive camera. The Instron tensile tester is not located in a dark room, therefore, the darkness had to be obtained by using black carton sheets and optical dark sheets. The darkness appeared to be quite good but some small noise was still observed, and to improve it the Instron should really be located in a fully blinded-room.

The Andor camera is an iXon Ultra 897 EMCCD. The EMCCD stands for Electron Multiplying Charge-Coupled Device. This technology converts a weak incoming light signal into an amplified electronic one that is then recorded. Such a sensitive camera can be used to detect single photons. The camera is used with a 35 mm objective with the original C mount of the camera.

In order to collect the maximal signal without any miss between successive images, a long exposure time of 0.5 s was chosen meaning that 2 images were taken per second. This long time of exposure was chosen in order to maximize the weak signal against the noise. Another argument for the long exposure time is that the camera then does not miss information between each frame which is the case for high acquisition frequency. The gain was set up at a high level of 500.

Treatment of the images obtained

Once the images were obtained for several samples with the Andor camera, a suitable data treatment had to be applied to quantify the signal properly. Indeed, the data suffers from an

amplification noise that needs to be removed. Other than this noise, the noise from lights that might come from the room is not removed in order not to change the signal obtained during the experiments. To remove the amplification noise, from each experiment, a square is selected out of the zone of interest (presenting therefore no signal). In this square, the average value is calculated over the different pixels for each image. The average value (often around 200 a.u. with our camera settings) is then subtracted to every pixel in the rest of the relative image. This simple background removal is then done for each experiment. Note that the background can vary temporally so that this subtraction has to be done for each image individually.

Once the samples are synthesised and the setup is ready, fracture experiments are carried out on the set of samples of Table 1. The procedure for the fracture test is similar to what is described in chapter 2 but the optical extensometer cannot be used so the elongation is calculated by the recorded displacement of the upper clamp or the value is taken from the movement of the upper clamp recorded by the Instron.

b) Example of a fracture experiment of the sample EA(d20)0.73(2.94)EA

The sample EA(d20)0.73(2.94)EA is chosen as an example to show the different images of a complete experiment. Once the images are recorded and once the noise is removed as described in the previous part, different usable images are obtained. In this part, to remove some more noise an additional median filter is used. The principle of this filter is to replace a pixel by the average of the neighboring pixels. In our case, each pixel is replaced by the value of the 2-by-2 neighborhood around the corresponding pixel. This treatment allows to weaken single rogue pixels that are normally errors, on the other hand it decreases the signal when the deformation is not very localized and weak. Also, this median filter will reduce the signal at the edges. This treatment was used here to reduce the noise with the goal of improving the quality of the visualization of the signal.

The stress-strain curve of the sample EA(d20)0.73(2.94)EA is displayed in Figure 21. The red arrows are referring to the images recorded simultaneously by the Andor camera and displayed in Figure 22. The stress-strain curve of Figure 21, is similar to what is expected with a sample entirely crosslinked with BDA. The interesting part of those two figures comes from the images displayed in Figure 22. In picture a, nothing can be seen, some small dots in the higher part are small reflections that can be observed on the upper clamp. This tiny reflection on the clamps is seen for all our images. Then in pictures b and c, some vertical dots can be observed on the left side of the pictures. Those points are attributed to a mechanoluminescent signal that is occurring in the bulk of the sample showing that some bond scission takes place. This was expected since dissipation (mechanical hysteresis) starts at around $\lambda = 1.4$ for this type of sample. Finally picture d shows a localized signal in an area that is located in front of the crack. This image shows that more extensive bond scission occurs ahead of the crack tip before the propagation starts.

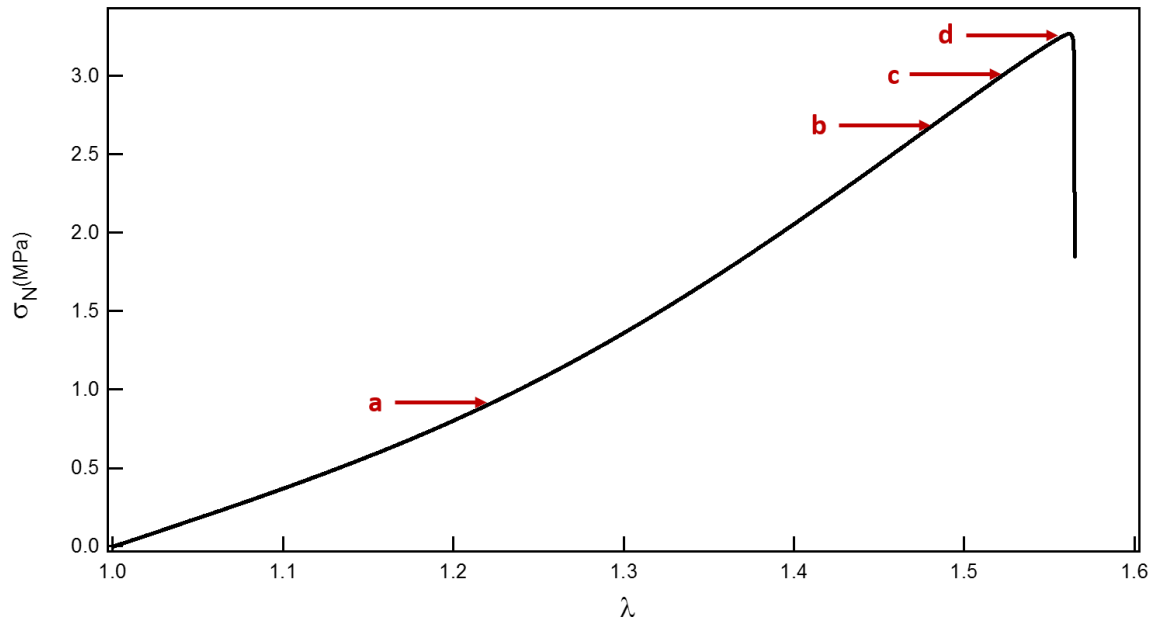

Figure 21: Stress-strain curve for the sample EA(d20)0.73(1)EA, the letters are referring to images taken at the same time.

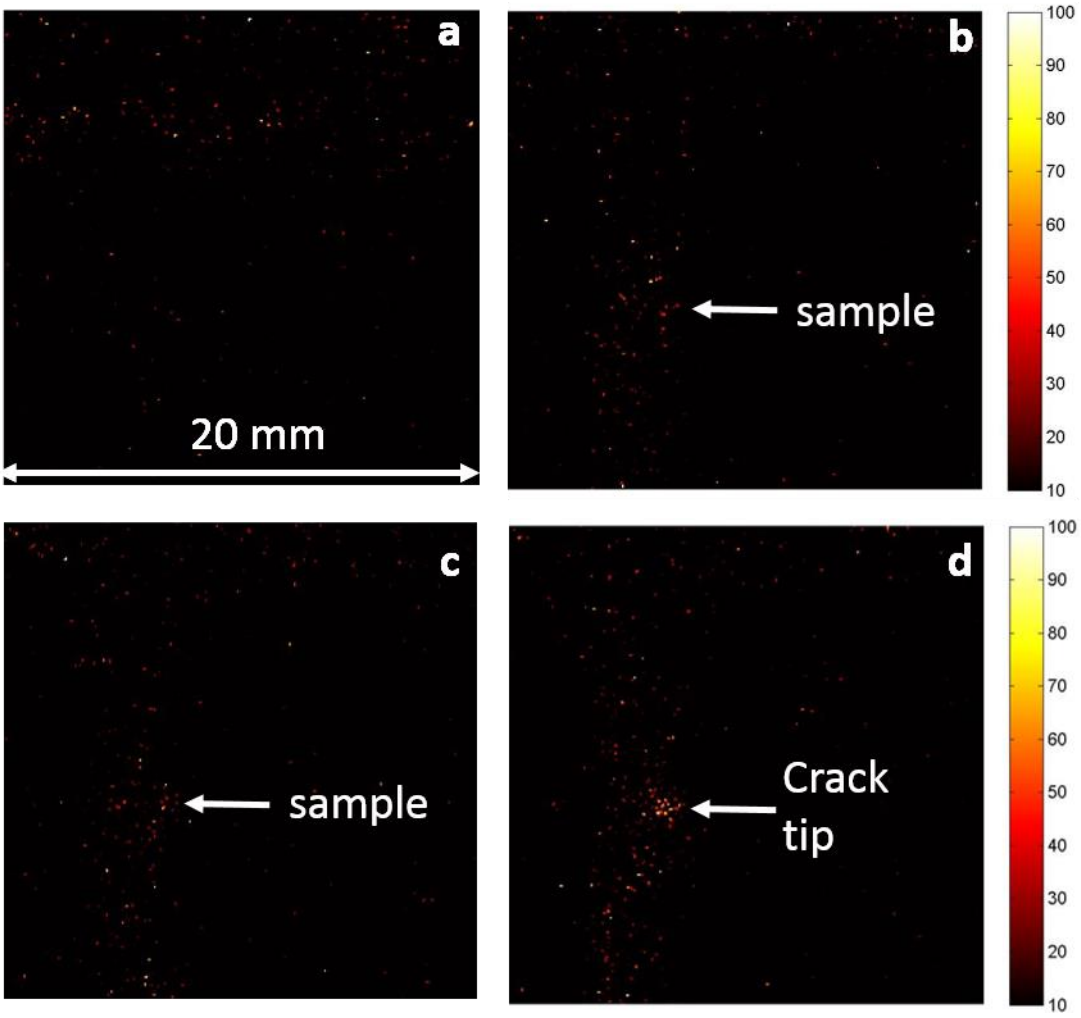

Figure 22: Images showing the mechanoluminescent signal for EA(d20)0.73(2.94)EA before propagation. The colour bar on the right is in arbitrary unit but similar for each picture.

We have seen that not only the propagation of the crack causes bond scission but some bond breaking is also occurring before the crack starts to propagate. In order to visually observe the dissipated energy before the crack propagates, the entire images that show a signal (after correction of the background) are summed together (in practice the 50 images before the propagation starts are taken: this number has been chosen and checked to be sure that no signal is lost). The result of this sum is displayed in Figure 23 on the left side. On the right side, the propagation image is displayed. Due to the fact that the exposure time is large and the propagation is fast, the entire propagation is recorded in the same picture.

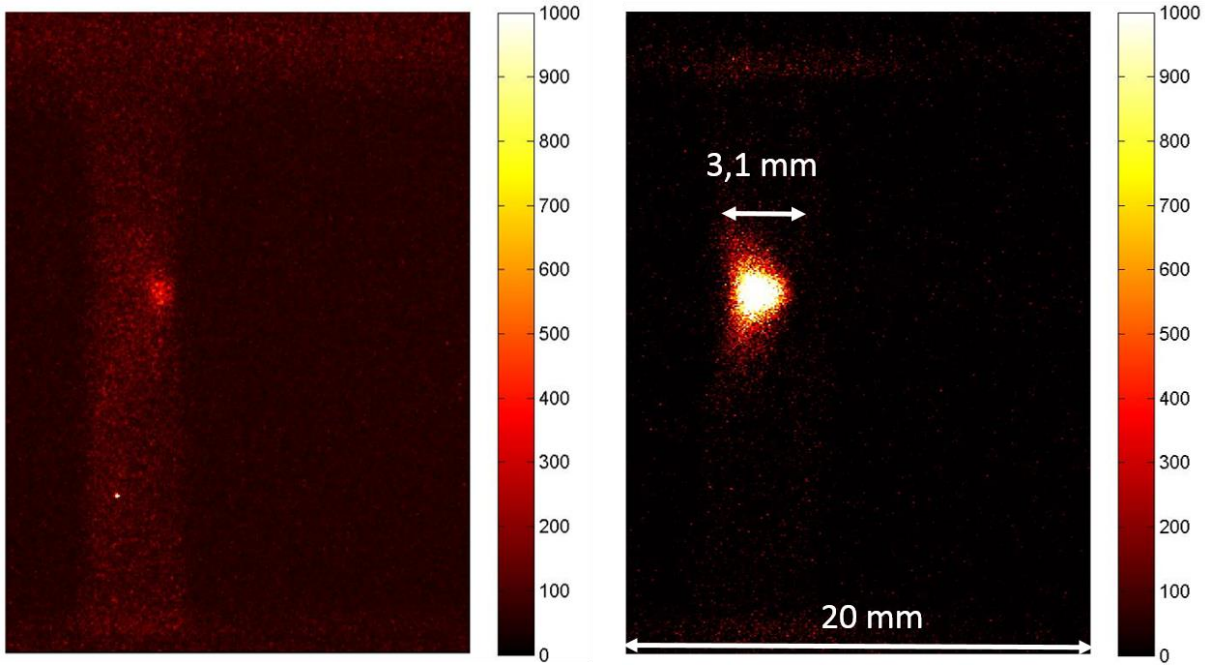

Figure 23: Left: Sum of the images before the propagation. Right: Image of the propagation.

On the left picture of Figure 23, the bond scission in the bulk can be clearly observed. Also a brighter area located at the crack tip shows a process zone with a higher concentration of bond scission occurring. On the right side, the propagation picture displays a bright signal integrating bond scission over the entire propagation process. The shape of this propagation is roughly a triangle and it can be seen that a large area is affected in the direction perpendicular to the crack propagation. The area where the mechanoluminescent signal is emitted measures 3.1 mm in the propagation direction and 6.7 mm in the perpendicular one.

Now that an example of the experiment conducted has been shown with the sample EA(d20)0.73(2.94)EA, the same treatment procedure is applied for the other samples to compare them.

c) Comparison of the signal obtained for the different samples

The first network displayed in Table 1, did not show a signal significant enough to be compared with the other samples. Also, this sample can be used to create many other network so its use is precious and not enough tests were tried on it to obtain a reliable result. Now that the

sample EA(d20)0.73(2.94)EA has been shown, the rest of the samples of Table 1 will be displayed, first with the sum of images before the propagation then the propagation itself and finally the sum of all images.

Sum of images before the propagation:

The same fracture experiment conducted for EA(d20)0.73(2.94)EA was done for the four other samples. For the sample previously studied, no slow propagation was observed but this could be the case for those materials. In order to see that, the stress versus time has to be plotted, the result is displayed in Figure 24.

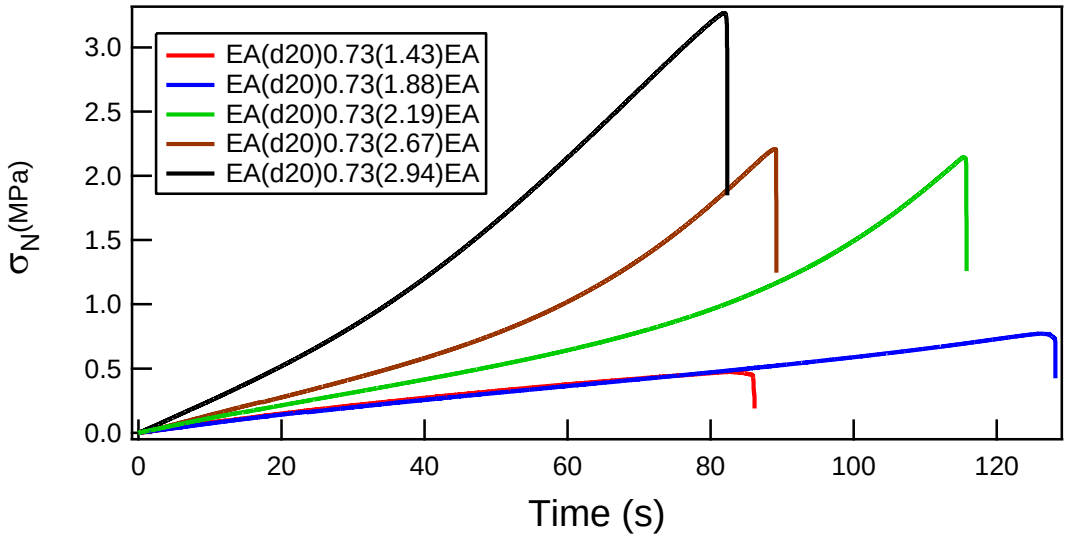

Figure 24: Stress versus time curve for the samples presented in Table 1. . $\dot{\lambda} = 8.10^{-3}s^{-1}$.

From the observation of Figure 24, we can observe that three samples have a fast propagation: EA(d20)0.73(2.94)EA, EA(d20)0.73(2.67)EA and EA(d20)0.73(2.19)EA. For those samples where the decrease of the stress is very fast after the maximum, there should not be a slow propagation stage. On the other hand the samples EA(d20)0.73(1.88)EA and EA(d20)0.73(1.43)EA show a slower decrease in stress during respectively 2 and 3 seconds. Therefore, some propagation should be observed before the last image. It can also be noticed that the sample EA(d20)0.73(2.67)EA shows an early breakage, at lower strain and at lower nominal stress than expected and also than EA(d20)0.73(2.19)EA. This will be confirmed by the mechanoluminescent signal recorded.

The same analysis procedure applied in the previous section was used for this set of data, the images for the four samples is shown in Figure 25.

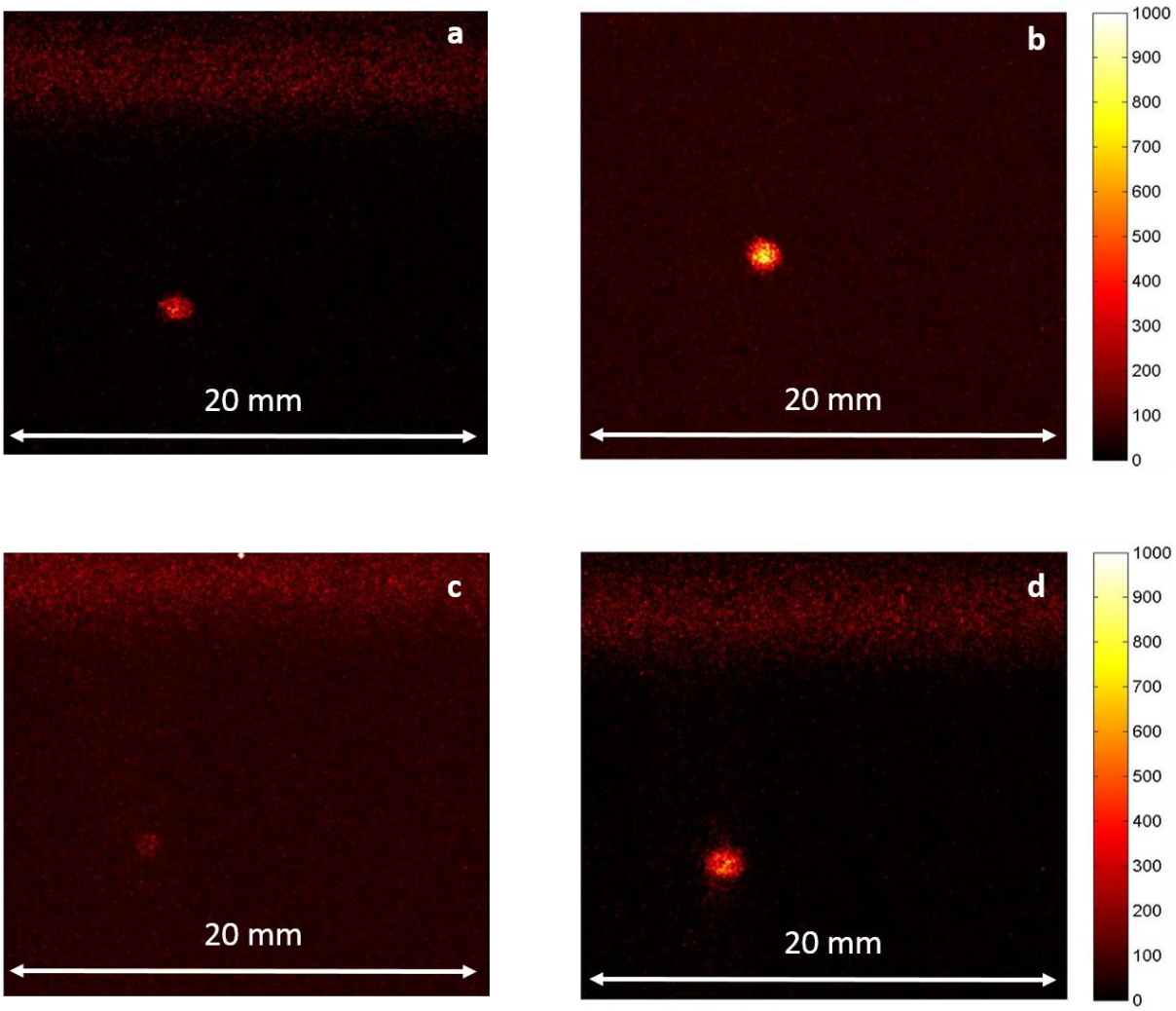

Figure 25: Images summed before the fast propagation for four different multiple networks: a) EA(d20)0.73(1.43)EA, b) EA(d20)0.73(1.88)EA, c) EA(d20)0.73(2.19)EA and d) EA(d20)0.73(2.67)EA. The crack is located on the right of each picture and propagates through the samples (5mm width) towards the left.

In Figure 25, the first noticeable difference with Figure 23 is that no mechanoluminescent signal is observed in the bulk of the samples. The only damages that are occurring in those networks are located in the process zone ahead of the crack tip. Due to the fact that a slow propagation was observed before catastrophic fracture for certain samples (see Figure 23), images a and b are showing part of the propagation process that could explain the high intensity. Image c show a very weak intensity meaning that only a quite small dissipation occurs before the fast propagation of the crack. On the other hand picture d shows a relatively high intensity of damage despite a fast propagation that could mean that this sample dissipates some energy ahead of the crack before the propagation starts. To have a better estimate of the intensity, the process zone will be integrated in the next part to be able to compare the sample.

Images of the propagation:

To complete the results of the images observed in Figure 25, it is necessary to display and analyse also the images corresponding to the fast propagation (the last 0.5 s). This is done for the four same networks, the result is presented in Figure 26.

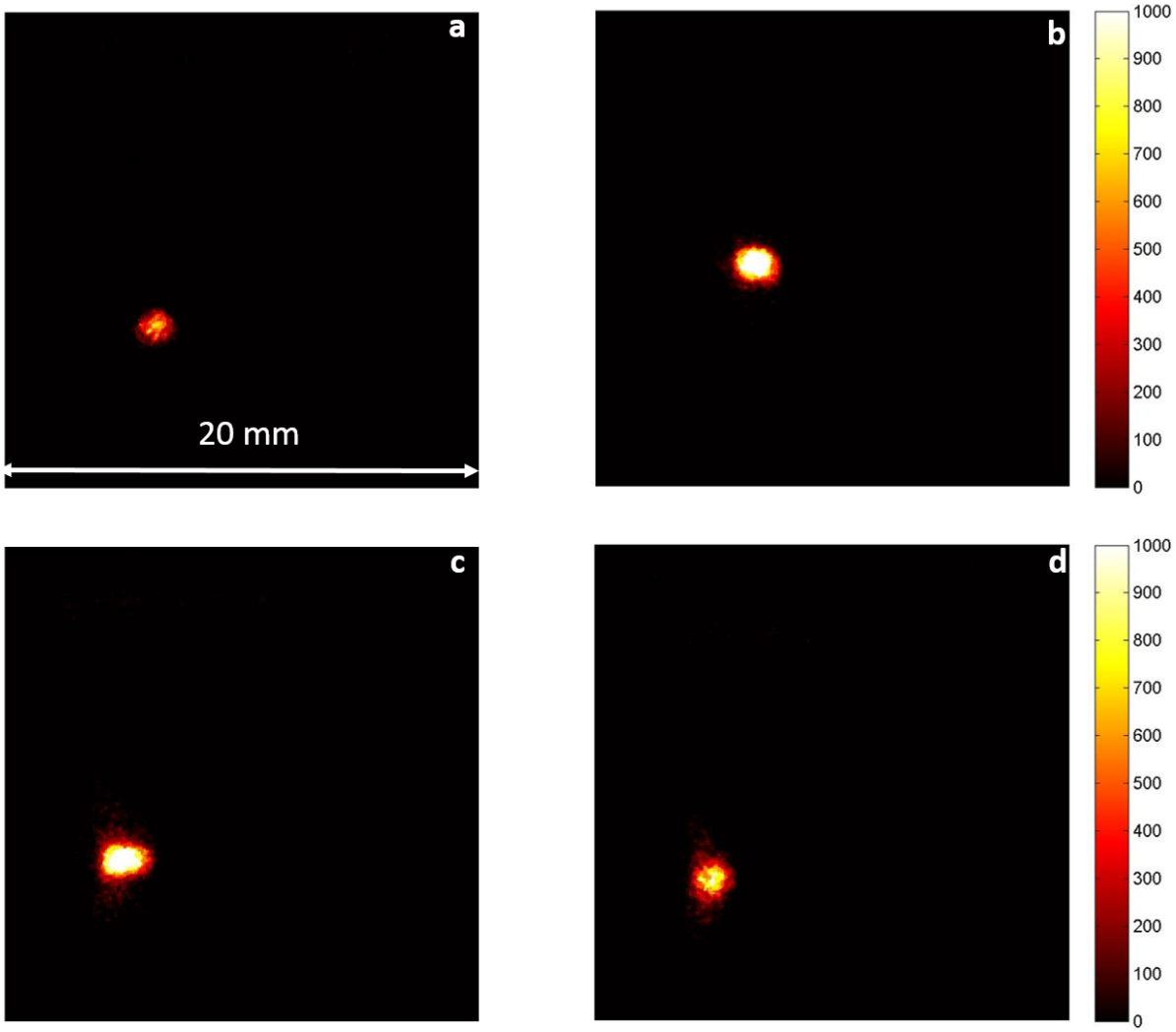

Figure 26: Images of the propagation for four different multiple networks: a) EA(d20)0.73(1.43)EA, b) EA(d20)0.73(1.88)EA, c) EA(d20)0.73(2.19)EA *and d) EA(d20)0.73(2.67)EA. The crack is located on the right of each picture and propagates through the samples towards the left.*

Figure 26 shows some differences between the different samples. First the length of the process zone during propagation is different for every sample. The samples EA(d20)0.73(1.43)EA, EA(d20)0.73(1.88)EA and EA(d20)0.73(2.67)EA seem to have a smaller propagation spot size than the two others. EA(d20)0.73(2.19)EA which had a small signal in Figure 25c, has a very large propagation signal on Figure 26c. If we compare the damage zone of those samples to that observed for EA(d20)0.73(2.94)EA in Figure 23, we can see that none of them has the same shape.

Since the same precrack (around 1 mm) is present in each sample, the same propagation spot size would be expected. Since it is not the case, the explanation might come from the slow propagation that has been observed for two samples in Figure 24. On the other hand, the total

signal observed at the propagation and before the propagation should have a similar horizontal size. For this reason, the images obtained in Figure 25 and Figure 26 can be summed to obtain the signal corresponding to the entire bond breaking phenomenon.

Sum of the entire mechanoluminescent signal:

The sum of the previous pictures corresponds to the signal that is emitted by all the dioxetane bonds that might have broken during the process of propagating a crack through those samples. The result of this sum is shown in Figure 27.

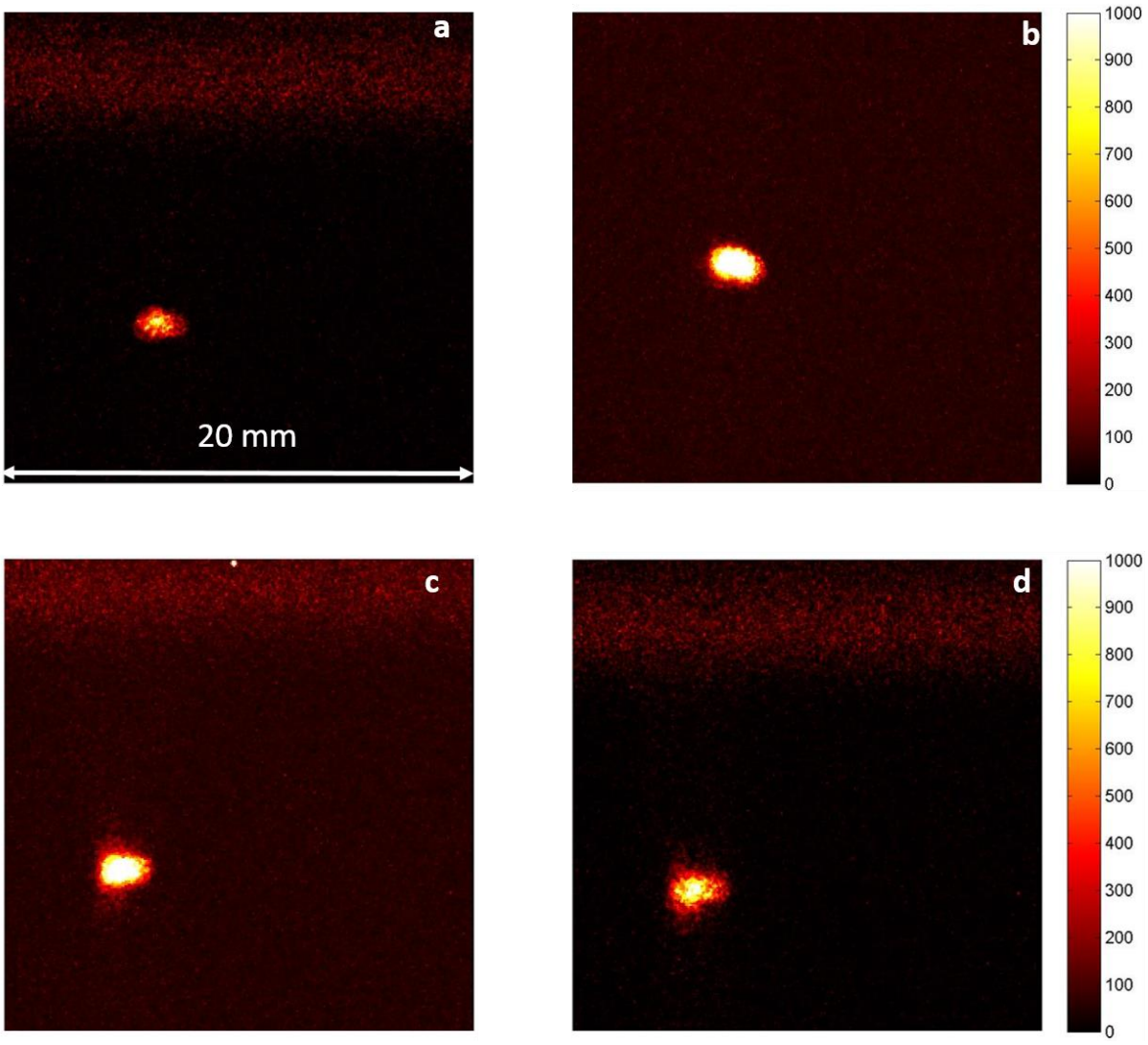

Figure 27: Images of the entire mechanoluminescent signal for four different multiple networks: a) EA(d20)0.73(1.43)EA, b) EA(d20)0.73(1.88)EA, c) EA(d20)0.73(2.19)EA and d) EA(d20)0.73(2.67)EA. The crack is located on the right of each pictures and propagates through the samples to the left.

Figure 27 first shows that the size of the sum of the entire signal is similar for each sample. Indeed, the measurement of the size of the spot for each sample gives some values between 2.6 mm to 3.2 mm. Also the total intensity is different. From the work of Ducrot [8], we expect an increasing mechanoluminescent signal with increasing prestretching. This seems to be the

case for the samples EA(d20)0.73(1.43)EA, EA(d20)0.73(1.88)EA, EA(d20)0.73(2.19)EA but the sample EA(d20)0.73(2.67)EA has a weaker signal.

Figure 27 is interesting to visualize the signal, on the other hand a suitable photon counting methodology needs to be used for a more efficient quantitative comparison between the samples. This will be the object of the following part.

d) Comparison of the intensity for different samples

Due to the uncertainty on the real amount of dioxetane crosslinker in each sample, a fully quantitative comparison of the mechanoluminescent signal is difficult. In this part, we will try however to compare the different samples as quantitatively as possible.

As a first step, the intensity of the mechanoluminescent signal has to be measured. To do so, an arbitrary rectangle of 150 pixels by 100 pixels is chosen to integrate the intensity of the process zone for every sample. The size of the rectangle shown in Figure 28 has been chosen so that the entire signal from the crack tip is located within the rectangle for the biggest propagation spot.

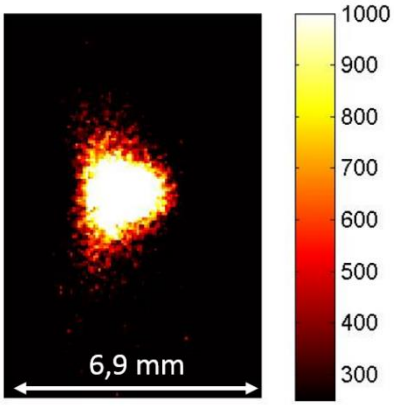

*Figure 28: Entire mechanoluminescent signal for the sample EA(d20)0.73(2.94)EA showing that it can be contained in a rectangle of 150*100 pixels.*

The rectangle is used to sum the value of each pixel over the area delimited by it. The sum of the pixels is made on the images shown in Figure 25, Figure 26, Figure 27 and Figure 28. This sum leads to the knowledge of the total signal emitted during the different stages of the process: before the final propagation, during the final propagation and both. This calculation is carried out for each sample. This operation gives a count in an arbitrary unit (a.u.) per surface of the measuring spot. Since the thickness is different for every sample, the count obtained for every sample is normalized by its thickness to obtain a value per surface unit. The width and length of the acquisition spot are fixed by the size of the rectangle and kept identical for each sample so that no other correction is needed.

Figure 29, shows the integrated signal calculated for the images before and during the propagation as a function of the prestretching and of the estimated value of the fracture energy calculated for every sample.

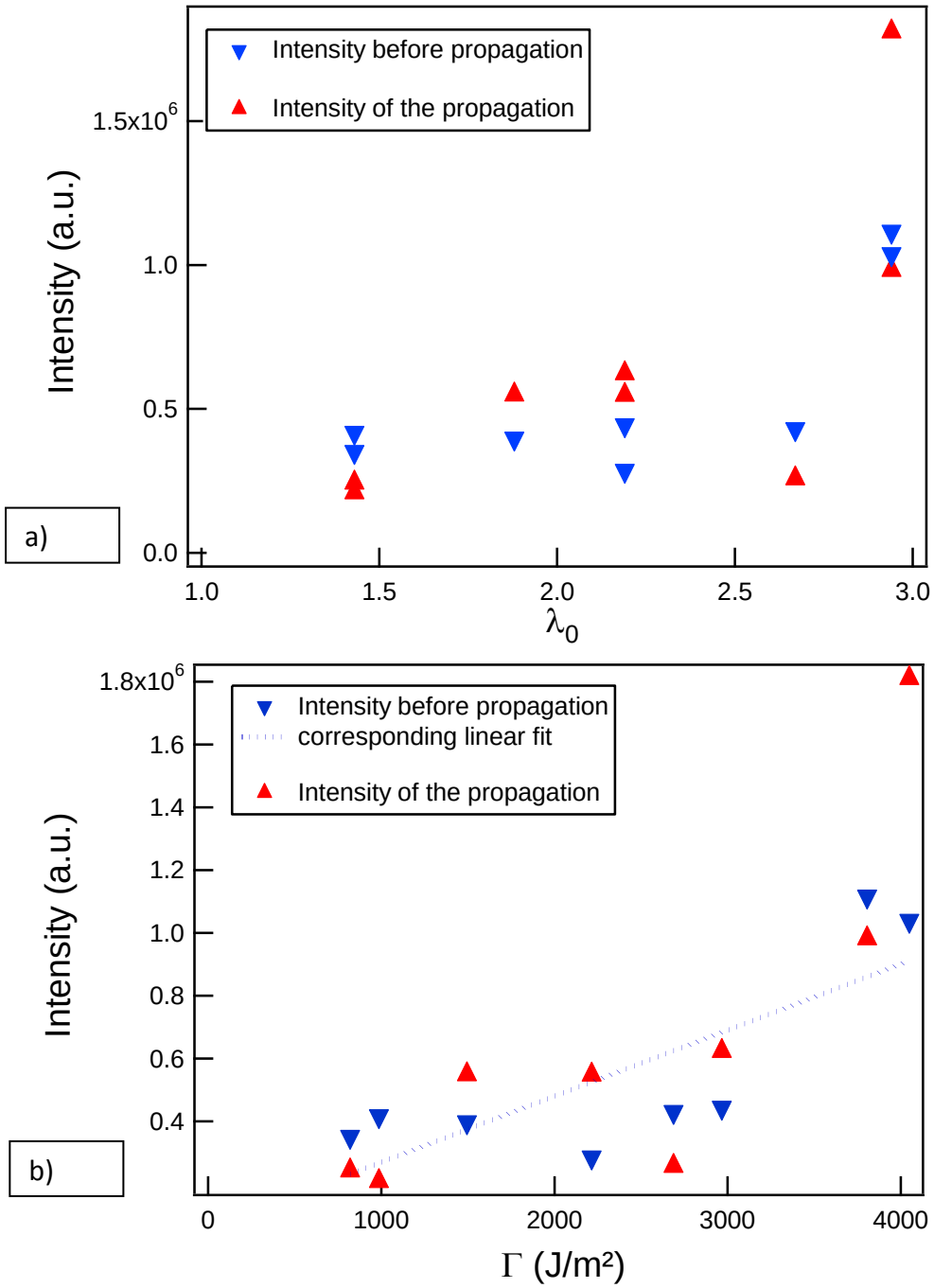

Figure 29: Intensity of the mechanoluminescent signal before and during the propagation as a function of the prestretching (a) and as a function of the fracture energy (b).

Figure 29a) shows that except for the sample EA(d20)0.73(2.94)EA (he one with the higher fracture toughness), the intensity obtained before the final propagation (blue symbols) does not seem to be affected much by the prestretching of the sample. This is in contradiction with previous results and this might come from the fact that the part before propagation is not well defined by the low amount of resolution obtained with our measurement technic in this case.

The fact that the signal before the propagation is higher for EA(d20)0.73(2.94)EA is due to the fact that not only the process zone emits light in this sample but also the bulk. Therefore the total signal obtained for EA(d20)0.73(2.94)EA is amplified by this phenomenon. This is less the case for the intensity obtained during the propagation. Due to the fact that some slow propagation can be observed, it is difficult to conclude using this curve.

Regarding Figure 29b), it seems that the intensity before the final propagation is an increasing function of the fracture energy. On the other hand, a linear fit is displayed (dashed blue line) showing that the increase is not linear. Until the fracture energy reaches 3000 J/m², the intensity might be increasing linearly but as soon as the sample starts to present some damages in the entire sample, it is not the case anymore which could be expected since the dissipation does not occur at the crack tip only anymore. The same observation can be made for the intensity of the propagation with a global increase of the intensity of the propagation with the fracture energy.

The fracture energy is certainly more related to the total intensity emission that does not take into account the arbitrary choosing of a final image. Therefore, the different light emissions of Figure 29, can be summed to obtain the total light signal for every sample. The resulting intensity is then plotted as a function of the fracture energy in Figure 30.

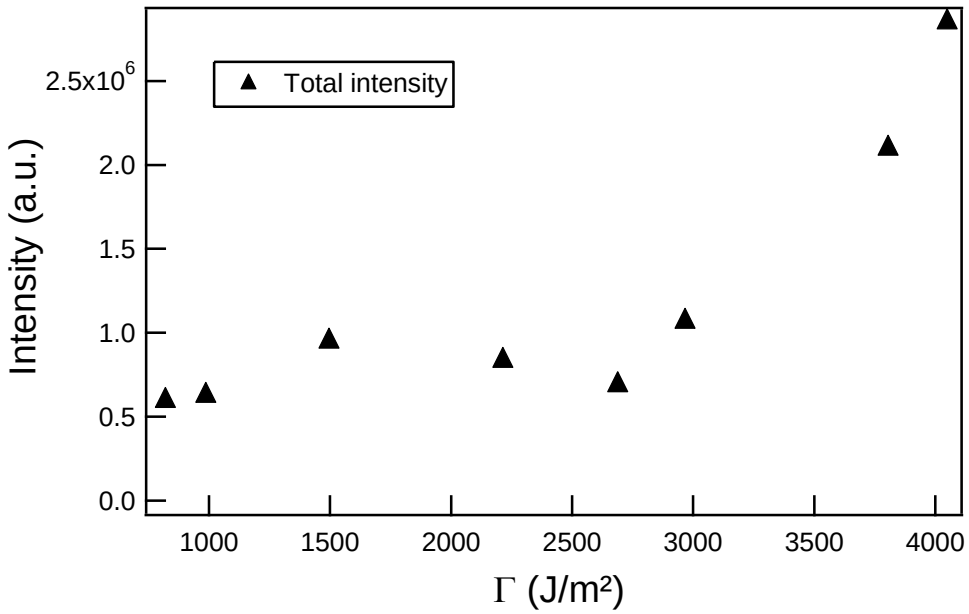

Figure 30: Intensity of the total mechanoluminescent signal as a function of the fracture energy.

From Figure 30, we can see that the intensity of the total mechanoluminescent signal is an increasing function of the fracture energy. However only a roughly and noisy linear increase can be observed up to 3000 J/m² followed by a sharp increase of the mechanoluminescent signal when bulk damages are observed. Figures 29 and 30 qualitatively confirm the results obtained by Ducrot, that the more prestretched a sample is, the more energy is dissipated at the crack tip. Indeed, a higher value of intensity means that the amount of broken dioxetane crosslinkers is higher. More broken crosslinkers mean that more bond scissions have occurred and have dissipated energy during the propagation process. However it is hard to argue from the data that the dissipation due to broken bonds is the only dissipation controlling Γ.

If we had more available material and more time, the ideal experiment would have been to calibrate the intensity observed with the camera in uniaxial traction with step cycle experiments. That calibration would have quantitatively related the hysteresis observed on the stress-strain curve and the mechanoluminescent intensity. With this calibration it would have been possible to obtain an approximation of the amount of broken chains around the crack tip for every sample.

In our case, the fraction of first network that is broken cannot be obtained quantitatively, but we can still compare the networks with each other. Indeed, we can assume that there is the same 20 % of dioxetane crosslinker for each network meaning that the only correction needed for the comparison is the fraction of first network. The correction by the amount of first network chains can be done in two ways: per bulk network chain or per surface chain crossing the fracture plane. In the first case we can divide the total mechanoluminescent intensity by the fraction of first network ϕ (the number density of crosslinker is in this case simply proportional to ϕ). Then, the comparison of the corrected signal gives an information of the average relative percentage of broken chains in the first network. Indeed, with that correction if the percentage of broken first network is constant at fracture, the corrected value will be constant. This corrected value is plotted as a function of the fracture energy in Figure 31.

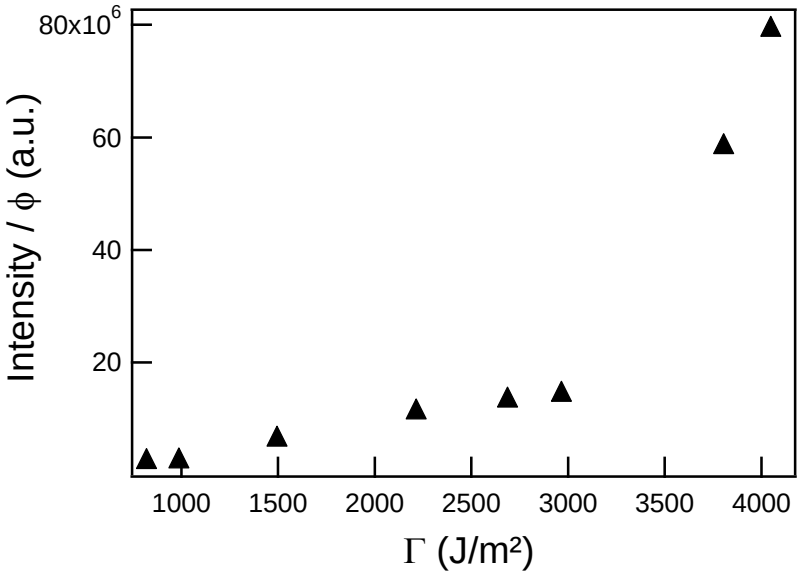

Figure 31: Total mechanoluminescent intensity corrected by the volume fraction of first network as a function of the fracture energy.

From Figure 31, it can be observed that this corrected intensity is never constant with the fracture energy and leads to the result that the percentage of broken first network is increasing linearly with the fracture energy until broken bonds are observed in the bulk.

However the measurement of the luminescence is made on a constant sample volume (thickness corrected) but remains inhomogeneous and concentrated near the crack tip.

A different correction can be applied on the total intensity measured to probe on the amount of broken chains per chain crossing the interface. This correction leads to the intensity being

divided by the dilution of the chains from the first network in the cross-section plane i.e. $\phi^{2/3}$. This result is presented in Figure 32.

The Figure 32 shows a similar tendency as the one observed in Figure 31 but the distribution of the corrected intensity is less broad. The physical interpretation of this graph is analogous to a thickness of the damage zone. Although we have no information on the spatial distribution of broken bonds for lack of spatial resolution, this normalized intensity reflects the number of broken chains per area and hence the average thickness of the damage zone (in a Dugdale sense). Up to 3000 J/m^2 this corrected intensity increases rather linearly and the onset of damage in the bulk (for the two points on the right of the graph) clearly shows the limits of the toughening mechanism where extensive bulk damage occurs before the crack propagates.

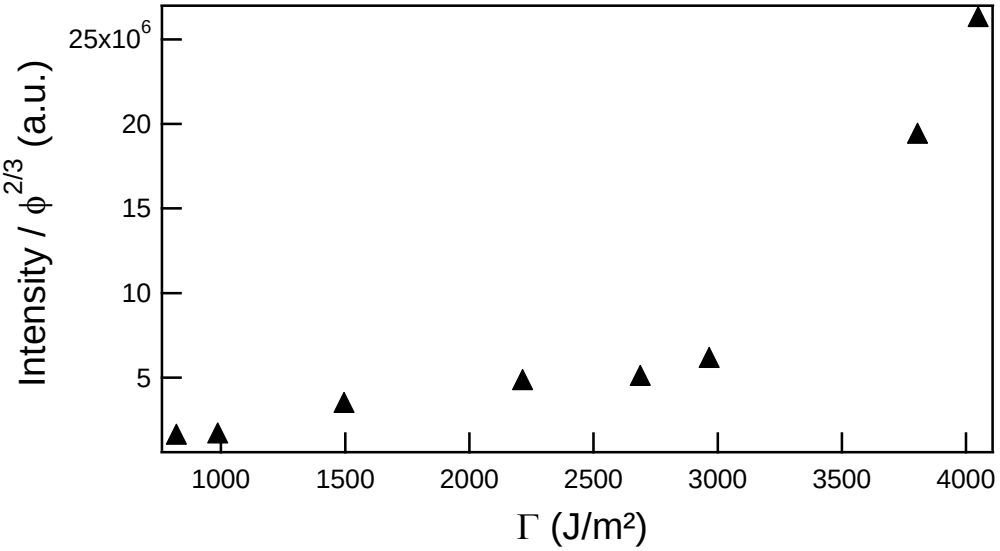

Figure 32: Total mechanoluminescent intensity corrected by the dilution of the chains of first network crossing the interface as a function of the fracture energy.

In the end it can be concluded that the fraction of broken dioxetane bonds in the first network is approximately 40 times higher for EA(d20)0.73(2.94)EA than for EA(d20)0.73(1).

This observation given by Figure 31 is only semi-quantitative and more experiments are needed to have an idea of the actual percentage of broken chains. By using the intensity values obtained for EA(d20)0.73(2.94)EA we tried to obtain an estimate of the fraction of broken bonds. To do so the signal has been corrected by the amplification, the probability to obtain the emission of a photon when a dioxetane crosslinker breaks and the area observed by the camera. The results gives a detected amount of broken chains that is six orders of magnitude smaller than the expected values. This difference was quite unexpected and could come from a problem in the synthesis or in the estimate of the broken bonds. This issue can be solved by systematic experiments with a proper calibration with cyclic experiments.

In conclusion, the mechanoluminescence experiments show bond scissions at the crack tip but they do not give information about the strain field that occurs at the crack tip. In order to investigate the local deformation in the process zone at the tip of the crack, another technique has been used during this work and is the subject of the following section.

2) Damage assessment from Digital Image Correlation (DIC)

a) Set up and principle of the technique

The mechanoluminescence experiments have led to the visualisation of the broken bonds during the opening and propagation of the crack and an approximate size of the damaged zone (i.e. where broken bonds are detected) as a function of the prestretching of the first network. In order to complete those observations, Digital Image Correlation was used to visualize the local deformation field at the crack tip. The goal is here to see the influence of the prestretching on the deformation field and to use the cyclic uniaxial tensile tests to calibrate and image the onset of local damage (mechanical hysteresis in uniaxial tension).

To perform the tensile test under a microscope, a deben microtensile stage is used, it has a span of 10 mm and a 200 N load cell. The elongation is performed with a rotating screw therefore limiting the strain rate. The sample is mounted horizontally under a binocular microscope equipped with a camera. The objective chosen gives a resolution of 2.47 µm/pixel. The depth of field being small, some adjustment must be done regularly during the stretching. For this reason, and because of the slow loading rate of the stage, the measurements were performed on the progressive opening of static cracks only. Therefore, the sample was stretched in steps of approximately 0.1 mm and a picture was taken at each step.

The samples used for these crack tip observations had a rectangular shape with approximately a length of 15 to 20 mm parallel to the crack direction and 5 mm distance between the clamps. The initial crack was made with a razor blade. To enhance the contrast for the DIC measurements, carbon black was applied with a brush all over the surface of the sample.

The general principle of the DIC technique is shown in Figure 33. Images taken successively are compared with each other. The first image is divided in a grid with a fixed mesh size (in our case the mesh size is 16 pixels). The grey value of each box of the grid is then measured. On the second image the software will find the previous grid in the new image. Therefore, the difference between the first grid and its new position in the second grid gives the local displacement field. In Figure 33, in the reference image on the left a Zone of Interest (ZOI) is defined, this same zone is tracked by the software in the deformed image, as shown on the right. From this, the local displacement of the ZOI can be deduced.

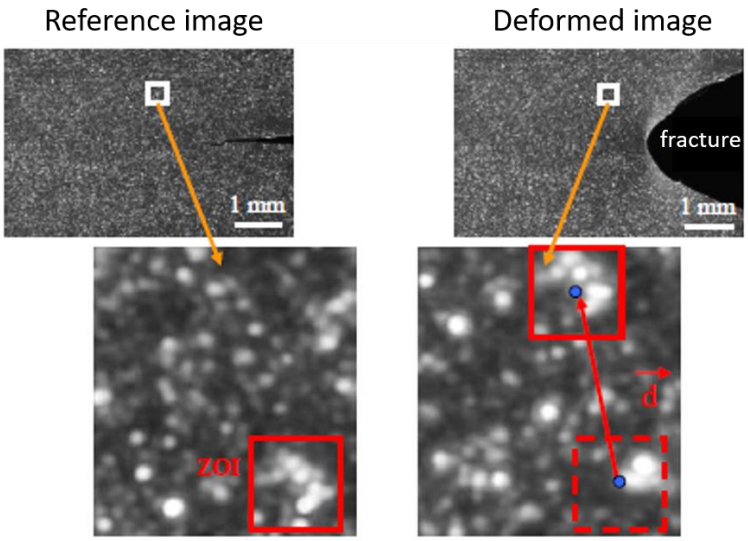

Figure 33: Images showing the principle of the DIC technic[12].

During this work, the software used is Correli Q4. It is a software developed at the LMT (Laboratoire de Mécanique et Technologie) laboratory in Cachan (France). This software runs on Matlab. It was previously described in Mzabi's thesis realized in our laboratory [12] and more recently used in the thesis of Demassieux [13]. An area located at the crack tip is defined as the region of interest (ROI), it is divided in boxes of 16 pixels. Correli is then minimizing the grey level difference to track the displacement of each box centre. The result is that the position of each box centre is then known for every image.

The DIC experiment was carried out on four different samples: EAe1.45(1), EAe1.45(1.68)EA, EAe1.45(2.55)EA and EAe1.45(3.42)EA. An example of the raw images obtained for EAe1.45(3.42)EA is shown in Figure 34. The red square represents the ROI that will be followed for each picture. In Figure 34, the stretch direction is vertical and it will be the same for all the presented figures of this section on DIC.

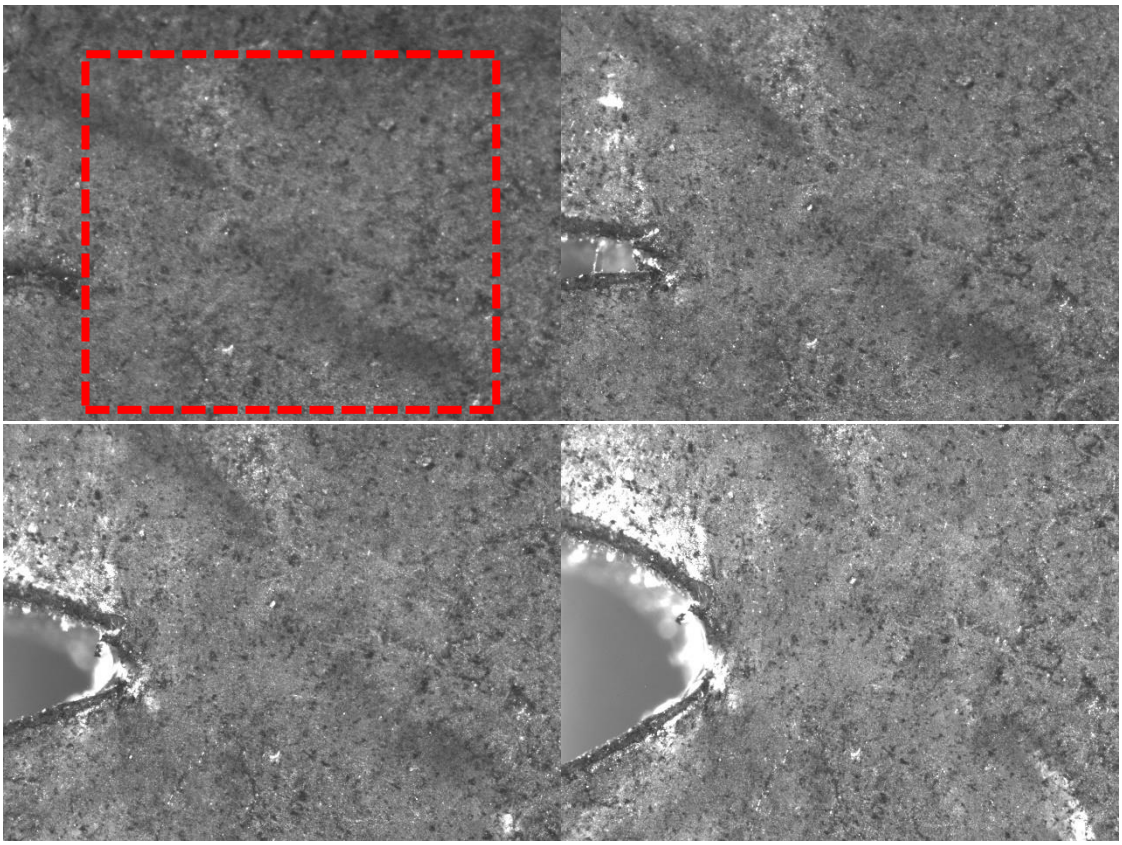

Figure 34: Raw images of a crack tip for the sample EAe1.45(3.42)EA. The red square in the first picture shows the initial position of the ROI.

Once the raw images are obtained for each sample, as shown in Figure 34, some data treatment is applied and will be the object of the following section.

b) Data processing and the use of the first stretch invariant

The software Correli gives the displacement of each box centre, U and V being the vertical and horizontal displacements. The goal of the data treatment is to be able to link the local displacement observed with our uniaxial tensile tests data. To do so the strain has to be calculated using the local displacement given by the software. As calculated and used by Demassieux [13], the two principal stretch values of the right Cauchy Green tensor are calculated using U and V. The root square of the two eigenvalues of the right Cauchy Green tensor gives the two principal stretches in the material. The largest is defined as λ_1 and the smallest as λ_2. Those two values can be used to define the strain state of the crack tip area. As done by Samaca et al. [14] , and then by Demassieux, an index of biaxiality I can be defined as shown in Eq. (4). This index describes the mechanical state of the sample ahead of the crack tip. The index is equal to 1 for pure shear, -1 for equibiaxial and 0 for uniaxial.

$$I = 1 - 2\frac{log(\lambda_2)}{log(\lambda_1)} \qquad \textbf{Eq. (4)}$$

This index can be locally calculated for each image of each sample. As an example, the value of the index is shown in Figure 35 for EAe1.45(3.42)EA. The displayed area corresponds to the red square shown in Figure 34. The crack is not represented and it is located at the left of every image, its tip is located at the very left of the images and at roughly 1900 pixels on the vertical scale.

In Figure 35, it can be seen that most of the region located ahead of the crack tip is displayed in red when the macroscopic elongation is high enough. The values of the biaxiality index are always above 0.85. From Figure 35, we can observe that our sample is deformed in pure shear on the entire region of interest. The same result can be observed for each sample.

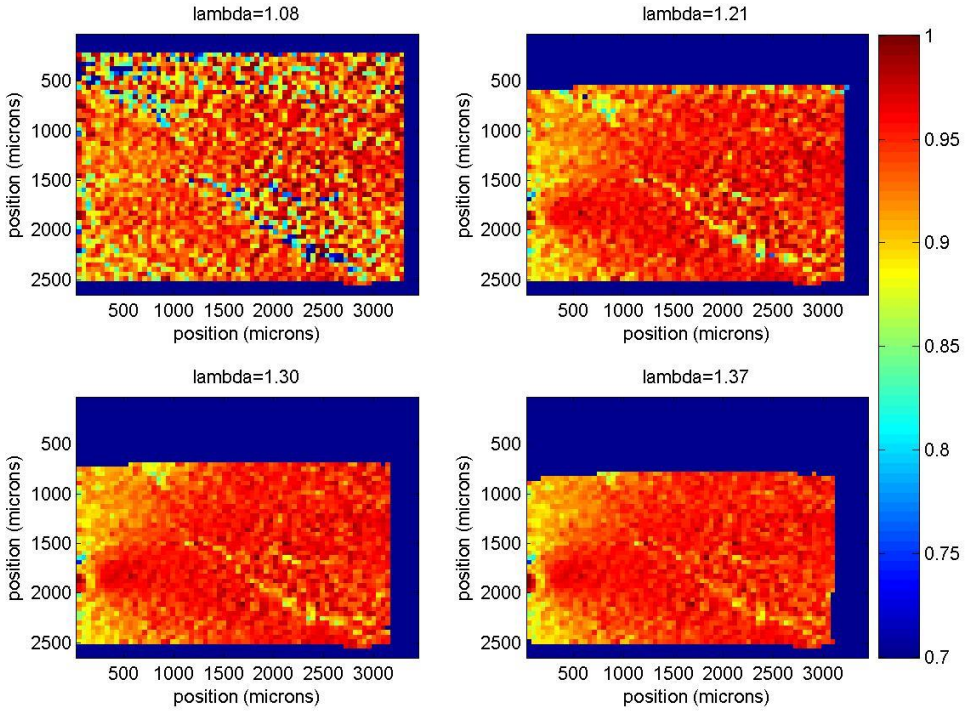

Figure 35: Index of biaxiality for four different macroscopic elongations (the macroscopic elongation is displayed above each image) for the sample EAe1.45(3.42)EA

The calculation of the biaxiality index shows that, for our different samples, the deformation is mainly in a pure shear mode. Therefore using exclusively the main direction of the stretch λ_1, to try to compare it with the deformation obtained in uniaxial tensile tests could lead to some errors. In order to link the uniaxial results obtained from chapter 3 and the local deformation given by the DIC experiments, we will use the first stretch invariant. Its expression is displayed in Eq. (5).

$$J_1 = {\lambda_1}^2 + {\lambda_2}^2 + {\lambda_3}^2 - 3 \qquad \textbf{Eq. (5)}$$

In Eq. (5), λ_1 *and* λ_2 are known, due to the assumption that the volume does not change in our sample upon deformation, λ_3 can be deduced as shown in Eq. (6). Therefore J_1 is known for every pixel boxes of every image.

$$\lambda_3 = \frac{1}{\lambda_1 * \lambda_2} \qquad \textbf{Eq. (6)}$$

It has been shown by Webber *et al.* [15] in their large strain experiments on double network hydrogels that the correct parameter to compare strain hardening obtained in uniaxial and biaxial experiments is the first strain invariant described in Eq. (5). Therefore, using the invariant as a measure of strain energy for both our uniaxial and DIC experiments should give us a reasonable way to link the results of both experiments. This means that the invariant value above which damages are observed in uniaxial tension can be used to define a damaged area around the crack tip in DIC experiments. There is no evidence that the invariant could also be used to predict yielding but we will assume that the invariant value for yielding in uniaxial tension can be used to characterize the occurrence of yielding in our multiaxial DIC experiments.

The stress-stretch curve in uniaxial tension is first converted in a stress vs. strain invariant curve for each used sample and an example is shown in Figure 36b) for the sample EAe1.45(3.42)EA (right) and compared to the original stress-strain curve (left).

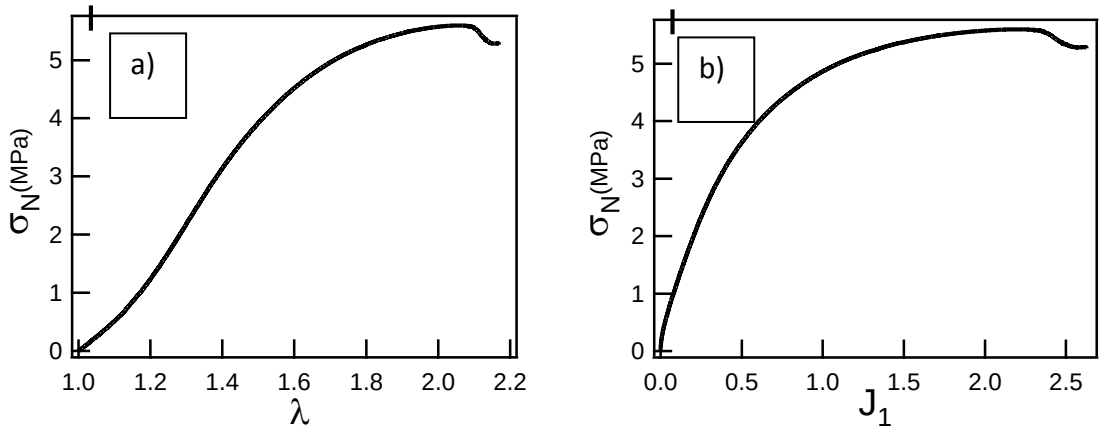

Figure 36: a): stress-stretch curve for the sample EAe1.45(3.42)EA. b): Stress as a function of the first stretch invariant for the same sample.

From the curves in Figure 36, a value of the invariant at yield can be obtained, 2.1 in the current example. The same analysis can be done for the sample EAe1.45(2.55)EA, the value is shown in Table 2. Using the cyclic experiments the critical deformation after which damages occurs can be measured for every samples leading to the corresponding invariant value as shown in Table 2.

Samples	Damages elongation	Damages invariant	Yield elongation	Yield invariant
EAe1.45(1)EA				
EAe1.45(1.68)EA	2.3	3.16		
EAe1.45(2.55)EA	1.7	1.07	3	6.67
EAe1.45(3.42)EA	1.4	0.39	2.1	2.36

Table 2: Invariant and elongation characteristic values for the different samples

Now that we have the value of the Invariant for the onset of mechanical hysteresis and for the onset of macroscopic yielding, we can use it to link the uniaxial cyclic tensile tests and the behaviour at the crack tip for the different samples.

c) Determination of the crack tip influence area

Determination of the macroscopic invariant

First, a macroscopic deformation has to be calculated for each image to determine the real amplification occurring around the crack tip. To do so we will calculate a macroscopic invariant. It is defined as the average value of J_1 far away from the crack tip at the extreme right of the region of interest where the crack has no influence. In this area, the material is deformed in pure shear. To calculate it, we calculate the mean value of 5 columns of pixel boxes located at the extreme right of the zone of interest for each picture. This DIC-based method will give the exact invariant and avoid the effects of slippage that could occur in the clamps. For the sample EAe1.45(3.42)EA, the result is presented in Figure 37.

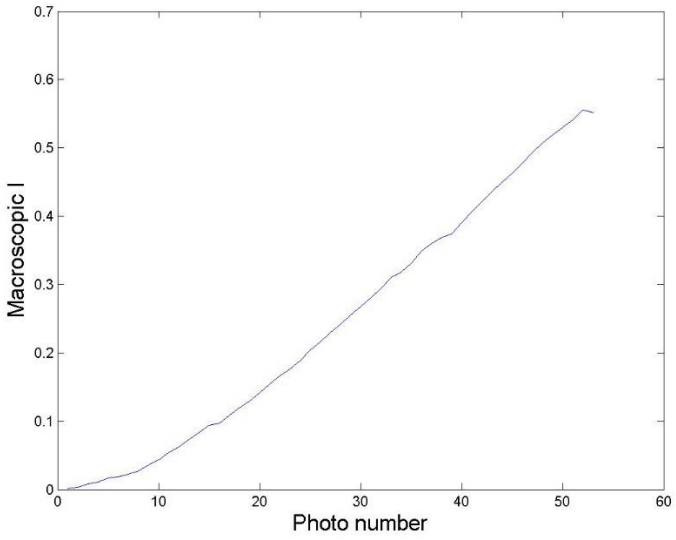

Figure 37: Macroscopic value of the Invariant as the photo number for the sample EAe1.45(3.42)EA

In Figure 37, it can be seen that the evolution of the macroscopic invariant from a photo to the next one appears to be quite linear after the ten first pictures. The slower increase at the beginning could be the result of an initial bending of the sample during its fixation into the clamps. Figure 37, shows the value of the macroscopic invariant that will be used as a reference for each corresponding picture. This procedure is carried out for every sample shown in Table 2.

Determination of the process zone of the crack tip

It has been seen that the area of interest is divided in pixel boxes. In this part, we will see how the crack tip has an influence on the different pixel boxes in the direction parallel and perpendicular to the crack propagation direction.

In the direction parallel to the propagation, a line where the actual crack tip has the most influence can be determined for each sample (pL for principal Line). However, as the crack opens this line is not always exactly a line of symmetry of the strain field but can be at an angle. Therefore, to have a more accurate result regarding the influence of the crack, three lines are considered, pL, pL+1 and pL-1. Those three lines are then averaged vertically into one line to plot an average intensity as a function of distance from the crack tip. A scheme to clarify which line is pL is displayed in Figure 38.

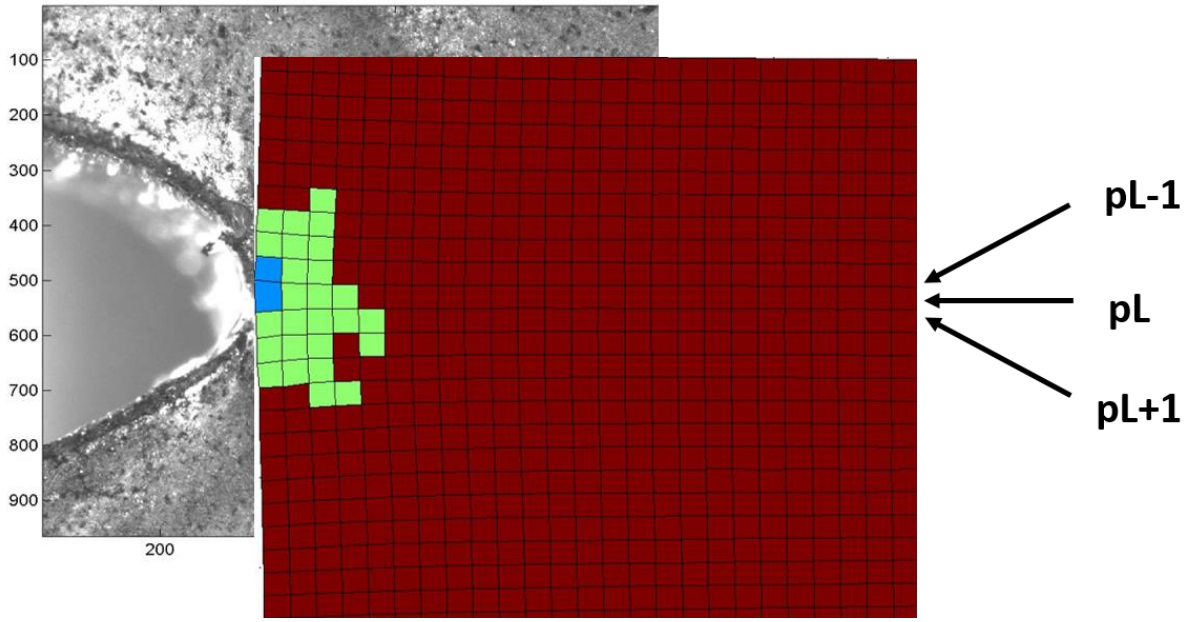

Figure 38: Scheme showing pL, pL+1 and pL-1. The grid shown, is the deformed grid corresponding to the picture of an open crack to visualize the selected lines of influence.

To observe the influence of the crack tip, the values of the local invariant for a certain number of pixel-boxes within a well-known distance from the crack tip are then plotted as a function of the macroscopic invariant. For the sample EAe1.45(3.42)EA, the result is presented in Figure 39.

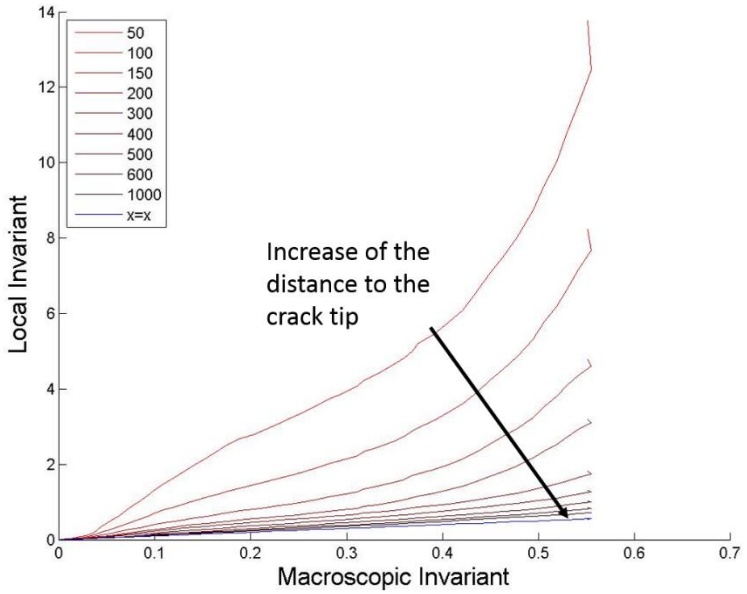

Figure 39: Local invariant as a function of the macroscopic invariant, the numbers in the legend correspond to the pixel-boxes distance to the crack tip in µm.

In Figure 39, the first thing that can be noticed is that far away from the crack, starting at 600 µm, the local invariant is equal to the macroscopic one. The pixel-box located at a distance of 500 µm, is affected only at a relatively high deformation, just before the propagation. The 5 curves showing a clear influence (from 50 to 300 µm), should be analysed in more detail. All five curves show two regimes, the first regime is roughly linear with different slopes for different distances from the tip. In the second regime, there is a strong slope increase which is more important when the distance to the crack is small. This amplification of the deformation at the crack tip could be due to the presence of a yielded area which would be an area with a large deformation but a slowly varying stress. Figure 39, shows a horizontal distance of influence around 500 µm. The use of a vertical plot will complete the determination of the size and shape of the zone.

For the estimate of the influence of the crack tip in the direction perpendicular to the propagation direction, another plot is needed. The same pixel-boxes are considered and the evolution of their value as a function of the vertical position is plotted for 4 different values of the macroscopic invariant and for different distances from the crack tip in each plot.

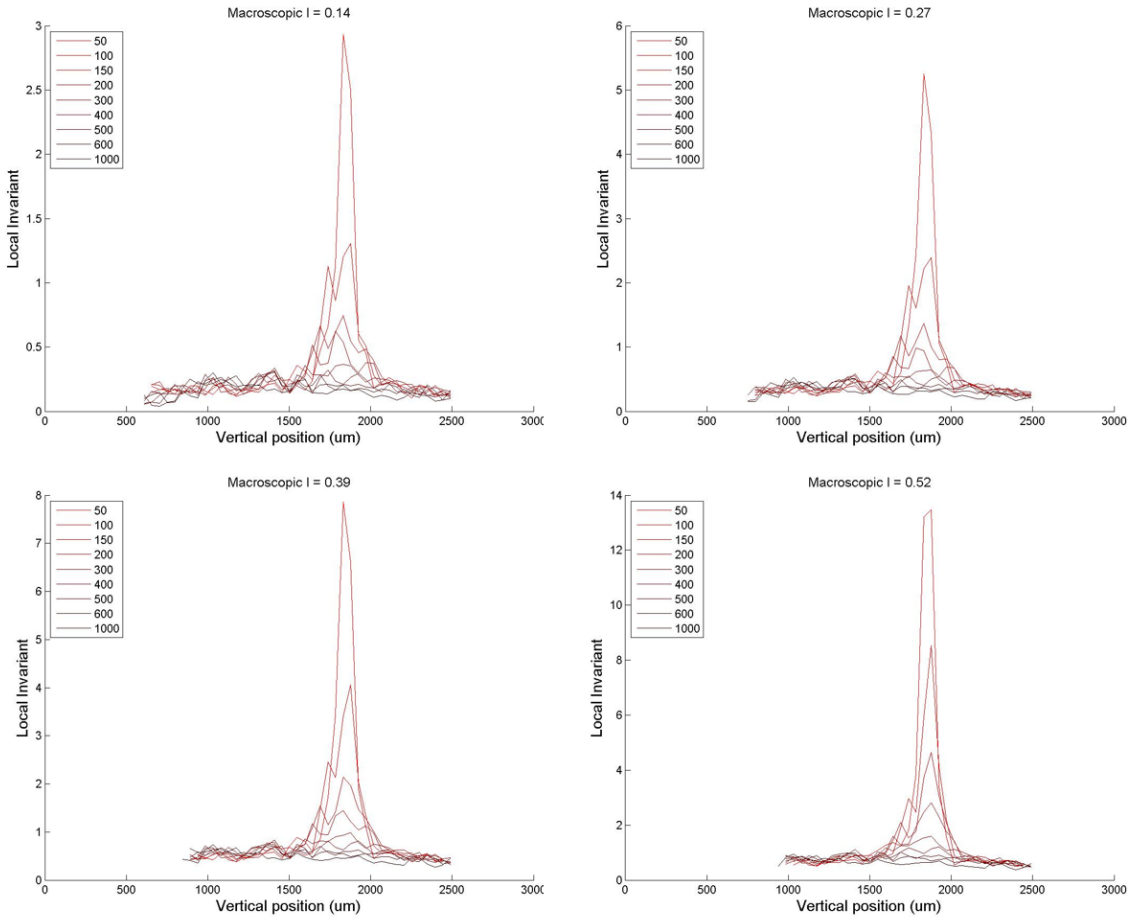

Figure 40: Local invariant as a function of the perpendicular position for four different macroscopic invariants. Top-left: macroscopic I = 0.14, top-right: macroscopic I =0.27, bottom-left macroscopic I = 0.39 and bottom-right: macroscopic I = 0.52.

Figure 40 shows the influence of the distance perpendicular to the crack. Note that the full scale is different from an image to another; to see better the influence of the crack even at low amplification levels such as in the top-left image. From those four images, the amplification of the deformation can be clearly seen to increase with the macroscopic invariant. The size of the affected area perpendicular to the crack seems to be defined at an early value of the macroscopic invariant and seems to be relatively constant around 400 µm. On the other hand, the noise on the signal does not really help visualizing the difference for columns located far away from the crack meaning that it is difficult to "precisely" define the influence of the crack tip in the vertical direction. It can still be noted that by zooming on each image and looking more closely at the curves corresponding to "50 µm", "100 µm" and "150 µm" from the crack tip, one can note that the peak at 50 µm, is narrower than that at 100 µm which is in turn narrower than the peak at 150 µm. The width of the peaks remains then stable for 150, 200 and 300 µm from the crack tip. This qualitative effect of the growing localisation of the singularity of strain was also seen by Mzabi *et al.* on SBR cracks [12].

In conclusion, the affected area in the perpendicular direction is less clearly detectable than that used for the parallel direction. The overall affected zone can be however estimated to be of 400 µm in the vertical direction and 500 µm in the horizontal one for that sample at a value of the invariant close to crack propagation.

For the samples EAe1.45(1.68)EA and EAe1.45(2.55)EA the horizontal analysis can be compared to the sample EAe1.45(3.42)EA presented earlier as shown in Figure 41.

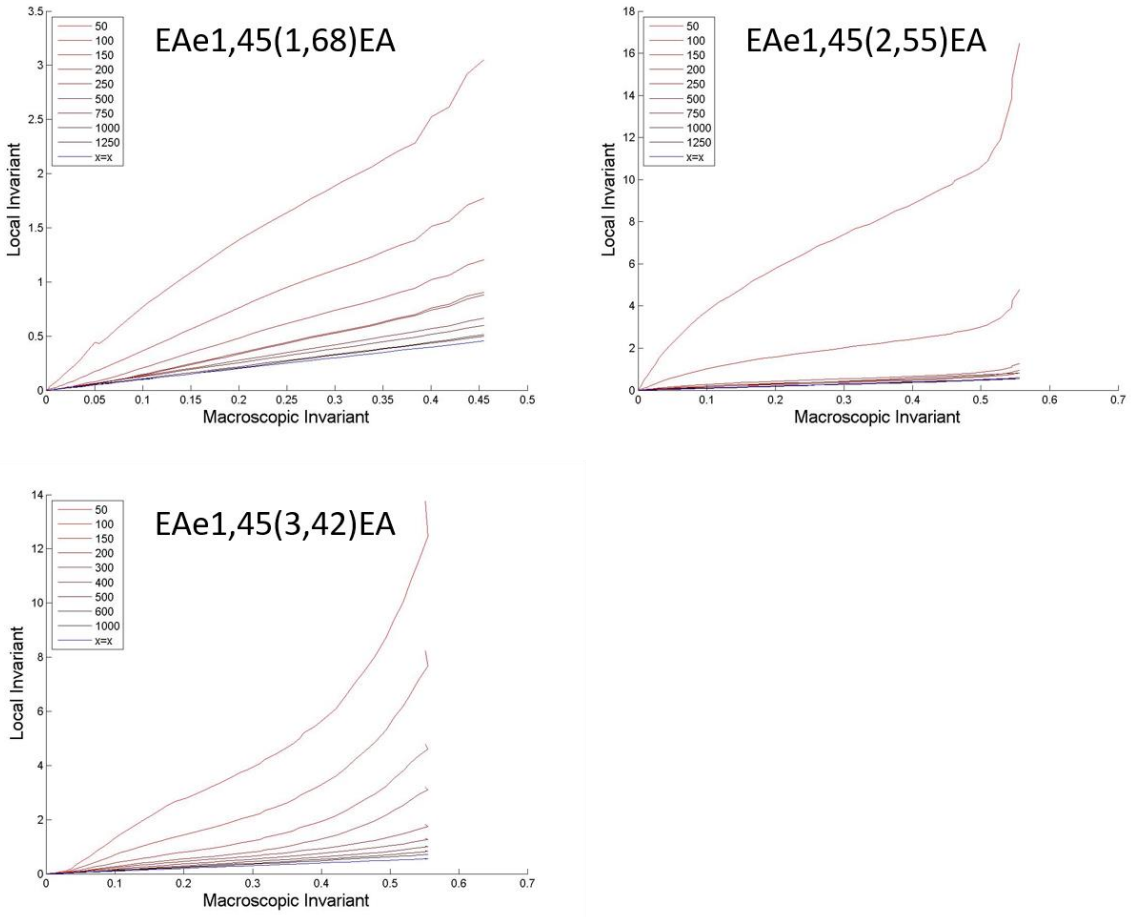

Figure 41: Local invariant as a function of the macroscopic invariant for three different samples, the numbers in the legend correspond to the pixel-boxes distance to the crack tip in µm.

Figure 41 presents the size of the process zone for three different samples through the amplification of the local invariant at the crack tip. For the EAe1.45(1.68)EA, the process zone seems to be approximately 250 µm long in the crack direction. The amplification level is quite small: before propagation occurs the macroscopic invariant reaches 0.45 while at the crack tip, the value can reach 3.2 for the local invariant, i.e. an amplification around 7. For the sample EAe1.45(2.55)EA, the last points of the graph show some propagation (very sharp increase of the slope) and the maximum of the local invariant before the propagation is around 11. For this sample, the process zone is surprisingly small in comparison to that of the sample EAe1.45(1.68)EA. The process zone appears to be confined to a 100 µm. On the other hand, the amplification is much larger reaching 20. In comparison the sample EAe1.45(3.42)EA shown in Figure 36 presents an amplification reaching 25 and a process zone up to 500 µm in the propagation direction. The analysis of the vertical zone of influence was also carried out but did not give much differences for the three samples. This might be due to the relative difficulty to estimate the influence with the noise quite largely present.

In order to obtain a better estimate of the affected area, in the next section we will focus on the visualisation of the local deformation at the crack tip in 2-D.

d) Visualisation of the local deformation at the crack tip

In the previous section, we have been able to estimate the size of the area affected by the crack. However, the use of the Correli Q4, can lead to a better visualisation. Indeed, with some data treatment, the shape and position of the centre of the initial pixel-boxes can be followed. Therefore, coupling those pieces of information with the value of the local invariant leads to a way to obtain a 2-D map of the local invariant at the crack tip. In order to improve the quality of the visualisation, each pixel-box does not have an individual colour as a function of the local invariant but different ranges of the local invariant are grouped together using the values shown in Table 2. In this case, the different ranges are the following:

- Red: the local invariant is inferior to the value leading to mechanical hysteresis (damage). Elastic deformation is predominantly occurring.
- Yellow: the local invariant is superior to the damages invariant. Dissipation occurs in this pixel-box.
- Blue: the local invariant is superior to the yield invariant. High dissipation occurs in this pixel-box with widespread breakup of the first network.

The different samples presented in Table 2 can also be compared with each other at the same values of energy release rate G. This energy release rate is calculated as described in Eq. (7) [12] where W is the density of elastic energy calculated from the integration of the area under the curve of the nominal stress versus the strain and h_0 is the initial size of the sample between the clamps.

$$\boldsymbol{G = W * h_0} \qquad \textbf{Eq. (7)}$$

The first value at which the three samples are compared is $G = 300\ J/m^2$. The first network is not compared to the others due to a very early breakage without any prior damages before the propagation. The comparison is shown in Figure 42. It is important to note that in this work and for the sake of the comparison with luminescence data, the strains are represented on a deformed grid that is changed by the crack opening whereas the common representation used in solid mechanics is the reference grid.

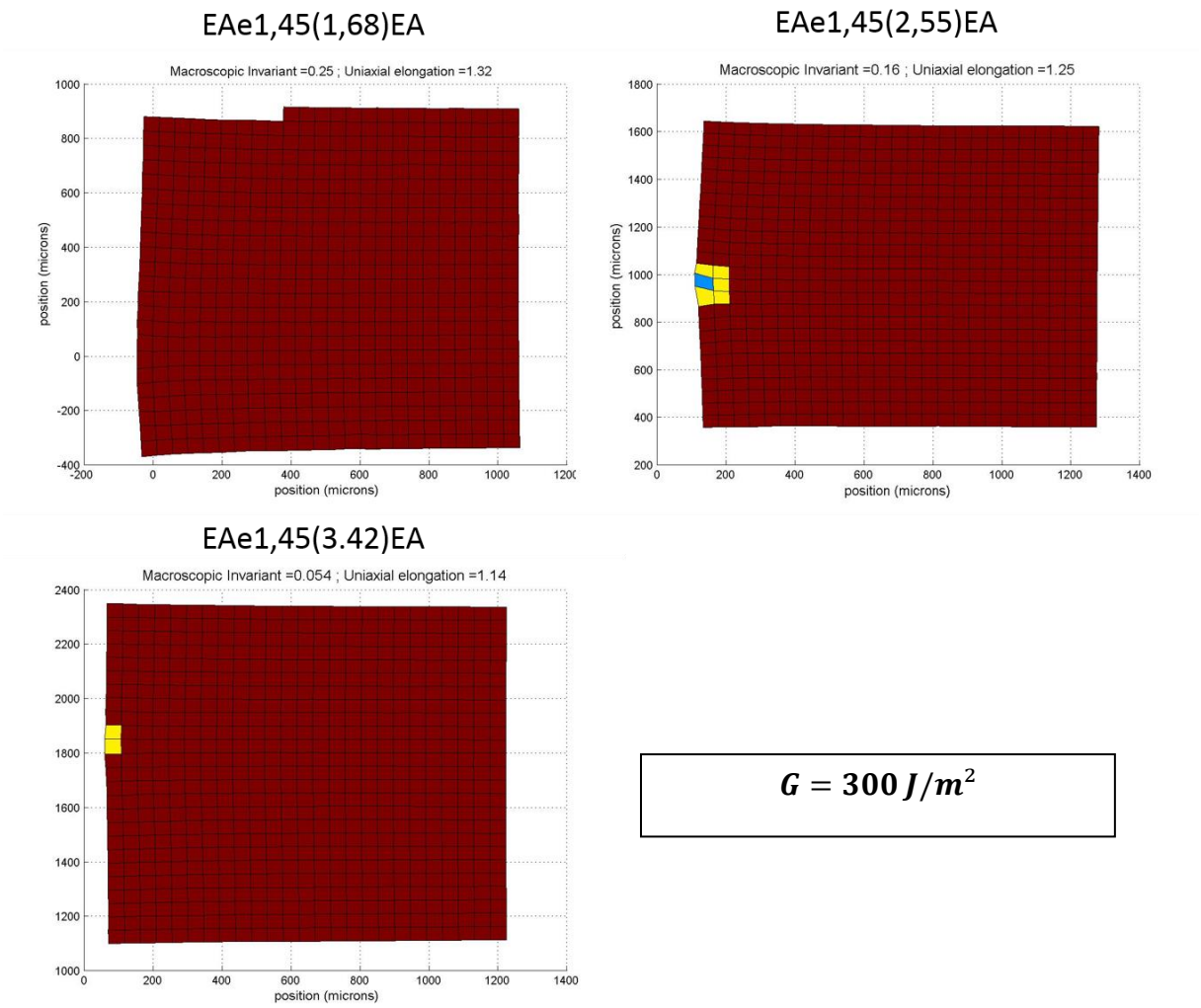

Figure 42: Comparison of the local invariant for the samples EAe1.45(1.68)EA, EAe1.45(2.55)EA and EAe1.45(3.42)EA for $G = 300\ J/m^2$. Macroscopic invariants are respectively 0.25, 0.16 and 0.054.

First, Figure 42 shows that the corresponding invariant and uniaxial elongation for $G = 300\ J/m^2$ is quite different for each network because of differences in stiffness (see Figure 23). At the local level, it is interesting to note that the less prestretched sample does not present any damage. On the other hand, the sample EAe1.45(3.42)EA presents two pixel boxes where the damages level is reached. The sample EAe1.45(2.55)EA even present some yielding at the very crack tip.

Then G is increased to $G = 500\ J/m^2$ which corresponds to Γ for the sample of EAe1.45(1.68)EA, the local invariant for each sample is presented in Figure 43.

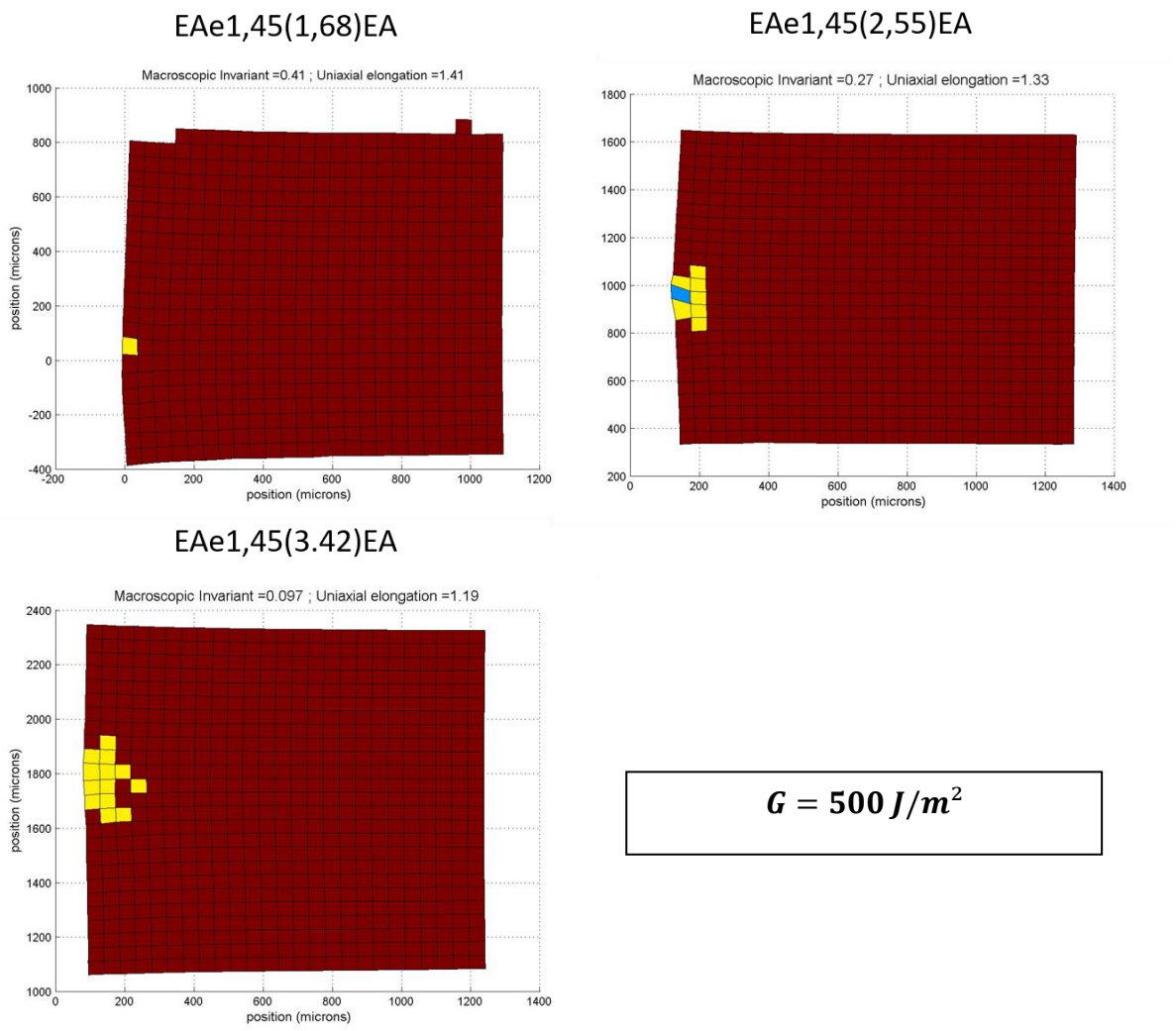

Figure 43: Comparison of the local invariant for the samples EAe1.45(1.68)EA, EAe1.45(2.55)EA and EAe1.45(3.42)EA for $G = 500\ J/m^2$. Macroscopic invariants are respectively 0.41, 0.27 and 0.097.

Figure 43 shows the finite elongation just before propagation for the sample EAe1.45(1.68)EA, and it can be observed that a small portion of the network is damaged prior to the propagation. It is interesting since this type of network is normally only elastic up to breakage in uniaxial elongation. For the two other samples the area affected by the crack tip becomes slightly bigger.

Continuing this approach, the value of G is increased up to Γ for the sample of EAe1.45(2.55)EA to $G = 1200\ J/m^2$. The local deformation is then compared to EAe1.45(3.42)EA in Figure 44.

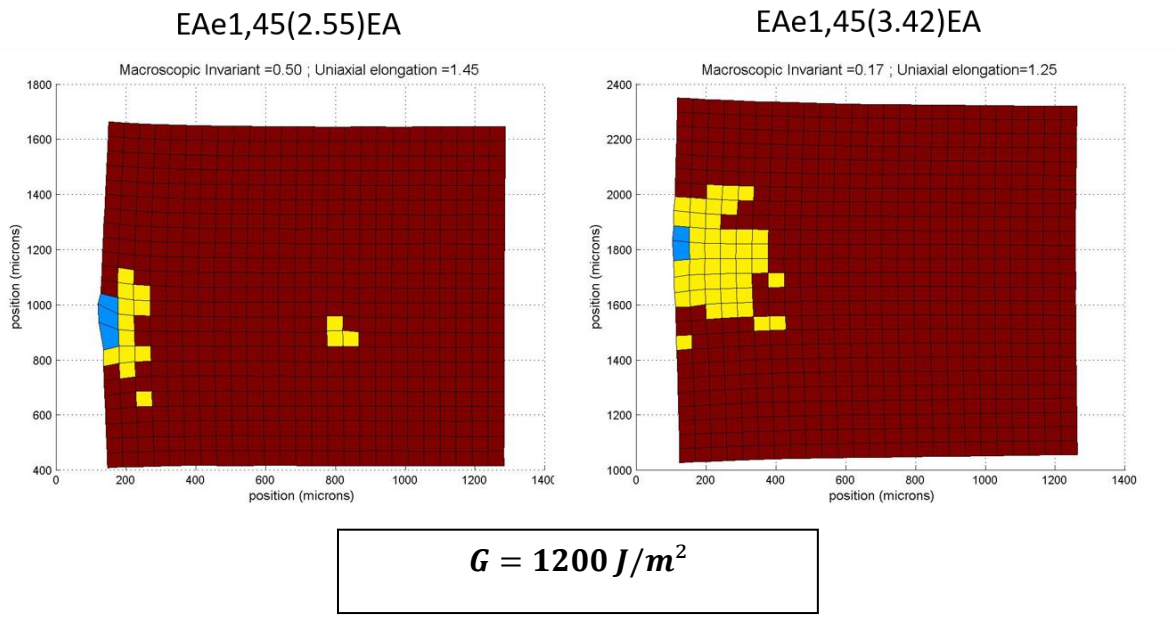

Figure 44: Comparison of the local invariant for the samples EAe1.45(2.55)EA and EAe1.45(3.42)EA for G=1200 J/m². Macroscopic invariants are respectively 0.50 and 0.17.

From Figure 44, it can be seen that the network EAe1.45(2.55)EA presents an enlarged damaged zone. This damaged zone reaches the approximate size of 150 µm by 300 µm. Also it can be seen that some local yielding is observed for that network while it was not possible to observe it macroscopically in uniaxial tension. For the sample EAe1.45(3.42)EA, the damaged area at the crack tip keeps increasing and localized yielding appears.

Finally, when EAe1.45(3.42)EA is stretched up to its maximal elongation before propagation, so that the invariant is increased up to Γ for this sample where $G = 4200\ J/m^2$. The local invariant at this deformation is shown in Figure 45.

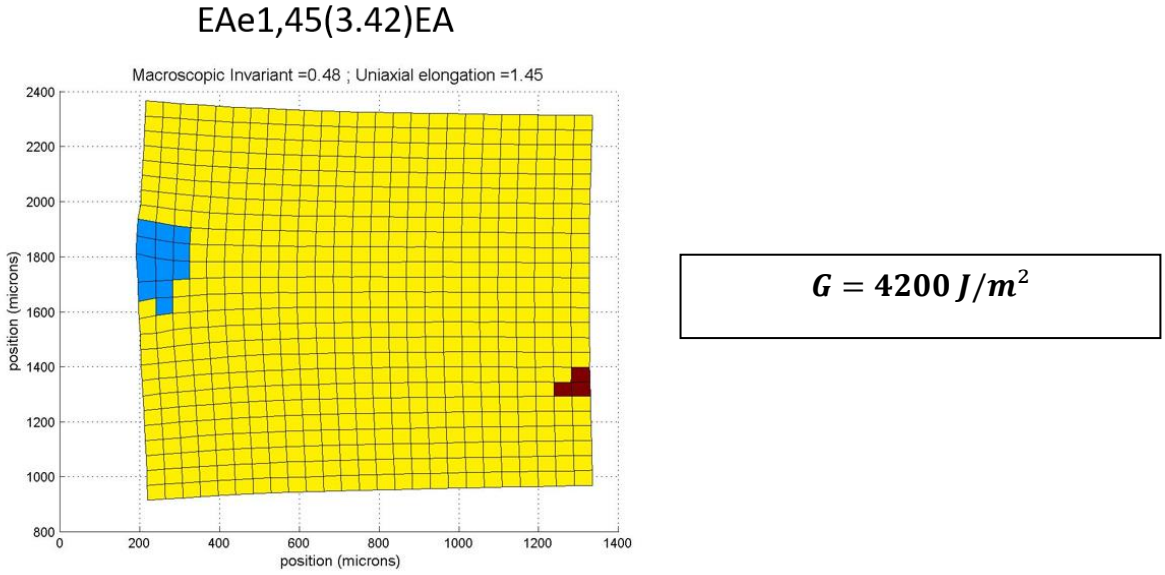

Figure 45: Local invariant for the sample EAe1.45(3.42)EA for G=4200 J/m². Macroscopic invariant is 0.48.

The first obvious conclusion of Figure 45 is that at this level of local invariant, the entire network is damaged in the bulk. Still a relatively large necked region can be observed at the crack tip. However, there is no real possibility to distinguish the affected area at the crack tip from the damaged bulk network with this representation. To refine our imaging, an arbitrary value of 1.2 times the macroscopic invariant has been chosen to show the area affected by the crack tip. This value has been chosen sufficiently high to be above the local noise to isolate the zone of influence. Therefore, when the local invariant exceeds $1.2*I_{macroscopic}$, the crack is responsible for part of the damages and the representation of this affected area is done in green in Figure 46.

EAe1,45(3.42)EA

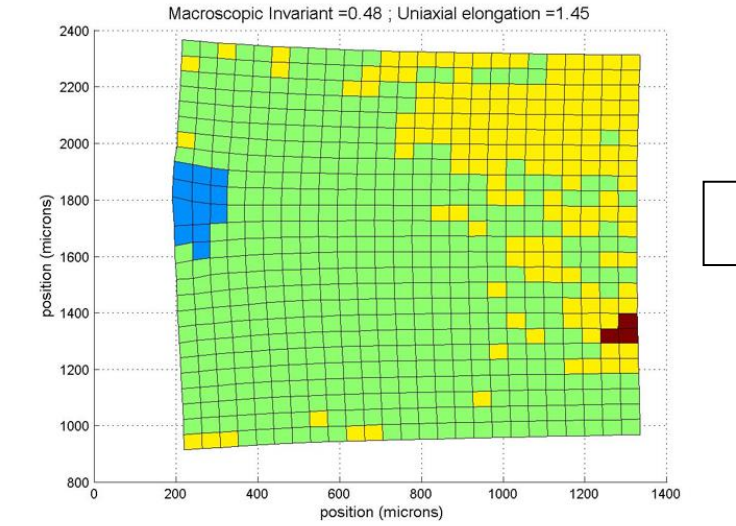

$$G = 4200\, J/m^2$$

Figure 46: Local invariant for the sample EAe1.45(3.42)EA for G=4200 J/m². The green zone correspond to 1.2 times the macroscopic invariant.

Figure 46 first shows that the estimate of the affected area obtained from the previous section is a bit wrong in comparison to the image of the bottom-right. The estimation of the affected area in the parallel direction at around 500 µm is underestimated, the size shown in the picture is closer to 800 µm. The value for the affected area in the perpendicular direction found using Figure 40 is also inferior to the value that can be observed in Figure 46. Using this figure, the correct value is at least 1500 µm.

Also Figure 46, confirms our expectation of the occurrence of an area where the sample macroscopically yields. This zone corresponds to an area where the first network is highly damaged and the local deformation is very high, with the local invariant being up to an order of magnitude higher than the macroscopic invariant. This locally highly damaged zone starts to form at a relatively low value of the macroscopic invariant and grows in size as the overall deformation increases.

The digital correlation experiments have offered the possibility to measure the local deformation at the crack tip and by comparing the data with uniaxial cyclic experiments, to estimate the size of this process zone. It should be noted however that the loading conditions being different, our analysis relies on the first invariant being a good parameter to characterize local damage. Reality could be more complex.

Conclusion

After studying the mechanical properties of our different networks in uniaxial tension in the two previous chapters, this chapter is dedicated to the impact of fracture.

It has been seen that despite a large variety of mechanical behaviours observed in tensile tests, the behaviours observed in fracture are not as wide. The Type 1 materials shows no reinforcement in fracture as expected, then Type 2 improves the fracture energy continuously with increasing prestretching. Finally the samples from Type 3 and Type 4 have relatively similar values of fracture energy despite an increasing level of prestretching and stiffening.

To visualize the local environment near the crack tip, two techniques have been used during this work, the mechanoluminescence and the DIC. The use of the two techniques gives a good characterisation of the crack tip. Mechanoluminescence shows the dissipative bond breaking mechanism that occurs during the crack opening and during the propagation. DIC gives a map of the strain field and can be used to estimate the damage zones during crack opening if properly calibrated with cyclic uniaxial tension data. Those two techniques appear to be complementary. It is difficult to compare the area affected by the crack tip for the different samples since they are not the same from one experiment to the other. If the size is compared for both most prestretched materials, it can be seen that the damaged zone before the propagation is of the order of 1 mm for both techniques.

The use of those techniques and especially the DIC have led to the observation of new dissipative mechanism for some samples. Indeed the sample EAe1.45(1.68)EA presented some damages before breakage that are not seen in tensile tests and EAe1.45(2.55)EA could show a yielding at the crack tip. This observation could explain the similar values of fracture energy for Type 3 and Type 4 since the same dissipation mechanism is observed.

On the other hand, the sample from Type 4 clearly showed some bulk dissipation that is artificially increasing the measured fracture energy with the technique used in this work. Indeed, to measure only the dissipation linked with the crack, the bulk dissipation should be removed. Therefore, maybe some of the Type 3 samples would be the most efficient to resist the crack propagation if the damages occurring in bulk would not be taken into account for the Type 4 samples.

Many topics are open for discussion here. The mechanoluminescence data (Figure 29) interestingly shows that the number of first network bonds breaking at the onset of crack propagation is rather similar and independent of the toughness if no bulk breakage occurs before propagation. However Figure 32 shows that the distance from the fracture plane over which this bond breakage occurs is proportional to the measured Γ. This striking result implies that the toughness is not controlled by the energy to break the bonds (or the strands) themselves, but to the volume (around the crack tip) over which the first network controls the mechanical behaviour of the material and imposes a hysteresis.

The damage during propagation would also be a very interesting quantity to determine but would require a more careful analysis with better temporally and spatially resolved data.

Nevertheless, it would be very interesting to compare the damage occurring before propagation, to that occurring during propagation with the idea of comparing this with simulations.

References:

1. Lake, G.J. and A.G. Thomas, *The strength of highly elastic materials.* Proceedings of the Royal Society of London, series A: Mathematical and Physical Sciences, 1967. **A300**: p. 108-119.
2. Gent, A.N. and R.H. Tobias, *Threshold tear strength of elastomers.* Journal of Polymer Science: Polymer Physics Edition, 1982. **20**(11): p. 2051-2058.
3. Rivlin, R.S. and A.G. Thomas, *Rupture of rubber. I. Characteristic energy for tearing.* Journal of Polymer Science, 1953. **10**(3): p. 291-318.
4. Greensmith, H.W., *Rupture of rubber. X. The change in stored energy on making a small cut in a test piece held in simple extension.* Journal of Applied Polymer Science, 1963. **7**(3): p. 993-1002.
5. Persson, B.N.J., et al., *Crack propagation in rubber-like materials.* Journal of Physics-Condensed Matter, 2005. **17**(44): p. R1071-R1142.
6. Gent, A.N., *Adhesion and strength of viscoelastic solids. Is there a relationship between adhesion and bulk properties?* Langmuir, 1996. **12**: p. 4492-4496.
7. Chen, C., W. Zhengjin, and Z. Suo, *Flaw sensitivity of highly stretchable materials.* Extreme Mechanics Letters, 2016.
8. Ducrot, E., et al., *Toughening Elastomers with Sacrificial Bonds and Watching them Break.* Science, 2014. **344**(6180): p. 186-189.
9. Chen, Y. and R.P. Sijbesma, *Dioxetanes as Mechanoluminescent Probes in Thermoplastic Elastomers.* Macromolecules, 2014. **47**(12): p. 3797-3805.
10. Chen, Y., et al., *Mechanically induced chemiluminescence from polymers incorporating a 1,2-dioxetane unit in the main chain.* Nat Chem, 2012. **4**(7): p. 559-562.
11. Ducrot, E., *Double Network Elastomers*. 2013, Université Pierre et Marie Curie: Paris.
12. Mzabi, S., *Caractérisation et analyse des mécanismes de fracture en fatigue des élastomères chargés*, in *Laboratoire PPMD-ESPCI*. 2010, Université Pierre et Marie Curie: Paris. p. 304.
13. Demassieux, Q. and C. Creton, *Structural changes in the process zone of a cyclic fatigue crack in filled natural rubber.* UMPC, 2016.
14. Samaca Martinez, J.R., et al., *Heat and strain measurements at the crack tip of filled rubber under cyclic loadings using full-field techniques.* 2015. **81**: p. 62–71.
15. Webber, R.E., et al., *Large Strain Hysteresis and Mullins effect of tough Double-Network Hydrogels.* Macromolecules, 2007. **40**(8): p. 2919-2927.

Chapter 6: Open general discussions

Chapter 6: Open general discussions

Introduction

During this work, we have tried to understand comprehensively the mechanical behaviour of multiple networks elastomers. It has been seen that the Young's modulus is controlled on the one hand by the presence of the additional entanglements brought by the interpenetrating networks and on the other hand by the degree of prestretching of the chains of the first network. This is especially seen at high prestretching levels, close to the limit of extensibility of the first network chains. Then the hardening phenomenon occurs and is observed at increasingly lower elongation as the prestretching of the first network increase. Fitting the uniaxial data with the Gent model showed that this phenomenon is controlled by the first network and its finite extensibility. We then showed that the stress during the hardening process could be rescaled by the areal density of first network chains crossing the interface. A master curve could be obtained for each family of materials stemming from the same first network, by correcting the stress by the areal density of first network strands and the strain by the prestretching of these strands. In conclusion, the uniaxial tensile curve is well understood up to the yield point. However, we still lack a molecular explanation for the macroscopic yielding and necking observed in some samples and not in others. Also, the details of the mechanism occurring during the necking after this yielding is not well understood.

In this chapter, we will open the discussion in order to answer these remaining questions regarding the end of the stress-strain master curve. The necking phenomenon will be discussed together with the yielding criteria and finally, the possible molecular mechanisms of fracture will be discussed.

I) Discussion around the mechanism involved during the necking process

The necking that is observed at high elongation for some of the multiple network elastomers is a very unique property in elastomers that was observed for the first time for those materials. This necking phenomenon has been observed macroscopically as described in chapter 3 section IV)1). The necking corresponds to a damage process occurring roughly in a plane normal to the tensile direction that propagates then through the entire sample along the tensile direction. Our hypothesis regarding this phenomenon is that at the yield stress, the first network is extensively damaged in a localized position. This localized area could be a zone with shorter first network chains. In this particular point of the sample, the extensive damages of the first network increase the local elongation and therefore create the necking phenomenon observed macroscopically. The fact that this necking does not lead to the failure of the sample but propagates in a stable manner along the sample implies that a strain hardening occurs at higher strains.

More specifically two damage fronts are created and propagate in opposite ways along the tensile direction. As the necked area grows in size, the high level of damage that takes place in the first network propagates progressively to the entire sample. At the same time the rest of the first network is not damaged more extensively than the level which is observed at the yield point. Then when one of the necking fronts reaches it, the damage becomes more extensive and the local stretch in the tensile direction increases. If this hypothesis is correct it should be observable in mechanoluminescence. Indeed, the two propagating fronts should be emitting light while the rest of the sample remains dark; if the first network breaks at this position.

In order to visualize directly the phenomenon, a piece of the sample EA(d20)0.73(2.94)EA used in chapter 5 section II)1) was used. We wanted to see if the mechanoluminescence could confirm our hypothesis that a more extensive bond breaking mechanism occurs at the necking fronts. To do so, the same set up described in chapter 5 section II)1) was used to record images. The un-notched sample was fixed in the clamps and the tensile test was carried out while recording some images with the Andor camera. The acquisition settings were similar to those used for the materials studied in chapter 5 with two images taken per second. At the same time, the Instron device recorded the stress-strain curve which is shown in Figure 1. The mechanoluminescent signal was recorded and a median filter (as used in chapter 5 section II)1)) was used to improve the signal visualisation on each image. Also, to improve the signal to noise ratio, every image was added to the next one giving therefore on each picture displayed the sum of two images. The results of this experiment is shown in Figure 1 for the stress-strain curve and in Figure 2 for some of the corresponding mechanoluminescence signal.

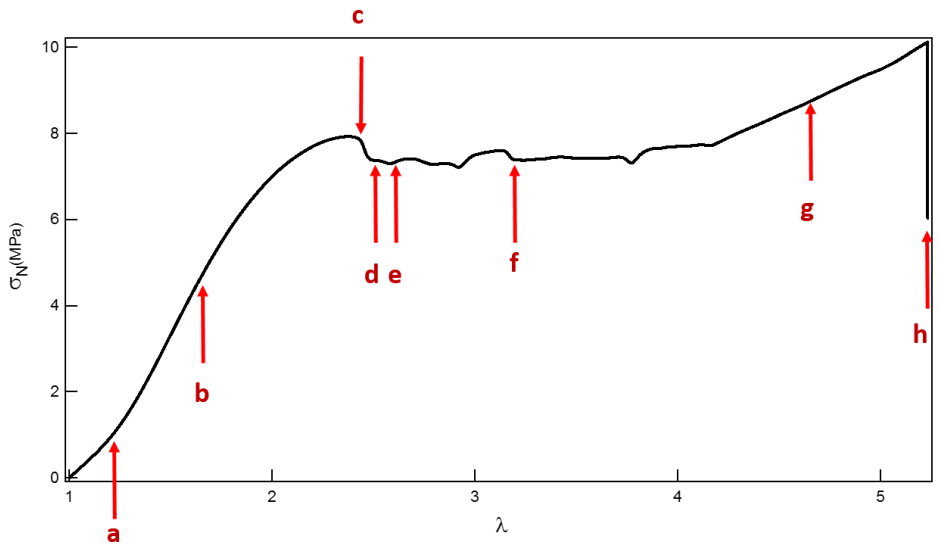

Figure 1: Stress-strain curve of for the sample EA(d20)0.73(2.94)EA. The signal was obtained while images were recorded, the different letters are referring to the images shown in Figure 2.

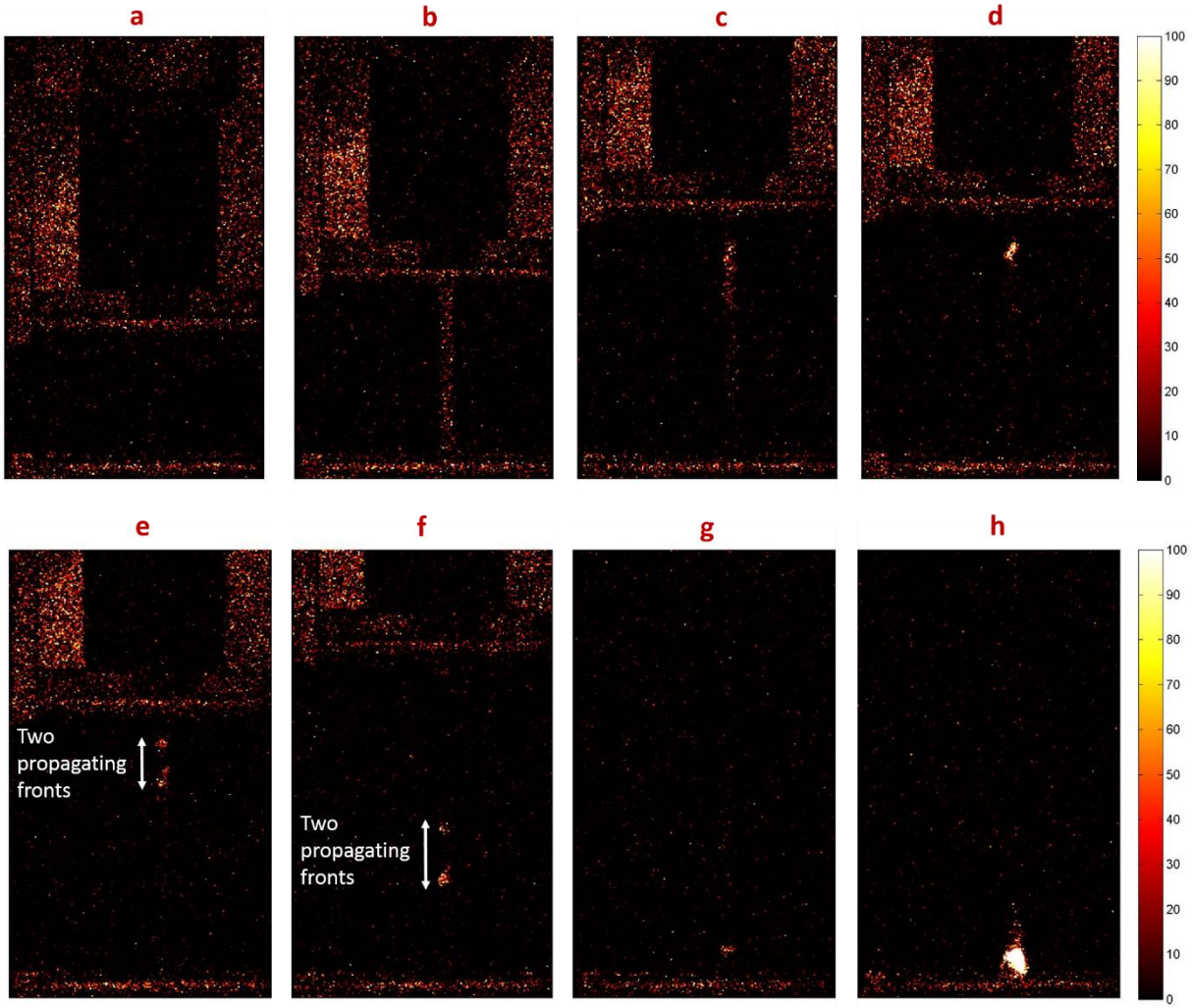

Figure 2: Images showing the mechanoluminescent signal of the sample EA(d20)0.73(2.94)EA. The letters are referring to the state of stress-strain of the sample (Figure 1) when the signal is recorded. The scale represents the count that can be compared between each picture but its unit is arbitrary.

The stress-strain curve recorded for this sample is shown in Figure 1. It can be seen that, as expected, the sample first yields with a maximum in nominal stress, then the force remains constant while the necked region propagates. Finally at high strain the nominal stress increases again. The different letters are referring to the corresponding images of the mechanoluminescent signal that have been taken simultaneously. Those images are displayed in Figure 2. The analysis of the different images is the following:

- a: No mechanoluminescent signal is observed, this image is taken at low elongation, no visible damages are occurring yet in the multiple network.
- b: This image is taken after the inflexion point of the strain hardening phenomenon ($\lambda > \lambda_h$), therefore bonds should be breaking, this can be observed by the homogeneous light signal observed over the entire sample.
- c: this picture is taken at the yield point, it can be seen that the signal appears to be less intense and is no longer homogeneous over the entire sample
- d: a very localized damage point can be observed, it corresponds to the area where the necking is initiated.
- e: The initiation observed in picture d is confirmed by picture e showing the two necking fronts going in opposite directions. The rest of the sample does not present any damages so is the part in between the two necking fronts.
- f: the necking front going up has been stopped by the end of the central zone of the dumbbell and the one going down has been stopped by certainly an inhomogeneous part (this corresponds to the increase of stress shown at an elongation of 3). Following this, a new necked area is created in the lower part of the sample and the two new fronts are shown in picture f.
- g: the necking has reached the end of the central zone. Bond breakage can be only seen in the bottom part, it has to be noted that the top grip and the top part of the sample are now out of the field of view of the camera.
- h: Macroscopic fracture of the sample occurs near the bottom clamp.

The images of Figure 2 are a clear evidence of the mechanism involved during the necking process. To complete the analysis of the phenomenon, the intensity of the signal has to be quantified. It has to be noted that on the different images of Figure 2 the clamps can be clearly seen for those experiments. The presence of the clamps (due to IR emission) has to be taken into account for the integration of the intensity signal. To obtain the mechanoluminescent intensity, a vertical column, that contains the entire sample all along the experiment, is used (witdh of 30 pixels). To remove the effect of the clamps in each image, a neighbouring column without signal is considered and the signal average is calculated for each line. Then to remove the clamps signal, this line average is subtracted to each pixel in the corresponding line in the column of interest. Then the sum of the signal of every pixel is counted for each image giving an intensity as a function of time. This intensity can be calculated as a function of deformation and presented in Figure 3. The noise level in the signal is significant but it will still give us information.

The intensity signal starts around 0 as expected with no signal at the beginning until the hardening is reached at $\lambda = 1.4$, there a sharp increase in the total intensity until it reaches a

maximum in the middle of the softening part. Following this maximum a slow decrease starts until a drop is observed when the actual necking starts. During the necking process of the central zone observed in the images of Figure 2, the total signal appears to be relatively constant. This constant value of the integrated signal is expected, since, two fronts are propagating and should break the same amount of first network chains in the entire sample.

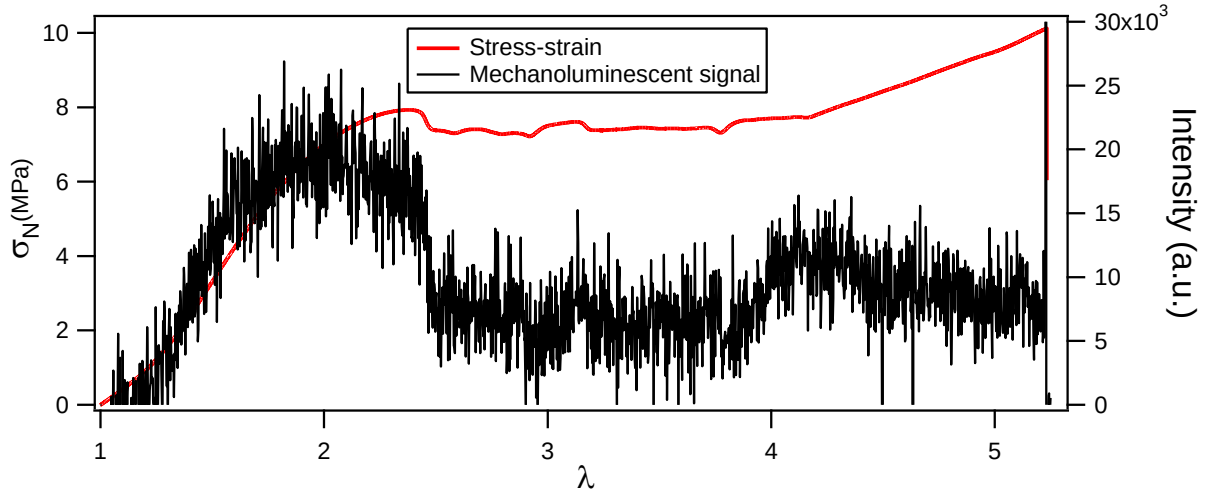

Figure 3: Stress-strain curve of for the sample EA(d20)0.73(2.94)EA along with the intensity of the mechanoluminescent signal.

Figure 3 confirms the necking mechanism: two fronts are propagating in the entire sample and breaking approximately the same amount of first network during the process. The intensity of the signal shown in Figure 3 can be summed for each image to obtain the evolution of the cumulated signal. This signal is shown in Figure 4. The different phases can also be observed on that figure, with at the beginning the absence of signal until the hardening starts followed by the necking that presents a smaller increasing slope and finally the second hardening. Figure 4 shows that the increase of the emitted light is not a linear function of the extension as opposed to the cumulative mechanical hysteresis shown in chapter 3 section II)2) on similar samples or what was observed by Ducrot [1]. This discrepancy between mechanical hysteresis and luminescence emitted should be investigated more extensively for different mechanoluminescent samples but suggests that the breakage of the first network is not the only dissipative mechanism involved especially when as the yielding and necking occur.

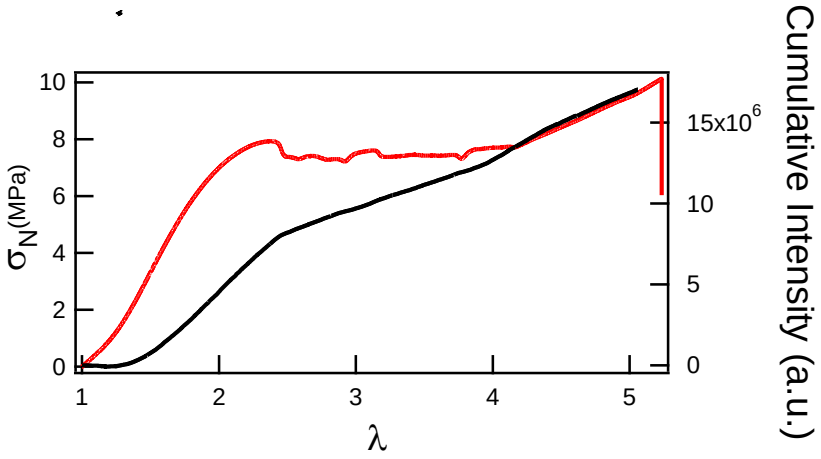

Figure 4: Evolution of the total intensity of the mechanoluminescent signal as a function of the elongation, along with the nominal stress.

The propagation of the necked region along the sample seems to be relatively well understood at this point. However the part following the necking ($\lambda > 4.2$) is quite surprising. In chapter 3 section II)4), during the cyclic experiments, we speculated that during the final strain hardening occurring after the necking, some additional bonds of the first network were breaking in a more homogeneous way. This hypothesis was made due to the fact that some unrecoverable hysteresis was still observed. Looking at Figure 2g, we can say that it is not the case, since the only signal appears to be coming from the bottom of the sample where the width of the sample increases in the shoulder part of the dumbbell. Note that the same thing might happen in the upper part of the sample that is outside of the camera window. The hysteresis observed in the cyclic experiments can come from two phenomena: either the necking region is propagating in the part with a larger cross-section (the shoulder). This would lead to a higher force but would mean that the central part of the sample is also submitted to a higher stress and continues to strain harden. The second process that could dissipate energy would be the second network breaking, this breakage would not emit any signal because the second network is not crosslinked with a dioxetane crosslinker. At this stage it is difficult to separate both processes.

This experiment was not reproduced due to a lack of material and time to do more mechanoluminescent experiments. Still this experiment proves the mechanism involved in the necking process and confirms our hypothesis by validating the entire damage mechanism scenario. First the deformation is elastic with no damage until the hardening kicks in. After that and before the yield stress the sample damages homogeneously and the first network breaks everywhere and dissipates energy. At the yield point, starting from a nucleation point in conditions that still need to be understood, a necking phenomenon starts. We have observed that this necking phenomenon is linked to a high amount of breakage of the first network that occurs locally. It is followed then by the creation of two necking fronts corresponding to an area were the first network is highly damaged. This area moves through the un-necked region until the entire sample is damaged in the same conditions. Finally, the last part of the curve after the plateau of nominal stress shows that this necked region has an intrinsic strain hardening after it is damaged and possibly some damages. The incorporation of the mechanoluminescent crosslinker in the second network could help to investigate the

strain hardening. Also, with quantitative mechanoluminescent experiments, the calculation of the evolution of the intensity with the measured hysteresis could give us answers regarding this final part.

We have now improved our molecular understanding of the stress-strain curve of our most prestretched samples by understanding what happens during the necking process. Still we need a model describing the failure criterion of the multiple networks and in the next part, we will try to apply Brown's model [2] to our system.

II) Discussion around Brown's fracture model of DN

1) Extensive description of Brown's model

Brown's model [2], has been quickly presented in chapter 1 section II)2). The goal of this model it to explain the failure mechanism involved in DN hydrogels to understand their toughness. In this paper [2], Brown describes a model that could be applied to DN hydrogels. In this section, we will discuss the use of this model for our system.

The first hypothesis of this model is that the first network does not break randomly at the molecular scale but micro-cracks occur at the early stage of energy dissipation suggesting the existence of a stress concentration mechanism. In the model, those micro-cracks do not lead to macroscopic failure because they are bridged by the presence of the second network in sufficient amount. This would lead to the nucleation of a large number of microcracks. The mechanoluminescent experiments conducted by Ducrot [1] have shown that in uniaxial traction the first network breaks in a spatially homogenous way at an early stage and the second network must therefore avoid macroscopic crack propagation otherwise the entire sample would break just as it does for a simple network.

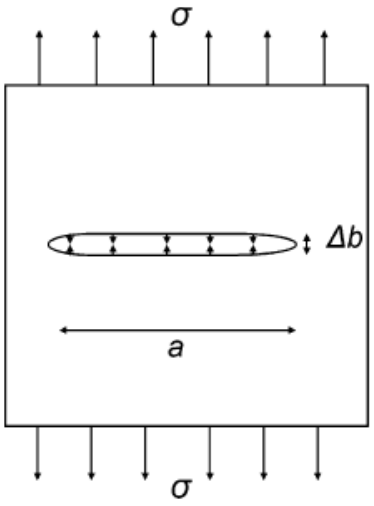

Figure 5: Schematic representation of a micro-crack in a DN gel [2]

Brown proposes Eq. (1) an estimated value of the strain energy release rate G calculated from the energy needed to close the crack shown in Figure 5. In Eq. (1), σ is the nominal macroscopic

stress and Δ_b is the extended length between crosslinks in the second network. When a micro-crack starts to appear in the first network for the critical energy release rate Γ_1, a nominal closing stress σ_a can be deduced as seen in Eq. (2).

$$G = \frac{\Delta_b * \sigma}{2} \quad \textbf{Eq. (1)}$$

$$\sigma_a = \frac{2 * \Gamma_1}{\Delta_b} \quad \textbf{Eq. (2)}$$

Then the second part of Brown's model considers the propagation of the macroscopic crack in the multiple network containing micro-cracks. Around the micro-cracks described in Figure 5, a highly damaged area is created on the tips of each crack. This area can be referred to as the Dugdale area [3]. The model assumes that the first network is highly broken in this area so the resulting material has mechanical properties close to that of the second network alone. In the model, this Dugdale zone has an elastic behaviour and a modulus equal to the one of the second network alone E_2. The rest of the network having a modulus E_1 mainly controlled by the first network. This behaviour around the crack tip is described in Figure 6.

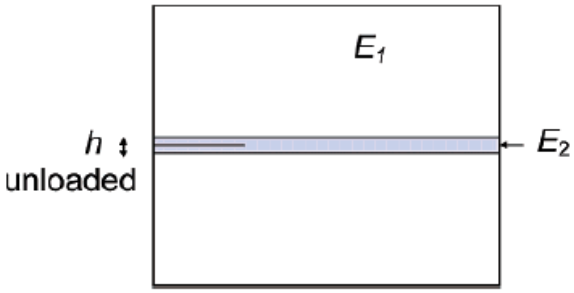

Figure 6: Elastic modulus around a micro-crack in a DN gel [2].

From Figure 6, to propagate a crack in the softened material, there has to be enough energy in the grey area that has an unloaded width h. The strain energy release rate available G_{local} to propagate a crack into the material is described by Eq. (3). For that crack to propagate through the entire sample, G_{local} has to be equal to the fracture energy of the second network Γ_2 this leads to an estimate of the maximal undeformed width of the damage zone h_{max} using Eq. (4).

$$G_{local} = \frac{h * (\lambda_m - 1)^2 * E_2}{2} \quad \textbf{Eq. (3)}$$

$$h_{max} = \frac{2 * \Gamma_2}{(\lambda_m - 1)^2 * E_2} \quad \textbf{Eq. (4)}$$

However, the experimentally measured fracture energy Γ_{global} corresponds to the energy needed to break the first network over this width h_{max}. Then, using an idealized representation of the stress-strain curve of a DN hydrogels shown in Figure 7, the global fracture energy of the sample Γ_{global} can be estimated with Eq. (5). Then using Eq. (2) and Eq. (4), another equation for Γ_{global} can be obtained as shown in Eq. (6), that can be also written using different parameters as shown in Eq. (7).

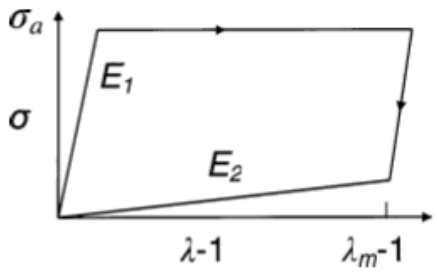

Figure 7: Idealized stress-strain curve of a DN gel [2]

$$\Gamma_{global} = h_{max} \ (\lambda_m - 1) \ \sigma_a \qquad \textbf{Eq. (5)}$$

$$\Gamma_{global} = \frac{4 * \Gamma_1 \ \Gamma_2}{(\lambda_m - 1) E_2 \ \Delta b} \qquad \textbf{Eq. (6)}$$

$$\Gamma_{global} = \frac{2 * \sigma_a \ \Gamma_2}{(\lambda_m - 1) E_2} \qquad \textbf{Eq. (7)}$$

Finally, Brown defines the enhancement of the fracture energy of the DN hydrogels by the ratio between the global fracture energy and the local fracture energy of the second network alone. The expression of that ratio is shown in Eq. (8).

$$\frac{\Gamma_{global}}{\Gamma_{local}} = \frac{2 * \sigma_a}{(\lambda_m - 1) E_2} \qquad \textbf{Eq. (8)}$$

Eq. (7) and Eq. (8) present the key results of Brown's model. Now let's try to apply it to our experimental system.

2) Use of Brown's model in our system

Now that Brown's model has been described we will try to see how it could be applied to our system. In the first part of the model, Brown developed the idea of micro-cracks occurring in the bulk material during deformation. For our materials, the mechanoluminescent experiments done by Ducrot [1, 4] and those presented in the first part of this chapter, show that some damages are occurring in the bulk. Those damages are coming from bond scission in the first network and are homogeneous at the spatial resolution of the camera but no macroscopic failure is observed. Based on this observation, we assume that many micro-cracks may indeed develop in the first network while the loose network keeps them at a microscopic size. We assume that the description of the mechanism involving micro-cracks in DN hydrogels can be applied to the system of multiple networks elastomers. Therefore in this part we will try to apply the results coming from that breakage mechanism.

The first part of the model regarding the creation of the micro-cracks, results in Eq. (2). In our complex system, only σ_a is well known for highly prestretched networks. Δ_b is not easily estimated for the different second networks. Indeed, transfer reactions to the polymer of the

existing networks are taking place at each polymerization step and there might be many trapped entanglements created over the different polymerisations. The fracture energy of the first network Γ_1 is well known for the simple network alone but not necessarily for the highly prestretched first network in multiple networks. In chapter 1 section I)6), a theoretical prediction of Γ_0 as a function of the network structure is proposed by using the model of Lake and Thomas [5] and is recalled in Eq. (9) for a simple network. If we assume that the areal density of chains crossing the interface is diluted by the swelling (Eq. (10)) we can estimate Γ_1 for the multiple networks using their mass fraction and the value of the fracture toughness of the first network (Eq.(11)).

$$\boldsymbol{\Gamma_0 \approx 2 * \Sigma_{SN} N U_{C-C} \approx \Gamma_{SN}} \qquad \textbf{Eq. (9)}$$

$$\boldsymbol{\Sigma_{SN(Multiple\ Network)} = \Sigma_{SN} \phi^{2/3}} \qquad \textbf{Eq. (10)}$$

$$\boldsymbol{\Gamma_1 \approx 2 * \Sigma_{SN(Multiple\ Network)} N U_{C-C} \approx \Gamma_0 \phi^{2/3}} \qquad \textbf{Eq. (11)}$$

Therefore an estimate of Δ_b can be obtained by plotting Γ_1 as a function of σ_a for the multiple networks displayed in chapter 3 table 1. The result is shown in Figure 8. It can be seen that the fracture energy of the diluted first network evolves linearly with the measured yield stress. The best linear fit does not cross the abscissa line in 0 but in 1.2 J/m² which is relatively close. Regarding the slope of the dashed line in Figure 8, it gives a value of 3.5, using Eq. (2), it gives an estimate of 7 µm for Δ_b. This value may be a bit higher than anticipated by Brown in his model but is nevertheless not unreasonable for the maximum width of a microcrack given that many transfer reactions coupling both networks must take place.

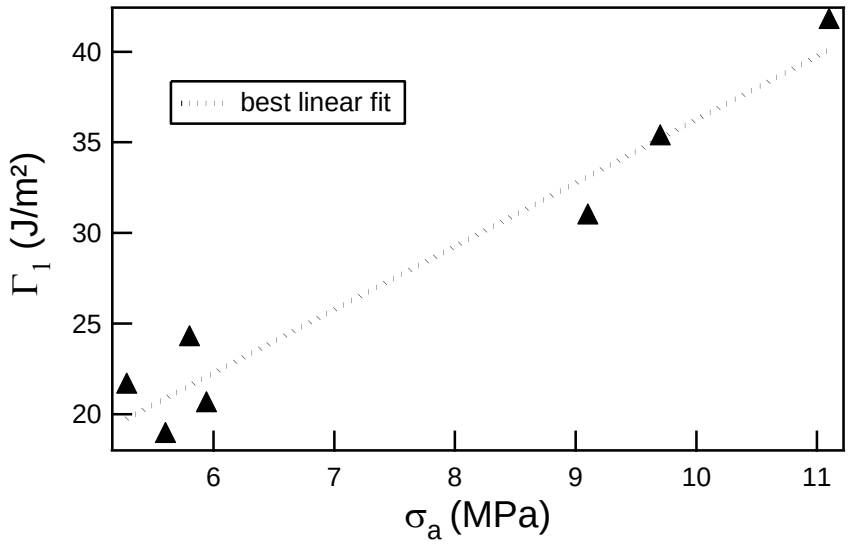

Figure 8: Estimated fracture energy of the first network as a function of the yield stress of multiple networks from the set of samples EAe1.45[EA]. The dashed line shows the best fit with a value at zero of 1.2 J/m² and a slope of 3.5.

Regarding the second part of the model, the hypothesis made by Brown is that in the area where the first network is broken, the material behaves as the second network alone. In chapter 3 we have obtained an estimate of the amount of broken bonds in the first network by using the step cycle experiments and assuming that the Lake-Thomas model is applicable

for chain scission in the bulk. We have been able to estimate that at the end of the necking process the fraction of broken chains in the first network is inferior to 5 % of the initial amount. For this reason, we think that the structure of the damaged area is different from that of the second network alone. For the materials that form a stable neck in uniaxial tension, the behaviour of the damaged area can be obtained experimentally. Indeed, at the end of the necking and before the failure of the material, the sample can be unloaded and the material in the necked state can be recovered. Also, the corresponding stress-strain curve can be deduced from the unloading curve (or the next loading) at the end of the necking in the steps cycles experiments shown in chapter 3. This curve can then be compared to that of the second network alone. We have carried out this procedure for the sample EAe1.45(3.42)EA and Figure 9 shows that the two mechanical behaviours are clearly different. The sample that has been entirely necked shows a higher modulus but also a strain hardening phenomenon. In Figure 9, it should be noted that both samples are reversibly elastic up to the maximal elongation shown.

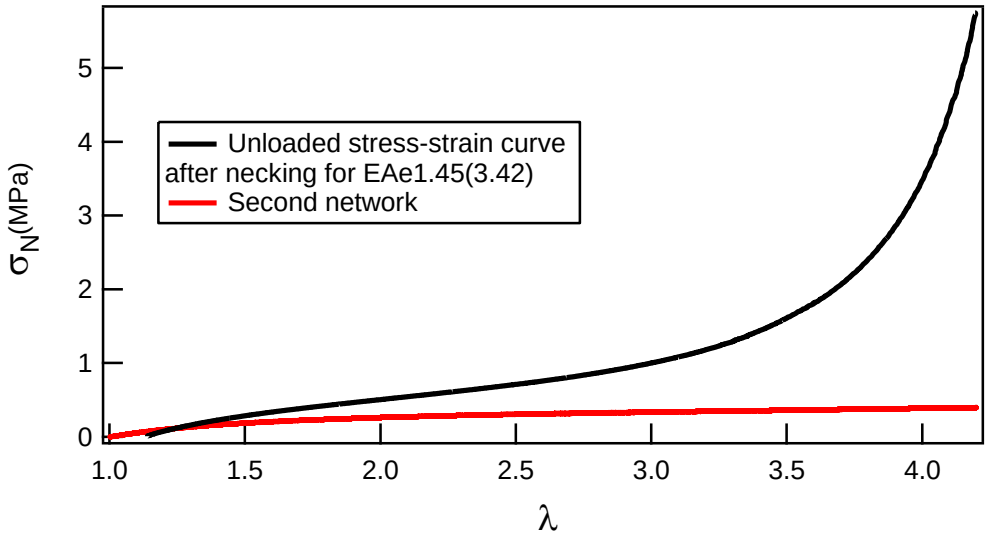

Figure 9: Stress-strain curves comparing the second network alone with the damaged material obtained after the propagation of the necking for the sample EAe1.45(3.42)EA

From the data of Figure 9, it can be deduced that the damaged material that Brown is referring to in his model is different from the second network alone for our system. Brown's model and equations are going to be applied on our materials but with the use of the necked material as the damaged material. The same stress-strain curve presented in Figure 7 can be obtained experimentally with the sample EAe1.45(3.42)EA, the result is shown in Figure 10. This curve plotted in Figure 10 will be used to estimate some values used in the model. This stress-strain curve gives the young modulus of the necked material, $E_2 = 1.1$ MPa and the value of the maximum elongation $(\lambda_m - 1) = 3.2$.

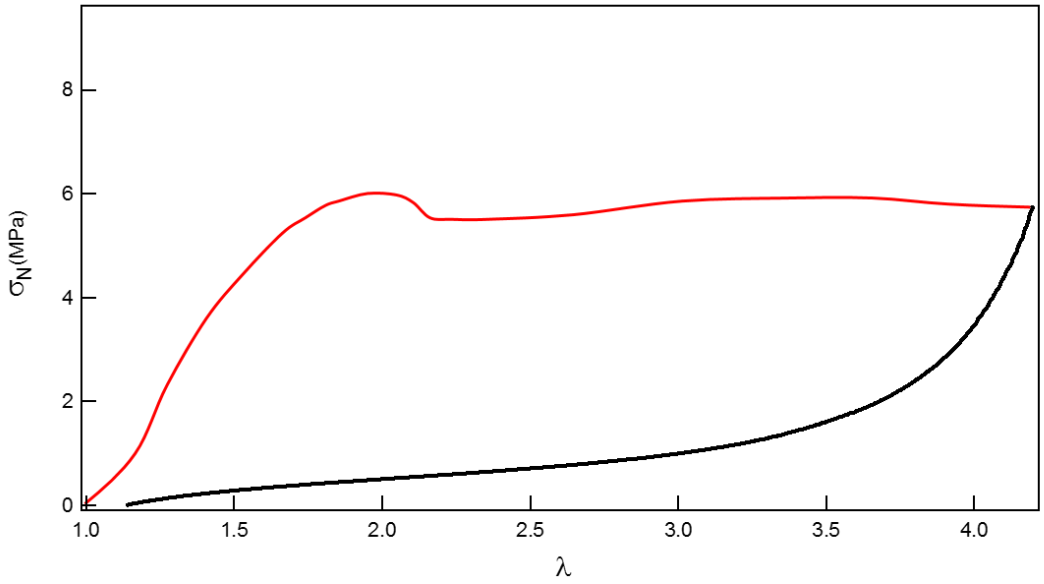

Figure 10: Experimental stress-strain curve showing the work to fully neck the sample EAe1.45(3.42)EA.

The DIC experiments shown in chapter 5 section II)2) have led to the observation of a yield zone around the crack tip. The undeformed width of this process zone would be the h_{max} that Brown is using in his model. Using Eq. (4) we will be able to estimate this value if Γ_2 is known. Γ_2 is the fracture energy of the necked network and can be obtained experimentally. To do so, a sample of EAe1.45(3.42)EA cut in a dumbbell shape is used, and a tensile test is performed on it. This tensile test is done very slowly, at a traction speed of 10 µm/s, to favour the necking phenomenon without breakage. When the necking occurs, we wait until it propagates to the entire central part of the sample to then stop the test and unload the sample. This damaged sample is then taken out of the Instron and a notch of 1 mm is made on the edge of the sample. Following the creation of an initial crack, a single edge notch test is performed. The result is presented in Figure 11 with the comparison of the fracture curve of a necked sample and that of an undamaged one. In this curve we can see the significant drop in modulus observed during the step cycles experiments in chapter 3 section II)4). Using the Greensmith approximation presented in chapter 5 section I)1), we can calculate the fracture energy of the necked sample. The fracture energy of the necked samples appears to be of an order of 1850 J/m². This value is 2 to 3 time lower than that of the undamaged sample.

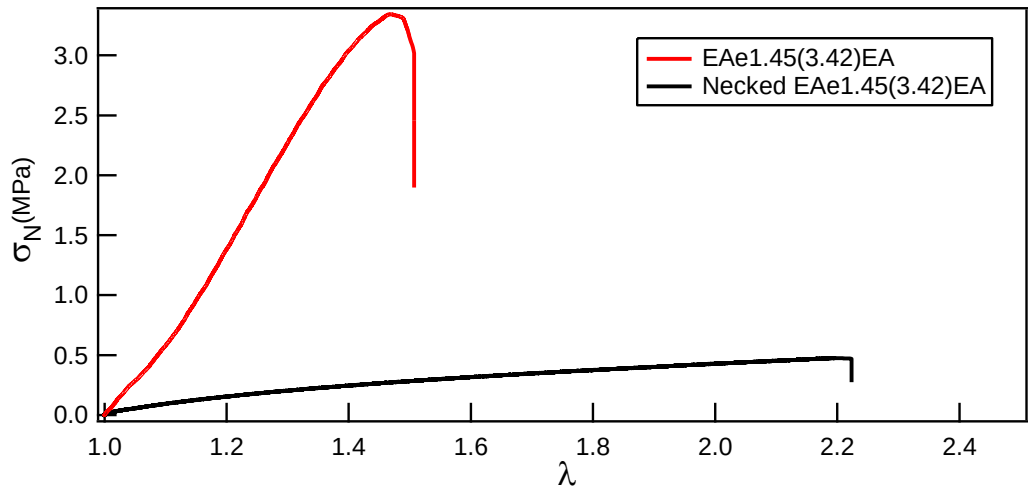

Figure 11: Stress-strain curves of two single edge notch tests. In red an undamaged EAe1.45(3.42)EA and in black a necked sample of EAe1.45(3.42)EA.

With this fracture energy, all elements of Eq. (4) are known for the sample EAe1.45(3.42)EA, and h_{max} can be calculated. For EAe1.45(3.42)EA, $h_{max} = 328$ µm, this value is of the order of magnitude of the value obtained for the same sample using the digital image correlation data. Indeed, the value of h at the maximum elongation before the crack propagates for the same sample was found to be 200 µm at a deformed state. The value obtained with the model might be overestimated due to an underestimation of the yield stress.

From the width of the Dugdale zone, an estimate of the total fracture energy can be made using Eq. (7). With $\sigma_a = 5.3$ MPa taken from Figure 10, this estimate gives 5570 J/m². This value should be compared with that obtained with a single edge notch sample in chapter 5 section I)2) for the sample EAe1.45(3.42)EA around 4000 J/m² for the standard loading rate of 100 µm/s. Considering that a slower traction speed could lead to values up to 6000 J/m², the value estimated by the model is in very good agreement with the experimental values. The magnitude of the amplification in Γ_{global} may not appear spectacular but actually the material is rather stiff and has still a much higher toughness than a much softer material.

Finally in his paper [2], Brown gives an estimate of the improvement of the fracture properties defined by the ratio between the global fracture energy and the fracture energy of the second network as shown in Eq. (8). For our system the comparison of the global fracture energy and that of the necked material gives a result of 2 or 3 in terms of ratio but this ratio does not make much sense as an enhancement ratio in this case since the necked material cannot be synthesised. The enhancement ratio in case of a comparison between a sample like EAe1.45(3.42)EA and the second network alone gives an enhancement of 15 times while the enhancement in comparison with the first network alone can go up to 40 times.

In the previous section we have examined in detail the applicability of Brown's model to our materials but especially to a single sample EAe1.45(3.42)EA. Indeed, this particular sample, where the necked region can be characterized, shows what is needed for the model to be checked experimentally. Unfortunately for most of the materials we synthesised, no macroscopic necking is observed and the yielded material cannot be characterized.

However, Eq. (5) can still be used. In this equation, two parameters have been obtained experimentally for most of our samples: the yield stress and the fracture energy. Therefore, for the set of samples used in chapter 3 section IV)2) and chapter 4 section I), the ratio of those two parameters can be plotted as shown in Figure 12. This ratio is equal to $h_{max}\ (\lambda_m - 1)$ and is expressed in µm.

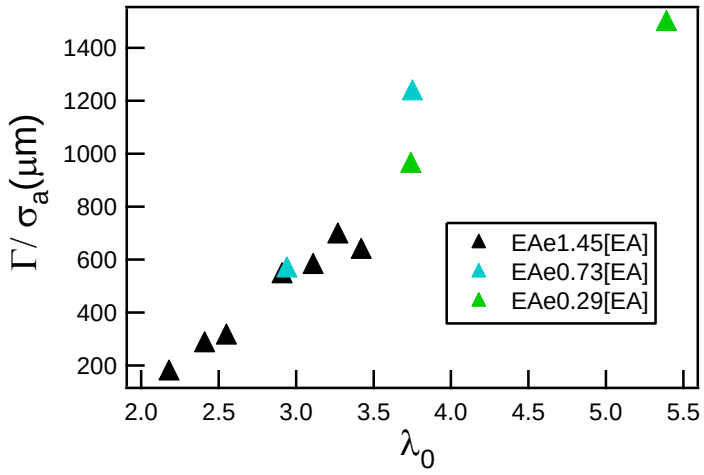

Figure 12: Γ/σ_a as a function of the prestretching of the first network for different multiple network made of various first networks.

Figure 12 shows the evolution of a characteristic ratio that has the dimension of a length, which is evolving linearly with the prestretching of the first network. Following Brown, if we interpret this distance as the width of the deformed damage zone when the crack propagates and make the assumption that $(\lambda_m - 1)$ does not vary much, then h_{max} increases almost by an order of magnitude with λ_0. This hypothesis is qualitatively in agreement with the evolution of the yield zone observed in chapter 5 section II)2) by DIC where the yield zone at the crack tip increases with λ_0.

To verify that, some more DIC or mechanoluminescent experiments should be done especially with multiple networks using EAe0.29(1) and EAe0.73(1) as first networks. Those experiments could help observing experimentally a yield zone and therefore confirm or not the good agreement with Brown's model.

In this part we have tried to verify the applicability of Brown's model to our elastomer system, and the results obtained using the different equations developed by Brown are in good or very good quantitative agreement with the performed mechanical experiments. Therefore, we can assume that the failure model proposed by Brown must be rather close to the real physical picture for our multiple networks elastomers. However a key missing point is the structure and properties of the broken network which controls the final crack propagation. It is clearly not a simple soft network but a network filled with broken pieces of first network which now acts as a discontinuous filler but a filler nevertheless. Such a structure will certainly depend very much on the details of the chemical connections between the networks during the various polymerization steps.

Conclusion

In this chapter we have summarized and completed our understanding of the stress-strain curves for networks with a highly prestretched first network. Indeed, the necking phenomenon is now much better understood. The use of the mechanoluminescence has led to the visualisation of the necking phenomenon with the breakage of the first network. Starting from a specific area where a nucleation of damages occurs in the first network, two fronts are created. Those two fronts are propagating by damaging the first network in two opposite directions until the entire gauge length of the sample reaches the same state. Following this necking, the subsequent strain hardening is still not understood and two hypotheses have been developed to explain the damages occurring during this part. It is either coming from the undamaged first network located on the edges of the dumbbell sample or the second network start to breaks.

Following the improvement of the understanding of the full stress-strain curve all the way to yielding the comparison of our different experimental results with the Brown's model has given good results strongly suggesting that the failure of the multiple networks is similar to that of the DN hydrogels. First micro-cracks appear in the bulk sample, those micro-cracks do not propagate thanks to the presence of the second network. The area affected by the micro-cracks grows until a critical value where the crack propagates and the entire material fails.

References

1. Ducrot, E., et al., *Toughening Elastomers with Sacrificial Bonds and Watching them Break.* Science, 2014. **344**(6180): p. 186-189.
2. Brown, H.R., *A model of the fracture of double network gels.* Macromolecules, 2007. **40**(10): p. 3815-3818.
3. Dugdale, D.S., *Yielding of steel sheets containing slits.* Journal of Mechanics and Physics of Solids, 1960. **8**: p. 100-104.
4. Ducrot, E., *Double Network Elastomers*. 2013, Université Pierre et Marie Curie: Paris.
5. Lake, G.J. and A.G. Thomas, *The strength of highly elastic materials.* Proceedings of the Royal Society of London, series A: Mathematical and Physical Sciences, 1967. **A300**: p. 108-119.

General conclusion

In 2003, Gong *et al*. introduced the principle of double network hydrogels [1]. The concept, based on the asymmetry of two interpenetrated networks led to a large improvement of strength and toughness for those materials. Starting from that work, ten years later, Ducrot *et al.* transferred the principle to multiple network elastomers made of acrylate monomers [2]. Instead of using a polyelectrolyte in water as a prestretched first network, Ducrot used a first network that was forced to swell in a monomer solution that will then create the second network. This technique led to a significant mechanical reinforcement, however, the underlying principle behind that reinforcement was not clear and needed some more experimental and theoretical analysis.

In the present work, systematic studies have been conducted on various parameters influencing the mechanical behaviour in order to investigate the mechanisms responsible for the improvement of the mechanical properties.

First, the influence of the degree of prestretching λ_0 of the first network was studied. This was realized by modifying the original synthesis conditions in order to obtain multiple networks, where the ratio between the first and the second network and therefore the degree of isotropic prestretching of the chains of the first network could be tuned to an arbitrary value. The uniaxial tension tests performed on those elastomers led to their classification in four different categories in terms of mechanical behaviour depending on λ_0 of the first network chains. Using Gent's model [3] to fit the strain hardening data showed that λ_0 also controls the onset of the hardening phenomenon, so that the onset of strain hardening occurred at the same value of the product $\lambda\lambda_0$ for a different set of materials. Using the same set of samples, we also analysed the process following the hardening i.e. the progressive damage of the first network. It was found that the stress was controlled mainly by the areal density Σ of strands crossing the plane normal to the tensile direction. Σ varies with the 2/3 power of the first network concentration ϕ. This result confirmed our hypothesis that the breakage is governed by the fraction of first network particularly the first network strands in the cross-sectional plane. Those analyses have led to a master curve which correctly describes the behaviour of all the different elastomers in large strain. The two key results obtained in chapter 3: normalization of the stretch by λ_0 and normalization of the stress by $\phi^{2/3}$ have then been used for the analysis of different networks.

After keeping the first network unchanged in chapter 3, chapter 4 was dedicated to the effect of molecular changes of the first network. Several important results were obtained.

First, the crosslink density of the first network governs the maximum extensibility of the chains and therefore the onset of the strain hardening phenomenon. However when the degree of crosslinking of the first network is too low, the fit of the data to the Gent model was not very good. This is in particular due to the fact that transfer reactions between networks become important so that the density of crosslink points introduced by transfer reactions becomes non negligible relative to the density of first network crosslinking points.

Second, the removal of the 50% solvent used in the synthesis of the first network led to a broader range of achievable mechanical properties. It was shown that a higher Young's

modulus and high stress at break could be obtained by this mean of synthesis which traps more entanglements.

The final change that was conducted on the first network was to use different monomers aside from the standard ethyl acrylate. Changing the monomer in the second network for larger acrylate monomers only led to difficulties upon the swelling of the first network. This change was conducted with the expectation of obtaining a micro phase separation but it did not improve the mechanical properties. The most interesting result from this part came from the use of a methacrylate monomer as first network. Methacrylate monomers have the specificity in comparison to acrylates to avoid transfer reactions between the chains, therefore the use of methacrylate in the first networks prevented connections between the first network and the networks that are synthesized afterwards. The mechanical properties of the multiple networks made in this way showed that this composition strategy could improve the mechanical properties by delaying the breakage of the entire sample and improving the elongation at break. However, those results were preliminary results, and as such more experiments should be conducted to confirm our hypothesis of a reinforcement by a better stress distribution in the networks. The first chapters of this work gave us the ability to control the final mechanical properties of our elastomers by understanding the effect of all the different aspects of the synthesis.

Chapter 5 was dedicated to the study of the fracture toughness. The most significant result observed in this part is that in our system of multiple network elastomers, the fracture toughness of the material increases with increasing Young's modulus. This result is contrary to what is commonly observed for standard unfilled elastomer networks and also in contradiction with Lake and Thomas's prediction [4]. The second part of chapter 5, dedicated to the observation of the local displacement field with DIC and the local damages with the mechanoluminescence, gave an explanation to this phenomenon. It appears that the increase of the prestretching, along with the modulus, tends to create a larger volume of influence at the crack tip leading to more energy dissipation. DIC experiments have shown that upon the increase of the prestretching the affected volume at the crack tip increases. The most interesting result there is the detection of local yielding at the crack tip while the sample remains fully elastic in uniaxial tension.

The mechanoluminescent experiments gave us a good knowledge of the extent of the damaged volume at the crack tip. It has been observed that this area increases with the prestretching. However, the most interesting results in mechanoluminescence were described in chapter 6 where these direct optical observations helped to confirm the mechanism leading to the necking phenomenon for materials containing a highly prestretched and diluted first network. Indeed, the observation of the two fronts experiencing molecular breakage confirmed the existence of two coexisting regions in this regime of the stress-strain curve. One region is already highly damaged and necked, and propagates through the progression of the two fronts to the rest of the sample. These two techniques, DIC and mechanoluminescence, provided new knowledge and methodology to investigate local strain and local breakage at the crack tip that could potentially be later applied to different materials. This could be useful for future multiple networks studies.

The last part of this work tried to link the different experiments that were carried out in this PhD with the model of Hugh Brown [5]. Brown showed that his model for double network fracture describes well the fracture of Gong's double network hydrogels, and we examined its relevance for the standard family of samples that were studied: EAe1.45[EA]. The results showed that Brown's model is quantitatively consistent with the observed behaviour of our materials and therefore strongly suggests that the first network progressively breaks in a non-random way by the formation of micro-cracks which are maintained at a microscopic scale by the presence of the second network in sufficient amount. A quantitative criterion for crack propagation based on material composition remained however elusive for lack of knowledge of the structure of the damaged material.

In conclusion, significant advances have been made in the understanding of the mechanisms by which these peculiar interpenetrated network structure provide a great mechanical reinforcement to otherwise brittle elastomers. We showed that the balance between stiffness and extensibility can be tweaked during synthesis resulting in a family of materials with rather different properties ranging from extensible with strain hardening to very stiff with a high strain at break.

This work has laid the groundwork for more experiments to be to done to lead to even better understanding: First, the use of mechanoluminescence just started to give some results at the end of the project, so quantitative experiments with better spatial and temporal resolution are a promising goal in order to map precisely the bond breaking mechanism around the crack tip or at the fronts of the necking. Also, the macroscopic yielding and necking that was first observed during this work for this type of soft materials is far from being fully understood. Indeed, it has been seen that a change in the monomer of the first network has an influence on the yielding values but the reason is not clear yet and more systematic experiments could improve the understanding of that phenomenon and lead to new applications.

References

1. Gong, J.P., et al., *Double-network hydrogels with extremely high mechanical strength.* Advanced Materials, 2003. **15**(14): p. 1155-1158.
2. Ducrot, E., *Double Network Elastomers*. 2013, Université Pierre et Marie Curie: Paris.
3. Gent, A.N., *A New constitutive relation for rubber.* Rubber Chemistry and Technology, 1996. **69**: p. 59-61.
4. Lake, G.J. and A.G. Thomas, *The strength of highly elastic materials.* Proceedings of the Royal Society of London, series A: Mathematical and Physical Sciences, 1967. **A300**: p. 108-119.
5. Brown, H.R., *A model of the fracture of double network gels.* Macromolecules, 2007. **40**(10): p. 3815-3818.

Annexes

Annex 1:

The two following graphs both show the absence of hysteresis for samples made with EA1.45(1) without solvent, meaning that only a very small amount of breakage occurs along the deformation for those samples.

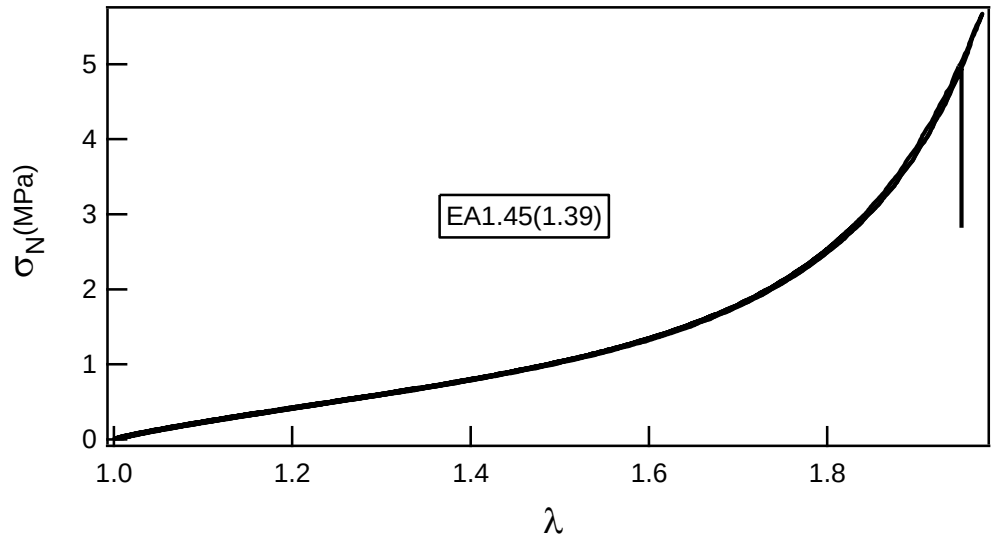

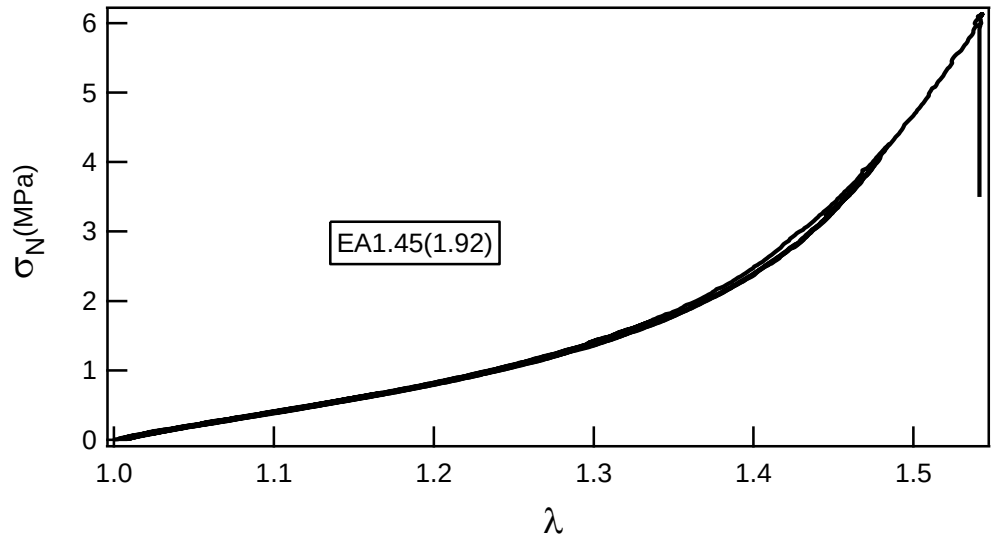

Annex 2:

Example of Gent fit's for the samples made with EA1.45(1) as first network. The good quality of the fit validates the use of this method to obtain the hardening elongation for the first networks made in the bulk.

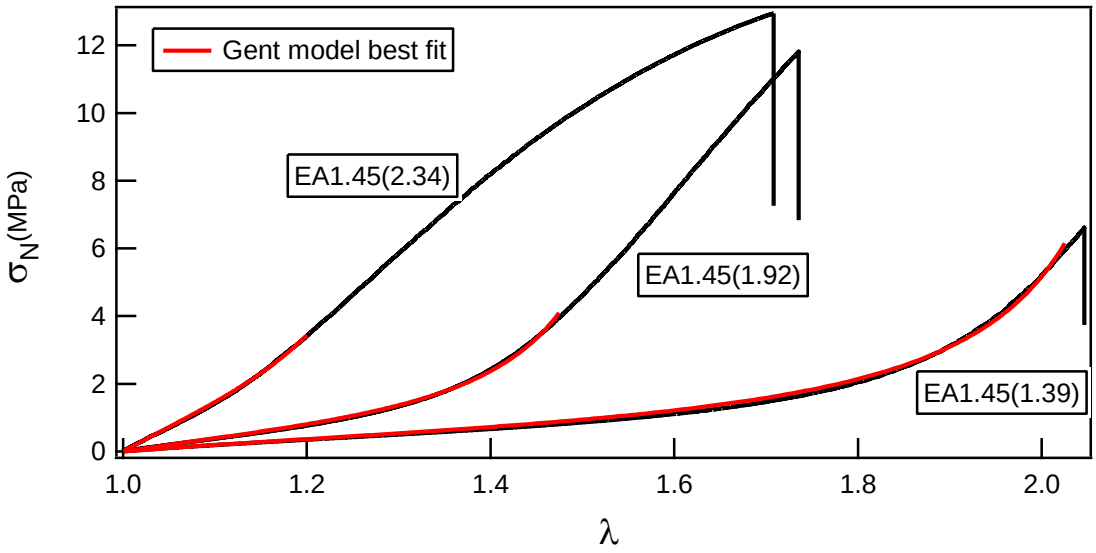

Annex 3:

DSC heat flow as a function of temperature for samples BAe1.86(1.59)EA (top) and BAe1.86(2.41)EA (bottom). Those two graphs both show a single glass transition temperature at -27 °C for BAe1.86(1.59)EA and at -23 °C for BAe1.86(2.41)EA. This result means that no phase separation occurs during the synthesis of multiple networks with BA and EA.

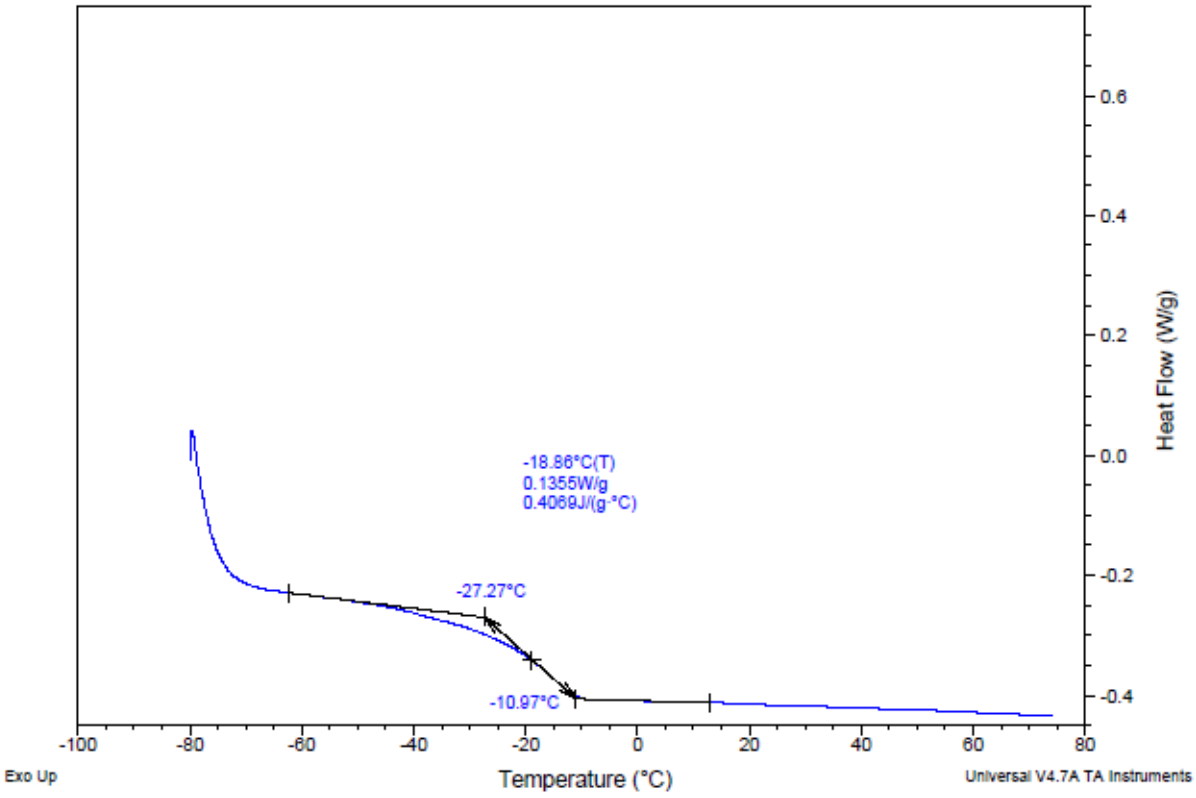

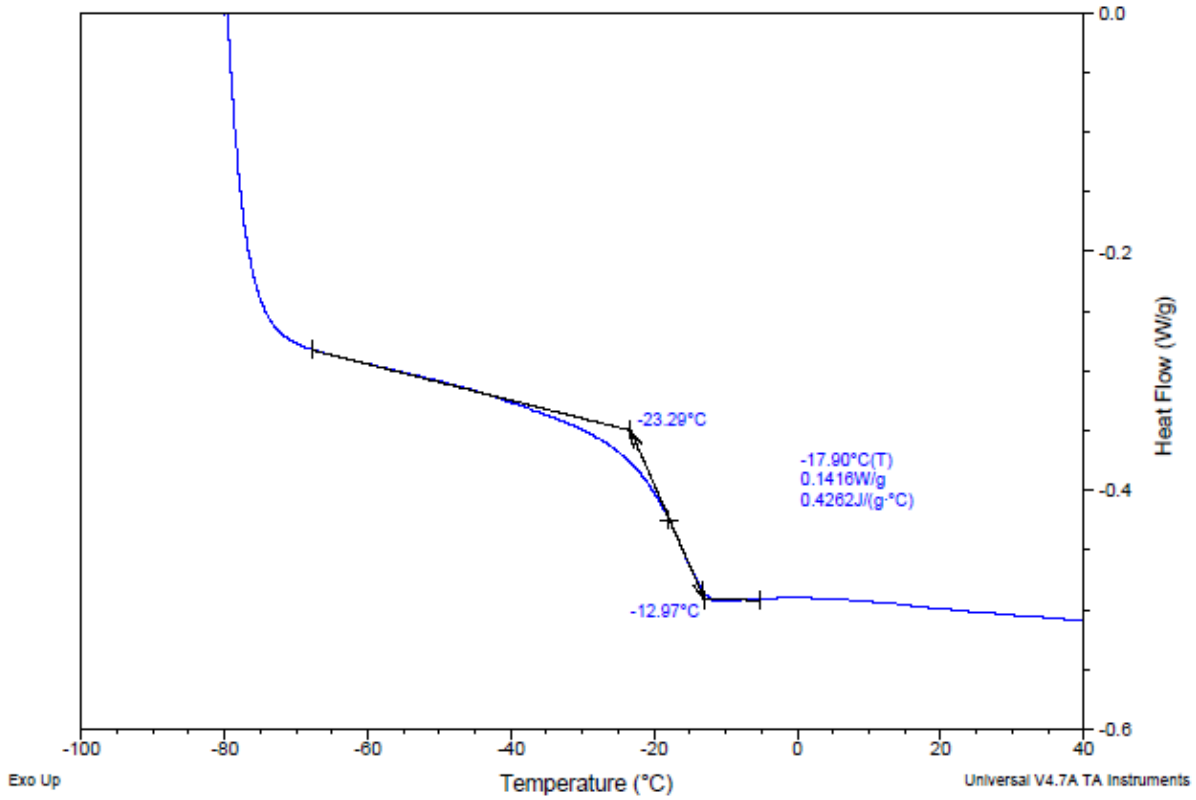

Annex 4:

DSC heat flow as a function of temperature for the sample EAe1.45(2)HA. Only one glass transition temperature can be observed, no micro-phase separation is detected for this sample.

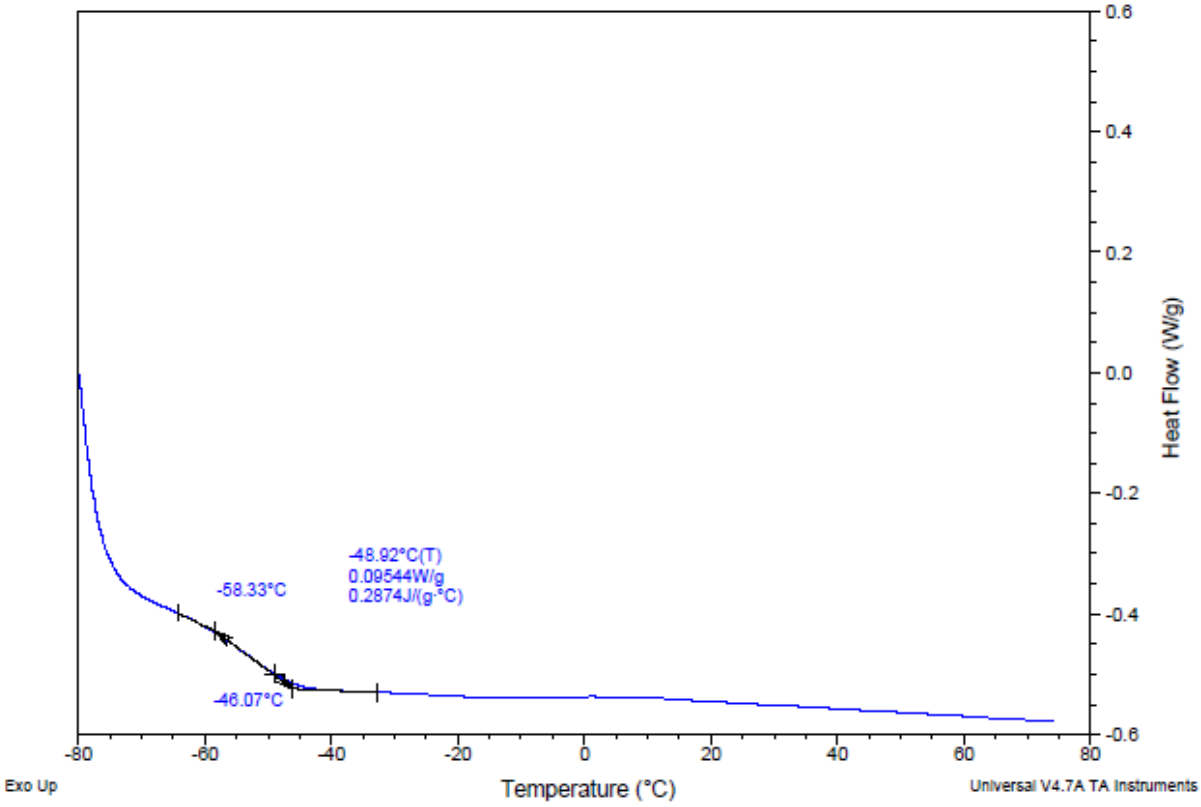

Annex 5:

This annex shows the stress-strain curves of EAe1.45[EA] samples in black and EAe1.45[HMA] in red. The multiple networks of the family EAe1.45[HMA] show poor mechanical properties due to the difficulty of swelling the first network with HMA which is a large monomer.

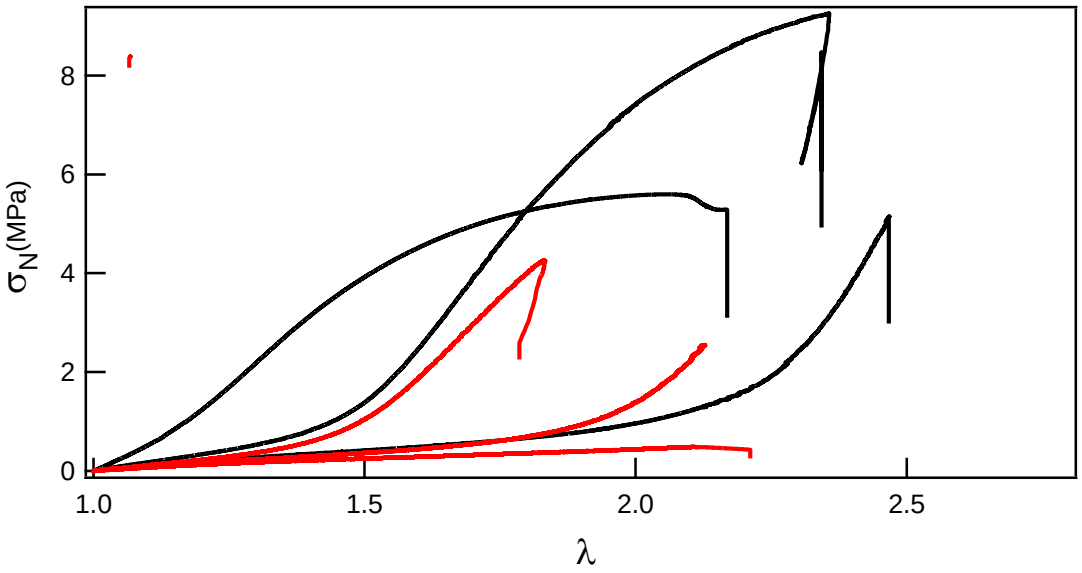

Abstract (EN): We investigated systematically the mechanical and fracture properties of multiple network elastomers synthesized by successive swelling/polymerization steps inspired by the molecular architecture of Gong's double network gels.

A more versatile synthesis method was used to vary continuously the isotropic degree of prestretching λ_0 of the first network resulting in a wider range of mechanical behaviours, where λ_0 controls the Young's modulus at small strain and the strain hardening at large strain. If the first network is diluted enough (<10%) molecular bond breakage occurs in this prestretched network at high strain while avoiding sample failure. The degree of dilution controls the amount of damage and therefore the slope of the stress-strain curve. Finally, for the most diluted systems (<3%), a yield stress and a necking phenomenon was observed. Changing the degree of crosslinking of the first network or the monomers used led to the same qualitative mechanical behaviour.

The fracture energy Γ was shown to be an increasing function of λ_0 however different regimes could be distinguished with macroscopic fracture occurring before or after bulk damage was detected. Visualisation techniques such as Digital Image Correlation and embedded mechanoluminescent molecules were used to map a damage zone in front of the crack tip, the size of which increased with λ_0.

Finally, the toughening mechanism of the multiple network elastomers could be understood in a nearly quantitative way within the framework of Brown's model of fracture of double network gels.

Abstract (FR): Durant ce travail, nous avons étudié les propriétés mécaniques et de fracture d'élastomères à réseaux multiples synthétisés par des étapes successives de gonflement/polymérisation inspirées de l'architecture moléculaire développée par Gong pour les doubles réseaux hydrogels.

Une méthode de synthèse plus versatile a été utilisée pour varier de façon continue le pré-étirement isotrope du premier réseau λ_0, qui contrôle le module d'Young et le durcissement. Dans le cas d'une dilution importante du premier réseau (<10%), une scission moléculaire apparaît à grande déformation dans le réseau pré-étiré sans rompre le matériau. Le taux de dilution contrôle la quantité d'endommagement et donc la pente de la courbe contrainte-déformation. Finalement, pour les systèmes les plus dilués (<3%), une striction est observée au-dessus d'un seuil de contrainte. Changer le taux de réticulant du premier réseau ou les monomères utilisés ont conduit par ailleurs à l'obtention de comportements mécaniques similaires.

L'énergie de fracture Γ est une fonction croissante de λ_0. Des techniques de visualisation locale comme la Corrélation d'Image Numérique et l'intégration de molécules méchanoluminescentes ont été utilisées pour décrire une zone d'endommagement en tête de fissure dont la taille augmente avec λ_0.

Enfin, le mécanisme de renforcement des élastomères à réseaux multiples a pu être partiellement décrit dans le contexte du modèle de Brown sur les doubles réseaux.